Faculty of Science and Engineering
Department of Spatial Sciences

An Evaluation of Surface Urban Heat Islands in Two Contrasting Cities

Mustafa Naem Hamoodi

This thesis is presented for the Degree of
Doctor of Philosophy
of
Curtin University

August 2018

Declaration

To the best of my knowledge and belief this thesis contains no material previously published by any other person except where due acknowledgment has been made.

This thesis contains no material which has been accepted for the award of any other degree or diploma in any university.

Signature:

Date:

Abstract

Urban Heat Island (UHI) is a common environmental issue facing modern cities, and refers to elevated surface and air temperatures relative to the surrounding rural areas. Impervious surfaces have a warming effect on urban land surface temperature (LST). The development of thermal infrared remote sensing provides opportunities to characterise the spatial and temporal structures of surface temperatures, especially for the urban areas. Therefore, analysis of urban surfaces via thermal remote sensing has played a significant role in monitoring and evaluating urban environmental quality. This work presents a comparative study on surface urban heat islands (SUHIs) in two cities, Baghdad and Perth, which were selected due to their different geographical locations, climatic conditions, and urban landscape patterns.

The first part of the study evaluates expansion of built-up areas and quantifies its effects on the SUHI. Multi-date Landsat data, acquired for the summers of 1976, 1984, 1992, 2000 and 2015 for Baghdad, and 1974, 1988, 1997, 2008 and 2015 for Perth, were used in this study. Linear spectral mixture analysis (LSMA) was used for mapping impervious surfaces. These maps were then divided into eight zones (pie sections) to quantify spatiotemporal dynamics of impervious surfaces. Spatial, temporal, and seasonal variations of LST were investigated using thermal maps, retrieved from thermal bands of Landsat data (except those in the 1970s).

The second part of the study examines the extent to which the urban thermal environment is influenced by spatial patterns of land use and land cover (LULC). Percent impervious surfaces area (PISA) and the impervious surface analysis tool (ISAT) were used to quantify the spatial distribution of impervious surfaces. In addition, a set of landscape metrics, including Shannon's diversity index (SHDI), modified Simpson's evenness index (MSIEI), Shannon's evenness index (SHEI), and patch density (PD) were used to assess urban landscape patterns. A statistical analysis between PISA, the landscape metrics and LST for both cities was examined and compared.

The final part investigates thermophysical behaviour of various urban LULC categories using surface albedo and LST parameters. These parameters were retrieved from two datasets, remotely sensed data (Landsat 8) and in-situ measurements using a

pyranometer and an infrared camera. A new method was developed and applied to adjust field data to the time of the satellite overpass. The adjusted field data were then verified using corrected surface albedo and LST retrieved from Landsat 8. The effect of various urban LULC surfaces on the urban thermal environment was then examined.

Impervious surfaces noticeably expanded in both cities over time. However, expansion rates and directions varied in each city. The area of impervious surfaces in Baghdad increased by 18.6% (161.9 km^2) from 1976 to 2015, whereas an increase of about 14.1% (68.6 km^2) from 1974 to 2015 was estimated for Perth. Landsat data reveal that the built-up category of Baghdad city is darker than Perth city, and hence exhibits higher temperatures. This finding indicates that the LST is affected by the spatial pattern of urban landscape, in addition to urban land use and land cover (LULC) characteristics. Inverse relationships for each of the correlations of landscape metrics with LST were found between Baghdad and Perth. Surface albedo and temperature of built-up categories are characterised by a greater impact on the environment compared with non-built up categories. The correlation between adjusted field measurements and Landsat 8 data was strong for surface albedo, and moderate for LST.

In conclusion, overlay ISA maps and then dividing the maps into zones is a powerful approach for precisely determining the amount and direction of impervious surfaces expansion. The PISA and landscape metrics were shown to be important parameters for inferring LST pattern. The adjustment of field measurements was demonstrated to be a practical method, and adjusted values were accurate in analysing the urban thermal environment.

Acknowledgements

I am immensely grateful to the Higher Committee for Education Development in Iraq (HCED) for granting me a scholarship and for supporting this PhD research.

I would like to thank my supervisors Dr. Ashraf Dewan and Dr. Robert Corner for their supervision, professional assistance and encouragement during this study. They were very supportive me during this journey.

I am very thankful to Dr. Ashty Saleem from Curtin University, Department of Spatial Sciences for his support and encouragement whenever I faced difficulties through the PhD journey. He has supported me in both my personal and academic life from the day one. I have learnt so much from him. Also, special thanks goes to members of the postgrad room for all the memorable fun times.

I wish to thank my fellow graduate students and staff members at Curtin University for sharing their proficiency and knowledge the intangible sources that actually went into producing this research.

I duly acknowledge the proof-reading/editorial services of Dr Andy Kiker.

Last but not least, my deepest gratitude to my beloved wife and kids, who are a source of immense joy and inspiration in both good and bad times, for their extreme support and patience, thank you all.

Related Publications

1. Naem, M., Corner, R., and Dewan, A. (2016). *Diurnal and seasonal surface temperature variations: A case study in Baghdad.* Paper presented at the Proceedings of the 3rd annual conference of Research@Locate, Apr 12-14 2016, pp. 65-70, Melbourne, Australia: CEUR.

2. Hamoodi, M., Corner, R., and Dewan, A. (2017). Thermophysical behaviour of LULC surfaces and their effect on urban thermal environment. *Journal of Spatial Science*, DOI: 10.1080/14498596.2017.1386598

Table of Contents

List of Figures

List of Tables

Abbreviations

ABS	Australian Bureau of Statistics
AUHI	Atmospheric Urban Heat Island
BOM	Bureau of Meteorology
BSh	Semi-arid Climate
Csa	Mediterranean Climate
DN	Digital Number
EPA	Environmental Protection Agency
GIS	Geographic Information Systems
IMO	Iraqi Metrological Organization
ISAT	Impervious Surface Analysis Tool
LCT	Land Cover Type
LSMA	Linear Spectral Mixture Analysis
LST	Land Surface Temperature
LULC	Land Use and Land Cover
NDVI	Normalised Difference Vegetation Index
NDWI	Normalised Difference Water Index
NIR	Near-Infrared
NOAA	National Oceanic and Atmospheric Administration
OLI	Operational Land Imager
PISA	Percent Impervious Surfaces Area
SUHI	Surface Urban Heat Island
SUHII	Surface Urban Heat Island Intensity
SWIR	Shortwave Infrared
TM	Thematic Mapper
UBL	Urban Boundary Layer
UCI	Urban Cool Island
UCL	Urban Canopy Layer
UDIA	Urban Development Institute of Australia
UHI	Urban Heat Island
USGS	United States Geological Survey
UTM	Universal Transverse Mercator

1. Introduction

1. 1. Research background

More than 50% of the population of the world currently live in urban areas, and the number is expected to increase to 66% by 2050, although most of the increase in population has occurred in developing countries (Seto et al., 2011; United Nations, 2014). According to Madlener and Sunak (2011), cities occupy around 2% of the earth's surface, and increase in urban population has resulted in the loss of previous agricultural land and vegetated areas.

The urban environment has been significantly influenced by a complex process, involving rapid urban growth, industrialisation, and other practices of land use attributable to increased human activities over time. Many environmental problems are driven by rapid urban growth, which appears to affect urban climate (Fall et al., 2010; Hamdi, 2010; Chapman et al., 2017), urban ecosystems (Jones et al., 1990; Turner, 1994), hydrological systems (Konrad & Booth, 2002; Jacobson, 2011), and the overall environment (Svirejeva-Hopkins et al., 2004; Lu et al., 2015).

Changes in land use/land cover (LULC) are causing changes in land surface properties, thereby affecting heat storage and albedo (Bounoua et al., 2002; Peng et al., 2011). At the local and regional levels, earth's climate has been significantly modified as a result of the interrelationship between land surface and the atmosphere (Voogt & Oke, 2003; Zhou et al., 2003). Consequently, urban climate is modulated by increasing surface and air temperatures, in addition to changes in climatic variables such as rainfall and humidity, for example.

One of the most common environmental issues that a city is currently facing is the urban heat island (UHI) phenomenon. This refers to elevated temperature (both surface temperature and air temperature) in an urban area compared with its surrounding rural areas (Oke, 1987; Voogt & Oke, 2003; Imhoff et al., 2010). This concept was probably first noticed by British scientist Luke Howard in 1818 who observed that air temperature in the city of London was higher than its undeveloped rural surroundings (Howard, 1833). The UHI phenomenon has attracted considerable attention due to the fact that urban climate is modified by changes in LULC. This issue was tested first by

Nieuwolt in 1964 based on work in Singapore (Nieuwolt, 1966). Subsequently, various data sources, methods, approaches, and models have been developed and employed to investigate UHI in a variety of environmental settings, especially in large cities. All of them have confirmed that urban areas have higher surface and air temperatures than their adjacent rural areas, primarily resulting from the conversion of natural surfaces into impervious surfaces. The main effect of urbanization is the variation of the land surface temperature (LST) pattern (Bektas Balcik, 2014). This variation is generally related to the nature and characteristics of LULC surfaces. In urban areas, increased ambient temperature is mainly associated with warmer surfaces (Synnefa et al., 2007).

The term "impervious surface" is defined as any man-made surface that prevents infiltrating of waters into the soil, such as building rooftops, streets, parking lots, and footpaths (Schueler, 1994; Arnold Jr & Gibbons, 1996). Impervious surfaces have a different absorption rate of solar radiation based on their properties (Uemoto et al., 2010), and normally have the thermal capacity high enough to store large amounts of solar radiation (Wang et al., 2007). Building and paving materials with high thermal capacities and higher conductivity, such as concrete, asphalt and bricks, lead to the development of UHI effects in their built environments (Stathopoulou et al., 2009; Kantzioura et al., 2012).

Previous literature has identified that the formation of UHIs is related to a number of factors that are mostly associated with LULC changes. Consequently, urban development, by adding more impervious surfaces, leads to elevated land surface temperature (LST), which contributes to the development of UHIs and is detrimental to the urban environment, affecting human health, comfort, and quality of life (Svensson & Eliasson, 2002; Santamouris et al., 2011). In 2018, NASA's Goddard Institute for Space Studies (GISS) reported that global average surface temperature anomaly increased to 0.9 °C in 2017 with a generally increasing trend for the period between 1880 and 2017 (NASA/GISS, 2018), as illustrated in Figure 1.1. In 2016, the historically highest global surface temperatures were recorded.

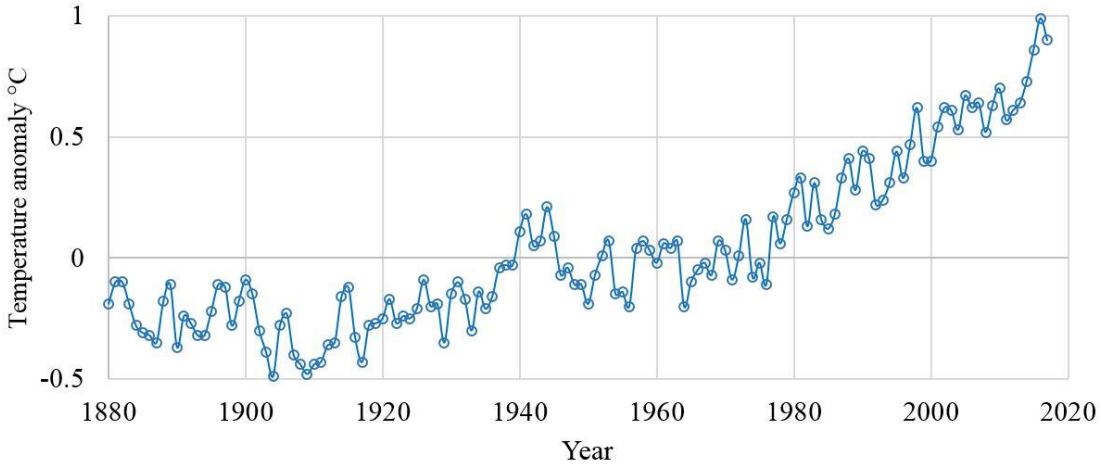

Figure 1.1 Annual global mean surface temperatures observed during the period from 1880 to 2017 (Source: NASA/GISS, 2018).

High rates of mortality and morbidity have recently been reported in many cities around the world due to the increasing frequency of heat waves (Confalonieri et al., 2007; Gabriel & Endlicher, 2011). Meanwhile, the expansion of impervious surface cover has adversely led to many significant climatic and environmental issues, including reduction of urban air and water quality (Hurd & Civco, 2004), the alteration of sensible and latent heat fluxes, and the increase of intense urban heat islands (Yang et al., 2003). In contrast, green cover and water bodies within urban areas positively affect urban climate and environment, due to reduction in UHI effects (Oliveira et al., 2011). Akbari et al. (2001) reported that urban heat islands emerged during hot summer days due to high absorption of solar radiation by impervious surfaces and concomitant lack of vegetation.

The above considerations are most relevant to hot climate cities in terms of the magnitude of their effect. However, the UHI effect is a common phenomenon in most cities, irrespective of the climatic region (Wong & Chen, 2008). Stewart and Oke (2012) noted that a UHI generally exists in most cities regardless of their size and geographic location. Moreover, surface and air temperatures differ across a city and are normally higher in densely built-up areas than in open green spaces (Jauregui, 1991; Onishi et al., 2010). These differences are attributed to changes in energy balance which are mainly brought about by urbanisation, which is in turn controlled by variations in urban structure, form, and urban cover (Oke, 1982). The term “urban

cover" describes land use surfaces within a city, including built-up areas, paving surfaces, green areas, bare land, and water bodies (Oke, 2006).

The human impact on urban landscape is significant. Urban expansion and refurbishment are constantly taking place in cities over time. Therefore, the spatial distribution and configuration of an urban landscape, including buildings, green cover, water bodies and other urban components, have been recognised as important factors affecting the urban thermal environment (Kottmeier et al., 2007; Bao et al., 2016).

The UHI effect can be intensified with loss of vegetation cover. Thermal properties of an urban area are influenced by the spatial patterns of urban development, particularly built-up areas, and changes in land use diversity and landscape fragmentation can initiate adverse environmental impacts (Weng, 2007; Shrestha et al., 2012). In contrast, summer air temperatures within an urban microclimate can be reduced by increasing the amount and spatial configuration of green spaces (Dimoudi & Nikolopoulou, 2003; Bao et al., 2016), as well as the presence of water bodies (Manteghi et al., 2015).

Remote sensing techniques have been used extensively in urban studies, climatologic studies, environmental studies, and specifically for UHI studies. Landsat data have been successfully used for mapping LULC and environmental monitoring. Use of multi-date Landsat data is useful for monitoring the spatiotemporal dynamics of impervious surfaces and to determine their impact on the urban thermal environment. However, field work instruments are still essential for studying certain issues in more detail. The integration of Landsat data with field work and geographic information systems (GIS) can provide valuable information for a comprehensive analysis of UHIs in different environments and for devising mitigating measures.

1. 2. Problem statement and designation of parameters

There is a lack of research on urban heat island (UHI) in Baghdad and Perth. Additionally, no detailed information about this phenomenon with regard to comparison between cities with contrasting climates, is available.

As detailed in the background, all cities around the world have generally experienced an increase in temperature resulting from the transformation of natural ecosystems into

human landscapes over time. However, temperature increase varies from city to city as a result of the differences in many factors associated with this phenomenon.

Baghdad has experienced a period of rapid population growth and accelerated economic growth along with a rapid conversion of rural lands to urban surface in the last five decades. On the other hand, political and economic conditions significantly influenced the urban fabric and form of the city which in turn contributed in creating a number of environmental problems, especially rising temperature in the urban areas during hot summer days.

The temperature in the urban environment of Baghdad has incrementally increased during the last few decades. This issue has attracted attention due to the fact that an increase in temperature during the last several summers was observed, during which high temperatures of more than 50 °C were recorded for several days by the Iraqi Metrological Organization (IMO, 2015). In a hot climate city like Baghdad, a consistent rise in temperature in the city has resulted in many problems (e.g. human health, quality and comfort of urban living, increasing energy consumptions).

Existing methods to study SUHIs rely mainly on land surface temperatures retrieved from thermal remote sensing, hence do not deliver satisfactory results for heterogeneous areas like a city. This is due to remote sensing data not offering a high thermal resolution for large-scale study areas. Therefore, integrating remotely sensed data with field work is a practical approach which is able to provide detailed explanations about thermophysical behaviour of urban surfaces in a certain urban area. However, some challenges remain. They are as follows:

1. Collecting in-situ data with regards to surface albedo and temperature for different LULC categories requires several working hours. The resulting problem is the difference in observation times among field measurements of various urban LULC surfaces. It is, therefore, essential to employ a new method for the adjustment of field data that can be used for further analysis.

2. There is a further challenge to be faced when combining Landsat data with field measurements, with regard to surface albedo and temperatures within the urban area. This challenge includes the “mixed-pixel” problem in urban areas

resulting from complex landscape types. Additionally, some natural land cover types have similar reflectance signatures to man-made surfaces.

The major aim of this thesis is to assess the effect of the surface urban heat island (SUHI) in two contrasting cities, Baghdad and Perth. This work was carried out using multi-date Landsat data for the 1970s, 1980s, 1990s, 2000s, and 2015, in addition to field observations of surface albedo and temperature. The following research questions will be addressed through this work:

1. What are the spatial patterns of impervious surfaces in the two cities over the last five decades?

2. Are there any significant differences in the spatial patterns of urban landscape between the two cities?

3. How do urban LULC categories for the two cities affect the urban environment?

The specific objectives are:

a) To evaluate expansion of built-up areas and quantify its effects on the SUHI;

b) To understand the extent to which the urban thermal environment is influenced by spatial patterns of LULC features;

c) To investigate thermophysical behaviour of various urban LULC categories in the two cities.

1. 3. Significance of the research

The significance of this research can be related to several aspects of urban studies, as outlined below:

- The urban heat island phenomenon has become one of the most important environmental issues, especially in large cities in developing countries, where the UHI negatively affects a community's environment and quality of life during hot summer days. It compromises human health and comfort, and

contributes to air pollution, greenhouse gases, impaired water quality, and increased energy consumption.

- Due to its indirect contribution to global warming through the emission of greenhouse gases resulting from human activities, the UHI phenomenon has become an important issue at both local, regional and even global scales (Alcoforado & Andrade, 2008; Emmanuel & Krüger, 2012).

- The proposed approach to adjusting field measurements, as a part of this work, may provide more accurate results for studying urban environments in greater detail.

- Until now, a considerable number of studies have been done on SUHIs around the world; however, a majority of them consider only one or two cities from the same spatial domain (e.g., a country). Therefore, this study attempts to understanding the pattern of surface temperatures in two contrasting climates one from the arid (semi-arid) zone (Baghdad) and one with a Mediterranean climate (Perth), with widely different urban development strategies. Consequently, it can enhance and add new scientific information.

- The SUHIs of Baghdad and Perth have not yet been investigated. There is no information about the thermal environments of these cities.

- The outcome of this study may be useful for researchers, urban planners, environmental engineers, and authorities in Baghdad in particular, and Iraq in general, to tackle the problem of rising temperatures within urban areas. This thesis could further help to achieve sustainable development goals in the urban environment.

1. 4. Field instruments, computer software, and data resources

1. LP PYRA 06 pyranometer to observe albedo
2. FLIR E5 infrared camera for recording LST
3. ENVI 5.1 for radiometric correction and dark-object subtraction processes
4. ArcGIS 10.2 for preparing all maps

5. FLIR Tools software to extract the exact values of the surface temperature
6. The ASTM E1918 procedure for albedo measurements
7. Metrological data for temperature, relative humidity, rainfall, wind speed, and the sunshine
8. Microsoft Word and Excel for thesis editing
9. Endnotes for thesis-references editing

1. 5. Structure of the thesis

The thesis is organised into seven chapters, as follows:

Chapter Two provides information about the urban heat island (UHI) phenomenon. Relevant literature and existing methods in terms of the relationships between impervious surfaces, landscape patterns, and LULC properties with LST are discussed. The chapter also provides information about the role of remote sensing in mapping impervious surfaces and LULC, and retrieving surface albedo and temperature;

Chapter Three provides a general overview of the two study areas and datasets;

Chapter Four summarises and discusses the results of, spatiotemporal dynamics of impervious surfaces for both Baghdad and Perth during the 1970s, 1980s, 1990s, 2000s, and 2015, spatiotemporal variations of LST for both cities during the 1980s, 1990s, 2000s, and 2015, as well as seasonal variations for both cities in 2015. Additionally, relation of LST to ISA growth;

Chapter Five analyses and discusses the influence of the urban landscape on LST patterns for both cities using percent impervious surface area and landscape metrics derived from Landsat data;

Chapter Six investigates and discusses how different types of urban LULC surfaces can influence urban thermal environments; and,

Chapter Seven presents conclusions of this thesis and makes some suggestions and recommendations for planning, management, and future work.

2. Literature review

2. 1. Introduction

This chapter presents the theoretical background on the phenomenon of the urban heat island (UHI), as well as related concepts. It initially provides an overview of the UHI phenomenon. Three main aspects of surface UHI, including impervious surface area (ISA), urban landscape pattern, and characteristics of urban land use and land cover (LULC) surfaces, are reviewed as well. In addition, this chapter emphasises previous studies that have investigated the relationship between the above concepts with surface UHI effects using remotely sensed data.

2. 2. Overview of urban heat island (UHI)

2.2.1. Definition and concept of UHI

The term "urban heat island" (UHI) is well-known as a climatological and environmental phenomenon, which is typified by urban areas that exhibit elevated surface and atmospheric temperatures relative to surrounding rural areas (Landsberg, 1981; Oke, 1987). It is a detrimental environmental problem in urban areas, affecting both climatic and ecological processes, particularly through hot summer periods. It describes urban areas that exhibit higher temperatures than their "background" as shown in Figure 2.1.

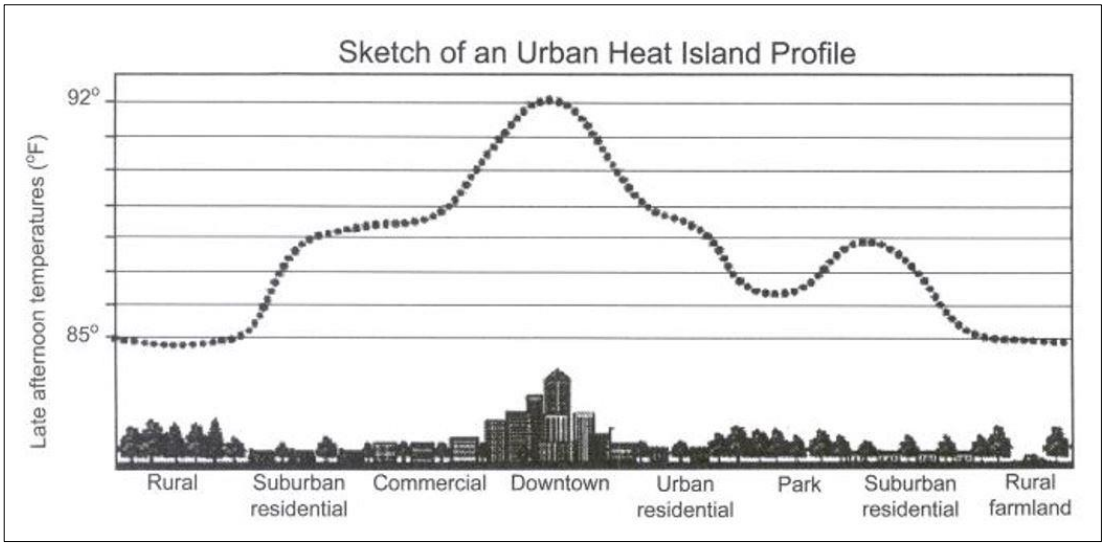

Figure 2.1 A general profile for the urban heat island effects (Source: U. S. Environmental Protection Agency (1992)).

UHI has been measured for many cities around the world at a range of scales. It has been found that the magnitude of UHI varies from city to city, influenced by several factors, such as geographical location, urban structure, building materials, vegetation cover, anthropogenic heat and pollutants. Some of the previous studies that measured the magnitudes of the UHI in many cities around the world, are listed in Table 2.1.

Table 2.1 Representative studies in cities around the world showing the magnitude of UHI.

City	Measured heat islands	Magnitude	Reference
Delhi (India)	Intensity of UHI	2.8 – 8.3 ℃ (D) 3.8 – 7.6 ℃ (N)	(Mohan et al., 2009)
Indianapolis (USA)	UHI	1 – 5 ℃ (D) 1 – 3 ℃ (N)	(Rajasekar & Weng, 2009)
Muscat (Oman)	Maximum intensity of UHI	2.3 ℃ (D) 4.3 ℃ (N)	(Charabi & Bakhit, 2011)
Kuala Lumpur (Malaysia)	Intensity of UHI	3.9 – 5.5 ℃ (N)	(Elsayed, 2012)
Bahrain	UHI	2 – 5 ℃ (D)	(Radhi et al., 2013)
Fuzhou (China)	Intensity of UHI	6.73 ℃ (D)	(Lin & Xu, 2016)
Erbil (Iraq)	SUHI	4.59 ℃ (D)	(Rasul et al., 2016)
Tehran (Iran)	SUHI	6 ℃ (D)	(Bokaie et al., 2016)
Madrid (Spain)	Intensity of UHI	5–6 ℃ (N)	(Núñez Peiró et al., 2017)
Turkey (Izmir)	Intensity of UHI	2.82 ℃ (D)	(Yavaşlı, 2017)
Mumbai (India)	UHI	3.4 ºC (D)	(Dwivedi & Mohan, 2018)
Paço do Lumiar (Brazil)	Maximum intensity of SUHI	11.50 ºC (D)	(Silva et al., 2018)
Tainan (Taiwan)	Maximum intensity of UHI	3 ℃ (D) 3.5 ℃ (N)	(Chen et al., 2018)

D= Daytime; N=Nighttime

The energy balance of the urban areas is a basis for the UHI formation. As the Sun is the primary source of energy for Earth's climate system, it is necessary to describe a basic energy balance in order to include the heat island phenomenon, and the urban surface energy balance is commonly defined as given in Equation 2.1 (Oke, 1987).

$$Q^* + Q_F = Q_H + Q_E + Q_S \quad (2.1)$$

Where:

Q^* = net all-wave radiation flux

Q_F = anthropogenic heat flux

Q_H = sensible heat flux

Q_E = latent heat flux

Q_S = ground conduction heat flux

The radiation balance can be expressed in a budget equation which consists of the net of all incoming and outgoing radiations of a surface.

$$Q^* = K^* + L^* = K\downarrow - K\uparrow + L\downarrow - L\uparrow \quad (2.2)$$

Where:

$K\downarrow$ = incoming direct and diffuse shortwave

$K\uparrow$ = reflected shortwave radiation

$L\downarrow$ = incoming longwave radiation from the atmosphere

$L\uparrow$ = outgoing longwave radiation from the surface

The energy balance partitioning of any surface depends on its characteristics, for example its surface reflection ability (albedo) (Christen & Vogt, 2004). This can commonly appear in cities with heterogeneous surfaces representing various building and paving materials and natural covers. Different surface energy budgets between urban and rural areas are recognised to be due to the differences in surfaces characteristics, land cover pattern and level of human activity (EPA, 2014). These factors can affect the generation and flow of heat that leads to different surface and air temperatures in cities, as compared to rural areas, and thus the formation of the UHIs.

2.2.2. Types of UHI

As defined above, the UHI reflects rising temperatures of urban surfaces or urban atmosphere in comparison to their surroundings. The UHI is categorised into two main types based on the altitude at which they are measured (Oke, 1995; Voogt, 2004):

1. Atmospheric Urban Heat Island (AUHI)

The atmospheric urban heat island (AUHI) refers to a warming of the urban atmosphere in comparison with the nearby rural surrounding atmosphere. It is directly measured by air temperature, recorded via weather stations. It dominantly appears in the evening, particularly after sunset, as a result of a slow release of heat from built-up areas into the cooler ambient air (Sheng et al., 2015). The atmospheric urban heat island includes two different types (Oke, 1976). These two types are defined as layers in the atmosphere, as illustrated in Figure 2.2.

- Urban canopy layer (UCL)

  The UCL exists in the layer of air where people live, extending from the ground surface upwards to approximately the top of roofs and trees. This type is the most commonly observed and is often what is referred to when the term UHI is used. The UCL is principally studied by measuring air temperature using thermometers in ground stations.

- Urban boundary layer (UBL)

  The UBL is located above the canopy layer, extending from the top of roofs and trees to higher atmospheric levels, although this layer normally extends no higher than 1.5 km from the surface of the earth.

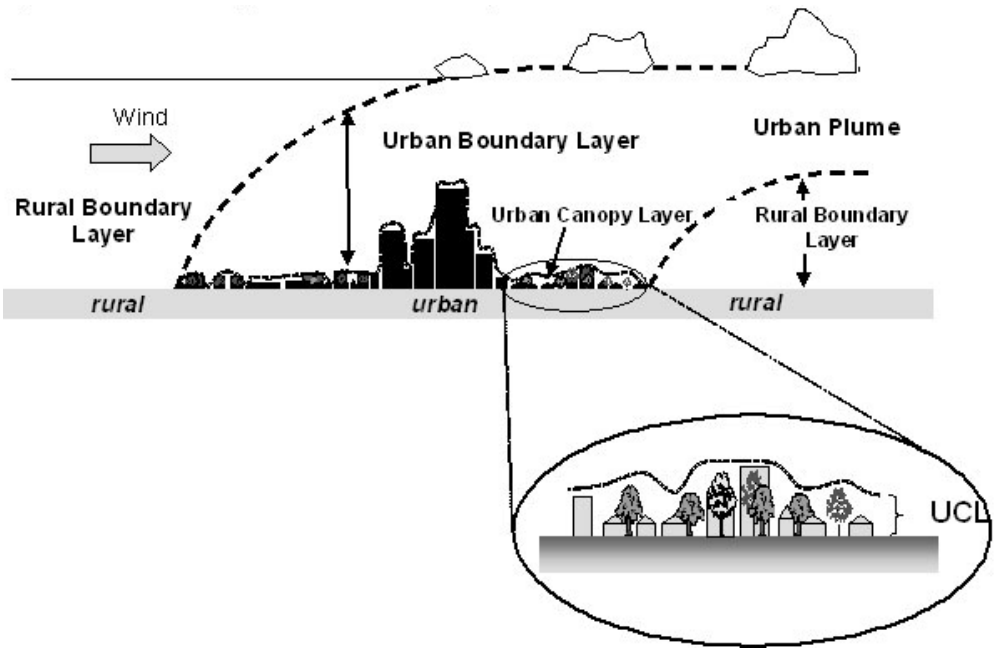

Figure 2.2 Vertical structure of the atmospheric heat island, showing the urban canopy layer and urban boundary layer (Voogt, 2004).

2. Surface Urban Heat Island (SUHI)

The surface urban heat island (SUHI) refers to the relative rise of land surface temperature (LST) in urban areas compared to their rural surroundings. It is typically characterised by a surface temperature recorded from upwelling thermal radiance observed or detected by thermal remote sensors such as ground-based, airborne, and satellite sensors. The term SUHI was proposed by Voogt and Oke (2003) when they employed LST to study the UHI effect. The surface urban heat island type is clarified in Figure 2.3.

Figure 2.3 Surface urban heat island type (Voogt, 2007).

2.2.3. Causative factors of UHI formation

The formation of the UHIs is influenced by several processes. In general, impervious surfaces such as buildings and pavements, play a key role in creating UHIs because they absorb and store heat and then release it again to the urban environment. Additionally, urban processes such as industrial processes, electricity generation, and human activities, give off heat directly to the urban environment. In this context, several processes which are associated with urbanisation have been characterised and documented as influential factors that can lead to the generation and enhancement of UHIs within the urban environments. For example, the factors listed below have been shown to influence the magnitude of the UHI (Oke, 1973; Karl et al., 1988; Atkinson, 2003; Voogt, 2004; Zhou et al., 2011; Phelan et al., 2015):

1. Factors relating to urban structure and form (see Figure 2.1)

- Changes in land cover
- Properties of building and paving materials
- Low surface albedo of built-up areas
- Spatial composition and configuration of urban green spaces
- Lack of green spaces and water bodies within urban areas
- Densely built-up surfaces

2. Factors relating to urban functions

- Increasing population density
- Anthropogenic heat
- Industrial processes and electricity generation

3. Others factors

- Weather conditions
- Geographic location
- Time of the day and season

2.2.4. Effects of UHI

Urban climates and environments have been negatively affected by a range of significant issues directly linked to elevated air temperature. The degree of influence varies from city to city based on the UHI intensity. The literature on the adverse effects of UHIs may be summarised by the following impacts:

1. Human health including human mortality and disease. Increased human mortality can be statistically related to elevated temperatures, and is exacerbated in heatwaves. Recently, a number of studies have stated that high rates of mortality and morbidity have been reported during the occurrence of, or due to the increased frequency of, heat waves in many cities around the world, for example, in Chicago (Semenza et al., 1996), in the United Kingdom (England, Wales, and London) (Rooney et al., 1998), in France (Fouillet et al., 2006), and in Berlin, Germany (Scherer et al., 2014).

2. Quality and comfort of urban living may be impacted due to increased human discomfort (Davies et al., 2007).

3. Increasing energy requirements, such as increased water and electricity consumption (Kantzioura et al., 2012). According to Akbari et al. (1992), the demand on electricity in six American cities (Los Angeles, Washington, Phoenix, Dallas, Tucson, and Colorado) increased by around 2-4% for each 1 °C increase in land surface temperature (LST).

4. Increased ozone and nitrogen oxides concentrations in urban environments (Akbari et al., 1992; Sarrat et al., 2006). According to Rosenfeld et al. (1998), the level of ozone in the city of Los Angeles can exceed 120 parts per billion by volume (ppbv) at 22 °C and could increase to be 240 ppbv at 32 °C.

5. Hydrological impacts and effects on soil properties in urban areas (Yang et al., 2016).

2.2.5. The relationship between surface and air temperatures

Surface temperatures have an indirect, but significant, influence on air temperatures, especially in the canopy layer, which is closest to the surface (i.e., the near surface climate). Previous studies (e.g., Unger et al., 2009; Zhou et al., 2014b) have proved that the LST is related directly to the nature and characteristics of LULC surfaces. Therefore, the temperature patterns in an urban region are highly influenced by the emissivity properties of urban surfaces and the heat capacity of erected structures (Schwarz et al., 2012). According to Lindén et al. (2015), changes in the surface energy balance of urban areas are affected by variations of surface properties (e.g., emissivity, albedo, surface roughness). Therefore, the relationship between surface temperature and air temperature varies over different LULC surfaces and at different times (EPA, 2014). The surface temperature is very sensitive to changing surface conditions, and consequently has a greater spatial and temporal variability than air temperature (Tzavali et al., 2015).

The effect of surface temperature on the atmosphere of urban-rural areas is therefore significant. At sunset, urban-rural differential cooling rates are at a maximum when rural areas start to cool rapidly; however, urban areas remain warm for longer and then cool at a slower rate (Goward, 1981). The difference in air temperatures was found to be greatest after sunset and least before sunrise (Tzavali et al., 2015). This was found to be due to impervious surfaces within urban areas that absorb and store heat during the daytime and then release it later to the atmosphere. Population density and built-up density, which have been used to distinguish urban and rural areas, also affect the temperature patterns in an urban region (Zhou et al., 2017). Streutker (2003b) observed that the urban air temperature in Harris County, Texas in 2000 became elevated as a result of increased surface temperature due to the increase in population and urban density. Figure 2.4 shows an example of surface temperatures being higher than air temperatures during the day, while convergent with them at night.

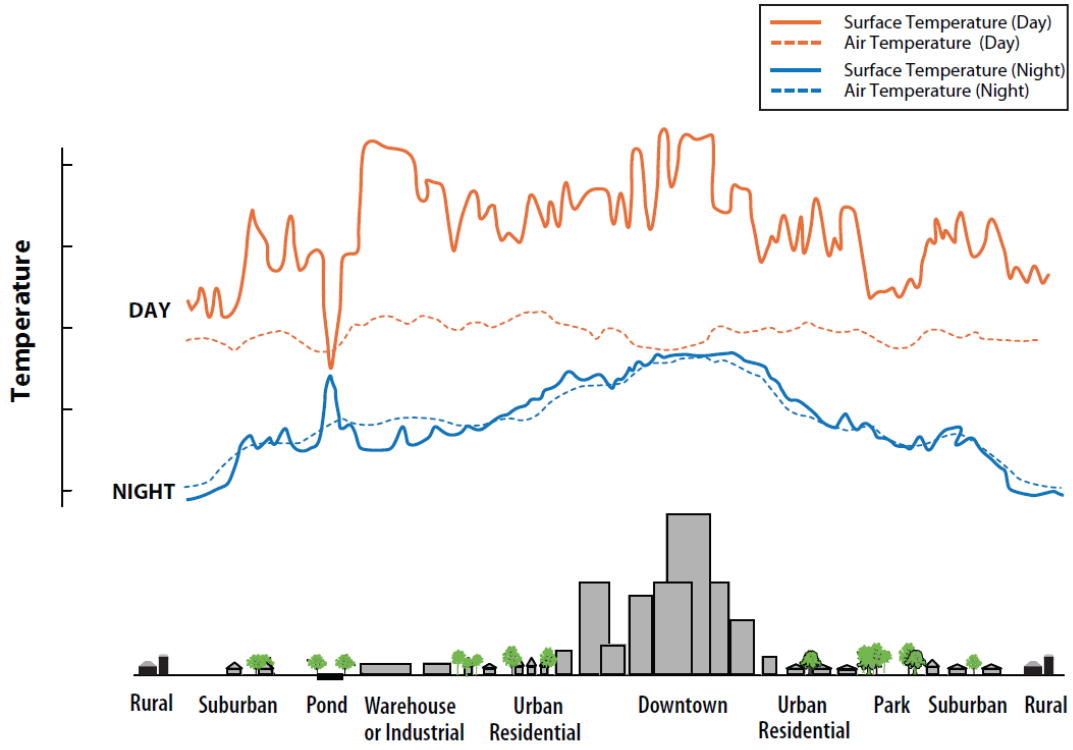

Figure 2.4 Sketch of surface and air heat islands during daytime and nighttime (Source: EPA (2014)).

Understanding the relationship between surface temperature and air temperature is essential for the analysis of urban heat islands via remote sensing. The mechanisms behind atmospheric urban heat island quantification and that of surface urban heat islands are different. Previous research on the analysis of SUHI has mainly employed LST measurements retrieved from satellite data, while atmospheric UHI has been studied using air temperatures recorded by weather stations (Streutker, 2002).

2. 3. Using remote sensing data for urban environmental analysis

Since the early 1960s, remotely sensed data have been employed for observing and monitoring the Earth and its environment in a range of applications. Study of the urban landscape has been one of the research concerns in the past few decades, with regard to its relationship to a variety of environmental parameters. For example, many applications, such as measurement of impervious surfaces, mapping urbanization, and

quantifying urban landscape patterns, have been linked to important climatic and environmental issues using satellite-based multispectral data.

Recently, the advent of thermal remote sensing has provided further information and extra applications for studying urban climates and environments. For instance, thermal imagery has been widely used to study urban heat islands (UHIs) using retrieved LSTs over urban areas. This technique was first applied by Rao (1972), who used surface temperature for a SUHI investigation. Since then, a number of studies have used remotely sensed thermal data for investigation of urban thermal climate, and these have been reviewed by Gallo et al. (1995); Voogt and Oke (2003).

Remote sensing imagery has been regarded as an effective data source for analysis of urban climate and environment. This is because a wide range of information can be obtained from various satellite data at different spatial, radiometric and temporal resolutions. In this context, a variety of satellite data such as the advanced very high-resolution radiometers (AVHRR), the moderate resolution imaging spectroradiometer (MODIS), Landsat, advanced spaceborne thermal emission and reflection radiometer (ASTER), IKONOS, and QuickBird satellites have been used to study urban areas at a range of scales and in various environments.

Previous studies have shown that Landsat imagery, as a medium resolution data source, is appropriate for studying urban thermal environments, since these data provide both multispectral and thermal data at the same time. In addition, spatial resolutions of the thermal bands are available at 120, 60, 100 m, for Landsat thematic mapper (TM) and enhanced thematic mapper plus (ETM+), and Landsat 8 (TIRS), respectively (Voogt & Oke, 2003; Weng & Hu, 2008; Martin et al., 2015). A considerable number of studies have demonstrated that Landsat has a capability to derive LST, ISA, and landscape metrics.

2. 4. Impervious surface area

2.4.1. Definition of impervious surface area (ISA)

Impervious surfaces are generally defined as any man-made land surface that prevents water infiltrating into the soil, such as building rooftops, streets, parking lots and

sidewalks (Schueler, 1994; Arnold Jr & Gibbons, 1996), while non-impervious surfaces include natural surfaces such as vegetation cover, water bodies, and bare land.

Estimating and mapping impervious surfaces from remotely sensed data has received considerable attention in the last two decades, since they have been used to determine the impacts of urbanisation. Imperviousness has been documented as an important factor related to water and ecosystem quality, urban climatic and environmental change, and socioeconomic conditions (Arnold Jr & Gibbons, 1996; Weng et al., 2009; Li et al., 2013a). Recently, ISA has been considered to be a critical factor for analysing the effects of the UHIs (Tang & Xu, 2016; Meng et al., 2018).

2.4.2. Extraction of ISA

Several approaches have been applied to mapping ISA from a variety of remote sensing data. The basic methods for mapping ISA were reviewed and summarised by Brabec et al. (2002); Weng (2012); Lu et al. (2014). These methods were grouped into six categories, based on the use of remote sensing variables and techniques, and are outlined in Table 2.2.

Table 2.2 Methods for mapping ISA.

	Category	Major techniques
1	Per-pixel based classification methods	Maximum likelihood classifier; decision tree classifier; expert rules
2	Object-based methods	Segmentation-based classification
3	Sub-pixel classification methods	Sub-pixel classifier; Artificial neural networks; ISA as one endmember
4	SMA-based methods	Addition of low and high albedo fractions; modified approach based on low-albedo, high-albedo, and land surface temperature; Spatially adaptive SMA; MESMA; temporal mixture analysis
5	Regression-based methods	Regression-based models which the ISA reference is used a dependent variable and various wavelengths were used as independent variables. An alternative is to use vegetation related variables, such as tasseled cap greenness and fraction vegetation cover
6	Threshold-based methods	Threshold based on NDISI; hybrid method based on NDVI and cluster analysis

The urban landscape is composed of different components, including, in general, impervious surfaces, vegetation, bare land, and water. However, impervious surfaces have a complex pattern in detail, created by the use of a wide range of building materials, which in turn lead to a wide variation in spectral signatures (Lu & Weng, 2004). In relation to this, the problem of mixed pixels among some categories may occur, where the same spectral signature can often appear for high reflectance impervious surfaces and for bare land. There is also a similarity in the spectral signature between dark impervious surfaces that have a low reflectance such as asphalt and other features like shadowless surfaces and water (Lu & Weng, 2004).

Linear spectral mixture analysis (LSMA) is considered to be an appropriate method for solving the mixed pixels problem in urban areas. It is based on the use of a single endmember or a combination of high and low albedo fraction images that was suggested by Wu and Murray (2003). Additionally, a number of studies have demonstrated that medium spatial resolution data, such as that for Landsat, may be used as an effective source for mapping ISA using the method of LSMA, especially over a large area (Wu & Murray, 2003; Lu & Weng, 2006).

2.4.3. Accuracy assessment

Accuracy assessment is a necessary task for the analysis of classified maps, since those maps are derived from remote sensing data that contain inevitable errors of various types (Maingi et al., 2002). The accuracy of remotely sensed data, in general, is determined by comparing the resultant thematic maps with reference data. Different methods have been used to assess the accuracy of produced thematic maps from remotely sensed data (Liu et al., 2007).

Error matrix analysis is currently a common method to assess the accuracy of image classification (Foody, 2002). It can provide a basis for accuracy assessment based on a simple cross-tabulation representing a number of pixels or polygons in a classified map against reference data (Jensen, 2005). This method can estimate accuracy by using several variables, as described below (Congalton, 1991; Jensen, 2005).

a. Overall accuracy (OA) is one of the most common accuracy measures and the simplest. It is calculated by dividing the total number of correctly classified pixels by the total number of pixels in the reference data. In addition, accuracies of individual categories can be computed in a similar way by dividing the number of correct pixels in each category by either the total number of pixels in the corresponding row or column pixels.

- Producer's accuracy (PA) measures errors of omission, which is a measure of how well real-world land cover types have been classified. It is computed by dividing the total number of correctly classified pixels in a category which represents the major diagonal of the matrix by the total number of pixels for that category from the total of the column.

- User's accuracy (UA) measures errors of commission, which represents the likelihood of a classified pixel matching the land cover type of its corresponding real-world location. It is calculated by dividing the total number of correctly classified pixels in each category by the total number of pixels that were classified for that category from the total of a row.

b. Kappa coefficient (Kappa) is a statistical measure of agreement between the results of classification and ground truth values. It is another accuracy indicator compares an observed accuracy with an expected accuracy. Therefore, it is considered to be a more reliable measure for assessing accuracy. A kappa result can take values of between 0 and 1, and a kappa coefficient equal to 0.8 or above it is considered to be a "very good" level of agreement; between 0.6 and 0.8 represents a "good" agreement; from 0.4 to 0.6 is considered to be "moderate"; and 0.4 or below is considered "poor" (Earl-Slater, 2002).

2.4.4. Methods relating to ISA

Several tools and statistics have been developed to quantify impervious surfaces for a particular area, based on a required objective, including the following:

2.4.4.1. Percent impervious surfaces area (PISA)

Percent impervious surfaces area (PISA) is a useful tool for investigating impervious surface cover, and its utility for examining the effect on the quality of urban environments was investigated by Arnold Jr and Gibbons (1996). Recently, Landsat imagery has been effectively used to quantify the amounts of impervious surfaces within a limited area. PISA is calculated by dividing impervious surface area for each cell or pixel by the total area of that cell or pixel. The values of PISA therefore range between 0 and 100%.

2.4.4.2. Impervious surface analysis tool (ISAT)

The impervious surface analysis tool (ISAT) is a technique designed to compute the percentage of an area covered by impervious surfaces within user-defined geographic areas (e.g., watersheds, municipalities, and subdivisions) from satellite data. This tool

was developed by the National Oceanic and Atmospheric Administration (NOAA) Coastal Services Center (NOAA Coastal Services Center, 2013) for coastal and natural resource managers and planners. ISAT was initially developed to determine estimates of the percentage of impervious surface area, and helps the user to perform an analysis that can determine the potential impact of additional impervious surfaces in new developments on water quality (Ward et al., 2015). It can also provide estimates of the typical amount of surface water pollution that may be related to increases in impervious surfaces over green covers (GWRC, 2010). It has been widely used as an indicator of the degree of urbanisation and environmental quality. For example, the variation of water quality conditions in the George Washington region during 1996-2006 has been mapped, based on the amount and percentage change of impervious surface area using ISAT (GWRC, 2010). Therefore, this tool can be usefully implemented to generate comparison maps for impervious surface evaluation.

2.4.5. Previous studies about the relation between impervious surfaces and urban heat environments

A review of the relevant literature on ISA indicates that extraction of impervious surfaces from Landsat data using linear spectral mixture analysis (LSMA) is a valuable and efficient approach. This approach has allowed for an increased focus on mapping impervious surfaces and analysing their spatiotemporal dynamics, since it works better to subdue the problem of mixed-pixel (Wu & Murray, 2003; Yuan et al., 2008; Weng et al., 2009; Kuang et al., 2014).

Elevated local surface and air temperatures in urban areas, compared with those in surrounding rural areas, are mainly associated with the modification of land cover and other land use practices (Streutker, 2003a). Impervious surface area, which is an important environmental indicator (Arnold Jr & Gibbons, 1996), has been identified as a key factor in the formation of the UHI effect (Kim et al., 2017). There are several factors with regard to ISA that have been documented as a cause of UHI: (1) changes in the physical characteristics of surfaces (surface albedo, aspect ratio, fabric density ratio, plan density ratio, green density ratio and thermal mass) (Kolokotroni & Giridharan, 2008); (2) changes in the heat fluxes resulting from the urban geometry (sky view factor and altitude) (Giridharan et al., 2007); (3) decreases in surface

moisture available for evapotranspiration (Xiao et al., 2007); (4) anthropogenic activities in urban areas (Murray & Heggie, 2016). Thus, the relationship between ISA and LST has been examined by a number of studies conducted using Landsat imagery in a range of settings.

The relationship between PISA and LST was investigated by Yuan and Bauer (2007) who studied surface urban heat island effects over the Twin Cities metropolitan area, Minnesota. Landsat data, including two images from Landsat 5 TM and two from Landsat 7 ETM+ in 2002, were used to retrieve LST from four different seasons. This study indicated that PISA was highly correlated to LST for all seasons. It also showed that the PISA is an appropriate indicator for efficiently studying the effects of SUHI.

The relationship between surface urban heat islands and PISA was investigated by Zhang et al. (2008) in Shanghai, China. ISA and LST were retrieved from a Landsat 7 ETM+ image acquired in 2001. LMSA was used to map imperviousness. The results showed a strong correlation between LST and PISA, both of which led to enhancing the effect of the UHI.

Using the city of Beijing as a case study, Hao et al. (2016) investigated changes in urban expansion and LST between 1990 and 2014. They also examined the relationship between PISA and relative mean annual surface temperature (RMAST). Landsat data, including TM, ETM+, and OLI were used to extract data for LST and ISA changes over time. The result revealed that an increase in PISA by more than 50% led to rising RMAST by more than 1.5 Kelvin. They concluded that land use covers, building morphology, and the spatial distribution of buildings and vegetation may have an influence on RMAST variations for the same PISA.

Tang and Xu (2016) examined the quantitative relationship between ISA and LST for six cities in China. Landsat ETM+ images were used to extract impervious surfaces by applying LSMA and to retrieve LST. They found that there was a significant positive correlation between ISA and LST for the six cities. They also showed that elevated LST was significantly associated with increased PISA in those cities.

2. 5. Urban landscape pattern

2.5.1. Concept and definition of urban landscape

The term “urban landscape” is a description of complex spatial patterns of different LULC types, and additionally, it can be regarded as a form of complex social, economic, and natural ecosystem (Wu, 2008). Luck and Wu (2002) point out that physical, ecological, and socioeconomic processes within cities can be influenced by their spatial patterns. Landscape ecology refers to three landscape characteristics, namely structure, function and variations of the landscape over time (Botequila Leitao et al., 2006). The linkage between the spatial pattern of cities and ecological processes can provide a better understanding of the urban ecosystem (Sukopp, 1998; Luck & Wu, 2002).

2.5.2. Landscape metrics

Landscape metrics or indices are broadly defined as quantitative measures to describe and evaluate the spatial pattern of a landscape (Herold & Menz, 2000; Reis et al., 2014).

Spatial metrics were first used in landscape ecology to quantify patterns of vegetation in natural landscapes in the 1980s (McGarigal & Marks, 1995; Herold et al., 2005). Since then, urban areas have received significant attention with regard to their ecosystems, and a number of landscape metrics have been suggested, developed, and investigated to examine the relationship between urbanisation and ecological conditions. In the last few decades, landscape metrics have been increasingly used for a range of applications, for example, to characterise urban patterns, to compare spatial patterns between different places, and to understand the spatiotemporal dynamics of urban patterns (O'Neill et al., 1988; Herold et al., 2005; Banzhaf et al., 2009). Recently, the relationship between landscape pattern and ecological processes has been investigated using various metrics (Turner, 2005). It is therefore important to understand the scientific context of existing landscape metrics in order to appropriately use them.

2.5.2.1. Levels of landscape metrics

Landscape metrics characterise a landscape on the basis of the level of heterogeneity, and may be grouped into three levels, including patch level, class level, and landscape level (Botequila Leitao et al., 2006) (Figure 2.5).

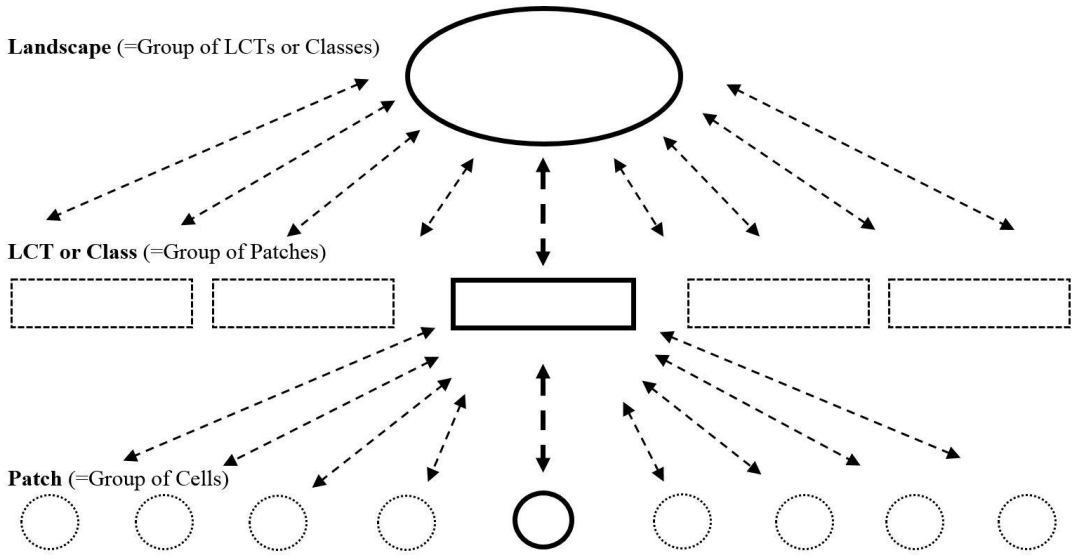

Figure 2.5 Patch, class, and landscape-level metrics (Botequila Leitao et al., 2006).

Each one of these levels may be explained as follows:

- Patch level: a patch can be defined as a relatively homogeneous land cover type which differs from its surrounding areas. It is represented as a region or polygon in spatial data models. The spatial character and context of the patches may also be defined and characterised at this level.

- Class level: a class is a group of patches (regions or polygons) that have the same type of land cover. Class level metrics measure and quantify characteristics of all patches at the same land cover type (LCT). Different parameters at the class level can be quantified, such as total extent, average patch size and degree of aggregation.

- Landscape level: a landscape is a group of all patches (regions or polygons) within the area of interest including all land cover classes. Landscape level metrics characterise the composition and configuration of the mosaic of

patches within the area of interest. Landscape metrics are generally types of landscape heterogeneity indices, and therefore, metrics at this level are used for overall landscape pattern recognition.

2.5.2.2. Components of landscape metrics

In general, spatial relationships among component parts can be used to distinguish landscapes. Two essential aspects of this, composition and configuration, may be used to describe a landscape via different metrics or indices (McGarigal & Marks, 1995).

- Landscape composition is easily quantified and refers to features associated with the presence and amount of different patch types on the landscape, but without explicitly describing their spatial features. Composition metrics are used at the landscape level because the measurement of composition requires integration over all patch types.

- Landscape configuration refers to the spatial or physical distribution of patches within the class or landscape level. Configuration metrics of individual patches are spatially explicit at the individual patch level, such as mean patch size and shape. Configuration can also be quantified by some metrics in terms of the whole class or landscape, and these metrics are spatially explicit.

2.5.3. Previous studies of urban landscape patterns and LST relationships by landscape metrics

The relationship between landscape patterns and ecological processes can be more clearly understood by quantifying the spatial heterogeneity patterns of the landscape (Turner, 1990; Turner et al., 2003). The impact of urban landscape patterns on urban ecosystems using various spatial metrics has been examined in a number of studies (e.g. O'Neill et al., 1988; Liu & Weng, 2008; Su et al., 2012). In addition, recent analysis of the relationship between the spatial patterns of landscape and LST patterns using landscape metrics has attracted attention, particularly in urban areas.

The relationship between landscape patterns and LST in terms of seasonal variations was investigated by Liu and Weng (2008) in Indianapolis, USA, using four Terra

ASTER images. In order to quantify the spatial characteristics of landscape patterns and LST zones, five class-based metrics and two landscape-based metrics were computed from dominant LULC types. The results showed that the spatial characteristics of urbanization and UHIs can be precisely characterised by quantifying landscape and LST patterns using landscape metrics.

The relationship between landscape metrics derived for urban, grassland, and agriculture, and LST zones over the southwestern Sydney metropolitan region and the surrounding fringe was quantitatively analysed by Zhang et al. (2013b). Two-temporal Landsat TM images from 1993 and 2006 were used to estimate LST and landscape indices, such as patch density (PD), perimeter-area fractal dimension index (PAFRAC), aggregation index (AI), and mean patch size (MPS), at the class level. The results showed that the spatial characteristics of each LULC category and the urban thermal environment can be precisely characterised using the relationships between landscape metrics and LST.

Assessing the effects of land use spatial structure on urban heat islands using HJ-1B remote sensing imagery in Wuhan, China, was a case study performed by Wu et al. (2014). In this study, the relationship between landscape metrics and LST using the HJ-1B satellite system were analysed at the class and landscape levels. Four types of LULC categories, including built-up areas, cropland, forest, and water were quantified for this analysis using a percentage of the landscape (PLAND), patch density (PD), edge density (ED), and landscape shape index (LSI) at the class level. Additionally, three other landscape-based metrics, such as contagion index (CONTAG), Shannon's evenness index (SHEI), and Shannon's diversity index (SHDI) were used as well. The results indicated that the UHI was affected by the landscape composition and the spatial configuration of the quantified LULC categories.

Asgarian et al. (2015) studied the influence of spatial patterns of green cover on LST in the urban area of Isfahan, Iran, using a Landsat ETM+ image from 2002. Five spatial metrics, including patch area (AREA), perimeter to area (PARA), core area index (CAI), shape index (SHAPE), and nearest distance (ND) were used in this analysis. They found that the spatial pattern of green space, determined by the magnitudes of landscape metrics, was significantly correlated with LSTs.

The influence of the spatial distribution of green spaces on the UHI pattern in Baotou, China was analysed by Bao et al. (2016). In this study, Landsat 5 TM images (from 2000, 2004, 2007 and 2011) and a Landsat 8 OLI image (from 2014) were used to describe the pattern of UHI intensity by extracting LST and deriving seven landscape metrics. These metrics included aggregation index (AI), class area (CA), evenness index (SHEI), landscape shape index (LSI), number of patches (NP), perimeter area ratio (PARA), and Shannon's mean patch fractal dimension (FRAC_MN). The results of this study demonstrated that optimising the spatial configuration of green spaces, along with their sizes, can play an important role in mitigating the UHI effects within an urban area.

2. 6. Characteristics of urban cover surfaces

The term "urban cover" describes land use and land cover surfaces in a city, generally included built-up areas, paving surfaces, green areas, bare land, and water bodies (Oke, 2006). Variations in surface characteristics with regard to the spectral reflectance and solar absorption, thermal capacity, and heat conductivity can directly influence LST pattern of an urban cover (Le-Xiang et al., 2006). Therefore, urban cover characteristics are considered to be an important factor in assessing urban thermal environments.

2.6.1. Optical and thermal properties of urban cover surfaces

Urban areas consist of heterogeneous patterns of urban LULC categories. Generally, conversion of LULC types, having different characteristics, can lead to significant changes in thermal conditions within urban areas. Furthermore, impervious surfaces with a variety of building and paving materials are known to alter the energy balance in urban environments by absorbing more than reflecting the incoming solar radiation (Stathopoulou et al., 2009). Santamouris et al. (2011) demonstrate that the use of materials that strongly absorb solar radiation is the main cause in generating the UHIs. Previous studies have indicated that surface albedo and land surface temperature (LST) may be effectively used to investigate and evaluate urban environments using remotely sensed data or field measurements, as follows:

- Surface albedo is defined as the fraction of the shortwave and near-infrared incident radiation that is reflected from a surface (Taha et al., 1988; Taha et al., 1992; Janjai et al., 2006). Surface albedo measurement plays a significant role in determining the effect of the thermal performance of urban cover on the environment (Li et al., 2013b), the energy balance of the ground surface (Akbari et al., 1990), the thermophysical properties of pavements (Kushari & Kanitpong, 2011), the radiative balance of the earth's atmosphere (Janjai et al., 2006), and urban climates and heat islands (Taha, 1997).

- Land surface temperature (LST) measurement is an important means of monitoring climatic and environmental phenomena, especially those related to thermal properties of Earth's surface (Becker & Li, 1990). Thermal imaging records the emitted radiation from the ground surface in the spectral range of 8-14 μm either by thermal remote sensing (Prakash, 2000) or by portable infrared cameras. Surface temperature measurements have been widely used to study UHIs (Voogt & Oke, 2003; Bechtel et al., 2012; Sobrino et al., 2013; Ahmed et al., 2014), for energy balance and ecological studies (Gillespie, 2014), and to monitor urban development (Khandelwal & Goyal, 2010; Thi Van & Xuan Bao, 2010).

2.6.2. Thermal behavior of LULC

Urban climates and environments have been widely investigated in terms of the effect of LULC characteristics at local, regional and even global levels. Surface albedo and LST, which can be retrieved from remotely sensed data, laboratory or hand-held instruments, have been used to determine the optical and thermal performance of urban covers.

An analysis of heat flux for various pavement materials in the Saitama University Campus, Tokyo, was carried out by Asaeda et al. (1996). In this study, they examined the effect of heat flux of several materials including asphalt, concrete, dry sand, macadam and bare soils, on the lower atmosphere during the summer season. Intensive measurements were taken in 1990 and 1991. Physical properties and ground temperatures were measured with thermocouples, heat flux was measured with a radiometer, and infrared radiation of the surfaces was measured by pyrgeometer. A

hand-held KANOMAX, CLIMOMASTER model 6511 meter was used to measure ambient air temperature, wind velocity and humidity. They found that asphalt had a greater ability to emit surface heat and a higher heat storage capacity than the other materials, such as concrete and soil.

Prado and Ferreira (2005) conducted a study in Brazil to measure albedo and analyse its effect on the surface temperatures of building materials. They used a spectrophotometer in the laboratory, with a range of 290 to 2500 nm, to measure the spectral characteristics of building materials. They examined many popular materials for roofs, including ceramics, fibrocement, aluminium, stainless steel, coated metal and coloured cement. They found that surface temperatures were lower than air temperatures for only red and white ceramics compared with many other materials that were measured under the established climatic conditions. They suggested that albedo or reflectance should be used as a parameter by manufacturers in determining the suitability of materials used for roofing.

Synnefa et al. (2007) examined optical properties and the thermal performance of cool-coloured coatings that had been developed to mitigate the effect of the urban heat islands. These coatings were applied on concrete pavement tiles and samples of these tiles were collected and placed on a horizontal platform. Surface temperature was measured by a sensor (thermocouples type K) connected to a data logging system, as well as to an infrared camera (AGEMA Thermovision 570, 7.5– 13 μm). A Devices and Services emissometer model AE was used to measure the infrared emittance. A UV/VIS/NIR spectrophotometer (Varian Carry 5000) was used to measure the spectral reflectance. They found that all the developed coatings had higher values of spectral reflectance than those of standard coatings, and consequently had lower surface temperatures.

Using the City of Athens as a case study, Stathopoulou et al. (2009) studied the surface heat island by measuring the optical and thermal properties of building and paving materials. They analysed SUHI using Landsat 5 (TM) and ASTER data during the daytime and nighttime. They furthermore examined the optical and thermal properties of the building materials that were commonly used in the study area, using a UV/VIS/NIR spectrophotometer (Varian Carry 5000) and the emissometer model AE to measure spectral reflectance and infrared emittance of the samples of materials,

respectively. A total of 78 building materials, including asphalt, concrete, marble, mosaic, ceramic, stone, rubber, coatings and membranes were selected. The results showed that the urban surfaces were cooler than open and non-urban surfaces in the city surroundings during the daytime. In addition, different spectral reflectance and emittance values were determined for the samples and these depended on the optical and thermal properties of those materials.

A study was carried out by Sobrino et al. (2013) in the City of Madrid to evaluate the surface UHI effect using remote sensing data. An ASTER image, Airborne Hyperspectral Scanner (AHS) (71-80 TIR bands), RAYTEK MID, and Heitronics radiometers, and an NEC TH9100 thermal camera were used to derive and record thermal properties of surfaces, such as surface temperature, emissivity and downward atmospheric radiance. They also used ASD FieldSpec3 and GER 1500 spectroradiometers to measure spectral reflectance. Images and ground-based measurements were acquired during June and July of 2008. In this study, they analysed different surface materials such as concrete, pavement, brick, asphalt, metal, steel, bare soil and green grass. The study showed that the use of LST maps with a Temperature Emissivity Separation (TES) algorithm, derived from thermal imagery, are an appropriate method to study surface urban heat islands.

Recently, the relationship between surface albedo and LST for urban cover surfaces has been investigated to assess the urban thermal environment. The relationship between surface albedo and temperature in Perugia and Aprilia, Italy, was examined by Bonafoni et al. (2017) using data retrieved from different satellite and airborne sensors. In addition, in-situ measurements of albedo were taken, using an albedometer Delta Ohm Pyra 05, at 12:00 Central European Summer Time in Perugia area. An inverse linear relationship between albedo and LST was found for both satellite and airborne observation, and for in-situ measurements.

2. 7. Knowledge gaps in previous studies

Since the UHI phenomenon has attracted significant attention, a considerable number of studies have examined and analysed UHIs at a range of scales. Many aspects have been considered as causative and contributive factors in the UHI formation by using different data sources, techniques, models, and approaches. However, previous

literature has typically evaluated SUHI using satellite data, and considering one or two cities from the same spatial domain (e.g. the same country). A single climatic zone has usually been representative for a study, and most studies have emphasised the impact of a specific category such as vegetation or built-up areas on the LST pattern. Additionally, most studies have considered a single factor in examining its effect on the SUHI.

In this thesis, a comprehensive analysis was carried out for evaluating the SUHI in two contrasting cities, Baghdad and Perth, with regard to urban development, landscape patterns, building and paving material characteristics, urban planning, legislation and regulations of city management, and socio-economic factors. Analysing and comparing SUHI patterns of the two cities with dissimilar climates using an integrated approach, including several aspects, such as spatiotemporal dynamics of built-up areas, spatial patterns of urban landscape, and urban LULC characteristics, to LST may enhance our understanding of the effect of SUHI. Comparing spatial patterns of SUHI in cities from both developed and developing countries is also expected to benefit researchers working on the urban thermal environment.

Through review of previous studies, it is apparent that it is better to develop and enhance existing methods for studying SUHI, particularly with regard to accuracy analysis. These methods are summarised below:

Regarding extraction of impervious surfaces from Landsat data, previous studies indicate that use of linear spectral mixture analysis (LSMA) is a valuable and efficient method. However, the problem of mixed-pixels among some categories still exists in some studies. In this thesis, therefore, an approach has been employed to be able to accurately map imperviousness by adding and enhancing some processes (as mentioned in Section 4.2.2). The produced maps have been overlaid and divided into eight zones for a better understanding of spatiotemporal dynamics of impervious surfaces.

- A few studies examined the relationship between landscape metrics and LST using Landsat data. Those studies focused on a certain land cover category, such as vegetation, in analysing its effect on the ecological environment (Zhang et al., 2013b; Asgarian et al., 2015; Bao et al., 2016). Additionally, existing

landscape metrics are not commonly used to examine relationships with LSTs. In this work, more specific landscape indices were employed, based on objective criteria regarding their relevance to the spatial analysis of urban areas, in order to investigate urban landscape and LST patterns. In addition, an appropriate scale with 100 × 100 m of the spatial resolution was adopted to apply metrics and examine LSTs at the landscape level.

- In terms of analysing the effect of LULC categories on the urban thermal environment using field measurements and remotely sensed data, the literature indicates the following:

a) Different procedures have been adopted for field measurements. The first involves taking samples from several categories for testing in a laboratory and using specific equipment. The second method collects samples from many categories in one place (such as a platform). The third method uses a hand-held instrument to record data in-situ directly. These methods, in fact, do not give a realistic representation of the thermal behaviour of the tested categories since:

   (1) Thermal performance of collected samples may be affected when their interaction with the local ambient conditions changes.

   (2) The differences in times among observed readings of several categories can affect the comparability of thermal measurements and hence influence the accuracy of the analysis.

b) For remote sensing data, using multi-sensor to examine the thermal pattern in the two cities is problematic, due to the differences in the time of image capture.

A detailed analysis of the SUHI based only on the parameters of albedo and LST retrieved from remotely sensed data is effective but not adequate. The use of field measurements is crucial to determine an actual representation of the thermal behaviour of urban LULC surfaces. In this thesis, therefore, a new method has been adopted to adjust field measurements and overcome the above-mentioned problems. This method has also been of assistance in comparing and integrating field derived data with satellite data.

2. 8. Chapter summary

This chapter provided an overview of the phenomenon of the UHI in terms of its definition, concept, causative factors, and effects. Additionally, it reviewed the main issues associated with SUHIs, including impervious surfaces, landscape patterns, and urban LULC characteristics. Previous studies have confirmed that linear spectral mixture analysis (LSMA) is an effective method for extracting and mapping imperviousness, particularly from Landsat data. They also consider that impervious surfaces are an important indicator for studying the UHIs. In addition, knowledge of surface temperature is important not only to obtain boundary conditions for the atmospheric temperatures, but also to understand the environmental effects on human beings. Landscape metrics were briefly introduced and the most relevant studies on their relationship with LST patterns were reviewed. The methods used for investigating the impact of optical and thermal properties of urban surfaces on urban climates and environments were also reviewed. Remotely sensed data may still not be sufficient to provide detailed information on urban thermal environments. Therefore, the integration of satellite data and ground data is very important in understanding thermal behaviour of various LULC categories within complicated urban areas.

3. Study areas and datasets

3. 1. Description of study areas

This chapter presents an overview of the two study areas: the central metropolitan regions of Baghdad and Perth. Several studies (e.g., Zhou et al., 2014a; Yang et al., 2017) have demonstrated that the patterns of the urban thermal environment differ from area to area due to climatic divergences. The different patterns of surface temperature have also been related to characteristics of land cover (i.e., physical and biochemical properties). Mathew et al. (2016) indicated that the spatial pattern of impervious surfaces significantly influence the LST patterns. In light of this evidence, Baghdad and Perth have been selected as the study sites, in order to determine factors affecting LST (and hence, SUHI) in different geographical locations and climates, as well as contrasting urban planning strategies, legislation and regulations for city management, landscape patterns, building materials, and socioeconomic factors.

In addition, SUHIs have not yet been studied for Baghdad and Perth. Studies on SUHI using remotely sensed data around the world have usually considered one or two cities from the same spatial domain (e.g. the same country). A single climatic zone has usually been representative for these studies, and most have emphasized the impact of vegetation or built-up areas on the spatial pattern of LST.

Evaluation of the thermal behaviour of two contrasting cities may therefore provide a potentially unique contribution to the field of thermal remote sensing, particularly to the phenomenon of UHI. Meanwhile, evaluation of SUHI for cities from both developed and developing countries is also expected to benefit researchers working on urban thermal environments. Studying two contrasted cities may be useful for formulating sustainable urban environmental management by determining the causative factors and devising pertinent strategies for mitigating the effect of SUHI in cities.

When studying urban thermal environments in two contrasting cities, it is necessary to identify the geographical characteristics of these areas. An understanding of the thermal and environmental conditions of these cities is therefore developed in this chapter.

Geographical location is considered to be a key element in determining the climatic effects of a region. The first study area, Baghdad, is located in central Iraq, which is in the Middle East. It is bordered by Turkey to the north, by Iran to the east, by the Arabian Gulf to the southeast, Kuwait and Saudi Arabia to the south, Jordan to the west, and Syria to the northwest. Perth on the other hand is situated in the southwest of Australia, and is bounded by the Indian Ocean to the west. It is the capital of Western Australia.

In the field of climatology, local characteristics of urban climate have been shown to be affected by urbanisation (Hu et al., 2006). Climate is defined as the average weather in an area (Washington State Department of Ecology, 2017). Average temperature, precipitation, humidity, and wind measurements can be used to describe climate over time in any particular place, and are also used in analysing urban climatic environments. In this chapter, mean monthly temperature (°C), rainfall (mm), relative humidity (%), wind speed (km/h), and sunshine hours have been adopted to define the climatic conditions and trends for each city. The average of the all monthly means for the periods of 2011, 2012, 2013, 2014 and 2015 for each variable was computed for the both cities. These data were obtained from the Iraqi Meteorological Organization for Baghdad (IMO, 2015) and from the Australian Bureau of Meteorology for Perth (BOM, 2015).

Temperature has been applied as the major parameter for studying urban heat islands (Oke, 1987), but other climatic elements have also used in investigating urban thermal environments. For example, wind speed and direction have been documented to monitor a cooling effect in urban areas, and the consequent decrease in UHI effects (Rajagopalan et al., 2014). Adebayo (1987) attempted to use relative humidity as a measure, but found that there was no significant effect on this caused by urbanisation.

Others factors such as nearby water, ocean currents, landform latitude, and vegetation cover may also have an influence on the climate of any particular place. The climate types of the Baghdad and Perth study areas, based on the Köppen-Geiger climate type map, are shown on Figure 3.1.

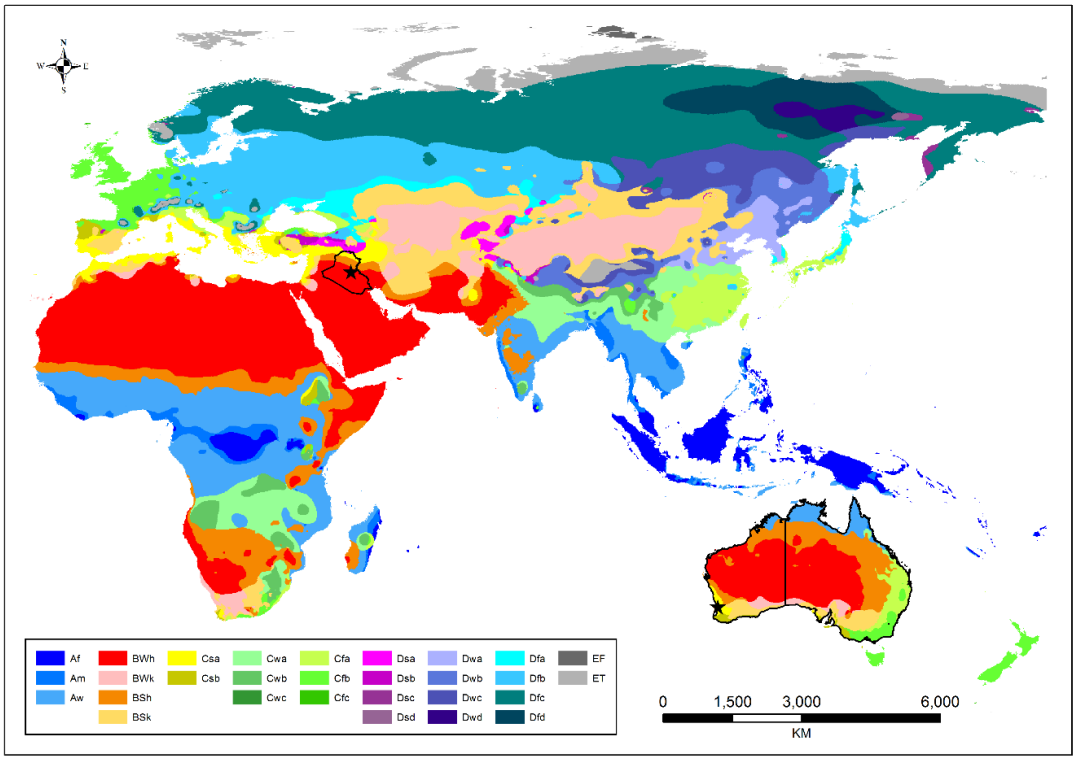

Figure 3.1 Köppen-Geiger climate type map of the world, showing the climate type of Baghdad and Perth (Peel et al., 2007).

Urban heat islands are also strongly associated with socioeconomic activities (Huang et al., 2011), and the demographic characteristics of a city in term of its population size (Oke, 1973). Urban expansion is mainly associated with population growth to accommodate an increasing population size (Marshall, 2007), and urbanisation is generally represented using population density and urban growth data (Seto et al., 2012). Angel et al. (2011) point out that urban areas of most cities around the world expand on average twice as fast as their local population growth rates. A general overview of both cities in terms of the geographical location, climate, and demographic characteristics are described below.

3.1.1. The study area of Baghdad

3.1.1.1. Geographical location

The study area of central Baghdad is located in the eastern-central part of Iraq, on both sides of the Tigris River with geographic extant of 33.18° N to 33.49° N latitudes, and 44.19° E to 44.57° E longitudes (Figure 3.2), covering a total area of 870.4 km^2. It has an average elevation of 32.1 m above mean sea level (USGS, 2016a). It is the capital and major city of Iraq, which is considered as the administrative, commercial and educational centre in the country.

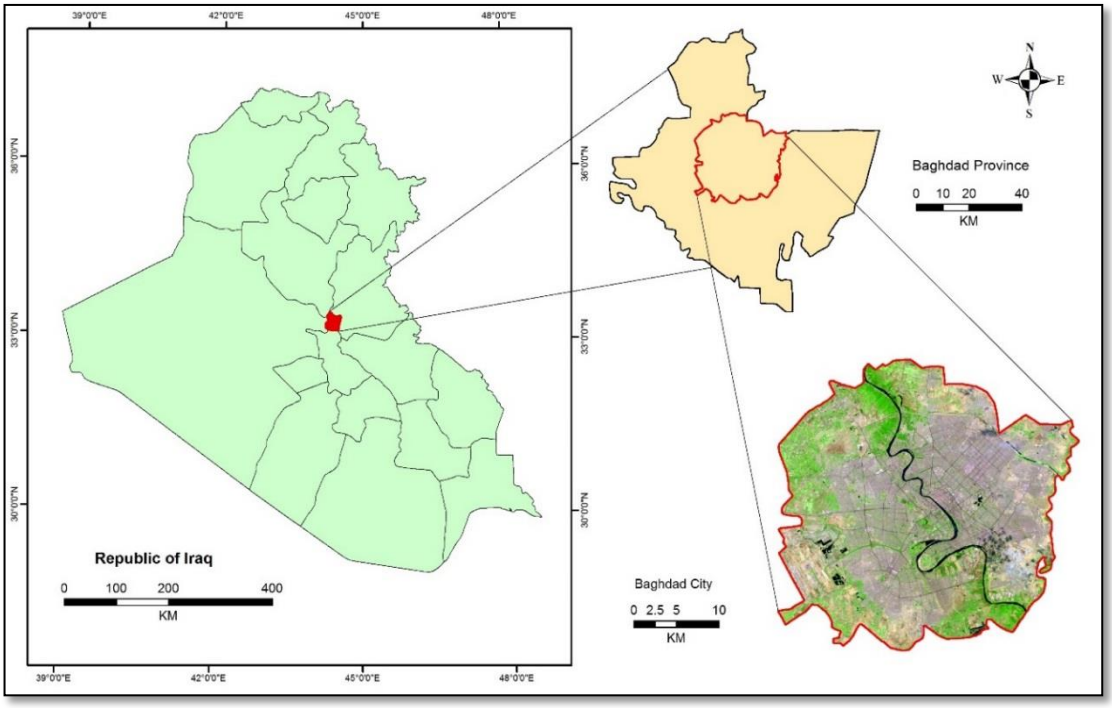

Figure 3.2 Satellite image showing the area and location of Baghdad study area (Landsat 8, bands 7, 5, 3).

3.1.1.2. The climate

According to the Köppen's climate classification system, Baghdad city is located in a semi-arid and subtropical desert climate type (BWh). Table 3.1 describes BWh climates (Peel et al., 2007).

Table 3.1 Köppen's definition of arid and semi-arid climate (BWh) (Peel et al., 2007).

Code	Type	Description
B	Dry climate / Desert	Annual evaporation higher than precipitations. No permanent rivers.
W	Dry (arid and semi-arid) climates	Annual precipitations < 250 mm.
h	Dry and heat	Annual average temperature > 18°C.

Figure 3.3(a) shows the mean monthly minimum temperatures (T_{min}) and maximum temperatures (T_{max}) in Baghdad. These values appear to have a similar trend during the period between 2011 and 2015. It should be noted that the difference between T_{min} and T_{max} was larger in summer and smaller in winter. The lowest mean monthly T_{min} and T_{max} were in winter, especially in December and January when they were 7.8 °C and 6.2 °C for T_{min} and 16.4 °C and 16.2 °C for T_{max}, respectively. Whereas, the highest mean monthly T_{min} and T_{max} were recorded during summers when they were 30.2 °C and 44.8 °C in July and 29.4 °C and 44.4 °C in August, respectively. The average of the annual mean maximum temperature was 30.6 °C for the period 2011-2015, while the average of annual mean minimum temperature was 18.5 °C.

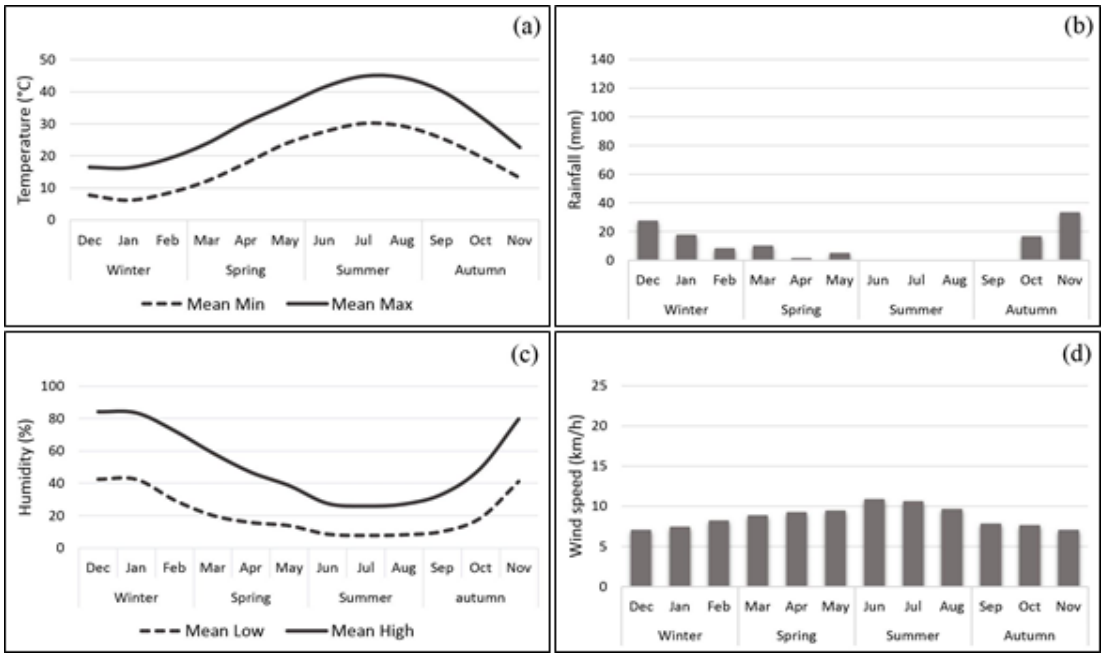

Figure 3.3 Mean monthly values of: (a) temperature; (b) rainfall; (c) humidity; (d) wind speed for Baghdad, 2011-2015.

The climate of Baghdad can be characterised as dry and extremely hot in the summer season, especially in July and August. High temperatures during summer are remarkable, reaching 51 ºC during heatwaves days in 2015 (IMO, 2015). This makes it one of the hottest cities in the world in terms of peak temperature. In contrast, the temperature decreases markedly during the short, cool winter months, which stretch from December to February, when temperature occasionally reaches 1 °C. The autumn months are September, October, and November, which have warm sunny days and cooler nights, with a mean maximum temperature of 26.1 °C. The spring months are March, April, and May, which are sunny and warm, with a mean maximum temperature of 24.2 °C.

As seen in Figure 3.3(b), the annual rainfall of Baghdad was 119 mm, and only occurs during winter, spring, and autumn, with most rainfall expected during the winter. Several studies have documented that the long-term annual rainfall of Baghdad is between 100-200 mm (Ali et al., 2015). Notwithstanding, the rainfall amounts for Baghdad decreased significantly during the period 1938-2008 (Al-Dabbas et al., 2015).

The trends in mean monthly high and low relative humidity in Baghdad during the period 2011-2015 are shown in Figure 3.3(c). The mean high relative humidity was lowest in the summer months, being 26% and 27.2% in July and August, respectively. Winter months such as December and January had the highest mean relative humidity, at approximately 84.2% and 83.5%, respectively. The mean low relative humidity followed the same trend as the high relative humidity through all months of the years, but with much lower values.

Mean monthly wind speed is illustrated in Figure 3.3(d). It ranged from 7 km/h to 10.8 km/h over the period 2011-2015. It increases in the spring and summer seasons and decreases through autumn and winter. The average annual mean wind speed is approximately 8.6 km/h. In Baghdad, the prevailing wind directions are generally north-westerly in spring and summer. These winds are dry and bring sandstorms from arid and semi-arid land surrounding Baghdad (Jassim & Goff, 2006).

In addition to these meteorological variables, sunshine hours is also an important meteorological variable that has been widely used in various fields and applications such as urban planning studies (Shao, 1991). Baghdad receives between 2800 to 3300 hours of annual bright sunshine (Alasady, 2011).

3.1.1.3. Demographic characteristics

According to statistical data from the Iraqi Ministry of Planning, Central Statistical Organization, the population growth of Baghdad province has been reported through censuses of 1947, 1957, 1967, 1977, 1987, and 1997, in addition to the estimated statistical data during 2003 and 2011. The population of Baghdad province increased dramatically through these years, as shown in Figure 3.4.

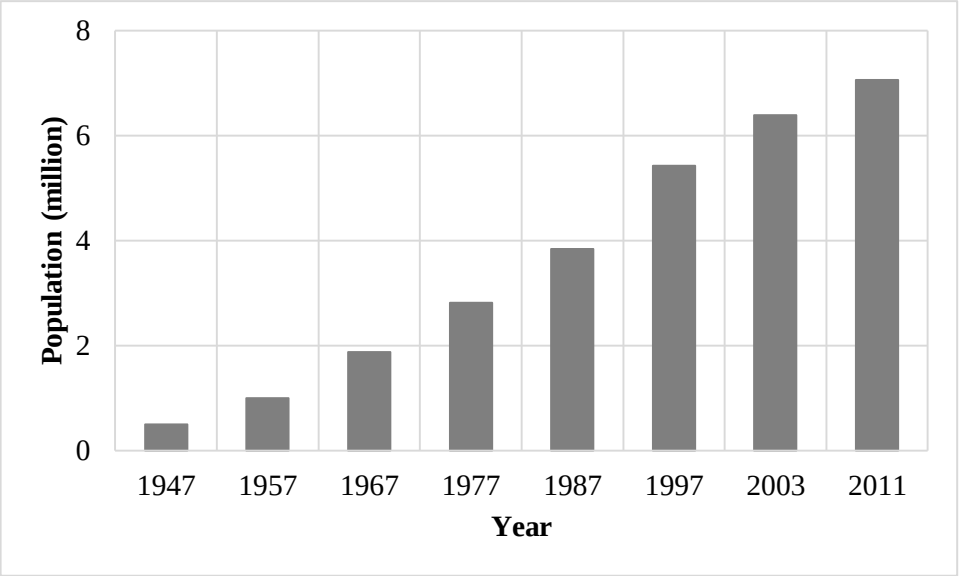

Figure 3.4 Population growth of Baghdad province (CSO, 2012).

Population growth has occurred as a result of natural increase in birth rate and internal migration from other provinces. According to the estimated data, the population was 7,057,736 in 2011. Baghdad is, therefore, the largest city in Iraq and the second largest city in the region. Figure 3.5 reveals the spatial distribution of population within the city of Baghdad classified by the administrative boundaries. It can be seen that the majority of people, around 78%, live within the boundary of Baghdad Mayoralty, compared with the remaining 22% inhabitants, who live in the suburbs.

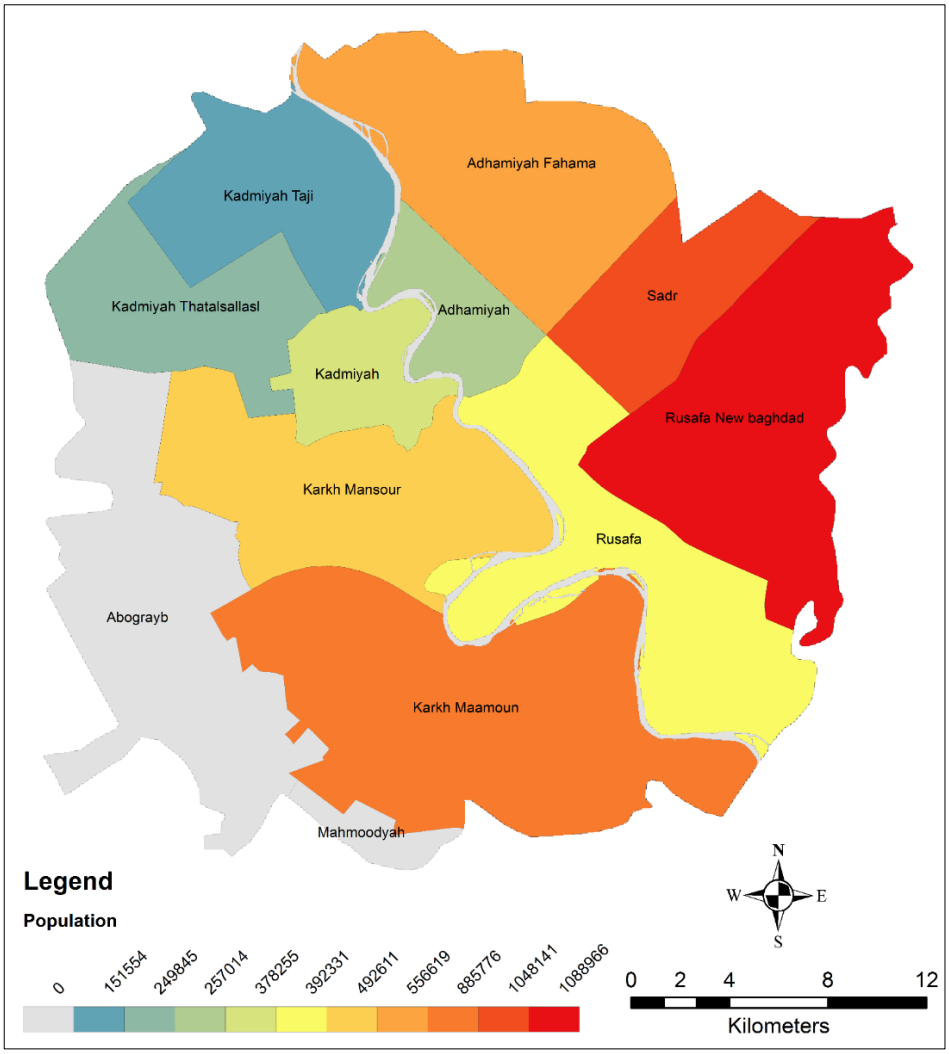

Figure 3.5 Spatial distribution of population in the districts of Baghdad (within the study area) during 2011.

During the study period, the urban growth of Baghdad fluctuated due to various factors (e.g., wars, political infighting, bursts of economic development, migration and population increase) that both encouraged and hindered growth. On one hand, Baghdad experienced a period of prosperity and economic growth since Iraq is one of the world's main exporters of oil. New modern districts and infrastructure, including sewerage, water systems, and highways, were built during that time. This rapid growth has seen an expansion of urban construction onto agricultural land and previously green areas have been transformed into built-up areas to accommodate residential, commercial and industrial expansions. On the other hand, during the wars of 1991 and 2003 Baghdad's infrastructure was severely damaged by the US-led coalition forces. Significant disturbance in the urban growth of Baghdad occurred during the first Gulf

War of 1991 and the subsequent economic sanctions, and the second Gulf War of 2003 and the subsequent political in-fighting. Despite the damage to Baghdad during the war of 2003, the city has subsequently experienced a significant increase in built-up areas as a result of further economic development, population growth, and attempts to redress the shortage in housing and infrastructure (Gunter, 2013).

3.1.2. The study area of Perth

3.1.2.1. Geographical location

Perth is situated in the south-western corner of Western Australia. It is surrounded to the west by the Indian Ocean and to the east by dense forest.

Perth is the capital and largest city in the state of Western Australia. The study area of the central Perth metropolitan region is located on the coastal plain of the Swan River, covering an area of 488.7 km^2. It has an average elevation of 21.4 m above mean sea level (Geoscience Australia, 2016). The geographic coordinates are 31.84° S to 32.11° S latitudes, 115.73° E to 115.99° E longitudes as shown in Figure 3.6.

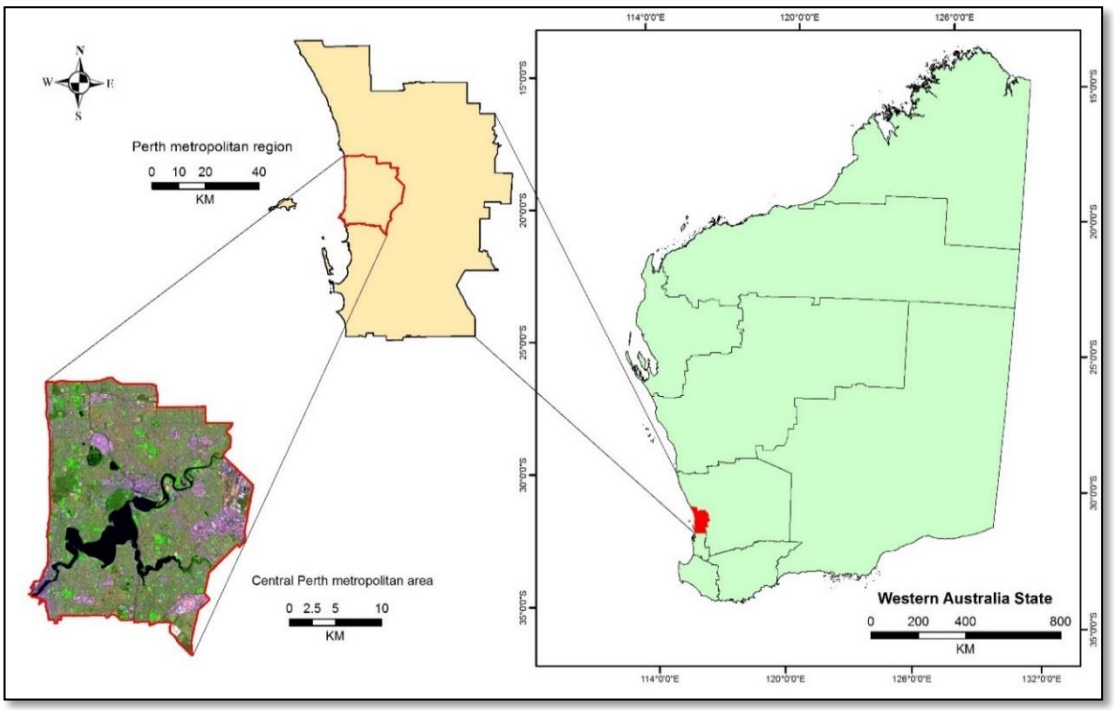

Figure 3.6 Satellite image showing the area and location of Perth study area (Landsat 8, bands 7, 5, 3).

3.1.2.2. The climate

In contrast to Baghdad, Perth climate is classified, according to the Köppen's climate classification system, as a Mediterranean climate (Csa). Table 3.2 shows the characteristics of Csa climates (Peel et al., 2007).

Table 3.2 Köppen's definition of Mediterranean Climate (Csa) (Peel et al., 2007).

Code	Type	Description
C	Hot moderate climate	The 3 coldest months average a temperature between -3°C and 18°C; Hottest month average temperature > 10°C; The summer and winter seasons are well defined
s	-	Dry season in summer
a	Hot summer	Average temperature of the hottest month > 22°C

The average values of temperature, rainfall, humidity, and wind speed for the period between 2011 and 2015 are presented in Figure 3.7 and are based on data obtained from the Australian Bureau of Meteorology (BOM, 2015).

Mean monthly minimum and maximum temperatures for Perth were recorded to be 16.2 °C, 18.5 °C, 18.9 °C, and 30.7 °C, 33.2 °C, 33.5 °C in the summer season of December, January and February, respectively, as shown in Figure 3.7(a). These months are usually dry and hot. The autumn months are March, April, and May which have warm sunny days and cooler nights. The winter months, which stretch from June to August, are rainy and mildly wet, with mean monthly minimum temperatures of 9.1 °C, 7.7 °C, 9.3 °C, and mean monthly maximum temperatures of 19.9 °C, 18.7 °C, and 20.3 °C, respectively. The spring months are September, October, and November which are sunny and warm. The average of annual mean maximum temperature was 25.8 °C, while the average of annual mean minimum temperature was 13 °C over the period 2011-2015.

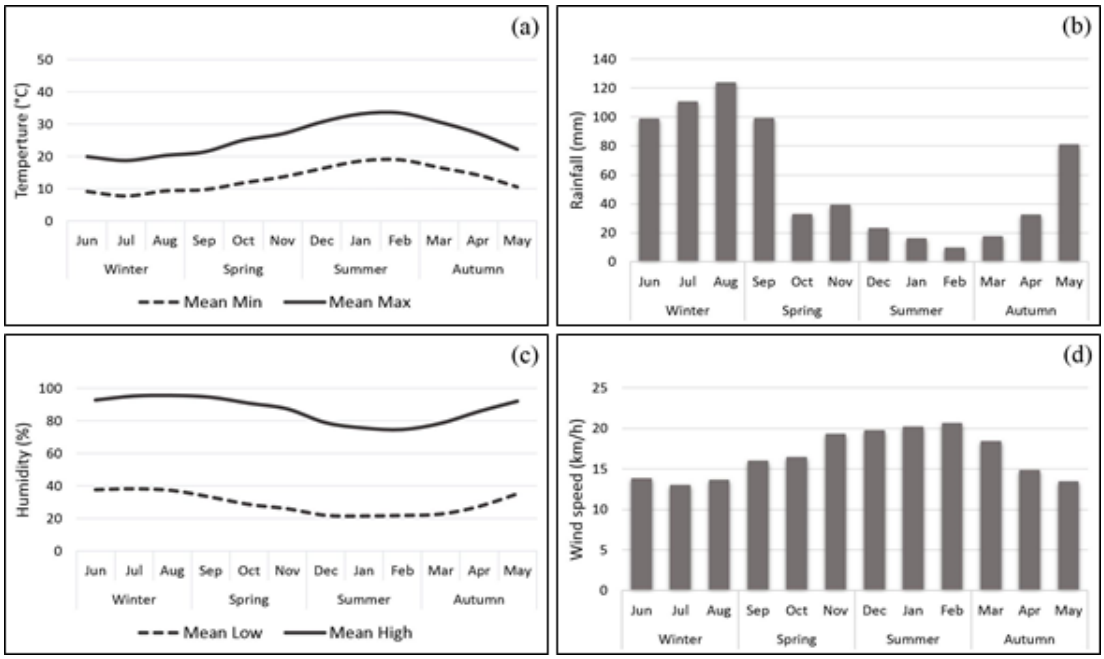

Figure 3.7 Mean monthly values of: (a) temperature; (b) rainfall; (c) humidity; (d) wind speed for Perth, 2011-2015.

The average annual rainfall in Perth was 683.15 mm during the period of 2011-2015 (Figure 3.7b). Perth receives relatively high rainfall in winter, followed by spring, autumn and summer. The average rainfall of Perth region has decreased by around 20 percent from long-term monitoring between 1910 and 2009 (Blakely & Carbonell, 2012), and based on projections for future rainfall, Suppiah et al. (2007) predict that the annual rainfall could decrease to 20 percent of the long-term average by 2030. However, the amount of rainfall in Perth is substantially greater than that of Baghdad.

In Perth, as shown in Figure 3.7(c), January and February may be characterised as the lowest humid months in the year, with mean monthly high and low relative humidity are about 75.5% and 74.6%, and 21.4% and 21.8%, respectively. The highest relative humidity was recorded in winter during July and August with high and low relative humidity about 95.2% and 95.6%, and 38.3%, 37.2%, respectively. The high and low humidity values show similar trends to each other throughout all months of the year. In general, relative humidity is higher in Perth than in Baghdad.

The average mean monthly wind speed for Perth is shown in Figure 3.7(d). It can be seen that the highest wind speeds of 20.2 km/h and 20.6 km/h were recorded in January and February, respectively, whereas, July had the lowest wind speed of 13 km/h. From

Figure 3.7(d), the average annual mean wind speed for the period 2011-2015 was approximately 16 km/h. This result is consistent with data obtained from Australian Bureau of Statistics (ABS) that considered Perth as the windiest region in Australia, with an average wind speed of 15.6 km/h (ABS, 2012). In contrast with Baghdad, Perth has generally higher wind speeds over the evaluated years.

The annual sunshine of Perth is between 2800 and 3000 hours, and is therefore, characterised as a sunny city with the Mediterranean climate (ABS, 2015). A significant similarity was found in terms of the amount of bright sunshine received by the two cities.

3.1.2.3. Demographic characteristics

Based on the Australian Bureau of Statistics (2012), the population of Perth gradually increased between 1947 and 2011 as shown in Figure 3.8. Perth is the largest city in Western Australia and the fourth most populous city in Australia, with an estimated population of 1,728,867 in 2011 (ABS, 2012).

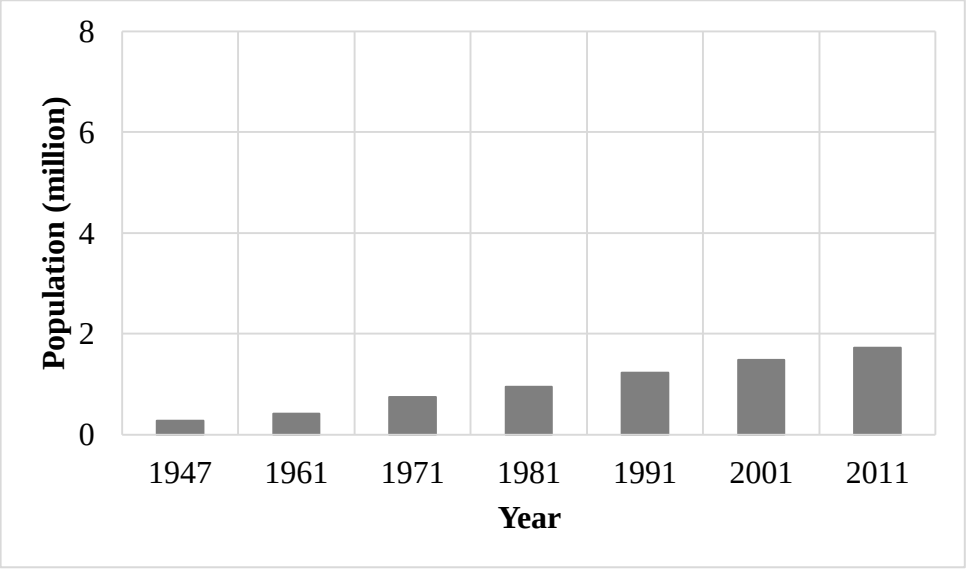

Figure 3.8 Population growth of Perth.

Figure 3.9 reveals that around 42% of people live within the central part of the study area of Perth, while a greater number of people (the remaining 58%) live in its suburbs.

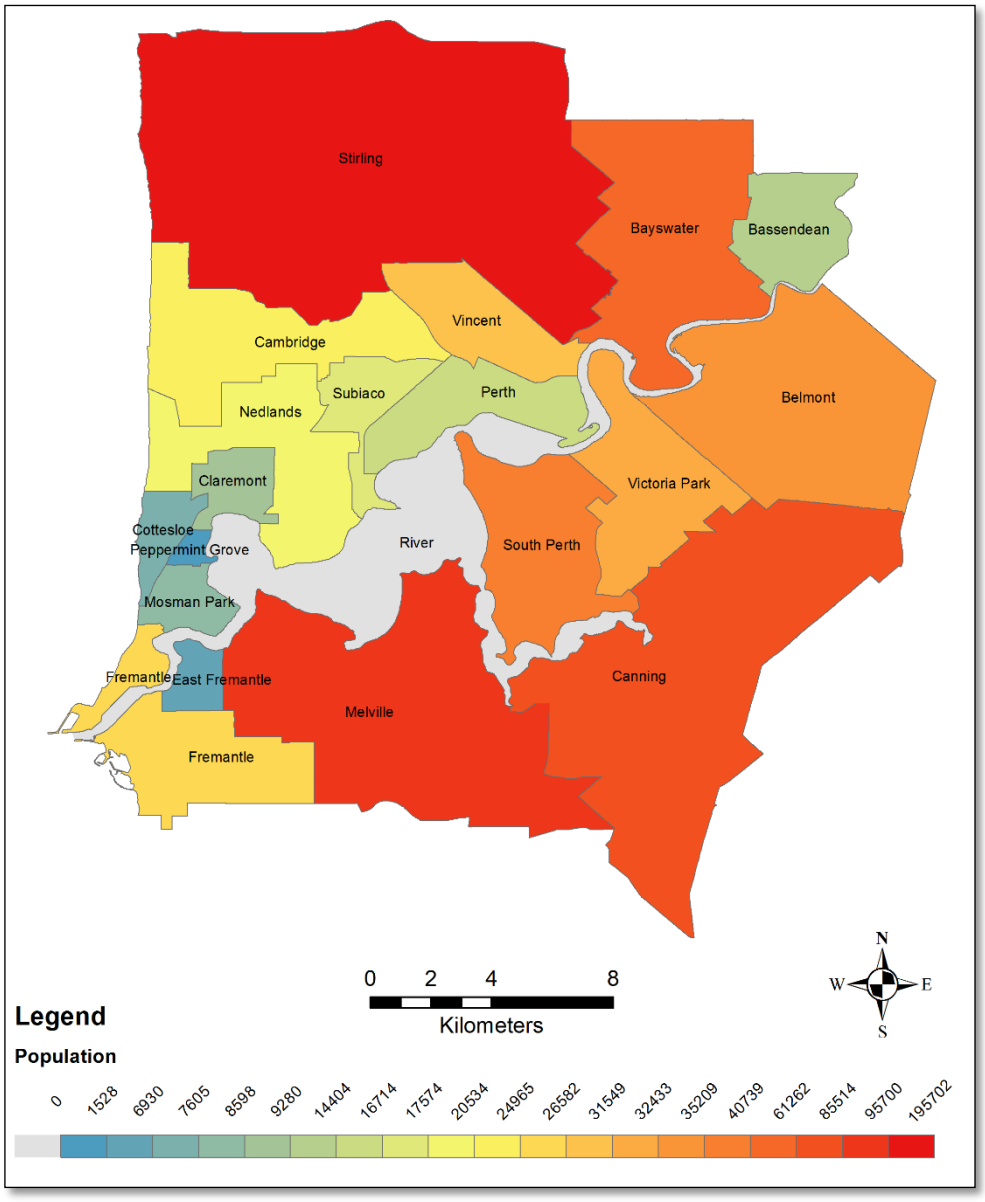

Figure 3.9 Spatial distribution of population in the districts of Perth in 2011.

The economy of Western Australia experienced remarkable growth, in line with population increase and urban expansion, during the last few decades, which was mainly related to the discovery and exploitation of new mineral resources in Western Australia (Pham et al., 2013). This development led to increasing inter-state and overseas migration to Western Australia, for work, as well as for investment, study and tourism. The city has experienced an increase in diversity in ethnicity and culture which has led to its boom over the past few decades (Kennewell & Shaw, 2008).

Based on the 2011census, population within the Baghdad area was 5 501 112 (Figure 3.5), and within Perth, 732 822 (Figure 3.9). The population density for Baghdad and Perth was found to be 6320.2 people/km^2 and 1499.5 people/km^2. In Baghdad, the highest population density was observed in the city core, while it is opposite in Perth, where the highest population density was located in the outer suburbs.

3. 2. Datasets

Datasets used in this study included remote sensing data and field observation data obtained by hand-held instruments. More details about these datasets are provided in the following sections.

3.2.1. Remotely sensed data

The term "remote sensing" is generally defined as the science of and technology for obtaining information about an object or area on the earth surface without touching them, by studying and analysing data from aircraft or satellite (Swain & Davis, 1978). Also, it is the term used for methods of detecting and measuring characteristics of targets by electromagnetic energy such as light, heat and radio waves that are remotely sensed (Sabins, 2007). Considerable applications to different fields such as studying and monitoring land cover, the atmosphere, the global environment, the weather etc., have been implemented using remotely sensed data. For Landsat satellites, there have been a series of platforms with a variety of sensors-the first one was an Earth resources satellite (Landsat-1) that launched in 1972, and other platforms in the Landsat series, with a variety of improved sensors (Figure 3.10), have been launched to study the Earth in multiple ways (Schowengerdt, 2006).

Figure 3.10 Landsat timeline (USGS, 2016b).

3.2.1.1. Landsat images pre-processing

Imagery selection for this study was based on suitability of data. All images were acquired under normal atmospheric conditions with less than 10% cloud cover. Three generations of Landsat data, including MSS, TM, and L8 were downloaded from the U.S. Geological Survey as Level-1 products (radiometrically calibrated and systematic geometric corrections) except for Landsat 8 2016, which is a Level-2 product (Level-1 and atmospheric corrections) (USGS, 2018a). These were acquired in the summers of 1970s, 1980s, 1990s, 2000s and 2015 for both study sites, as well as to summer 2016 for the study area of Perth (Table 3.3), providing a close anniversary date for each image. Images were acquired at approximately 10:00 am local time for both Baghdad and Perth cities.

Table 3.3 List of the Landsat images used in this study.

City	Datasets	Acquisition date	Local time AM	Path/Row
Baghdad	Landsat 2, MSS	23-07-1976	09:48:51	181/037
	Landsat 5, TM	27-08-1984	10:03:39	168/037
	Landsat 4, TM	09-08-1992	09:42:20	168/037
	Landsat 5, TM	23-08-2000	10:11:21	168/037
	Landsat 8, OLI-TIRS	01-08-2015	10:33:14	168/037
	Landsat 8, OLI-TIRS	05-01-2015	10:33:40	168/037
	Landsat 8, OLI-TIRS	02-04-2015	10:04:02	169/037
	Landsat 8, OLI-TIRS	23-07-2015	10:39:23	169/037
Perth	Landsat 1, MSS	19-01-1974	09:33:00	120/082
	Landsat 5, TM	11-02-1988	09:35:09	112/082
	Landsat 5, TM	28-02-1997	09:31:02	112/082
	Landsat 5, TM	11-02-2008	09:56:07	112/082
	Landsat 8, OLI-TIRS	21-02-2015	10:11:27	113/082
	Landsat 8, OLI-TIRS	20-01-2015	10:11:37	113/082
	Landsat 8, OLI-TIRS	19-04-2015	10:04:50	112/082
	Landsat 8, OLI-TIRS	15-07-2015	10:11:11	113/082
	Landsat 8, OLI-TIRS	12-10-2015	10:05:28	112/082
	Landsat 8, OLI-TIRS	23-01-2016	10:11:43	113/082

Other sets of remotely sensed data, including high spatial resolution satellite images and aerial photographs, were mainly used as reference data to assess the accuracy of derived products. These references data included a Corona image from 1972, an IKONOS image from 2001, and a Quickbird image of 2009 for Baghdad city. Five aerial photographs were obtained from the State Land Information Portal (SLIP Enabler, 2015) for Perth city, covering the years of 1974, 1985, 1995, 2008 and 2015.

Image pre-processing methods below were performed using ArcGIS 10.2 and ENVI 5.1 (ESRI, 2013; EXELIS, 2013).

- Atmospheric correction was performed using the dark object subtraction (DOS) method to remove atmospheric effects (path radiance) using a two-step process (Chavez, 1988). Firstly, the digital numbers (DN) were converted to the top of atmosphere (TOA) reflectance. Values of the darkest pixels were then subtracted from each Landsat image to make all images comparable to each other. DOS is perhaps the simplest of available methods, mostly used for image atmospheric correction for many applications (Song et al., 2001). It was also suitable for the historical images because this method does not require climate data.

- Image registration of the enhanced images was the next step in data pre-processing in order to map and quantify the genuine changes and enable direct comparison of values among the evaluated images.

- All images were clipped based on boundaries of the two study sites for all subsequent processing.

3.2.2. Field measurement instruments

Surface albedo and surface temperature measurements were taken during field work using the pyranometer and the FLIR E5 infrared camera.

3.2.2.1. Pyranometer instrument (Albedometer)

The LP PYRA 06 pyranometer operates in the spectral range of 0.305 to 2.8 µm (Figure 3.11a) and is composed of a second class pyranometer that conforms to ISO 9060. It is based on a pair of thermopile pyranometers; the upper one measures the incident radiation on the ground (↓) and the lower one measures the reflected radiation (↑) from the objects on the ground (LP PYRA 06, 2007). A Delta-Ohm DO9847 Data logger connected to the LP PYRA 06 albedometer was used to record and read the observed data (Figure 3.11b).

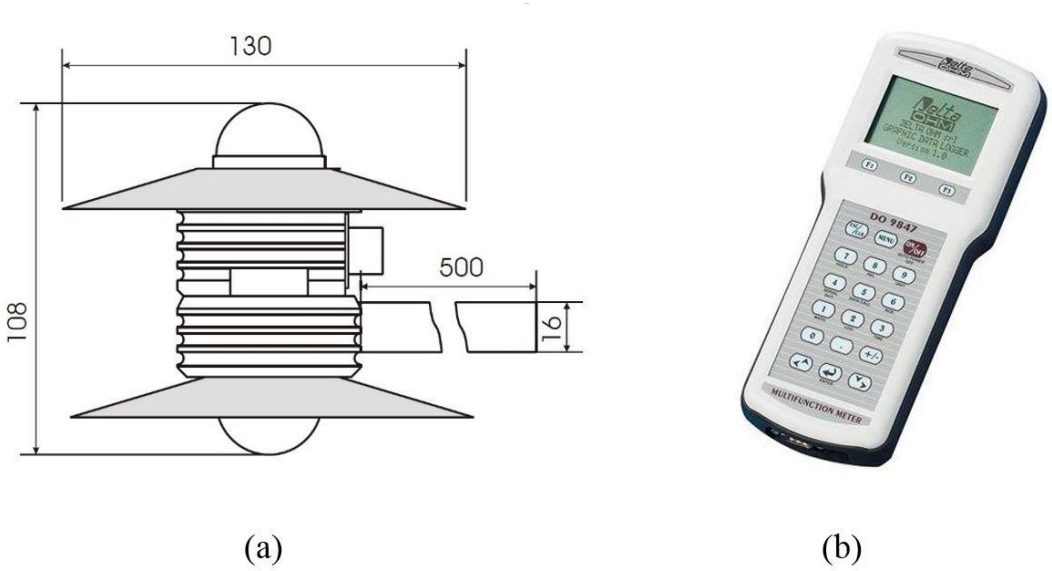

Figure 3.11 (a) LP PYRA 06, (b) Data logger 9847.

3.2.2.2. Infrared camera

The FLIR E5 infrared camera records thermal data in the spectral range of 7.5–14 µm (Figure 3.12) and was used for recording thermal information of surfaces in the study area. It works within a temperature range of 2 to 250 °C and has a variable material-specific emissivity setting (0.1 to 1.0). It has an accuracy of ±2% and a thermal sensitivity of < 0.07 °C. The resolution of the thermal image is 120 × 90 pixels. This camera has an exclusive function that is known as multi-spectral dynamic imaging (MSX). This function provides extraordinary thermal detail that simplifies interpretation of an image. The captured images can be stored and analysed using FLIR Tools software (FLIR E5, 2014).

Figure 3.12 The FLIR E5 infrared camera.

3. 3. Chapter summary

This chapter provided an overview of Baghdad and Perth, including their environmental settings, climatic conditions, and demographic characteristics. The geographical location and climate classification of the two study sites are markedly different. In addition, there are variances between the two cities in their climatic variables such as temperature, rainfall, humidity and wind speed. However, despite these differences, both cities have dry summer season, and receive high, and approximately similar amounts, of sunshine. Monitoring of temperature for the five year period of 2011-2015 revealed that the temperatures have increased for both Baghdad and Perth, but significantly higher in Baghdad. A contrast between the population growth and distribution of both cities was observed. Fundamental information on the datasets used in this study, including remotely sensed data and those from hand-held instruments, were also described.

4. Impact of impervious surfaces expansion on land surface temperature

4. 1. Introduction

Urban impervious surfaces expansion is generally understood as a spatial dynamics phenomenon, resulting from urbanisation and industrialisation that mainly relates to growth in population and the economy (Kinga, 2015). It increases the dominance of buildings and paving in areas primarily used for public, residential, commercial, industrial and transportation areas (Bagan & Yamagata, 2012). From a remote sensing perspective, urban growth is defined as a process occurring when the pixels belonging to non built-up areas in the previous image are categorised as built-up areas in a later evaluated image (Cabral et al., 2005). Recently, ISA has been recognised not only as an indicator of the degree of urbanisation but also used as an important parameter in issues related to the environment, hydrology, ecology and socioeconomics (Arnold Jr & Gibbons, 1996; Slonecker et al., 2001). The quality of the urban thermal environment is significantly affected by ISA, particularly in cities experiencing rapid urbanisation and industrialisation (Oke, 1987; Chen et al., 2006; Stathopoulou et al., 2009; Hamdi, 2010; Kumar et al., 2012).

For many years, a range of remote sensing data with various spatial and temporal scales has been used to map and quantify land use and land cover, to characterise spatiotemporal dynamics through change detection. These data are an effective tool for studying and monitoring land surface due to their ability to provide a large-scale synoptic overview, availability of images at regular intervals, and simplicity in processing and deriving statistics (Ford, 1979; Lo, 1981; Hathout, 2002; Lo & Quattrochi, 2003). Recently, medium spatial resolution images, such as those provided by Landsat, have become an important source of images for mapping impervious surface areas using unmixing techniques at local, regional and global scales (Wu & Murray, 2003; Lu & Weng, 2006; Deng et al., 2012). Unmixing techniques have been traditionally used with hyperspectral data to reduce correlation between bands and were later expanded to use with Landsat data for distinguishing the spectra of different LULC categories from the typically mixed pixels of urban areas precisely (Lu & Weng, 2004; Kärdi, 2007).

It is therefore important to quantify spatiotemporal changes to impervious surface areas to understand and monitor climatic, environmental and socioeconomic issues related to urban areas. The "urban heat island" effect, for instance, has been identified as a problem resulting from urbanisation. This chapter aims to evaluate growth in the built-up areas of the study areas for the last five decades and quantify its effects on SUHI. To address this aim, the chapter objectives are:

1) to quantify the spatiotemporal dynamics of impervious surfaces;

2) to investigate spatiotemporal variations of LSTs, and temporal and seasonal variations of SUHIs.

4. 2. Datasets

Two sets of data were used in this chapter. First, a temporal series of Landsat satellite data including MSS, TM, and L8 was acquired, representing the summers of the 1970s, 1980s, 1990s, 2000s and 2015. They were acquired at approximately 10:00 am local time (as described in Section 3.2.1). Secondly, high spatial resolution satellite images and aerial photographs were used as reference data to assess the accuracy of the generated impervious surface maps. These data included a Corona image from 1972, an IKONOS image from 2001, and a Quickbird image from 2009 for Baghdad city. Five aerial photographs, obtained from State Land Information Portal (SLIP Enabler, 2015), representing the years 1974, 1985, 1995, 2008 and 2015, were used for Perth city.

4. 3. Methods

Pre-processed images (as described in Section 3.2.1.1) were used to estimate ISA and LST. The workflow for the methods used to quantify ISA growth on SUHI is shown on Figure 4.1.

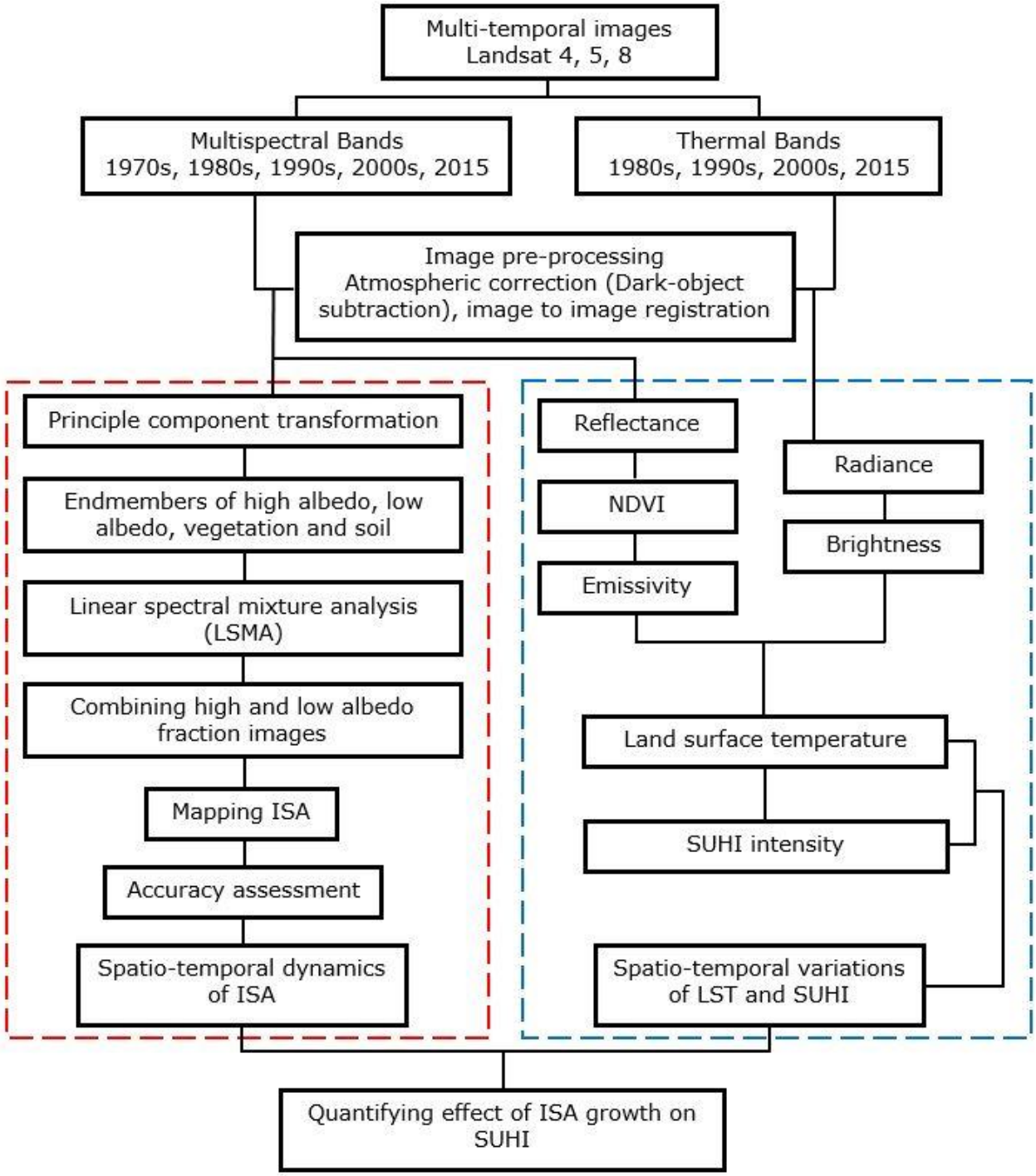

Figure 4.1 Flowchart showing methods for estimating ISA and SUHI intensity.

4.3.1. Impervious surface area mapping

The processing steps began with masking water bodies for all images to obtain accurate results for principle component analysis (PCA). The outcome of PCA was then used to calculate the impervious surface area. The final process was to evaluate the accuracy of the ISA maps. A more detailed explanation of these processes are given in the following sections.

4.3.1.1. Water masking

Water has spectral characteristics similar to those of other land use/land cover (LULC) surfaces, such as asphalt, shadows and green areas. Furthermore, water and other low albedo objects are often mixed, affecting the endmembers of the analysis, unmixing results. Thus, it was necessary to mask water bodies from all images before further processing, and especially before undertaking principle component analysis (PCA) transformation. Water masking was carried out using the normalised difference water index (NDWI) as suggested by McFeeters (1996) and the modified normalised difference water index (MNDWI) as developed by Xu (2006). Water indices are commonly used with Landsat images to extract water surfaces, for which index values range from -1 to 1. The NDWI was calculated for Landsat images MSS using Equation 4.1:

$$\mathrm{NDWI} = \frac{(\rho(\mathrm{Green}) - \rho(\mathrm{NIR}))}{(\rho(\mathrm{Green}) + \rho(\mathrm{NIR}))} \tag{4.1}$$

Where:

ρ (Green) is the spectral reflectance of green band

ρ (NIR) is the spectral reflectance of near-infrared band

For Landsat images TM and OLI, MNDWI was calculated using Equation 4.2:

$$\mathrm{MNDWI} = \frac{(\rho(\mathrm{Green}) - \rho(\mathrm{SWIR\_1}))}{(\rho(\mathrm{Green}) + \rho(\mathrm{SWIR\_1}))} \tag{4.2}$$

Where:

ρ (Green) is the spectral reflectance of green band

ρ (SWIR_1) is the spectral reflectance of short wave infrared band

Water features are normally characterised by threshold values greater than zero (McFeeters, 1996). In this study, values were typically > 0.1 and were converted to polygons prior to masking.

4.3.1.2. Extraction of impervious surfaces

The steps used to map impervious surfaces from Landsat images (Figure 4.1) are described below:

1. According to Green et al. (1988); Boardman and Kruse (1994), transformation of the multispectral images into a new dataset can be performed by using two different approaches: principal component analysis (PCA) and minimum noise fraction (MNF). These approaches can be effectively used to identify image end-members and to derive high quality end-members (Lu & Weng, 2006; Kuang et al., 2014). In this study, both approaches were tested and principle component analysis (PCA) was eventually used, primarily because a better result was obtained based on a visual check, but also because, as a data transforming technique to convert Landsat multispectral images into a new dataset (i.e., to reduce the six reflective bands to three principle components), PCA was free from cross-correlation and minimised noise. Three PCA images were generated based on eigenvalues that best fit the variations in the dataset;

2. Four endmembers, including high albedo surfaces, low albedo surfaces, green areas and bare land, were chosen from the scatterplots of three PCA components;

3. Linear spectral mixture analysis (LSMA) was used to convert each image into four fractional images;

4. The high and low albedo fraction images were combined, to create an ISA layer as described by Wu and Murray (2003);

5. The combined image of ISA was classified into 32 classes and a threshold value was defined based on a comparison with the original image. A binary dataset was then created to separate ISA and non-ISA parts;

The binary ISA data classification was subsequently converted to polygons to facilitate post-classification editing.

4.3.1.3. Accuracy assessment

According to Foody (2002), accuracy of classified maps, produced from remote sensing data, is essential for assessing the reliability of outcomes.

In this work, ground reference data, collected from high resolution data (as described in Section 4.2), were used to assess accuracy of impervious surface area maps. One hundred samples were extracted from high-resolution data (where each sample represented 3 × 3 Landsat pixels). These samples were evaluated against the relevant impervious surface maps. As described in Section 2.4.3, several variables, including overall accuracy, kappa coefficient, producer's accuracy and user's accuracy were used to evaluate accuracy of impervious surface maps.

4.3.2. Retrieving land surface temperature (LST)

In this study, Landsat 4 and 5 (TM) and Landsat 8 datasets were employed to retrieve LST. A single thermal band of Landsat 4 and 5 (TM) and two thermal bands of Landsat 8 (bands 10 and 11) were used. Unfortunately, there were some artifacts (e.g., stray light) resulting from thermal energy that affected the data collected in the Landsat 8 TIRS bands. In particular, band 11 was substantially more contaminated than band 10 by stray light. Therefore, U.S. Geological Survey (USGS) have suggested that only band 10 should be used for LST retrieval (https://landsat.usgs.gov/using-usgs-landsat-8-product).

Several algorithms have been proposed to retrieve LST from Landsat data. These algorithms may be roughly grouped into three categories: single-channel methods, multi-channel methods, and multi-angle methods (Li et al., 2013c). The most popular algorithms from the single-channel methods are the Mono-Window (MW) algorithm

(Qin et al., 2001) and the generalised Single-Channel (SC) algorithm (Jiménez-Muñoz & Sobrino, 2003). For the multi-channel methods, the most popular is the Split-Window (SW) algorithm (Becker & Li, 1990), and an algorithm proposed by Sobrino et al. (1996) has been preferred for the Multi-Angle (MA) method. Historical data from a TM sensor and a single band from TIRS-Landsat 8 (Band 10 only) were used in this work, and these were not suitable for the split-window and multi-angle methods, because their algorithms require two channels to retrieve LST (Jiménez-Muñoz & Sobrino, 2003). Additionally, multi-angle methods can only be used for homogeneous areas (e.g., the sea surface or densely vegetated forest) but not for heterogeneous areas (Li et al., 2013c).

For the single-channel methods, the mono-window algorithm has been proposed to retrieve LST using two parameters, atmosphere transmittance and mean atmospheric temperature. Whereas, the generalised single-channel algorithm requires a distribution of both atmospheric temperature and water vapour content. Sobrino et al. (2004) proved that the single-channel algorithm provides better results than the mono-window algorithm, generating root mean square deviation values of 0.9 K and 2 K, respectively, when radio-sounding data is not used. These algorithms were also tested by Vlassova et al. (2014) who found that the root mean square deviation values were 1 °C and 2.3 °C for the single-channel algorithm and mono-window algorithm, respectively. The main disadvantage of these methods is that certain atmospheric parameters must be available.

In order to retrieve LST from historical Landsat datasets, there are often difficulties in obtaining in-situ atmospheric profile data during the satellite overpass. In this study, radiosonde data and atmospheric water vapour content were unavailable for the images used. Therefore, an image-based method (single-channel-based surface emissivity) was the only method that could be applied to retrieve LST from geometrically corrected Landsat data. Land surface emissivity (LSE), which is considered to be a modifying parameter for atmospheric correction methods and surface characterisation, has been proven to be related to the Normalised Difference Vegetation Index (NDVI) (Valor and Caselles, 1996). Therefore, land surface emissivity (LSE) computed from the NDVI, based on (Sobrino & Raissouni, 2000), was adopted as a parameter for atmospheric correction when retrieving LST in this study.

Ding and Xu (2008) conducted a comparison among the image-based method, the mono-window algorithm and the generalised single-channel algorithm, over the city of Fuzhou, China. They found that the image-based method provided superior results than mono-window algorithm and single-channel algorithm. Furthermore, this method has proved to be straightforward and has been widely used in various settings (e.g., Weng & Yang, 2004; Xiao & Weng, 2007; Zhang et al., 2013a; Ayanlade & Jegede, 2015; Estoque & Murayama, 2017; Fathizad et al., 2017; Pal & Ziaul, 2017; Dai et al., 2018; Madanian et al., 2018; Silva et al., 2018; Xiao et al., 2018).

Thermal bands of Landsat data were used to retrieve LST. The thermal bands of Landsat 4 and 5 have a spatial resolution of 120 × 120 m and Landsat 8 has that of 100 × 100 m. These thermal bands had already been resampled to 30 × 30 m by USGS. A three-step process was used to calculate LST.

Step 1: Conversion of digital number (DN) values of Landsat thermal bands to top of atmosphere (TOA) spectral radiance using the Equation 4.3.

$$L_\lambda = M_L \times Q_{cal} + A_L \quad (4.3)$$

Where:

L_λ = TOA spectral radiance

M_L = Band specific multiplicative rescaling factor (radiance multi-band x, where x is the band number)

A_L = Band specific additive rescaling factor (radiance add band x, where x is the band number)

Q_{cal} = Quantized and calibrated standard product pixel values (DN)

Step 2: Conversion of spectral radiance to at-satellite brightness temperature (Tb) in Celsius (°C) using Planck's law, as in the Equation 4.4.

$$T_b = (K_2 / \mathrm{Ln}((K_1 / L_\lambda) + 1)) - 273.15 \quad (4.4)$$

Where:

T_b = Effective at-satellite temperature in Kelvin (K)

L_λ = TOA spectral radiance

K_1 = First calibration constant

K_2 = Second calibration constant

The thermal constants of band 6 (TM) and bands 10 and 11 (TIRS) are shown in Table 4.1 and are available in metadata for the images used (USGS, 2015b).

Table 4.1 K_1 and K_2 calibration constant values for thermal bands of Landsat data.

	K_1 (W m^{-2} sr^{-1} μm^{-1})	K_2 (Kelvin)
TM band 6	607.76	1260.56
TIRS band 10	774.89	1321.08

Step 3: Correction of Land Surface Temperature (LST): this step was used to retrieve land surface temperature (LST) from T_b imagery and atmospherically corrected emissivity data using the Equation 4.5, developed by (Artis & Carnahan, 1982).

$$LST = T_b / (1 + (\lambda \times T_b / \rho) \times Ln(\varepsilon)) \quad (4.5)$$

Where:

λ = Wavelength of emitted radiance (the peak response and the average of the limiting wavelengths (λ = 11.5 μm)

ρ = h c / σ (1.438×10^{-2} mK)

h = Planck's constant (6.26×10^{-34} Js)

c = the velocity of light (2.998×10^{8} s^{-1})

σ = Stefan–Boltzmann's constant (1.38×10^{-23} J K^{-1})

ε = Surface emissivity

Surface emissivity (ε) was computed from NDVI using Equation (4.6) as suggested by Stathopoulou et al. (2007).

$$\varepsilon = 0.017\ P_v + 0.963 \quad (4.6)$$

Where: P_v = proportion of vegetation that was computed from the NDVI according to Equation (4.7)

$$P_v = (NDVI - NDVI_{max})^2 / (NDVI_{max} - NDVI_{min})^2 \quad (4.7)$$

Where: NDVI = Normalised Difference Vegetation Index. The NDVI was computed from the red and NIR bands of Landsat data.

4.3.3. Normalisation of LST

The relative radiometric normalisation (RRN) technique was used to normalise multi-temporal LST data. That is required to remove radiometric differences between multi-temporal data in order to make those data comparable (Hajj et al., 2008). This technique has been widely utilised for a variety of purposes, including thermal data, vegetation indices, change detection, etc. (Heo & FitzHugh, 2000; Yang & Lo, 2000; Santra et al., 2017). Since LST represents different sources or different years, normalisation was needed.

4.3.4. SUHI intensity

To help understand the intensity of thermal properties for each study area, the intensity of the surface urban heat island (SUHII) was obtained by calculating the difference between the mean urban surface temperature and that of the surrounding rural areas. The selected urban pixels were represented by the city core, while rural pixels included more vegetated areas. SUHII was computed using Equation 4.8 (Tiangco et al., 2008).

$$SUHII = LST_U - LST_R \quad (4.8)$$

Where: LST_U= the average values of LST within the urban area

LST_R= the average values of LST for the rural area

4.3.5. Quantifying change to impervious surfaces

In this chapter, consecutive Landsat images were used to determine spatiotemporal growth of impervious surfaces. The adopted approach for quantifying spatiotemporal dynamics of impervious surfaces was based on division the impervious surface maps into zones. This approach divided each study area into eight zones (pie sections), based on the cardinal and inter-cardinal directions, in order to assess precisely growth of impervious surfaces for each city. Urban development and the resultant ISA dynamics for both cities were examined for different five periods: the 1970s, 1980s, 1990s, 2000s and 2015.

4. 4. Results and analysis

Spatiotemporal dynamics of impervious surfaces in both study areas are presented in Figures 4.2 and 4.3 for Baghdad and 4.5 and 4.6 for Perth. Figure 4.4 for Baghdad and Figure 4.7 for Perth summarise quantitative measures of the amount and direction of the expansion of impervious surfaces over the course of the study periods.

The overall accuracy and kappa coefficient of the impervious surface maps, derived using the method in Section 4.3.1.3, ranged from 87% to 91% and between 0.75 and 0.83, respectively for Baghdad; and from 87% to 93% and between 0.73 and 0.85 for Perth (Table 4.2). User's accuracy and producer's accuracy of impervious and non-impervious categories ranged from 80% to 100% and 75% to 100% for Baghdad and from 79% to 100%, and 73% to 100% for Perth, further details for each year are presented in Appendix A. The accuracy of all impervious surface maps was above levels recommended by the USGS website; hence these results can be considered suitable for subsequent analysis.

Table 4.2 Accuracy assessment and kappa coefficient of the ISA maps for Baghdad and Perth cities.

	Baghdad			**Perth**		
	Year	Overall accuracy (%)	Kappa coefficient	Year	Overall accuracy (%)	Kappa coefficient
1	1976	88	0.75	1974	87	0.73
2	1984	91	0.83	1988	93	0.85
3	1992	87	0.75	1997	89	0.78
4	2000	90	0.80	2008	87	0.73
5	2015	89	0.77	2015	90	0.80

Impervious surface growth are presented in Table 4.3 and Table 4.4 for both study areas. The study area of Baghdad covers an area approximately 870.4 km^2. Impervious surfaces were estimated to be approximately 139.25 km^2, 229.82 km^2, 246.89 km^2, 257.04 km^2 and 301.16 km^2 in 1976, 1984, 1992, 2000 and 2015, respectively. During the periods of 1976–1984 and 2000–2015 Baghdad experienced a higher growth of impervious surfaces than the other periods (1984–1992 and 1992–2000).

In contrast to Baghdad, the study area of Perth covers an area of approximately 488.7 km^2. Estimated impervious surfaces areas were approximately 133.53 km^2, 161.36 km^2, 182.67 km^2, 191.62 km^2 and 202.20 km^2 in 1974, 1988, 1997, 2008 and 2015, respectively. It is apparent that impervious surfaces areas increased during the periods of 1974–1988 and 1988–1997 substantially more than the other periods (1997–2008 and 2008–2015).

Table 4.3 Area in km^2 and percentage of temporal expansion of ISA in Baghdad and Perth.

Baghdad			**Perth**		
Year	ISA (km^2)	ISA (%)	Year	ISA (km^2)	ISA (%)
1976	139.25	15.99	1974	133.53	27.32
1984	229.82	26.40	1988	161.36	33.01
1992	246.89	28.36	1997	182.67	37.37
2000	257.04	29.53	2008	191.62	39.20
2015	301.16	34.59	2015	202.20	41.37

There was significant expansion in impervious surfaces in both cities. In Baghdad, impervious surfaces increased from 139.25 km^2 (15.9% of the total area) in 1976 to 301.16 km^2 (34.59% to the total area) in 2015, with a total expansion of approximately 161.9 km^2 (18.6%). Perth's impervious surfaces also increased by 133.53 km^2 (27.3% of the total area) and 202.2 km^2 (41.37% of the total area) in 1974 and 2015, respectively. Expansion in the period from 1974 and 2015 was therefore approximately 68.67 km^2 (14.1%). At present (as of 2015) impervious surfaces covered approximately 34.6% of Baghdad and 41.37% of Perth metropolitan area.

Table 4.4 Rates of ISA expansion for Baghdad and Perth during the study periods.

Baghdad			**Perth**		
Year	ISA (km^2)	ISA (%)	Year	ISA (km^2)	ISA (%)
1976-1984	90.57	10.41	1974-1988	27.83	5.69
1984-1992	17.07	1.96	1988-1997	21.31	4.36
1992-2000	10.15	1.17	1997-2008	8.95	1.83
2000-2015	44.12	5.06	2008-2015	10.58	2.17
1976-2015	161.91	18.6	1974-2015	68.67	14.05

4.4.1. Spatiotemporal dynamics of ISA

Combining the maps of the impervious surfaces with the zones division was performed to determine the amount and direction of the expansion of ISA in each zone.

A more detailed analysis of the growth in impervious surfaces during each period and zone is described in the following sections for each city.

4.4.1.1. Baghdad city

The impervious surface maps of Baghdad city are shown in Figures 4.2 and 4.3, depicting the spatial distribution of ISA for each year and their directional changes. The figures indicate that impervious surfaces expanded at different rates and in different directions throughout the study period, moving from the city centre towards surrounding rural areas that were mainly comprised of high-density orchards, agricultural fields and pastures.

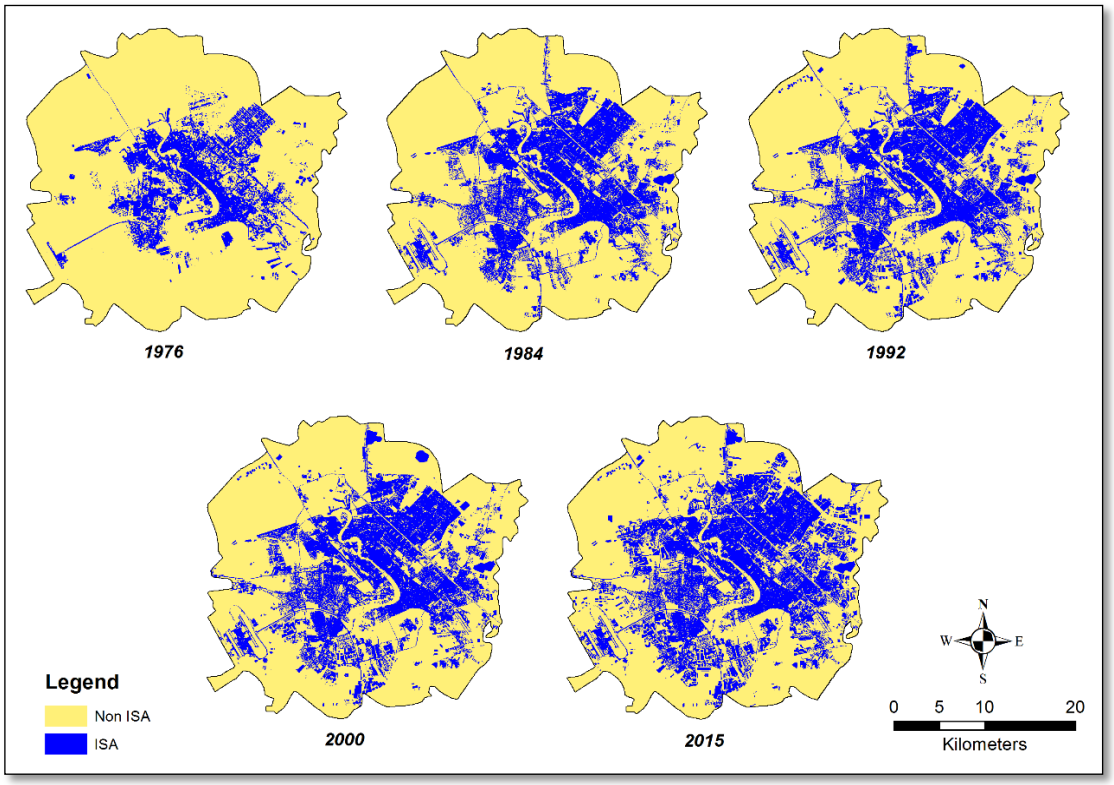

Figure 4.2 Impervious surface maps of Baghdad city, 1976 to 2015.

Figure 4.3 shows the directions of impervious surfaces. The greatest expansion can be observed in zones 1 (N–NE), 2 (E–NE) and 5 (S–SW).

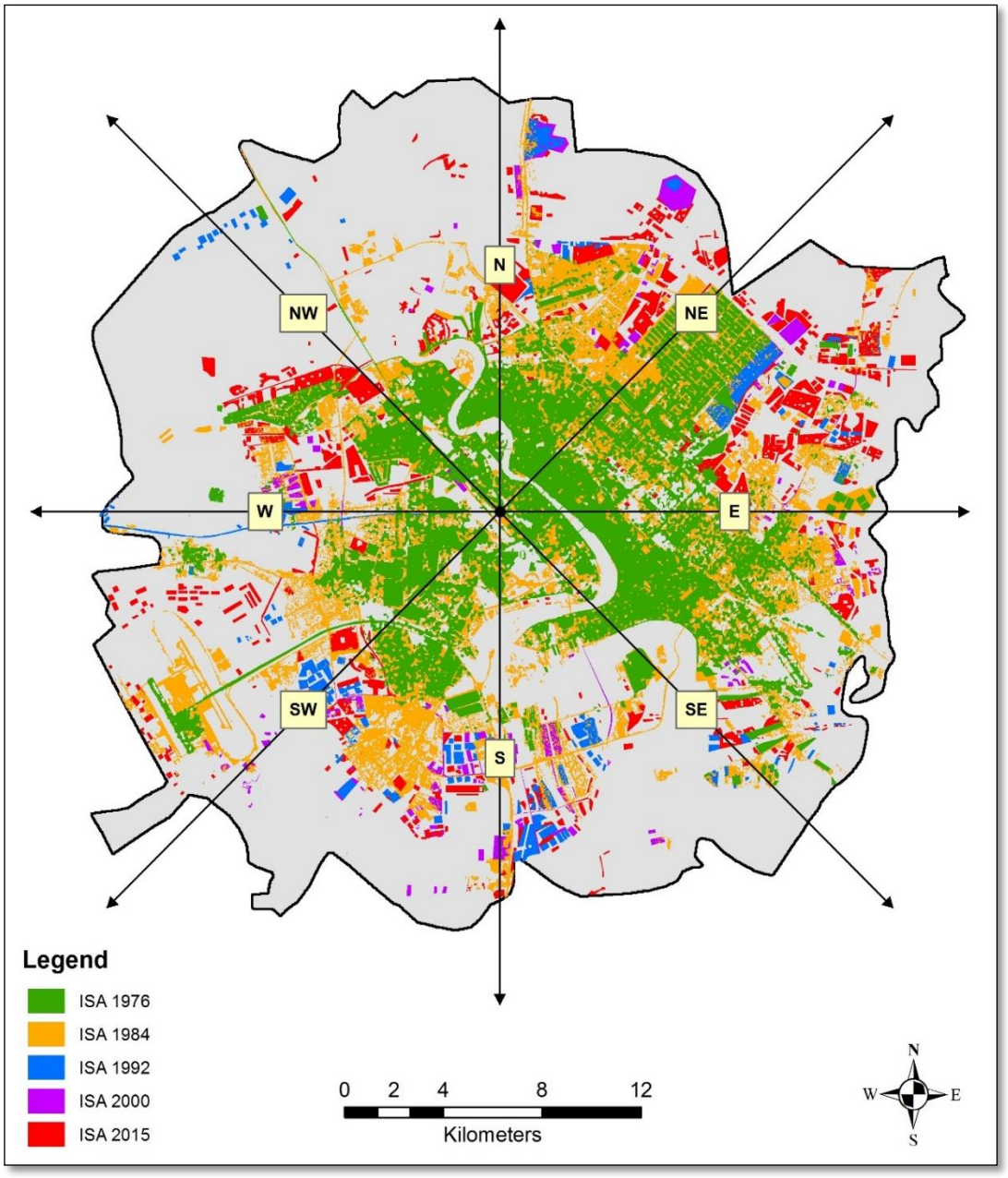

Figure 4.3 Spatiotemporal expansion of impervious surfaces in Baghdad, 1976 to 2015.

The amount and direction of impervious surface areas in Baghdad is also displayed in Figure 4.4. The spatiotemporal dynamics of ISA in each zone and direction appear to have different extents, over the various periods from 1976 to 2015. The proportion of ISA becomes greater over time, especially in the city core.

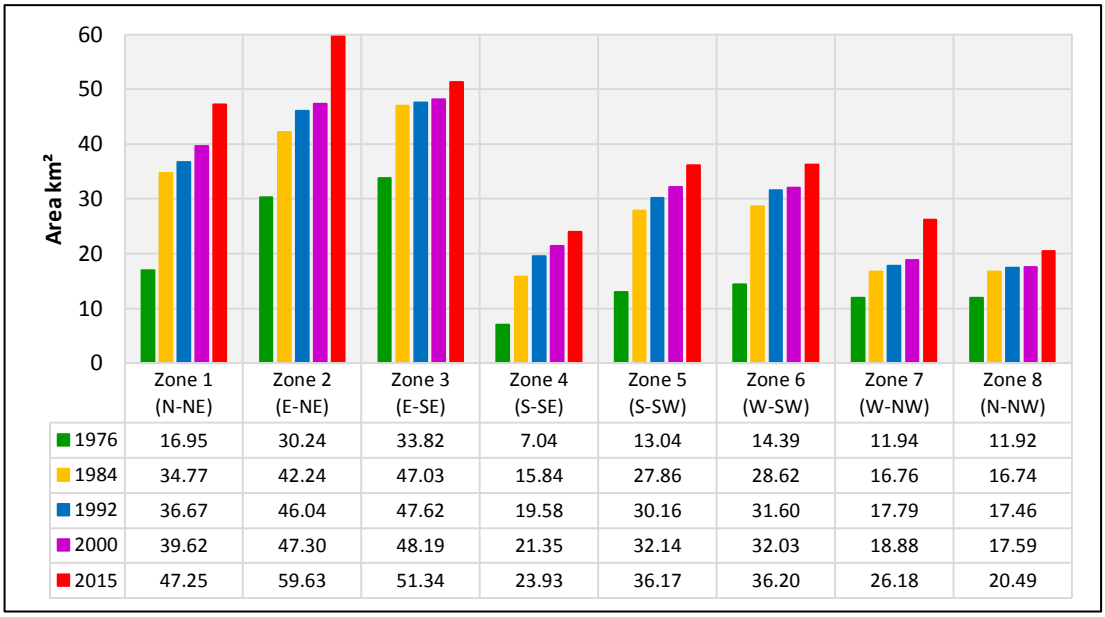

	Zone 1 (N-NE)	Zone 2 (E-NE)	Zone 3 (E-SE)	Zone 4 (S-SE)	Zone 5 (S-SW)	Zone 6 (W-SW)	Zone 7 (W-NW)	Zone 8 (N-NW)
1976	16.95	30.24	33.82	7.04	13.04	14.39	11.94	11.92
1984	34.77	42.24	47.03	15.84	27.86	28.62	16.76	16.74
1992	36.67	46.04	47.62	19.58	30.16	31.60	17.79	17.46
2000	39.62	47.30	48.19	21.35	32.14	32.03	18.88	17.59
2015	47.25	59.63	51.34	23.93	36.17	36.20	26.18	20.49

Figure 4.4 Growth in imperviousness in each zone (km^2) in Baghdad city, 1976 to 2015.

The spatiotemporal dynamics of impervious surface expansion in Baghdad can be summarised as follows:

- In the first period (1976–1984), Baghdad experienced a much greater increase in ISA, of approximately 90.57 km^2, compared with other periods. Considerable expansion occurred in all directions, but was most noticeable in zone 1 (N–NE), and to a lesser extent zones 5 (S–SW) and 6 (W–SW). Expansion was less in zones 7 (W–NW) and 8 (N–NW).

- In the second period (1984–1992), the expansion of ISA was 17.07 km^2, with the majority seen in zones 2 (E–NE; 3.8 km^2), 4 (S–SE; 3.74 km^2) and 6 (W–SW; 2.98 km^2).

- In the third period (1992–2000), ISA increased by approximately 10.15 km^2. This period had the lowest increase in ISA throughout the study period. Most of the ISA growth was observed in zone 1 (N–NE; 2.95 km^2), while zone 8 (N–NW; 0.13 km^2) had the lowest growth.

- The fourth period (2000–2015) covers the longest time span in the study period. Impervious surfaces grew from 257.04 km^2 in 2000 to 301.16 km^2 in 2015; this was apparent in all directions but by differing amounts. Significant growth

occurred in zones 2 (E–NE; 12.33 km^2), 1 (E–NE; 7.62 km^2) and 7 (E–NE; 7.3 km^2). Zones 8 (N–NW; 2.89 km^2) and 4 (S–SE; 2.58 km^2) had lower amount of growth.

4.4.1.2. Perth city

The spatiotemporal dynamics of impervious surface areas were evaluated in five different years: 1974, 1988, 1997, 2008 and 2015. Results of the changes in spatial extent of ISA for each year are shown on Figure 4.5. It may also be observed that ISA gradually expanded in different directions, as shown in Figure 4.6. A detailed statistical analysis of the growth of ISA is shown in Figure 4.7. Impervious surfaces in Perth city expanded from 133.5 km^2 in 1974 to 202.2 km^2 in 2015 but with a variety of expansion rates and directions over time.

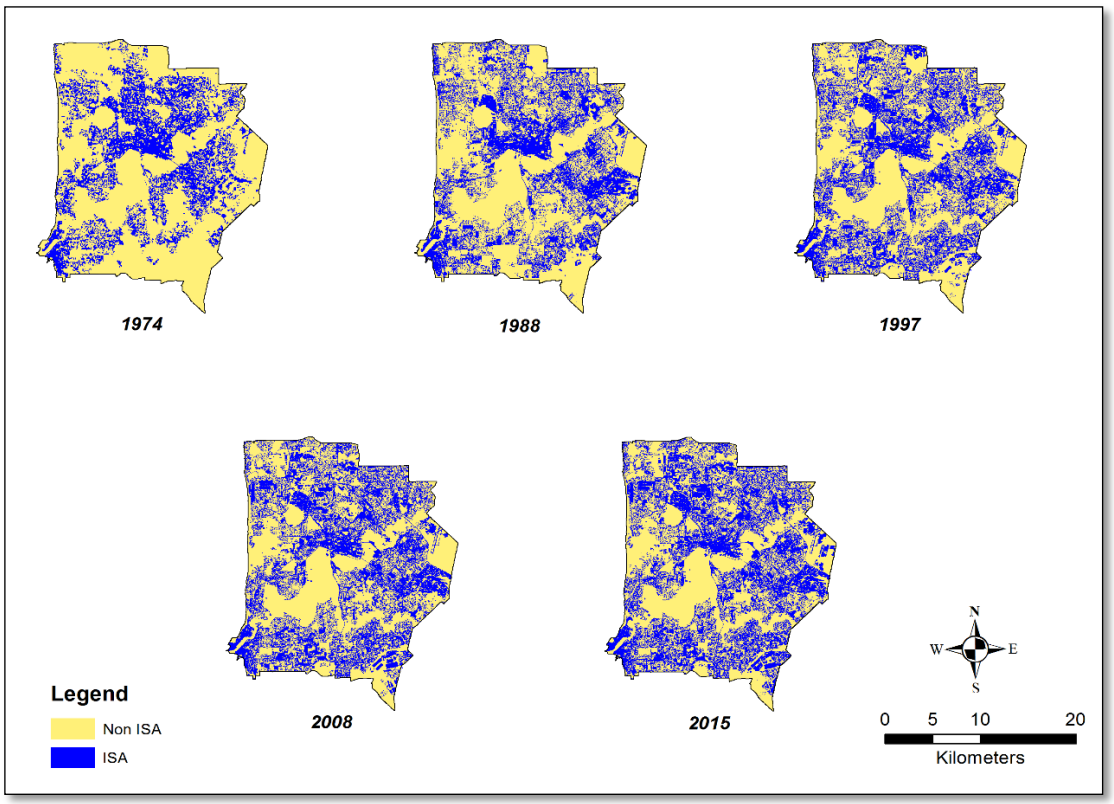

Figure 4.5 Impervious surface maps of Perth, 1974 to 2015.

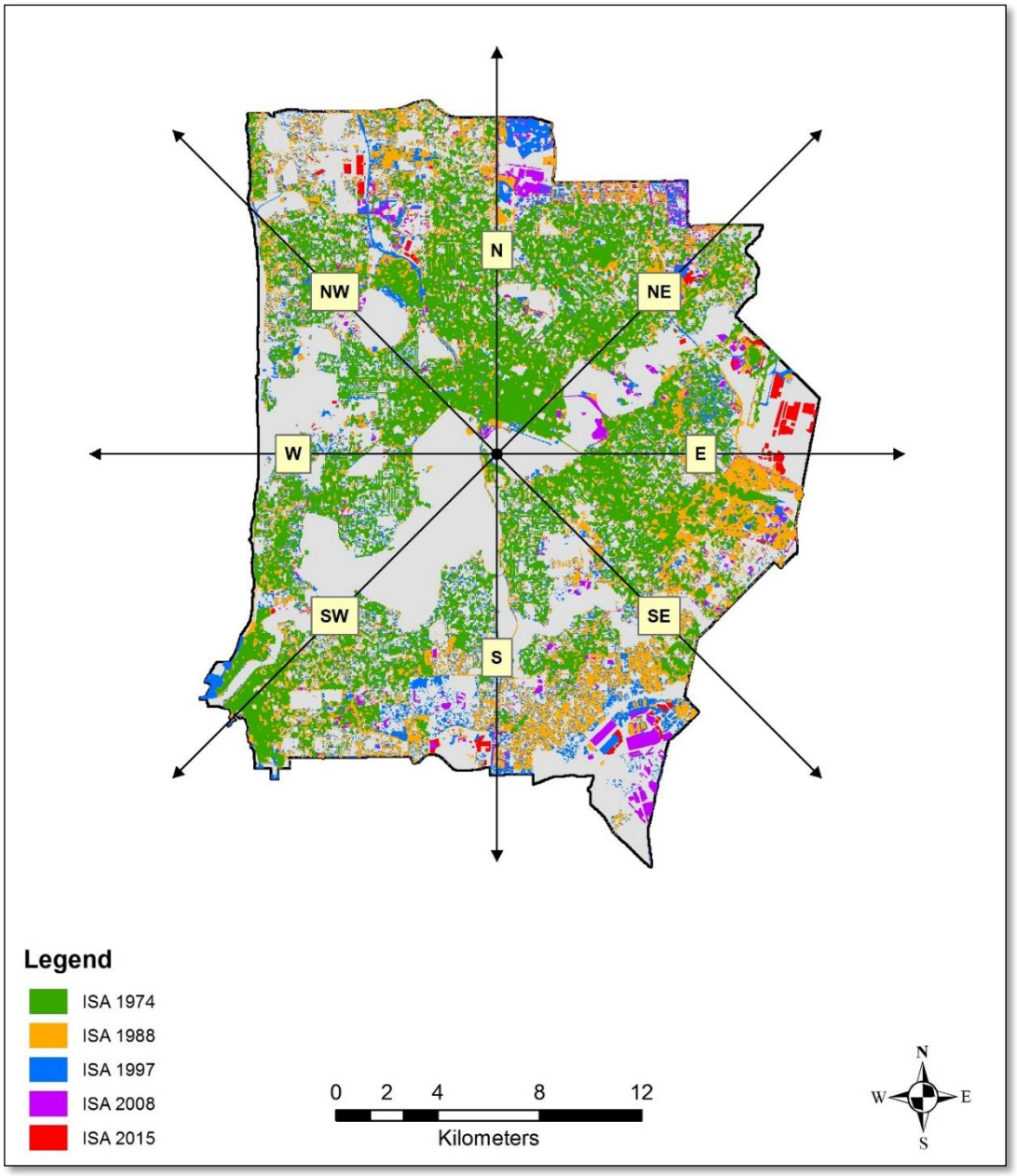

Figure 4.6 Spatiotemporal expansion of impervious surfaces in Perth, 1974 to 2015.

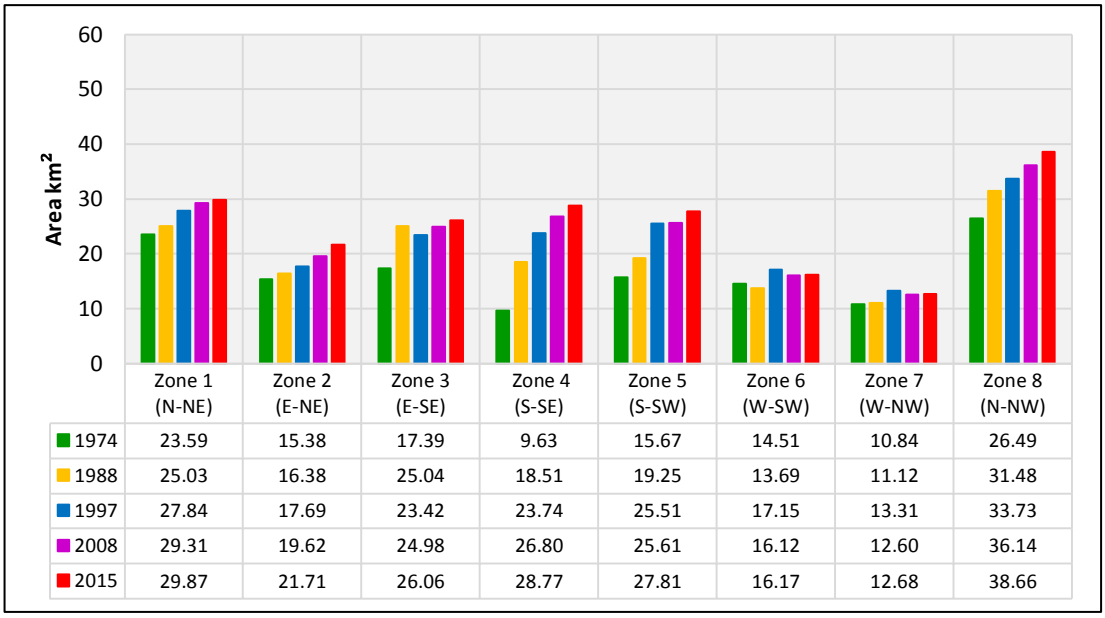

	Zone 1 (N-NE)	Zone 2 (E-NE)	Zone 3 (E-SE)	Zone 4 (S-SE)	Zone 5 (S-SW)	Zone 6 (W-SW)	Zone 7 (W-NW)	Zone 8 (N-NW)
1974	23.59	15.38	17.39	9.63	15.67	14.51	10.84	26.49
1988	25.03	16.38	25.04	18.51	19.25	13.69	11.12	31.48
1997	27.84	17.69	23.42	23.74	25.51	17.15	13.31	33.73
2008	29.31	19.62	24.98	26.80	25.61	16.12	12.60	36.14
2015	29.87	21.71	26.06	28.77	27.81	16.17	12.68	38.66

Figure 4.7 Impervious surfaces growth in each zone (km^2) in Perth, 1974 to 2015.

The results obtained from the analysis of the spatiotemporal dynamics of ISA growth in Perth are summarised below:

- In the first period (1974–1988), a substantial expansion of impervious surfaces (an increase of 27.83 km^2) was observed. The direction of the impervious surfaces growth was mostly distributed across zones of 4 (S–SE; 8.87 km^2), 3 (E–SE; 7.65 km^2) and 8 (N–NW; 4.99 km^2).

- In the second period (1988–1997), approximately 21.3 km^2 of land was converted to impervious surfaces, and the expansion was mainly located across zones of 4 (S–SE; 5.23 km^2) and 5 (S–SW; 6.26 km^2).

- In the third period (1997–2008), Perth experienced the lowest expansion of impervious surfaces, that of approximately 8.95 km^2. The majority of this growth occurred in zones 4 (S–SE; 3.06 km^2) and 8 (N–NW, 2.4 km^2).

- In the fourth period (2008–2015), impervious surfaces expanded to cover 202.2 km^2 (41.3%) by 2015, amounting to approximately 10.58 km^2. Impervious surfaces expansion was mainly located in zones 8 (N–NW, 2.52 km^2), 5 (S–SW, 2.2 km^2), 2 (N–NE, 2.09 km^2), and 4 (S–SE, 1.97 km^2).

4.4.2. Spatiotemporal variations of the LST pattern

The LST maps retrieved from Landsat data for the years of 1984, 1992, 2000 and 2015 for Baghdad city and the years of 1988, 1997, 2008 and 2015 for Perth city were employed to examine the spatiotemporal distributions of LSTs for both study areas.

In Baghdad, surface temperature increases were noticeable for built-up areas and bare lands, which had expanded significantly over areas that were previously categorised as vegetation. The variations of LSTs for bare lands and built-up areas were ranged from 44.1 °C to 51.9 °C and 42.3 °C to 49.8 °C, respectively over time, as well as to over space (Figure 4.8). Areas of water, and orchards with other vegetation cover corresponded to LSTs that were considerably lower than bare lands and built-up areas, ranging from 30.6 °C to 35.4 °C and 33.6 °C to 45.5 °C, respectively. The Tigris River passes through the middle of the city and a high density of orchards have been planted on both banks, particularly to the north and south. These low surface temperature areas decreased in extent as a result of ISA expansion.

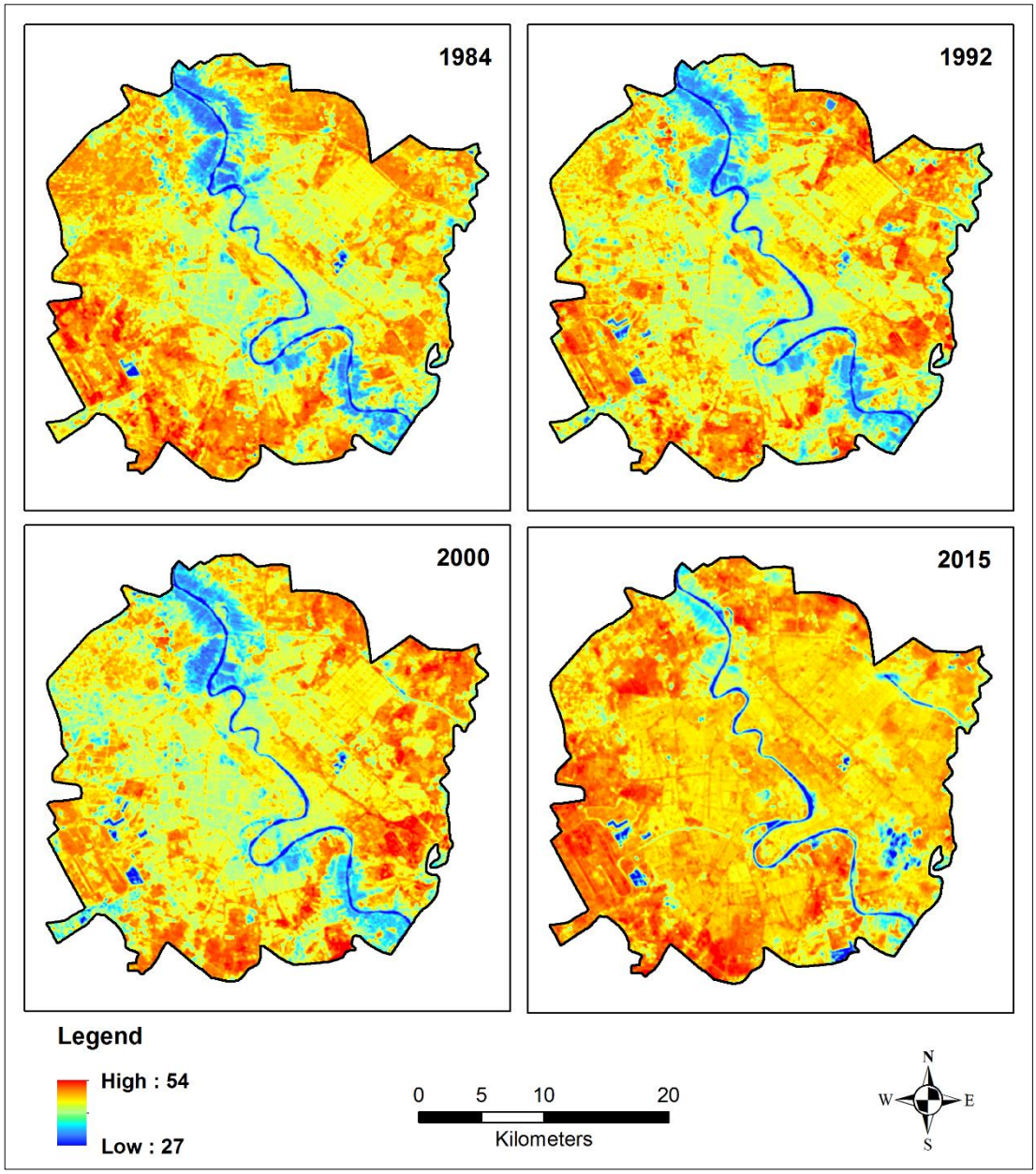

Figure 4.8 Thermal maps of Baghdad city for 1984, 1992, 2000 and 2015.

In comparison, Perth had smaller variations in LSTs between 1988 and 2015, with bare lands and built-up areas ranging from 34.5 °C to 38.7 °C and 31.6 °C to 36.2 °C, respectively over time (Figure 4.9). Changes in urban expansion over time seem to have had a negligible effect on LST. LST variation for the larger water bodies in Perth, including the Swan River, ranged from 25.1 °C to 26.8 °C, and from 29.9 °C to 32.1 °C for areas with vegetation cover.

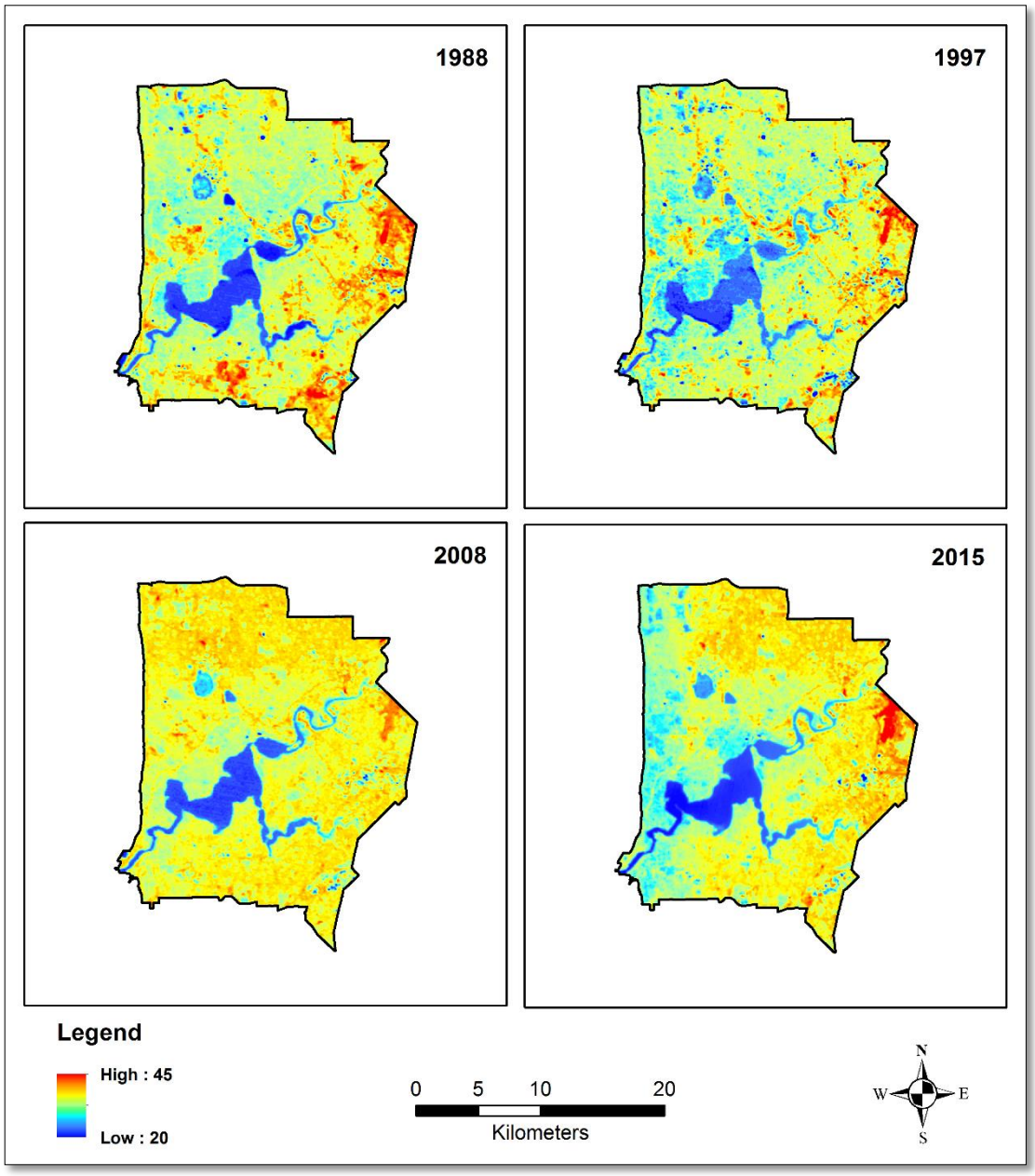

Figure 4.9 Thermal maps of Perth city for 1988, 1997, 2008 and 2015.

4.4.3. Temporal trend of SUHI intensity with impervious surface growth

The SUHI intensity was computed from LST data for all years, based on the difference between the average surface temperatures in urban areas and that in surrounding rural areas. The results show that the SUHI intensity of Baghdad was 7.26 °C, 8.28 °C, 7.9 °C, and 8.64 °C in 1984, 1992, 2000 and 2015, respectively. The maximum SUHI intensity was observed in 2015 (Figure 4.10 a).

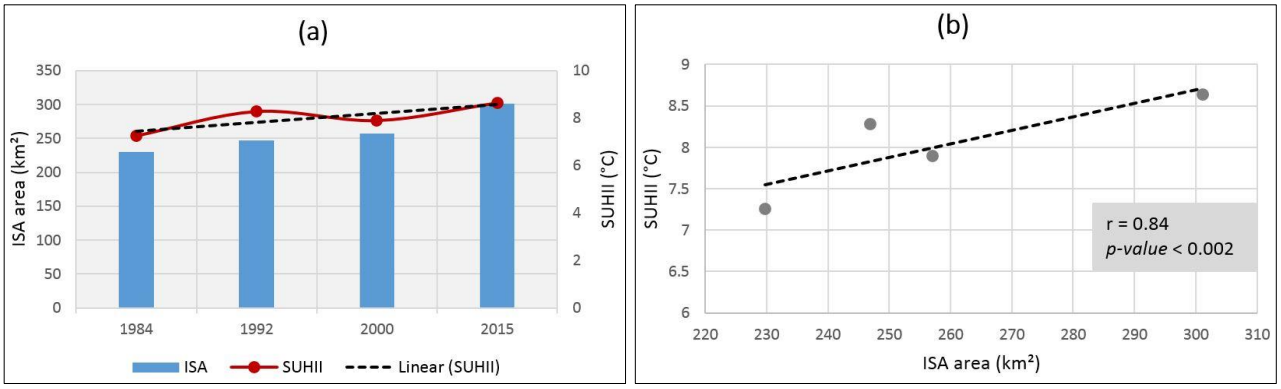

Figure 4.10 Relation between SUHII and impervious surface growth in Baghdad, 1984 to 2015.

For Perth, the results show that SUHI intensity was 2.86 °C, 2.93 °C, 3.01 °C, and 3.68 °C in 1988, 1997, 2008 and 2015, respectively. The increase of SUHI intensity was found to be about 0.82 °C between 1988 and 2015 (Figure 4.11(a)).

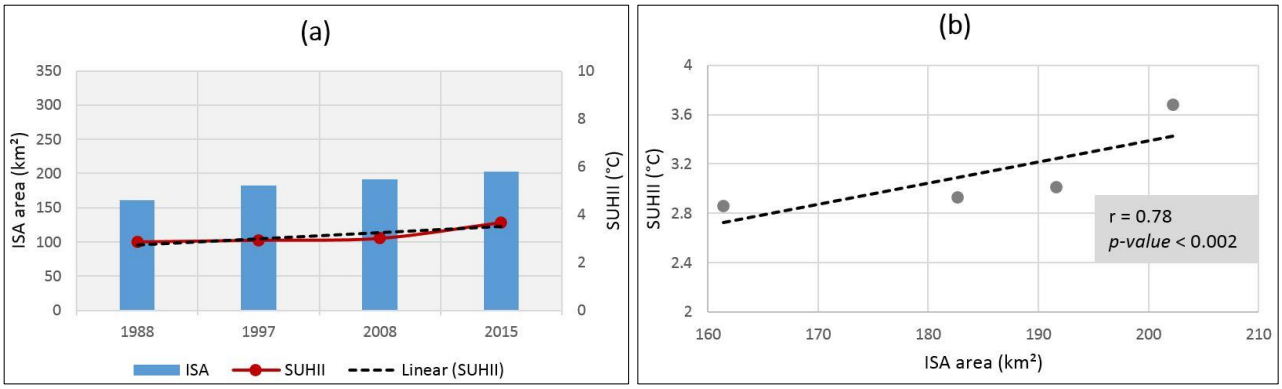

Figure 4.11 Relation between SUHII and impervious surface growth in Perth, 1988 to 2015.

The relationship between the UHI effect and city size was explored in earlier studies. This relationship was first examined by Oke (1973), who pointed out that UHI intensity is positively affected by the city size. A recent study also confirmed this (Li et al., 2017).

In this study, a comparison of SUHI intensity with impervious surface growth was examined as data related to other factors was not available at this time of this work. The analysis indicated that both cities experienced an increase in SUHI intensity with

an increase in impervious surfaces. For Baghdad, the SUHI intensity was 7.26 °C in 1984, and then increased to 8.64 °C in 2015, coincident with an increase in built-up area of 71.34 km^2 between 1984 and 2015 (Figure 4.10(a)). It may be seen that the trend line shows an increase in SUHI intensity for Baghdad city between 1984 and 2015 (Figure 4.10 a). Impervious surface area in Baghdad is positively correlated to SUHI intensity to a statistically significant degree ($r = 0.84$) (p-value < 0.002) for the SUHI intensity (Figure 4.10 b). In Perth, the SUHI intensity was 2.86 °C in 1988, and increased to 3.68 °C in 2015, coinciding with an increase in built-up area of 40.84 km^2 between 1988 and 2015 (Figure 4.11(a)). There is also a statistically significant (p-value < 0.002) positive relationship ($r = 0.78$) between SUHI intensity and ISA growth in Perth over this period (Figure 4.11(b)).

Although weather patterns (such as wind and cloud cover) and geographic location (climate and topography) can strongly influence the magnitude of urban heat intensity (EPA, 2014), expansion of impervious surfaces (i.e., various development forms and levels of urban pattern) has important role in SUHI intensity. For example, Zhang et al. (2012a) state that UHI magnitude was affected by the size and shape of the urban area, the spatial distribution of ISA within the urban area, and land cover composition of the surrounding rural area. Other studies (Tan & Li, 2015; Estoque & Murayama, 2017) showed that the intensity of UHI increased with concomitant growth in urban areas. Therefore, the influence of impervious surfaces expansion on SUHI intensity would appear to be a significant factor, despite larger-scale climatic and meteorological effects.

4.4.4. Seasonal variations of SUHI

Statistical details of daytime SUHII for each of the seasons (including winter, spring, summer and autumn), for both study areas in 2015 were assessed using LSTs. The results showed that the intensity of SUHI varies with the seasons in the two study areas.

In Baghdad, the mean value of LST pixels in the urban area was the highest in summer (50.05 °C), followed by spring (30.82 °C), autumn (30.45 °C), and winter (16.56 °C). Similarly, the highest mean LST values in the rural areas was found in summer (41.41

°C), followed by spring (25.35 °C), autumn (25.32 °C), and winter (14.52 °C). Based on the difference in LST for temperatures in urban and rural areas, SUHII was computed for all seasons. The results (Figure 4.12) showed that the highest SUHII was found in the summer season (8.64 °C), while the lowest SUHII occurred in the winter season (2.03 °C). The spring season was determined to have (5.47 °C) a slightly higher SUHII than the autumn season (5.14°C).

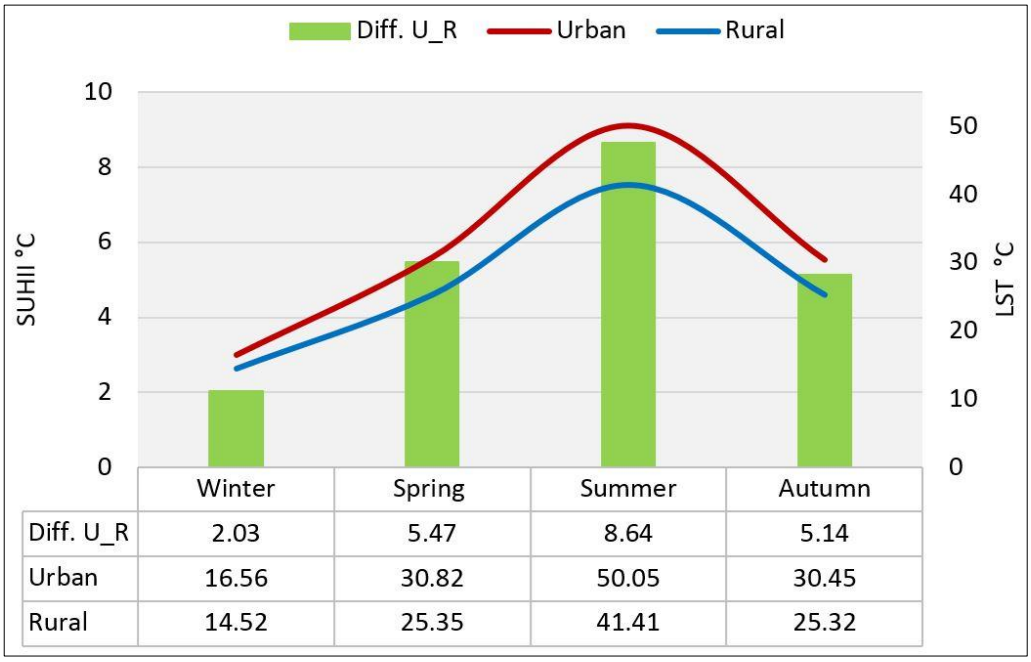

	Winter	Spring	Summer	Autumn
Diff. U_R	2.03	5.47	8.64	5.14
Urban	16.56	30.82	50.05	30.45
Rural	14.52	25.35	41.41	25.32

Figure 4.12 Seasonal variations of the daytime SUHII of Baghdad in 2015

In a similar trend to Baghdad, the LST of Perth varied with the seasons but with lower mean LST values for all seasons. The mean LST value in the urban area was the highest in summer (37.87 °C), followed by spring (34.99 °C), autumn (26.1 °C), and winter (15.13 °C). Similarly, the mean LST value in rural areas was highest in summer (34.19 °C), followed by spring (32.81 °C), autumn (24.33 °C), and winter (13.67 °C). The results (Figure 4.13) indicate that SUHII was highest in the summer season (3.68 °C), followed by the spring season (2.18 °C), the autumn season (1.77 °C), and lowest in the winter season (1.46 °C).

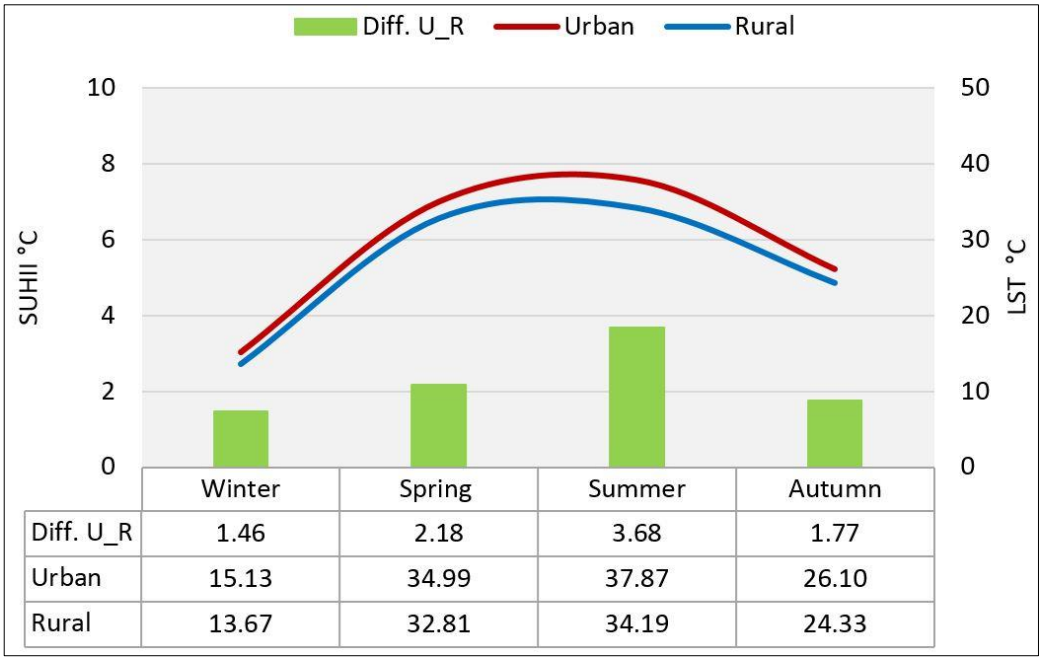

	Winter	Spring	Summer	Autumn
Diff. U_R	1.46	2.18	3.68	1.77
Urban	15.13	34.99	37.87	26.10
Rural	13.67	32.81	34.19	24.33

Figure 4.13 Seasonal variations of the daytime SUHII of Perth in 2015.

The observed seasonal variation in SUHII may normally be related to seasonal climatic weather conditions, which in turn depend on the geographical location for each city. According to Kim and Baik (2002), seasonal variation of UHI magnitudes are associated mainly with the differences in the weather conditions. Despite this, it may be noted that SUHII in Baghdad was significantly higher than Perth during all seasons, even though both cities recorded similar climate-related trends of the SUHII over the four seasons.

4. 5. Discussion

Both Baghdad and Perth cities showed significant growth in impervious surfaces, due to urban expansion, during the study periods. Land cover change has contributed to an increase in LST, as a result-increases in ISA appear to coincide with the change in temperature patterns of the two urban areas. Impervious surface area increased as urban space was converted from a mixed pattern of impervious and other land cover types, mainly from green areas to built-up categories. As a result, the spatial form and patterns of the two cities were changed. The analysis shows that urban impervious surface expansion was not concentrated in all directions and was variable during the

study periods. The pattern of impervious surface expansion was driven for each city by various reasons, which can be summarised as follows.

In Baghdad, fluctuations in the rate of urban growth may be attributed to factors such as political infighting, bursts of economic development, and population increase. Although population in Baghdad changed in response to political and economic conditions, the average annual rate of population growth during the study period was approximately 2.7 per cent, which increased pressure on existing land use. However, factors, both encouraging and hindering the urban growth of Baghdad, varied in each time period. For example, during the first period (1976–1984) rapid urban expansion occurred in parallel with economic growth of the petroleum sector (United Nations, 2001). A reduction in urban growth during the second period (1984–1992) possibly related to the Iraqi-Iranian war that took place mainly during this period, during which the bulk of the Iraqi budget was apportioned to the armed forces, and thus infrastructural development was mainly neglected (United Nations, 2001; Nordhaus, 2002). Economic deterioration due to the Gulf war and subsequent economic sanctions resulted in the lowest rate of urban growth during the third period (1992–2000) (Nordhaus, 2002). Consequently existing built-up areas came under intense pressure as people migrated from surrounding rural areas and other provinces to the capital in search of work. Finally, despite political infighting during the period of 2000–2015, a remarkable degree of urban growth occurred, which was linked to economic development, population growth, and attempts to redress the shortage in housing and infrastructure (Gunter, 2013). In 2015, the Ministry of Construction and Housing for Baghdad stated that there was a serious crisis in housing. They identified that around 380,000 houses were required to accommodate the growing population. Many large slums were built over vacant lands in addition to buildings constructed over areas that were previously residential garden lots, and therefore the growth of built-up areas intensified. All these circumstances and factors were influential in reshaping the urban fabric of Baghdad.

On the other hand, Perth generally experienced more stable urban growth, especially after World War II. The increase of urban areas in Perth city reflected the outcome of robust urban management plans developed by the city authorities, and enforced regulations in the housing sector. However, variation in urban growth still occurred,

mainly resulting from economic development. Other factors also had a considerable effect on Perth's urban development, including population growth from both internal and overseas migration, growth in the mining sector, investment in real estate, and the development of tourism. Mining played an important role in boosting the economic growth of Western Australia (Pham et al., 2013), and was one of the prime factors influencing urban development. As urban dynamics are strongly linked to population dynamics (Moghadam & Helbich, 2013), Perth's urban growth was also the result of the natural population increase due to births exceeding deaths and overseas migration that occurred in roughly equal proportions (Connoley, 2013), although the population growth rate varied in each period. The city's population has increased substantially in the last few years, but only 42% live in the central sub-region (Table 4.5).

Table 4.5 The distributions of Perth's populations in 2012 (UDIA calculations, ABS 3218.0).

Sub-regions	Estimated populations	Share of Perth population
Central	672,857	42.4%
North-West	240,733	17.6%
North-East	169.447	11.4%
South-East	147.786	10.8%
South-West	165.351	13.0%
Peel	59.895	4.8%

Economic migrants and students can be considered as the main drivers of Perth's economic growth (Colebatch, 2016). The first period (1974–1988) experienced a remarkable increase in impervious surfaces followed by rapid economic growth in the mining sector. According to Yiftachel and Hedgcock (1993), central Perth experienced massive urban development during the early 1970s, for example, 250,000 m2 of office floor space was added between 1977 and 1984 and central city parking spaces increased by 16,800 bays between 1971 and 1986. The city experienced a massive office development boom again in the middle of 1980s (Yiftachel & Hedgcock, 1993). Between 1988 and 1997, the growth of impervious surfaces continued, but the rate was not so high. Between 1997 and 2008 impervious surfaces had lowest growth rate among the study periods. It is possible that this decline in urban expansion may be explained by renewal projects that focused on derelict or redundant land on

waterfronts, on old industrial buildings, old bond stores and former railyards, particularly in the East Perth project (O'Connor et al., 2001). It also might be explained as a response to the uncertainty associated with the decreased average annual population rate, the lowest during this period being 1.8% between 1991 and 1996 and 1.6% between 1996 and 2006 (Connoley, 2013). During 2008–2015, the city again experienced growth in impervious surfaces, probably related to an increase in mining activities and results of other economic development. Population also gradually increased to an annual average of 3.1% in 2006–2011 and 3.4% in 2011–2012 (Connoley, 2013).

Regarding to the relationship between SUHII and the growth of built-up areas, Figures 4.10 and 4.11 show that SUHII is positively correlated to impervious surface growth. The high growth of ISA in Baghdad, in comparison to Perth (Tables 4.3 and 4.4), may have led to higher magnitudes of SUHI, particularly in summer daytimes. This is consistent with previous studies in which urban expansion has been shown to boost SUHI effects (Yuan & Bauer, 2007; Yu & Lu, 2014). This is also consistent with the higher urban LST in Baghdad, as compared with its rural LST.

Although different magnitudes of the intensity of the SUHI were found between the two cities for each season, a trend of the seasonal variations for both cities was similar (i.e., high in summer and low in winter). This may be related to the fact that the differences in the seasonal weather conditions and fluctuations in both cities.

SUHI in Baghdad was found to be higher than that of Perth. In general, city form, building patterns, and the composition and configuration of LULC features may have contributed to this contrast between the two cities. Urban planning and management may therefore have played an important role in developing SUHI, since political and socio-economic conditions have been influential factors on the form and pattern of urban development (Davis, 2016). This finding is in agreement with another study that found that unplanned and uncontrolled rapid growth causes serious negative effects on urban environments (Chadchan & Shankar, 2012).

Increasing LST values in urban areas are possibly linked with urban expansion and the decrease in vegetation cover over time, and hence a developing in SUHI. This is apparent in the city of Baghdad, which experienced significant changes in its LULC

categories over time, as more buildings, using heat-retaining building materials, were added. Meanwhile, since 2003, the city of Baghdad has experienced widespread growth of unplanned housing (urban slums) (Figure 4.14). Slums and informal settlements in the city of Baghdad have been recently created as a result of the war and subsequent insurgency in Iraq since 2003, with consequences including security problems, sectarian displacement and tribal conflicts. Migration from rural areas to the capital city of Baghdad, due to lack of work and extreme housing crises, was also a contributing factor toward the growth of slums. Another important factor resulting from the absence of monitoring and follow-up by relevant governmental entities has been the dredging of agricultural land and its resale. According to a report by the Ministry of Planning and the United Nations Human Settlements Programme (UN-Habitat) (Miran, 2017), more than 1000 settlements were created in Baghdad after 2003 and this number is increasing as a result of the aforementioned causes. Recent studies (e.g., Scott et al., 2017) pointed out that temperature in informal settlements increased by several degrees Celsius as a result of their density and lack of vegetation cover. Therefore, slums and informal settlements, which represent large areas of impervious surfaces with heat-retaining building materials, may have negatively contributed to developing the SUHI in Baghdad.

Figure 4.14 Urban slums in Baghdad (Source: Google images).

In addition to slums and informal settlements, man-made activities such as private and shared electricity generators, which have been widely used in Baghdad (Figure 4.15) may also be accountable for increasing LST.

Figure 4.15 Typical electricity generators used in Baghdad (Source: Google images).

Use of these generators may introduce thermal pollution, which may be a contributing factor to an increase in LST. More than 10,000 electricity generators of different sizes are being used in Baghdad province, based on data released from Baghdad Provincial Council (2015). Furthermore, high density residential areas have more generators than low density ones. Hot summer days result in significant daytime generator use and increased thermal emissions across the city, which contributes to both environmental and health issues (Al-Waeely et al., 2014).

In Perth, regulations on city planning and management, relating to urban greening and the kinds of building materials used, may have positively contributed to more environmentally-sustainable urban development. In addition, the nature, distribution, and intensity of green cover may have had a significant effect on the magnitude of SUHI.

In summary, the fact that the average intensity of SUHI (SUHII) in Baghdad is higher than Perth may partly be related to differences in urban form, landscape pattern, types of building and paving materials, and regulations in city planning. This may be also attributed to large green spaces and higher density of vegetation cover, as well as its distribution, throughout the city of Perth. In addition, the majority of houses in Perth

are designed for a single family and are also relatively covered by trees, compared with the city of Baghdad. These factors will be analysed and discussed in more detail in the next two chapters.

4. 6. Chapter summary

Information about patterns of urban growth via the measurement of impervious surfaces during the past few decades is important, particularly when it sheds light on related environmental issues. In this chapter, the spatiotemporal development of impervious surfaces in two cities, Baghdad and Perth, was quantified using multi-date Landsat data. The results showed that overlaying ISA maps and then dividing into eight zones is a powerful approach in monitoring urban development, since it supports the precise determination of the amount and direction of the growth of impervious surfaces in each zone. In both cities, impervious surfaces expanded noticeably; however, the rate of increase fluctuated in response to different specific circumstances. The analysis showed that the area of impervious surfaces in Baghdad increased by 18.6% (161.9 km^2) from 1976 to 2015, while an increase of about 14.1% (68.6 km^2) from 1974 to 2015 was estimated for Perth. The analysis provides useful information about patterns of impervious surfaces in different periods for the two cities. This information is therefore useful for a better understanding of how both cities have developed over time. These results are important in identifying the composition and configuration of urban landscape patterns and the characteristics of urban cover surfaces which appear to have effect on urban thermal environments.

5. Spatial pattern of urban landscape and its relation with LST

5. 1. Introduction

Rapid urban expansion appears to have an effect on urban climate (Fall et al., 2010; Hamdi, 2010) and on the overall environment (Svirejeva-Hopkins et al., 2004), including urban ecosystems (Jones et al., 1990; Turner, 1994) and hydrological systems (Konrad & Booth, 2002; Jacobson, 2011). Increasing surface and air temperatures are the most serious impacts of rapid urban expansion (Oke, 1987). The spatial distribution and configuration of an urban landscape such as buildings, green spaces, and water bodies are the key drivers affecting the urban thermal environment (Kottmeier et al., 2007; Bao et al., 2016).

Satellite imagery has been widely used to assess urban environments. Impervious surface area (ISA) and land surface temperature (LST) are recognised as main indicators in assessing the effect of an urban environment (Lu & Weng, 2006). These parameters can be easily quantified, and may help to address environmental problems caused by urban growth (Arnold Jr & Gibbons, 1996; Rashed et al., 2001).

Numerous studies have been conducted for mapping impervious surface area using Landsat data (Wu & Murray, 2003; Lu & Weng, 2006; Deng et al., 2012). Yuan and Bauer (2007) and Weng and Lu (2008) for example demonstrated that LST is positively correlated with impervious surface area (ISA). Meanwhile, the LST intensifies with the enhancement of built-up cover; similarly, LST is negatively correlated with vegetation cover in an urban area.

The urban heat island (UHI) effect can be intensified by the loss of vegetation cover resulting from urban expansion. As urban area expands, land use diversity and landscape fragmentation take place that can produce adverse environmental impacts (Weng, 2007; Shrestha et al., 2012). In contrast, the introduction of urban vegetation with appropriate distribution (Dimoudi & Nikolopoulou, 2003; Bao et al., 2016), combined with the presence of water bodies (Manteghi et al., 2015), can reduce temperature within an urban climate.

While the previous chapter has analysed and quantified spatiotemporal developments of impervious surfaces in Baghdad and Perth during the study periods, the overall aim of this chapter is to understand the extent to which the urban thermal environment is influenced by the spatial patterns of land use and land cover (LULC) features.

Specifically, the objectives of this chapter are:

1) to quantify the spatial distribution of major land use and land cover categories;
2) to determine the intensity of impervious surfaces;
3) to examine the relationship between the proportion of impervious surface area and land surface temperature; and
4) to explore the effect of the spatial pattern of urban landscape on LST.

5. 2. Datasets and methods

5.2.1. Datasets

In this chapter, Landsat 8 (OLI and TIRS) data during summer of 2015 were used (as described in Section 3.2.1).

5.2.2. Urban cover classification

Urban cover maps were prepared from Landsat images for both study areas for the period of summer of 2015. A hierarchical image classification was used to classify study areas into four main land use and land cover categories, including built-up area (ISA), green surface, bare land and water. The hierarchical method calculates each category separately. Firstly, water bodies were estimated using the modified normalised difference water index (MNDWI) (as described in Section 4.3.1.1). Secondly, built-up area was extracted using ISA techniques (as described in Section 4.3.1.2). Thirdly, vegetation cover was determined using the normalised difference vegetation index (NDVI), which is used to describe vegetation characteristics such as green biomass and chlorophyll content. NDVI is calculated using red (0.63–0.69) and

near infrared (0.77–0.89) bands from Landsat images (Equation 5.1) and its value ranges from (-1 to 1) (Rouse Jr et al., 1974; Tucker, 1979; Tucker et al., 1985).

$$\mathrm{NDVI} = \frac{(\rho(\mathrm{NIR}) - \rho(\mathrm{Red}))}{(\rho(\mathrm{NIR}) + \rho(\mathrm{Red}))} \quad (5.1)$$

Where:

ρ (Red) is the spectral reflectance of red band

ρ (NIR) is the spectral reflectance of near infrared band

Threshold values greater than 0.2 were used to determine vegetation cover using NDVI. The resultant image was reclassified and converted to polygons, and masked from the image as a separate category. Finally, based on a vector boundary file, the three categories, water, ISA and vegetation cover were clipped so that the remaining pixels represented the category of bare land only.

5.2.3. Calculation of PISA and ISAT

Percent impervious surface area (PISA) is a useful parameter for investigating impervious surface cover, and its utility to examine the effect on the quality of urban environments was first shown by Arnold Jr and Gibbons (1996). In this study, a grid with a cell size of 100 × 100 m was created to match the spatial resolution of TIR Landsat 8 image for subsequent analysis. This grid was overlaid with ISA maps to compute percent impervious surface area of each cell using ArcGIS 10.2 software (ESRI, 2013). A PISA map was prepared to show the percent impervious surface of the total area. The outcome of this operation ranges between 0 and 100%. The PISA maps were calculated for built-up areas using ISA maps that described in Section 4.2.2.2.

Map generation using the impervious surface analysis tool (ISAT) was carried out in several steps: the first was to generate a grid with a cell size of 100 × 100 m over the study area with a unique identifier; the second was the calculation of percentage impervious surface area within each grid cell; the third was the calculation of imperviousness coefficients based on major land use/land cover categories (i.e., high

(impervious surfaces), moderate (vegetation), and low (water and bare-land)); finally, the fourth step was to implement the tool using the above coefficients, as suggested by NOAA Coastal Services Center (2013). The output provides three categories, defined as low (1–10), medium (10–25) and high intensity (25–100) development. The results may be used to evaluate and predict the impact of impervious surfaces on the local environment. In this work, ISAT is only used to describe the distribution and amounts of impervious surfaces using low, medium, and high intensity values in the two study areas. Hence, the information derived from this tool is useful and may enhance our understanding with regard to the effect of impervious surfaces on the land surface temperature patterns.

The relationship between PISA and LST was examined for two cities, Baghdad and Perth. A grid was generated over the study areas with a dimension of 100 × 100 m, to match the original spatial resolution of the thermal data. Therefore, the value of each grid cell represents the mean value of approximately nine pixels (30 × 30 m spatial resolution) for the impervious surface data. Sampling at higher of 500 and 1000 points per area did not improve the resulting correlations for relationships under investigation. Therefore, 100 sample grid points were considered to a sufficiently rigorous sample to evaluate the relationship between PISA and LST. These samples were randomly distributed over parts of the study areas that contained impervious surface footprints. The sample locations were then used to extract precise values from the PISA maps and LST maps.

5.2.4. Landscape metrics calculation

Based on the urban LULC maps derived from the Landsat 8 image, landscape metrics were calculated to quantify the spatial pattern of urban landscape for each city. A number of landscape metrics have been developed to measure and describe the spatial patterns of landscapes. These metrics have been extensively employed to study ecological quality (McGarigal et al., 2002), but are not commonly used to assess urban thermal environments. However, landscape metrics are generally used as ecological variables to understand the interaction of spatial patterns of land use with the environmental and ecological process (Turner et al., 2001; Wu et al., 2014).

Overall, addressing a particular objective, independent of the metrics, and scale of analysis, as well as comparison of two or more different landscapes, can be considered as criteria for the selection of an appropriate landscape index (Turner et al., 2001). Therefore, selection of landscape metrics was made based on previous studies, which meet these criteria, to determine changes in landscape spatial and temporal patterns (Jai & Zeng-Xiang, 2003; Siyuan et al., 2007).

Yang et al. (2017) demonstrated that urban landscape patterns are considered to be one of the most important factors relevant to surface urban heat islands. Therefore, in this chapter, a set of landscape metrics, including Shannon's diversity index (SHDI), Shannon's evenness index (SHEI), the Modified Simpson's Evenness Index (MSIEI) and patch density (PD) (Table 5.1) were used to analyse urban landscape patterns, and subsequently, to examine their influence on the LST pattern for both cities. These landscape metrics were derived from the major land use and land cover categories, and the values of each index were calculated based on a 100×100 m grid cell size.

In some previous studies, these metrics have been named differently. Recently, a number of studies (e.g., Jai & Zeng-Xiang, 2003; Wang et al., 2003; Siyuan et al., 2007; Wang et al., 2009) have referred to these metrics as the landscape diversity index (H), landscape dominance index (D), landscape homogeneity index (E), and landscape broken index (C), respectively. However, in this work the original spatial metrics have been adopted and are briefly defined below:

- Shannon's diversity is one of the most commonly-used metrics for measuring landscape diversity. "Diversity" refers to how evenly the proportions of land cover types are distributed (O'Neill et al., 1988; Turner et al., 2001).

- The Shannon's index of evenness is probably the most widely-used measure of dominance in landscape. "Dominance" is the extent to which a few land cover types dominate the landscape (Griffith et al., 2002).

- Modified Simpson's Evenness Index (MSIEI), which is a metric that considers only the evenness of patch sizes and not the number of patches, may be used to measure homogeneity in a particular landscape (Schindler et al., 2008). "Homogeneity" refers to the degree to which landscape is controlled by a few patch types (Wang et al., 2009).

- Patch density is a metric of landscape structure used to measure the areal density of landscape patches. It measures the spatial heterogeneity of a given landscape through the number of patches per unit area of LULC categories (Zhang et al., 2015).

Table 5.1 Descriptions of the four selected landscape metrics (McGarigal et al., 2002).

Metric	Description	Computing equation	Range
Shannon's diversity index (SHDI)	Equals minus the sum of the proportional abundance of each patch type multiplied by the Ln of that proportion	$\mathrm{SHDI} = -\sum_{i=1}^{m} P_i \times \ln P_i$ Pi: proportion of landscape in cover type i ; m: the number of different patch types	SHDI ≥ 0
Shannon's evenness index (SHEI)	Equals minus the sum of the proportional abundance of each patch type multiplied by that proportion, divided by the Ln of the number of patch types	$\mathrm{SHEI} = \frac{-\sum_{i=1}^{m} P_i \ln(P_i)}{\ln m}$ *Pi:* Proportion of landscape in cover type *i; m:* the number of different patch types	0 ≤ SHEI ≤ 1
Modified Simpson's Evenness Index (MSIEI)	Equals minus the Ln of the sum of the proportional abundance of each patch type squared, divided by the Ln of the number of patch types	$\mathrm{MSIEI} = \frac{-\ln \sum_{i=1}^{m} (P_i)^2}{\ln m}$ Pi: proportion of landscape in cover type i ; m: the number of different patch types	0 ≤ MSIEI ≤ 1
Patch density (PD)	Equals the number of patch types (i.e. land cover categories) in the landscape, divided by the area of that landscape	$\mathrm{PD} = \mathrm{N}/\mathrm{A}$ N: the number of different patch types; A: total landscape area	PD > 0

5. 3. Results

5.3.1. Urban LULC classification

The urban LULC classification conducted for both Baghdad and Perth cities provides an overview of the urban landscape for one period of time (summer 2015), as well as comparable information on the spatial distribution of LULC categories. The hierarchical method used to calculate each LULC category provided a reasonably accurate representation of the actual land cover distribution for each study area. The accuracy of the classified maps for 2015 was assessed using the method described in Section 4.3.1.3. The overall accuracy and kappa coefficient were 79% and 0.69 for Baghdad and 88% and 0.83 for Perth, respectively. User's accuracy and producer's accuracy for each category and each city are presented in Appendix A. Built-up and man-made surfaces (ISA) are represented in red. Green areas represent orchards, agricultural fields, and vegetation, while blue represents water category (e.g., rivers/streams and artificial lakes). Areas of bare land (open space without artificial and vegetative cover, and cultivated land) are shown in yellow.

The classification maps revealed that the distribution of LULC categories within the core of Baghdad city was dominated by impervious surfaces within the high density built-up area, while vegetated areas are located around the city margins. Green surfaces occurred mainly in the northwest, southwest, and southeast as agricultural areas, and along both sides of the Tigris River. Bare land category in Baghdad is mostly distributed within and around the built-up area (Figure 5.1).

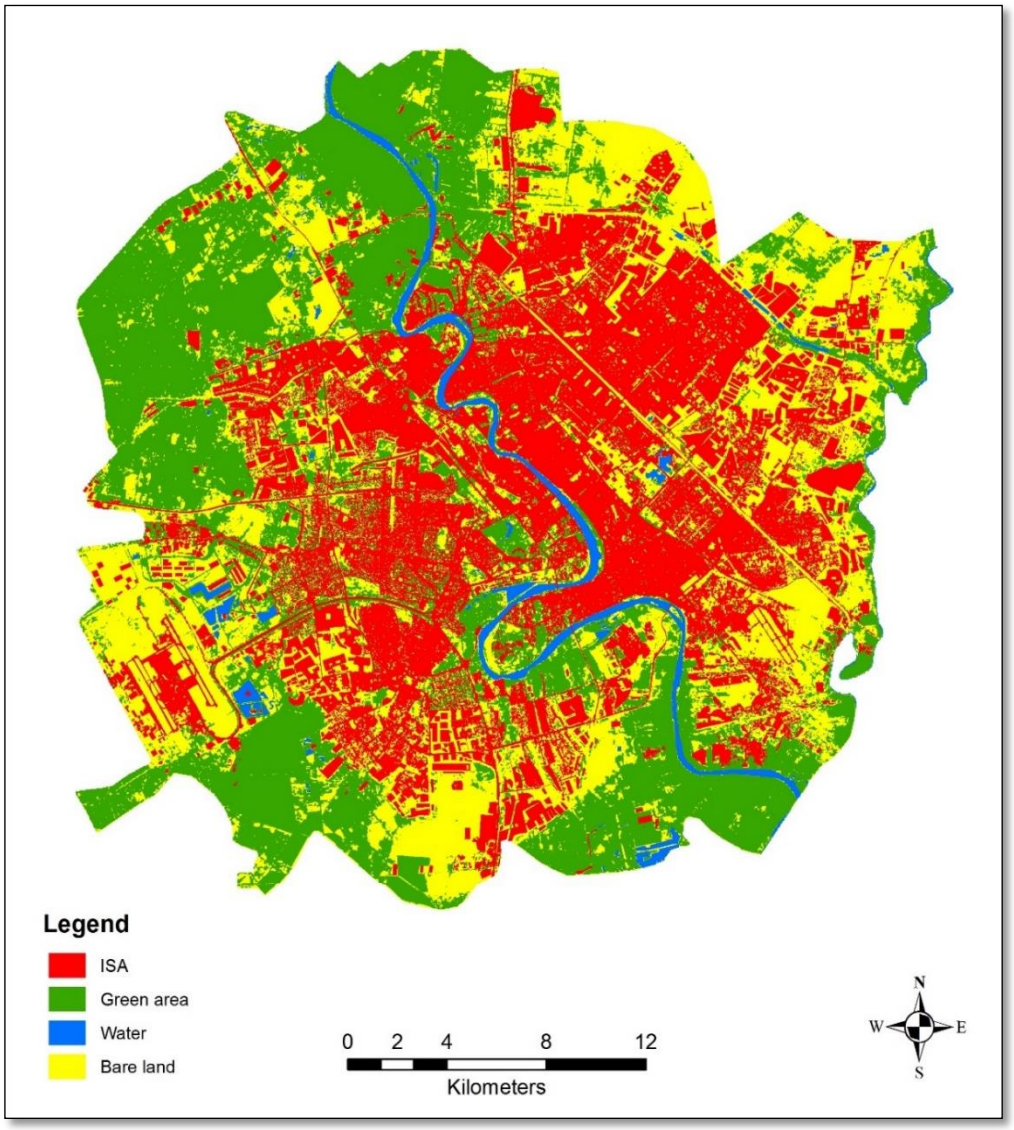

Figure 5.1 Major land use and land cover categories in Baghdad, 2015.

In Perth, it is observed that green space occupied the largest area, while bare land category occupied a very small portion of the city (Figure 5.2). Since the water bodies cover a large area, Perth perhaps has a tendency for having more green space near the coast, on the dune fields, and around rivers and lakes.

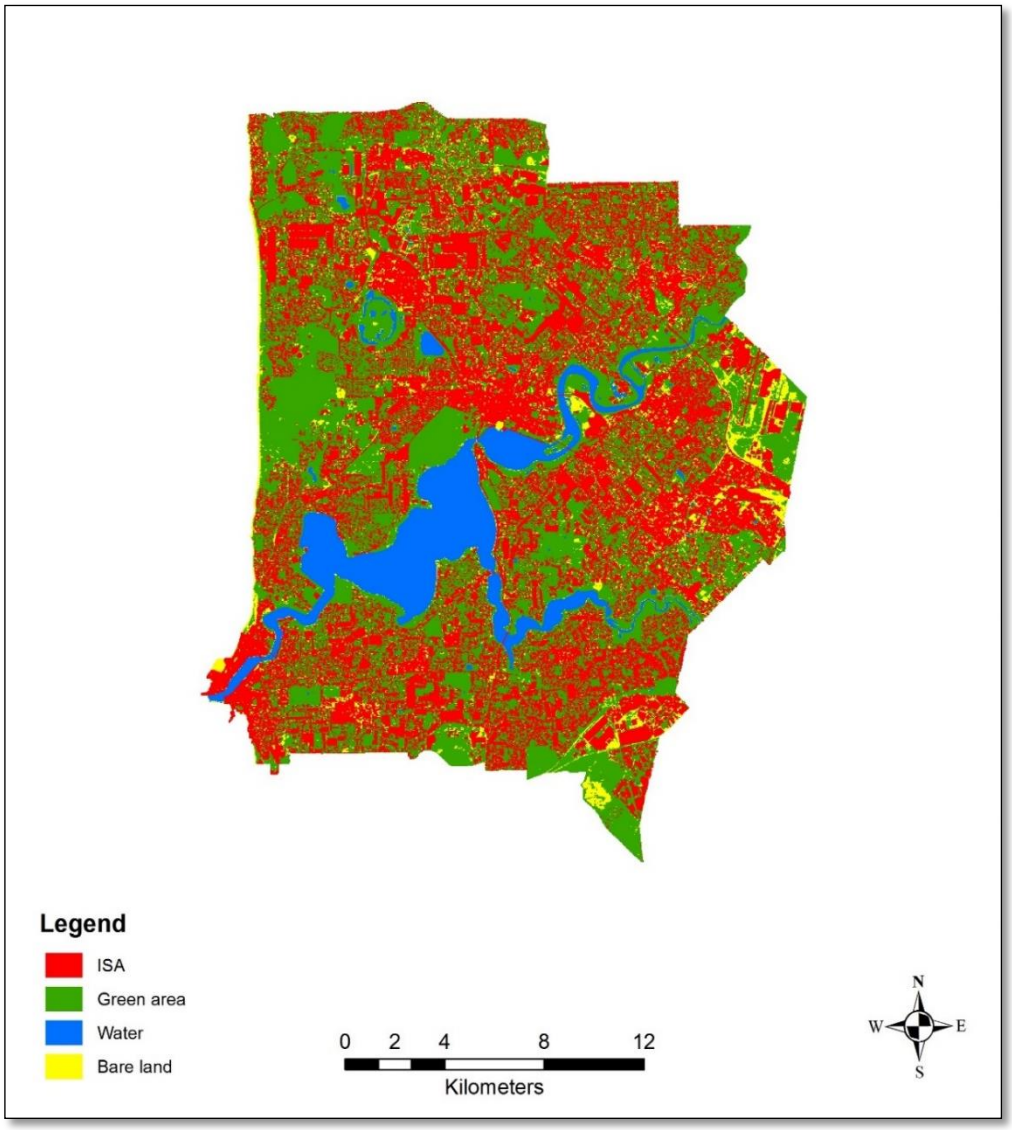

Figure 5.2 Major land use and land cover categories in Perth, 2015.

The analysis revealed that built-up area (ISA) constitutes around 35% (301 of a total 870.4 km^2), followed by green space 34% (298 km^2), bare land 29% (249 km^2) and small areas of water 3% (23 km^2) in Baghdad city, as shown in Figure 5.3. In contrast, green surface covered the highest percentage area of 45% (219 of a total 488.7 km^2) followed by 41% impervious surfaces (202 km^2) in Perth city. Water bodies occupied 8.2% (40 km^2) and a small proportion of Perth was found to be under bare land category (5.62%, 27 km^2) (Figure 5.3).

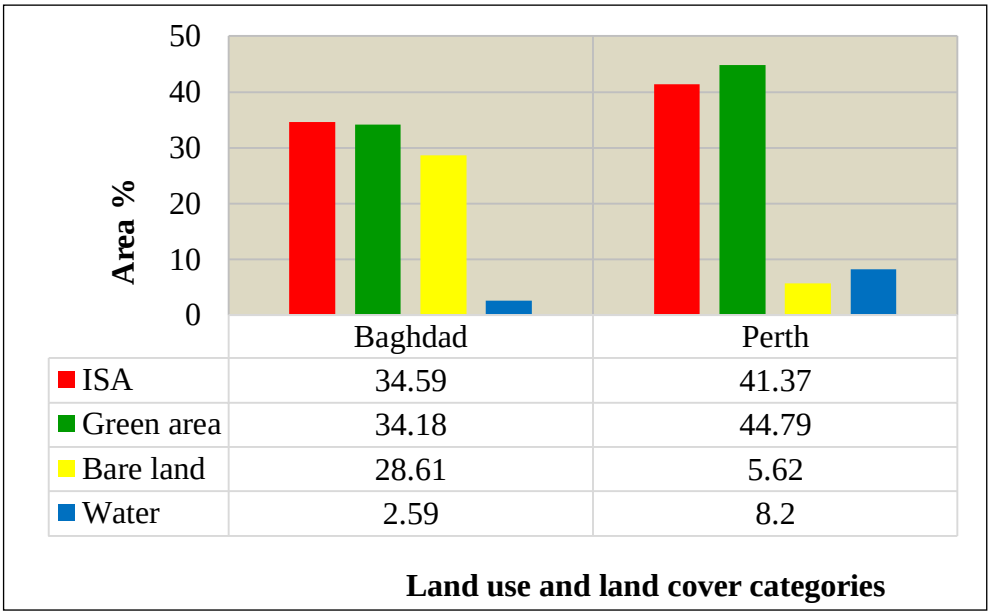

Figure 5.3 Percent (%) of urban land cover categories in Baghdad and Perth.

5.3.2. Relationship between percent impervious surface area and LST

In Baghdad city, Figure 5.4(a) clearly shows that the higher percentages of impervious surface area are mostly distributed in the core area.

The development intensity coefficient values for the impervious surface analysis tool (ISAT) range from low (less than 10%), medium (10–25%) to high (>25%). For Baghdad city, consistent with the percent impervious surface area values, the high-intensity values covered most of the built-up category within the study area. Medium intensity values of the urbanised area were limited. A large area covered by low-intensity values, which mostly represented rural areas (Figure 5.4(b)).

On the LST map (Figure 5.4(c)), the high value of LST are mostly concentrated in the areas where dense built-up areas are widespread. These areas have a mean LST of between 48 °C and 54 °C, and are mainly distributed in the city centre, to the south, to the southwest and to the west of Baghdad. Nevertheless, the value of LST in a pixel decreases substantially where built-up areas becomes less dense and mixed with some natural cover such as vegetation and water bodies.

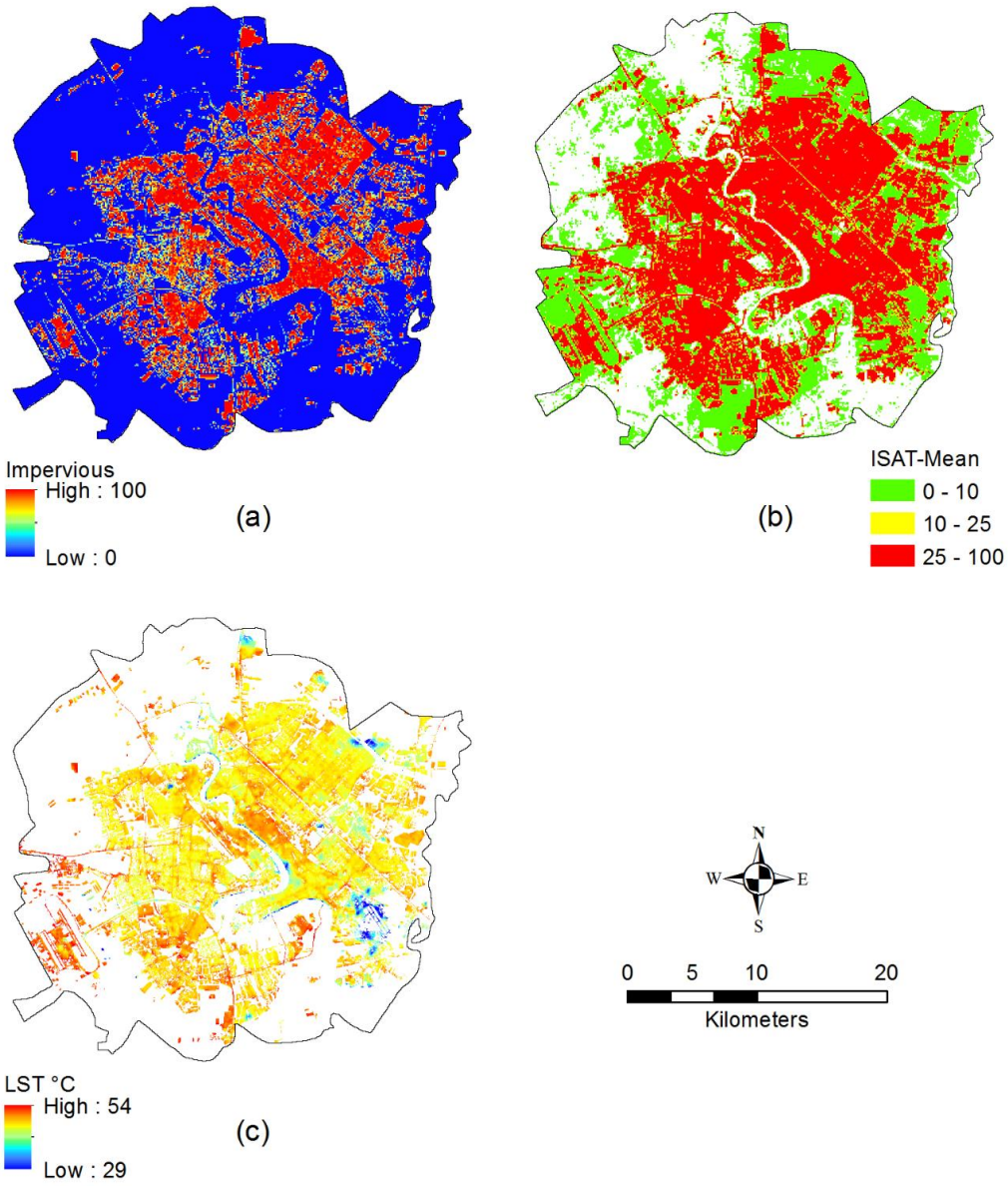

Figure 5.4 Spatial pattern of ISA and LST in Baghdad: (a) percent impervious surface area (PISA); (b) impervious surface analysis tool (ISAT); (c) land surface temperature (LST).

Figure 5.5 reveals the results of a statistical analysis comparing PISA and LST for Baghdad city. The following regression equation was obtained, which indicates that an increase in PISA is correlated to an increase in LST over Baghdad.

$$LST = 0.1013\ ISA + 39.476 \quad (5.2)$$

The relationship between PISA and LST is strongly and positively correlated, as indicated by the coefficient of determination (r^2=0.669), suggesting that PISA has a significant effect on the distribution of LST in Baghdad city (Figure 5.5(a)). In this figure, some outliers at around 60 PISA% with LST values of around 40 °C, which were beyond the expected range of LST of built-up areas (42.3 °C to 49.8 °C as mentioned in Section 4.4.2), were removed. Those outliers may be the result of a mixture of different LULC categories (i.e., with those of lower LSTs) with ISA, leading to reduce LST values for those cells in the grid.

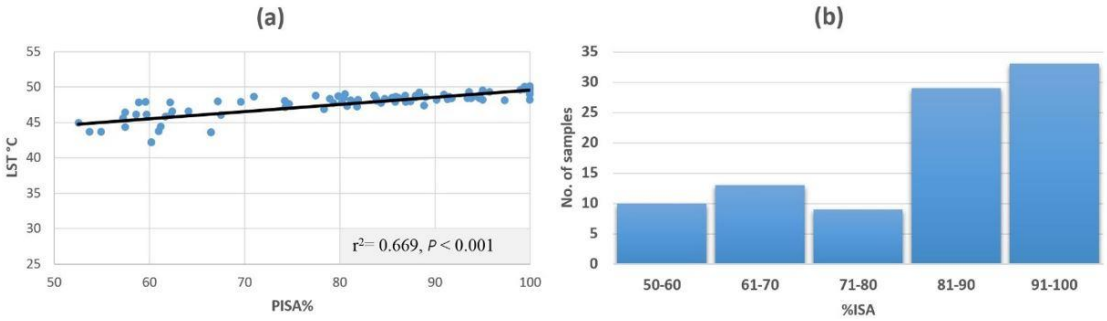

Figure 5.5 Relationship between LST and percent impervious surface area for Baghdad city.

Nearly 67% of the total variation of the mean LST sampled is accounted by the linear relationship with built-up area data. Based on the obtained linear regression function as described in Figure 5.5(a), the increases in PISA may be partly responsible for increases in LSTs. It can be seen from Figure 5.5(a) that the ISA was cut off at 50% which is the result of ISA grid cells having been chosen in densely built up areas between 50% and 100% ISA. Figure 5.5(b) shows that the majority of ISA values were clustered between 80% and 100%. In this context, the majority of the percentages of impervious surface area associated with high LSTs were high values of around 70% or more. The correlation plot indicates that very dense built-up areas in the city of Baghdad are associated with noticeably elevated LST. In contrast, the low density built-up areas contain natural surfaces which may have contributed to reducing the LST.

The percent impervious surface area in Perth city is relatively homogeneous across the study area (Figure 5.6(a)). Figures 5.6(a, b, c) further indicate that green space and

water bodies are widespread in Perth and may account for relatively low LSTs in the city core and beyond.

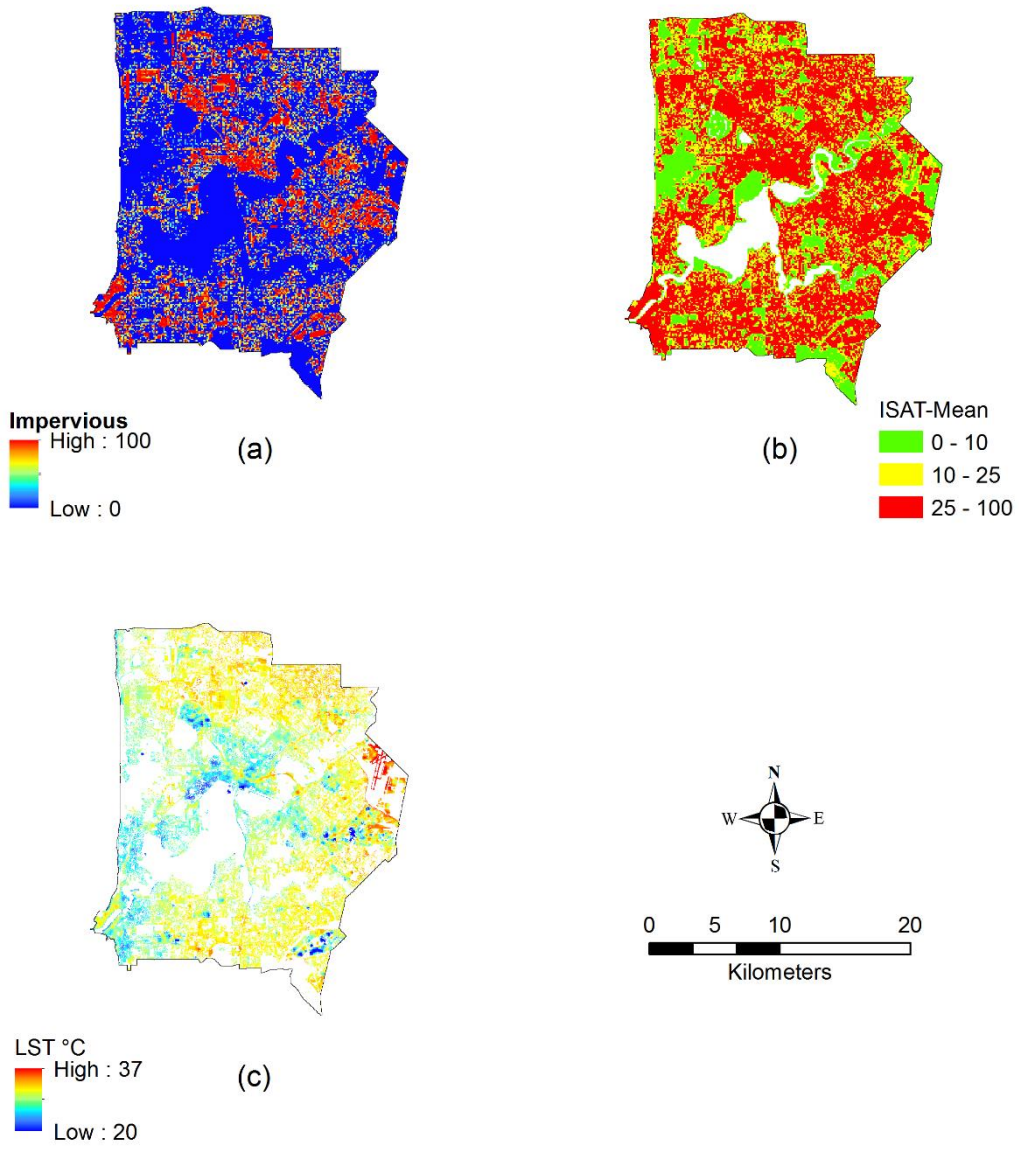

Figure 5.6 Spatial pattern of ISA and LST in Perth: (a) percent impervious surface area (PISA); (b) impervious surface analysis tool (ISAT); (c) land surface temperature (LST).

The relationship between PISA and LST was examined by a linear regression. Following linear relationship was obtained (Figures 5.7(a)), which showed that for Perth the coefficient of determination ($r^2 = 0.777$) is strong and somewhat higher than

that of Baghdad. That means about 78% of the total variation of the mean LST is explained by the linear relationship with the percent of ISA.

$$LST = 0.0973\ ISA + 23.794 \quad (5.3)$$

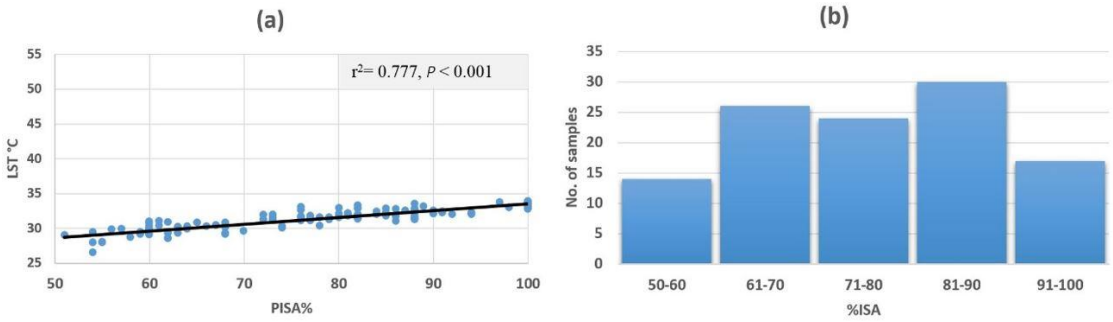

Figure 5.7 Relationship between LST and percent impervious surface area for Perth city.

Despite the fact that density of ISA in Perth is relatively low compared to that of Baghdad, the values of ISA samples were also obtained over densely built-up surfaces (%ISA > 50). Compared with Baghdad, it can be seen that there is a roughly peaked distribution with higher values between 60% and 90% ISA and lower values on either extreme for Perth (Figure 5.7(b)). In Perth, the extent of vegetation cover and number of water bodies is high, which may contribute to local areas of low LST. However, in both cities, the spatial pattern of LST indicates that LST is relatively high within urban areas, particularly in high density built-up areas.

5.3.3. Landscape metrics and LST analysis

The observed increase of built-up surfaces in both cities (Baghdad and Perth) during the study period reflects landscape shapes in each city that became gradually more complex because of the changes in land use and land cover. In order to compare landscape patterns of the two cities, it is necessary to examine the composition and configuration of the urban landscape in detail.

The relationships between landscape metrics of urban spatial composition and mean LST can provide more detail about the complexity, composition, and configuration of

urban landscape. The outcome of such an analysis may be an important aspect in assessing LST, and comparing the nature of surface urban heat islands between the two cities.

The selected landscape metrics, including the Shannon's diversity index (SHDI); Shannon's evenness index (SHEI); modified Simpson's evenness index (MSIEI); and patch density (PD) were calculated at the landscape level (as described in Section 2.5.2) for the major land use and land cover categories. Scatter plots were generated to examine any correlation between the landscape metrics and LST. The results provided a clear contrasting picture between the two cities with regard to the diversity, dominance, homogeneity, and heterogeneity metrics.

5.3.3.1. Baghdad city

Figure 5.8 shows the spatial distribution of each landscape index in Baghdad. The values of the Shannon's diversity index (SHDI), Shannon's evenness index (SHEI), modified Simpson's evenness index (MSIEI), and patch density (PD) ranged from 0 to 3.433, 0 to 1, 0 to 1, and 0 to 20.689, respectively. The results indicate that the west side of Baghdad is more homogenous, diverse and broken relative to other parts of the city. On the other hand, the Shannon's evenness index (SHEI) showed that the city core has more impervious surfaces whilst beyond the city core vegetation cover is more dominant.

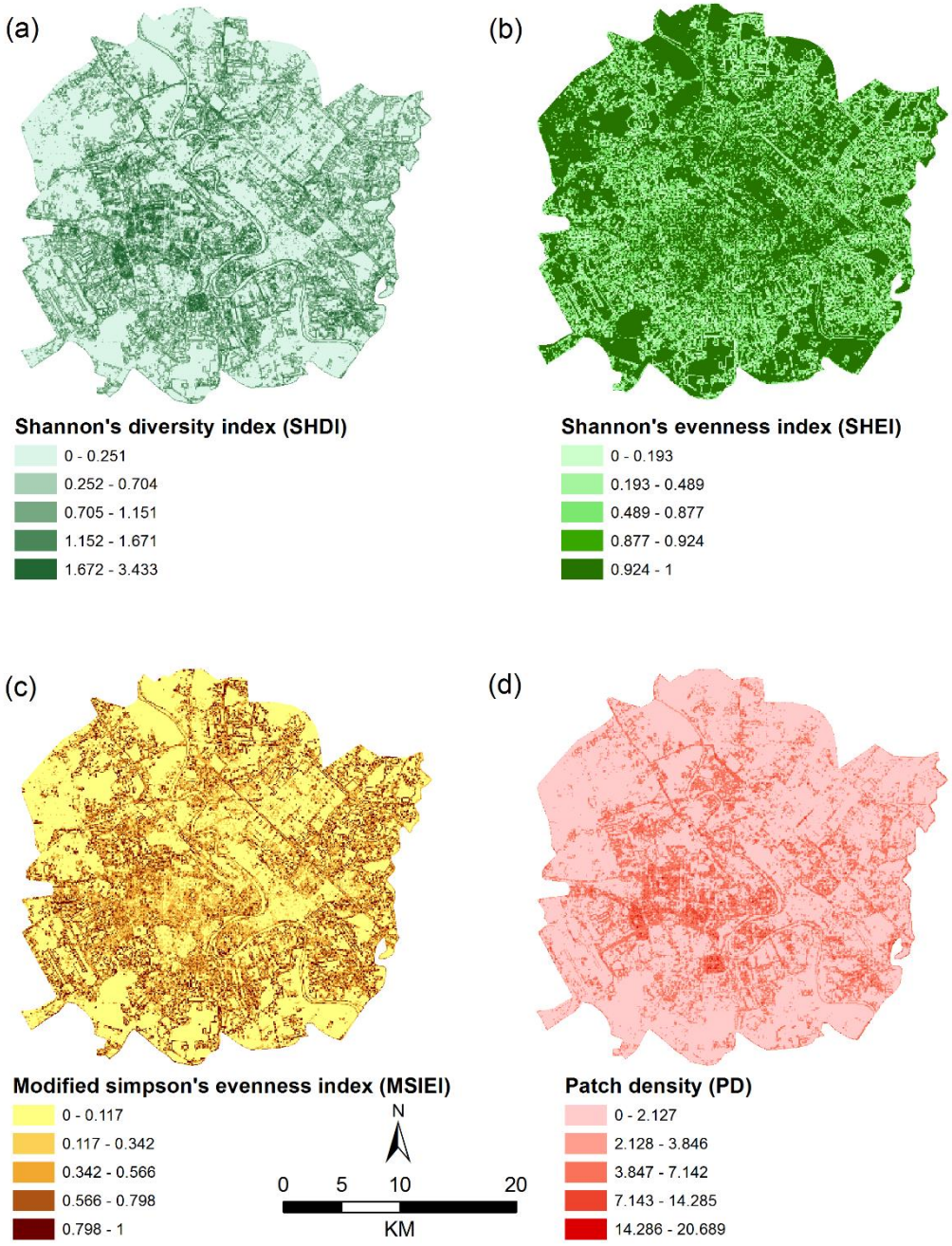

Figure 5.8 Spatial distribution of landscape metrics in Baghdad: (a) Shannon's diversity index; (b) Shannon's evenness index; (c) Modified Simpson's evenness index; and (d) Patch density.

The correlation between LST and each of landscape metrics was examined and is shown in Figure 5.9(a-d). The correlation coefficients for LST and Shannon's diversity index (SHDI), Shannon's evenness index (SHEI), modified Simpson's evenness index (MSIEI), and patch density (PD) were found to be ($r = -0.61$, p-value < 0.001), ($r = 0.62$, p-value < 0.001), ($r = -0.56$, p-value < 0.001), and ($r = -0.45$, p-value < 0.001),

respectively. These results indicate that the Shannon's diversity index (SHDI) had a strong inverse relation, and modified Simpson's evenness index (MSIEI) and patch density (PD) had a moderate inverse relationship with LST. However, the Shannon's evenness index (SHEI) showed a strong positive correlation with LST. These results are consistent with the study conducted by Jai and Zeng-Xiang (2003) showed that the Shannon's evenness index (SHEI) is inversely related to the Shannon's diversity index (SHDI).

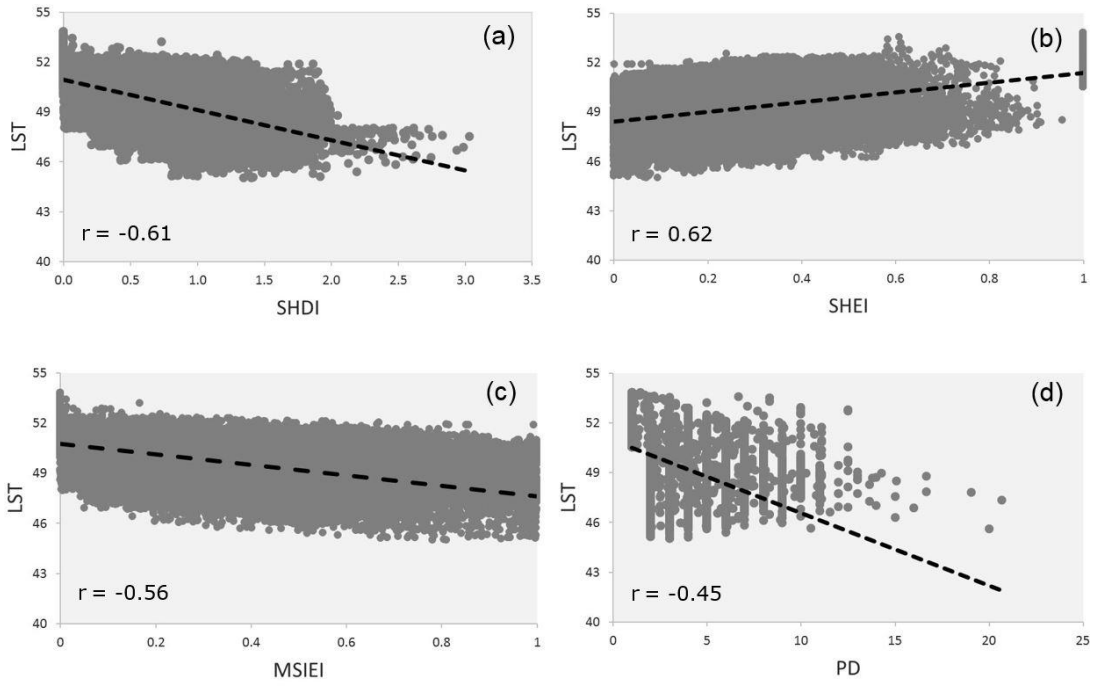

Figure 5.9 Scatter plots between LST and landscape metrics in Baghdad: (a) Shannon's diversity index; (b) Shannon's evenness index; (c) Modified Simpson's evenness index; and (d) Patch density.

5.3.3.2. Perth city

The spatial distribution of each of the landscape metrics for Perth city are shown in Figure 5-10(a-d). Compared with Baghdad, different ranges of values of landscape metrics were found for Perth. The values of the Shannon's diversity index (SHDI), Shannon's evenness index (SHEI), modified Simpson's evenness index (MSIEI), and patch density (PD) ranged from 0 to 1.911, 0 to 1, 0 to 1, and 0 to 50, respectively. The results indicate that Shannon's diversity index, modified Simpson's evenness index, and patch density are distributed across the study area except for the centre of Perth, which contains the Swan River and some relatively large vegetation covers. It can be

seen from Figure 5-10(b) that those central areas have high values of the Shannon's evenness index (SHEI), indicating that there is less diversity of landscape.

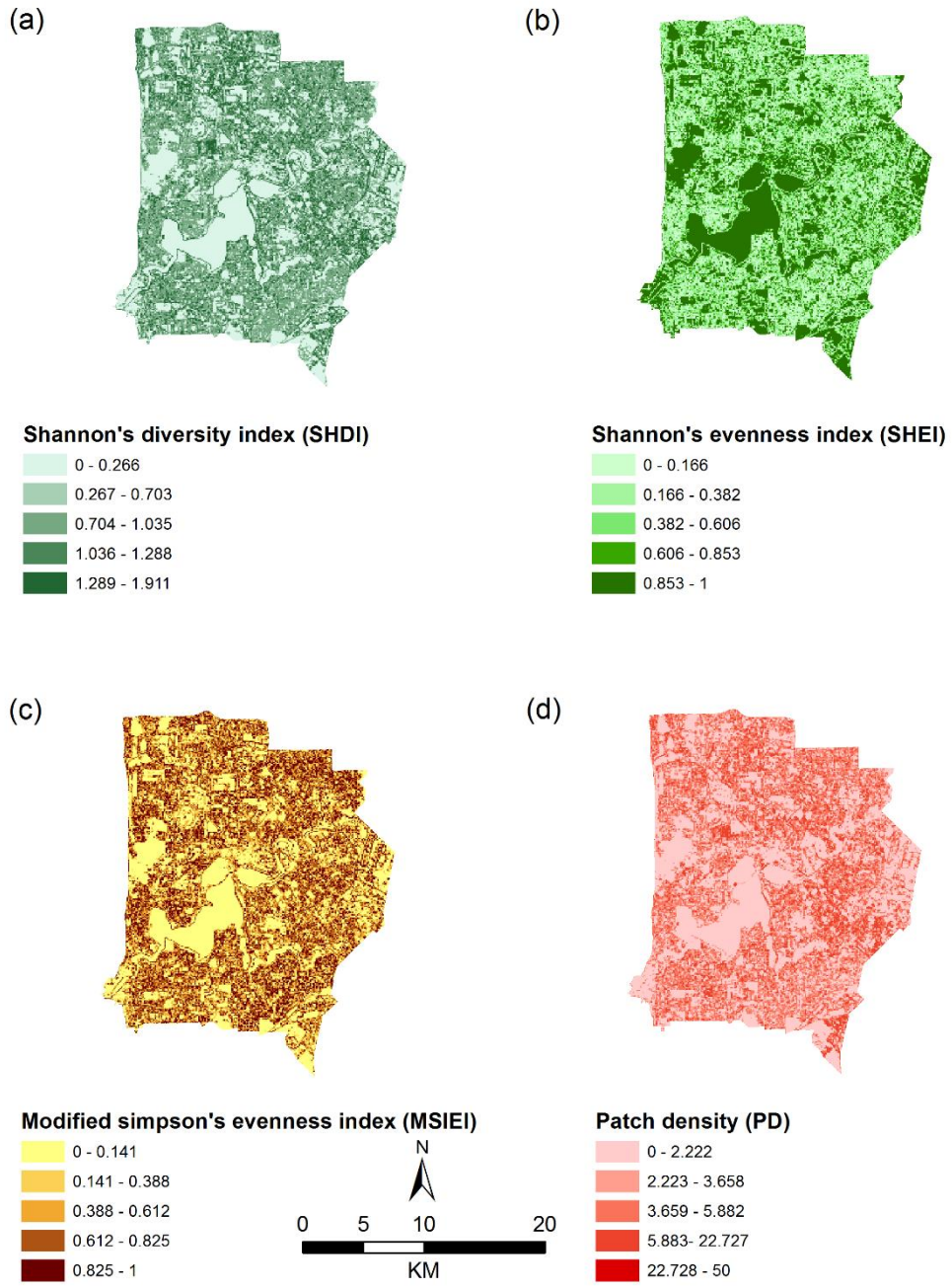

Figure 5.10 Spatial distribution of landscape metrics of Perth: (a) Shannon's diversity index; (b) Shannon's evenness index; (c) Modified Simpson's evenness index; and (d) Patch density.

The results of statistical analysis between each of the landscape metrics and LST are shown in Figure 5.11(a-d). It can be seen from the scatter plot in Figure 5.11(a) that there is a strong and a significant correlation between the Shannon's diversity index (SHDI) and LST ($r = 0.68$, p-value < 0.001). The correlations between LST and modified Simpson's evenness index (MSIEI), and patch density (PD) were found to be strong ($r = 0.64$, p-value < 0.001) and moderate ($r = 0.51$, p-value < 0.001) (Figure 5.11(c, d)), respectively. However, a strong negative correlation was found between LST and the Shannon's evenness index (SHEI) ($r = – 0.75$, p-value < 0.001) (Figure 5.11(b)). Therefore, the relationships observed for the two cities were consistently opposite to each other.

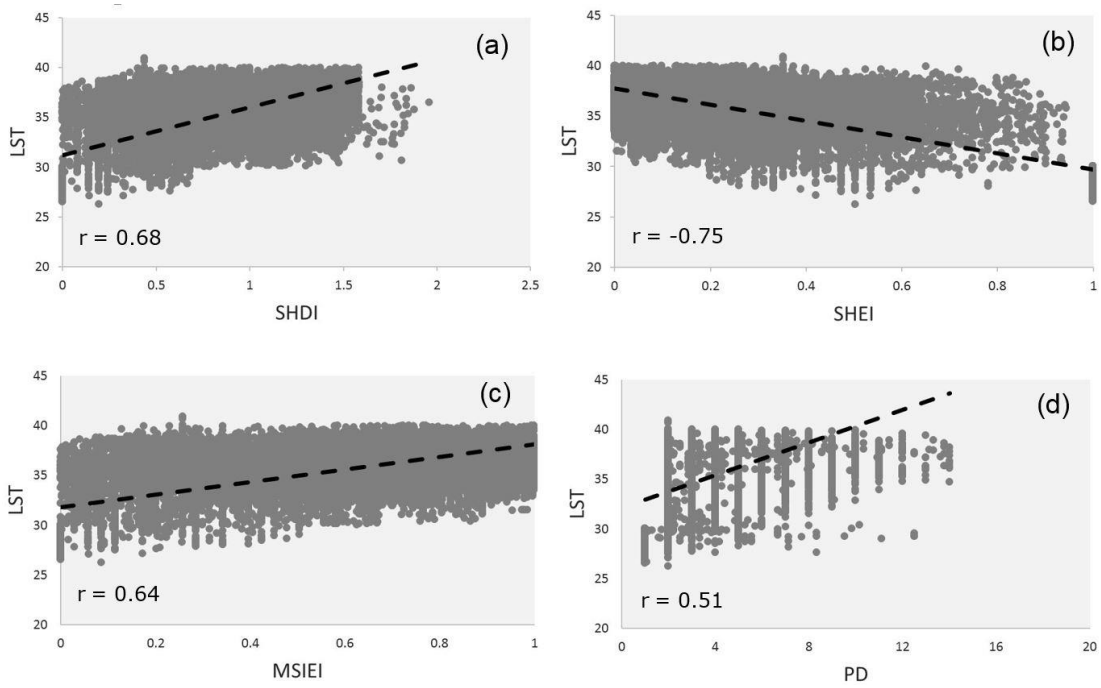

Figure 5.11 Scatter plots between LST and landscape metrics for Perth: (a) Shannon's diversity index; (b) Shannon's evenness index; (c) Modified Simpson's evenness index; and (d) Patch density.

5. 4. Discussion

As mentioned in Section 4.4.1, both Baghdad and Perth cities experienced a significant urban expansion during the last five decades. Land cover change has contributed to an increase in impervious surfaces, hence an increase in LST. An increase in impervious surface area seems to be affecting the temperature patterns of the two cities. The impervious surface area is increasing with time at the expense of other land cover types, especially green covers and open spaces.

5.4.1. Impact of impervious surfaces on LST

Uncontrolled and unplanned development in Baghdad city resulted in an increase of dense built-up areas in line with growth of population (as described in Section 3.1.1.3). Furthermore, commercial and industrial activities within residential areas in districts have also expanded in line with urban development. This agrees with the observation that cities in developing countries are becoming compressed due to urban growth (Jenks & Burgess, 2000).

In contrast, natural surfaces such as vegetation cover and water bodies play a key role in mitigating LST. For example, having greater green cover in Perth greatly enhances the quality of the urban environment for city dwellers (Oliveira et al., 2011; Duarte et al., 2015). In the city of Baghdad, green cover is significantly diminishing as a result of urban expansion. Areas with green cover are mostly restricted to privately-owned houses that have areas of 600 m^2 or more; orchards, which are mostly planted on the north and south banks of the Tigris River; and limited public parks and gardens. Green areas are not factored into planning for developments in Baghdad, and as a result, much of the old districts, and commercial and industrial areas do not have adequate vegetation.

The observed LST pattern revealed elevated temperatures in the city core, to the south, to the southwest and to the west of Baghdad. The city centre includes commercial, industrial and old residential areas. The south and southwest districts are mostly covered by industrial areas and military bases. The western region includes Baghdad international airport. All these areas predominantly covered by highly impervious surfaces. Referring to Figure 5.12(a, b, c), one can find that areas located in the city

centre are characterised by highly dense impervious surfaces. Meanwhile, green surfaces and open spaces are very sparse in these areas. Hence, elevated LST would be expected due to these impervious surfaces and human activities. The commercial areas (Figure 5.12(a)), while distributed widely, are concentrated in the city centre, especially the older areas. These areas are very crowded throughout the year, since they are of significant commercial importance for Baghdad and Iraq. Many other new commercial markets have also been built around the city centre because of urban population growth.

Several industrial areas (Figure 5.12(b)) are also located in and around the city centre of Baghdad based on older master planning. In more recent times, the existence of these large areas have become a problem for the constructional, environmental and socioeconomic aspects of urban planning. The old districts with narrow alleys (Figure 5.12(c)) within Baghdad city are in general high characterised by dense residential areas and mostly historical and heritage areas, and extend across a large, historically established area. In addition, the past few decades have seen the construction of other residential areas, which became highly dense as a result of the small size of units (as discussed in Section 4.5).

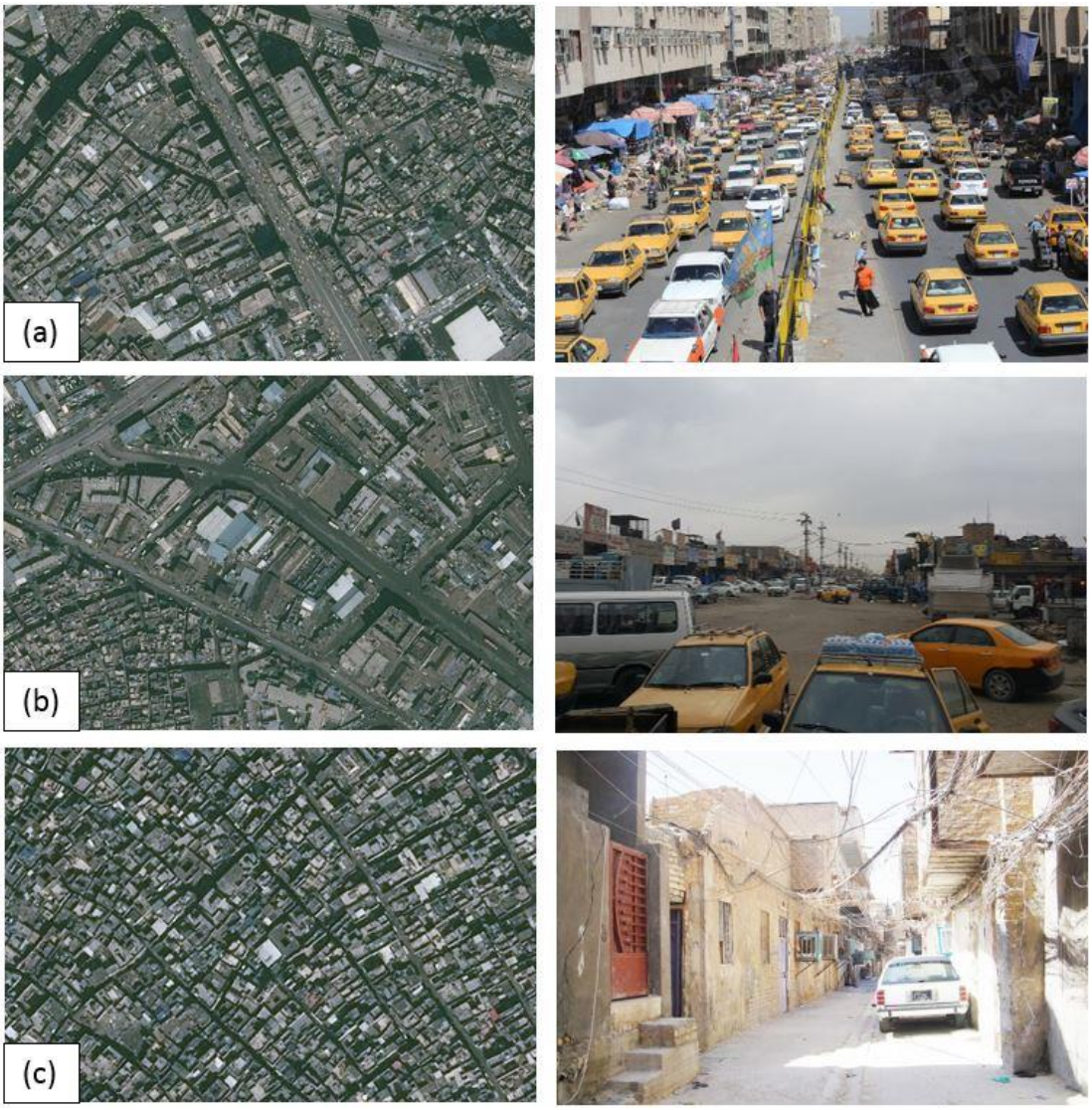

Figure 5.12 Satellite images (left) and photographs (right) showing: (a) commercial area; (b) industrial area; (c) old residential district (narrow alley). These images show highly dense impervious surfaces with almost no green cover or open spaces in the core of Baghdad city (Source: Google maps and images).

Urban development in Perth city is markedly different to Baghdad, since urban environmental issues have been considered throughout the planning and management stages of urban development. The amount and distribution of vegetation, vegetated open spaces, and parks allocated in planning has contributed to lower LST. Green areas have been planted amidst commercial, industrial and residential areas, as can be found in the satellite imagery (Figure 5.13(a, b, c)).

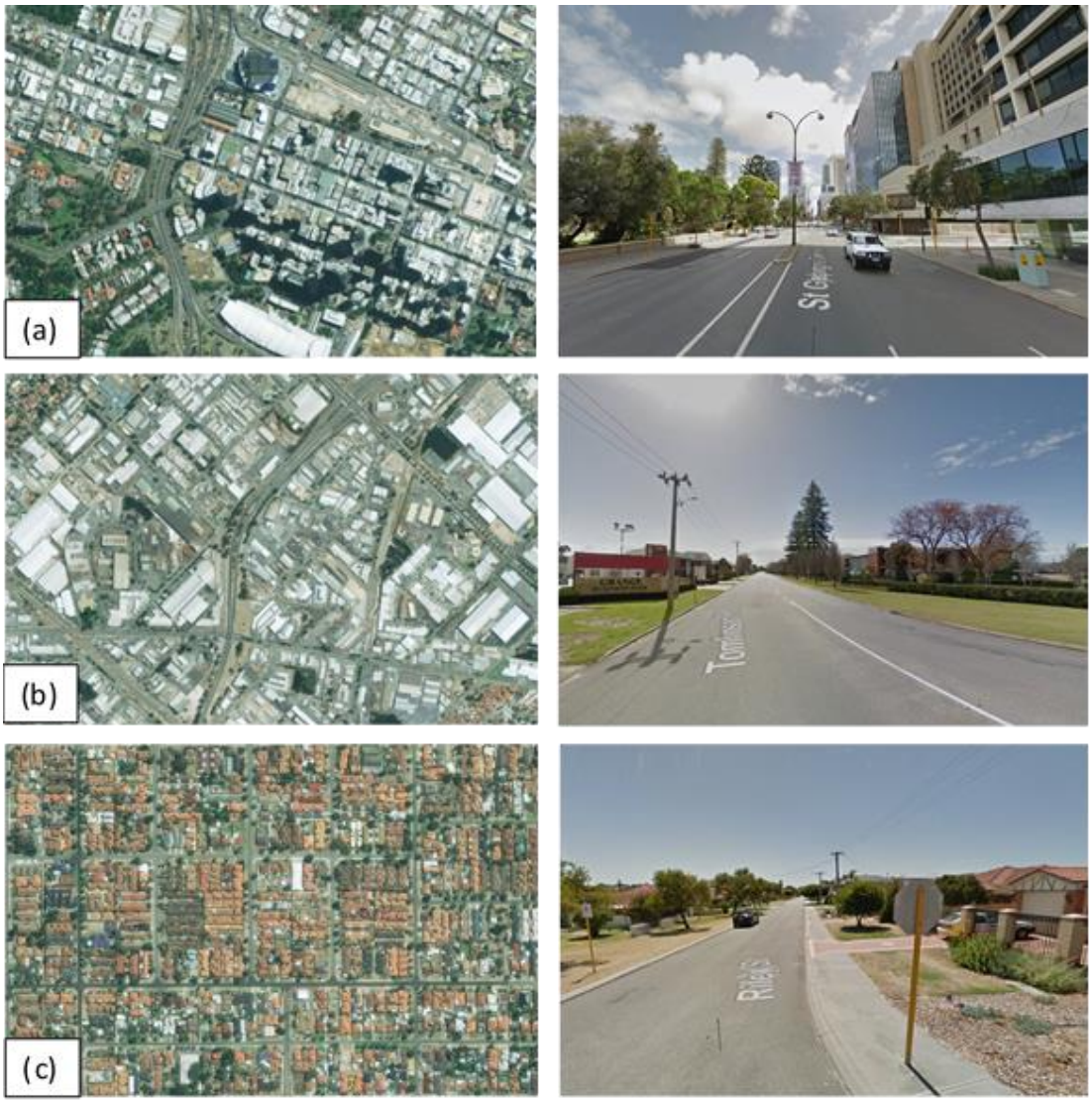

Figure 5.13 Satellite images (left) and photographs (right) showing: (a) commercial area; (b) industrial area; (c) residential area. In these images, green cover and open spaces are clearly visible in Perth (Source: Google maps).

The plan of the "urban forest" has been applied as an objective strategy to improve city liveability and to promote community health and well-being. Urban forest is a valuable amenity of the city infrastructure that includes trees, green spaces, and other vegetation (City of Perth, 2016b). This strategy aims to improve canopy cover in the city by implementing nine goals as mentioned in Figure 5.14. In the early 20th century, there was a focus on modern town planning. Accordingly, Australian capital cities established town planning associations during the period of 1913-1916. Thenceforth, a number of new plans, strategies and regulations were prepared to control development and improve the urban environment of Perth through public policies

(Freestone, 2009). By 1929, redressing the defects of the past, and planning for future in an orderly manner were the aims of the Western Australian association. The principles of ecologically-sustainable development were adopted during the 1990s. Recently, an environmental strategy for the city of Perth has been developed to empower the city to achieve a high level of environmental management, and an environmentally sustainable city (City of Perth, 2016a).

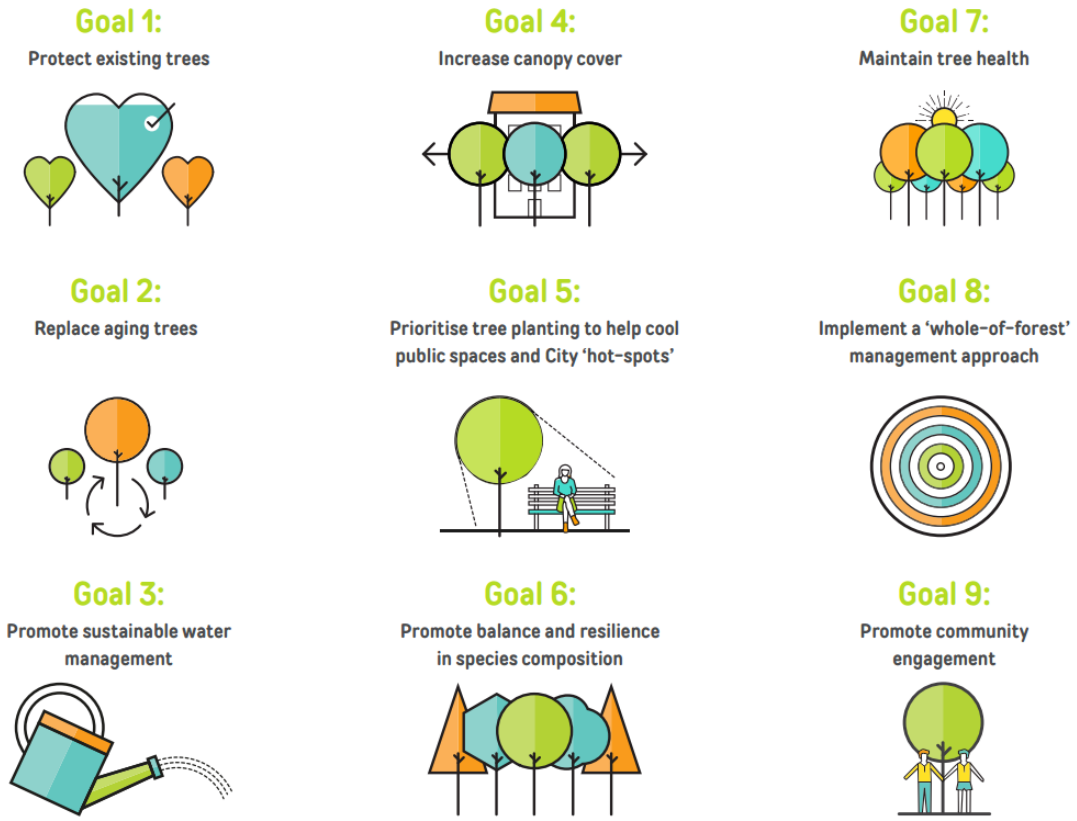

Figure 5.14 Nine goals of the urban forest plan for Perth city (Source: (City of Perth, 2016b).

In general, Perth is covered by a large amount of green infrastructures, including parks, public gardens, private gardens, golf courses, etc. The selection of suitable plants (usually those native to WA), and a spread of vegetation, green spaces and water bodies throughout built-up areas, have decreased the percentage and continuity of impervious surfaces. The higher amounts of green cover in Perth City resulted in lower amounts of impervious surfaces throughout the study area. While, the majority of impervious surface cells in Baghdad (70% or more) had high mean LSTs (and more agglomeration), mostly representing the city centre. These are consistent with (Yuan

& Bauer, 2007), who mention that the density and characteristics of impervious surfaces in each grid has a significant effect on the pattern of LST, and that amounts and diversity of green cover across impervious surfaces can inversely affect LST. The variation of land surface temperature between Baghdad and Perth is related to the amount of impervious surfaces and characteristics of the urban fabric. These findings are in agreement with previous studies which identified the relationship of impervious surfaces and vegetation with LST elsewhere (Yuan & Bauer, 2007; Tang & Xu, 2016).

It can be concluded from above discussion that green infrastructure within Perth is widespread as a result of supporting and regulating the local, state and federal governments in Australia to protect vegetation, therefore protecting the urban environment from the influence of heat islands. While Perth has significant financial penalties for any breach of a planning scheme outlined in the Planning and Development Act 2005, no such strong planning regulation has been implemented in Baghdad. From this analysis, it is evident that planning regulation may have a serious impact on the urban thermal environment.

5.4.2. LST relationships to landscape metrics

The correlations between landscape metrics and mean LST indicate that land surface temperature may be influenced by landscape patterns in the two cities. The results highlighted that Baghdad has substantial built-up area and bare land categories with relatively low amounts of green areas and water bodies. The LST map for Baghdad in 2015 (described in Section 4.4.2) revealed that, the categories of bare land (51.9 °C) and built-up area (49.8 °C), had relatively higher LST than greenery areas (45.5 °C) and water bodies (35.4 °C). Also, the complexity and irregular shapes of built-up areas, particularly in the old districts, are related for elevating LST. In contrast, Perth within its urban core has a larger amount of, and more homogeneous, vegetation cover (32.1 °C) and water bodies (26.8 °C) that had lower LST compared with bare land (38.7 °C) and built-up area (36.2 °C). In addition, shapes of built-up patches are regular, which may have contributed to lower LSTs than Baghdad.

It should be mentioned that the correlations for each city are quite opposite as shown in Figures 5.9 and 5.11 and Table 5.2.

Table 5.2 Correlation coefficients (r) between landscape metrics and LST for Baghdad and Perth.

Landscape metrics	Baghdad	Perth
	LST	
	r	r
Shannon's diversity index (SHDI)	– 0.61	0.68
Shannon's evenness index (SHEI)	0.62	– 0.75
Modified Simpson's evenness index (MSIEI)	– 0.56	0.64
Patch density (PD)	– 0.45	0.51

This difference seems to be reflecting the influence of land use and land cover categories and their spatial pattern. For Baghdad, the result for the Shannon's evenness index (SHEI) (Figure 5.8(b)) shows that the majority of cells were impervious surfaces and bare land, especially in the areas of commercial, industrial, and old districts. Therefore, the correlation of the Shannon's evenness index (SHEI) with land surface temperature may have been strongly positive (r = 0.62) due to their dominance. On the other hand, the Shannon's diversity index (SHDI), modified Simpson's evenness index (MSIEI), as well as patch density (PD) were found negatively correlated with LST (r = – 0.61, – 0.56 and – 0.45, respectively). This may have resulted from mixing those cells of dominated categories such as impervious surfaces and bare land (having high LST) with other low LST categories such as water and vegetation.

In contrast to Baghdad, Perth appears to have inverse correlations for each of the landscape metrics with LST. The reason may be linked to the existing land use and land cover pattern, i.e., a large number of cells are covered by green area and water bodies. An increase in these cells may act to reduce LST. The Shannon's evenness index (SHEI) had a strong inverse correlation with LST (r = – 0.75). In detail however, decreased values of the Shannon's evenness index (SHEI) occur normally as a result of mixing those cells with other high LST categories like impervious surfaces and bare land that led to elevated LST. Therefore, in the case of Perth, the Shannon's diversity index (SHDI), modified Simpson's evenness index (MSIEI), and even patch density (PD) contributed to elevated land surface temperature, hence resulting in positive correlations (r = 0.68, 0.64 and 0.51, respectively).

These findings are in agreement with previous studies that examine the relationship of LST with landscape patterns. LST was observed to decrease as a result of a more homogeneous dispersed pattern of vegetation patches around built-up areas (Asgarian et al., 2015). Another study conducted by Liu and Weng (2008) pointed out that decreases in building densities can minimize LST in urban areas.

5. 5. Chapter summary

This chapter has demonstrated how land surface temperature was affected by dense built-up areas and spatial patterns of the urban landscape in both Baghdad and Perth cities. Both study areas were classified into four main categories by a hierarchical image classification method. The classified maps provided quantitative information about the distribution of LULC. These maps were employed to produce an impervious surface analysis tool (ISAT). Percent impervious surfaces area (PISA) and the impervious surface analysis tool (ISAT) were used to quantify the spatial distribution of impervious surfaces. Then, the relationship between percent impervious surfaces area and LST was examined. In addition, landscape metrics such as the Shannon's diversity index (SHDI), Shannon's evenness index (SHEI), modified Simpson's evenness index (MSIEI), and patch density (PD) were used to investigate the impact of spatial patterns of the urban landscape on LST. The results revealed that the factor of the percent impervious surface area may be an important tool for inferring the land surface temperature pattern. Results also indicated that the LST had been affected by the spatial pattern of urban landscape for both cities.

In this chapter, the influence of spatial composition and configuration of land use and land cover on LST was examined. However, the variation in land surface temperature in urban areas can result from other important factors, such as characteristics of urban cover surfaces, and this will be investigated in the next chapter.

6. Thermophysical behaviour of urban LULC categories

6. 1. Introduction

The previous chapter analysed and evaluated the effect of the spatial pattern of urban landscape on land surface temperature for Baghdad and Perth. This chapter focuses on investigating thermophysical behaviour of urban LULC surfaces within the urban environment. This is designed to assist in the examination of urban heat islands (UHIs) in the two cities.

Generally, impervious man-made surfaces absorb more heat, and therefore exhibit increased temperature, in comparison to natural surfaces, such as vegetation cover, due to greater absorption of solar radiation (Uemoto et al., 2010). This effect is known as the urban heat island (UHI) phenomenon, and is typified by urban areas that exhibit higher temperatures than their expected background temperature. Many studies have been carried out on UHI around the world, especially in large cities. All of them have confirmed that urban areas have a higher surface and air temperature than their surrounding rural vegetated areas. Santamouris et al. (2011) demonstrated that materials that absorb and retain heat are accountable for such effect. According to Day and Roaf (2007), the building and construction sector is considered one of the leading sectors for high raw materials consumption, energy consumption, waste production, and release of polluting gases to the urban environments. Large areas of dark surfaces like concrete, bricks, and asphalt absorb and store solar radiation during the day and release it in the evening (Oke et al., 1991; Yow, 2007).

In this chapter, two essential parameters are used to study the urban cover. These parameters are surface albedo and land surface temperature. The thermal behaviour of most common LULC categories is examined using field measurements and remotely sensed data. Many recent studies have investigated the relationship between directly measured surface albedo and surface temperature for urban cover surfaces to assess the thermal environment of an urban area. According to Menon et al. (2010), the land surface temperature (LST) in urban areas decreases approximately 0.008 K for an average increase of 0.0003 albedo during the summer season in the USA. Another study carried out by Taha (1997) showed that increasing surface albedo in cities in the USA has contributed to the decrease of the urban heat islands effect through a decrease

in air temperature of between 2 and 4 °C. In another experiment, raising the surface albedo of the pavement at Portland State University, Oregon, USA from 0.37 to 0.91, led to a corresponding decrease in air temperature of 1.3 °C (Taleghani et al., 2014). In addition, increasing surface albedo of built-up surfaces can reduce the amount of energy consumed for cooling. Akbari et al. (2006) pointed out that energy consumption for cooling reduced by up to 20% as a result of improving the surface albedo of rooftops from 0.1 to 0.6.

There are a number of challenges to be faced when studying and analysing urban areas with field work and remote sensing data. These include the complex nature of landscape types, limitations in the spatial and spectral resolutions of remotely sensed data, similar reflectance signatures of some LULC surfaces, and the problem of mixed-pixels in urban surfaces. Different experimental procedures have been used to measure surface temperature and spectral reflectance of building materials. Some studies used a spectrophotometer (Varian Carry 5000) to measure samples in the laboratory (Stathopoulou et al., 2009; Synnefa et al., 2009). Other studies tested collected samples of different materials on a horizontal platform (Synnefa et al., 2007). Difficulties faced by these studies related to the time of data acquisition, and problems with LULC categorisation.

In this context, there are also a limited number of comparisons between remote sensing data and field measurements of surface albedo and LST. Therefore, the combined field work and remote sensing data in this study is of great benefit to studies of the thermal urban environment. In order to overcome these problems, a new method has been developed to temporally adjust field observations, and then compare them with Landsat-derived parameters to examine the thermal behaviour of a variety of LULC surfaces.

The aim of this chapter is to investigate the thermophysical behaviour of urban LULC categories in Perth. This chapter first describes data collection methods, followed by a description of the new method required to adjust the field measurements of surface albedo and LST. Then the relationship between adjusted field measurements and Landsat-derived surface albedo and LST is examined. The effect of various urban LULC surfaces on the urban thermal environment is then analysed.

6. 2. Materials

6.2.1. Field work instruments

The LP PYRA 06 pyranometer and the FLIR E5 infrared camera were employed to record surface albedo and surface temperature, respectively. The major features of these instruments were described in Section 3.2.2.

6.2.2. Satellite image

A Landsat 8 image, acquired on the 23rd of January 2016 at 10:11:43 am Perth local time (as described in Section 3.2.1.), was used for the analysis in this chapter.

6. 3. Methodology

Surface albedo and surface temperature were measured for the main urban LULC surfaces using portable instruments, a pyranometer (LP PYRA 06) and an infrared camera (FLIR E5), to investigate their thermal behaviour. The observed data from the field were scheduled on the same day and days surrounding the expected overpass of Landsat 8 over Perth. A new method was developed and applied as an adjustment to the field measurements. Next, the relationships between adjusted values collected from the field with values retrieved from the Landsat 8 image for both surface albedo and surface temperature were examined. Finally, the adjusted data was used to analyse the thermophysical behaviour of the selected urban land cover surfaces. In this chapter, this methodology was applied within the central Perth metropolitan area.

6.3.1. Field measurements

For this study, 24 materials from different rooftops and ground surfaces, representing built-up areas, vegetated surfaces, bare land and water bodies were selected. Appendix B shows visible and thermal images of the samples taken from the field. As shown in Table 6.1, field measurements were taken with the pyranometer and the infrared camera over a number of days, around the time of the Landsat overpass on 23th of January 2016. All observations were carried out between 9 am and 3 pm in hot and clear summer days. The shortness of the experimental period during daytime and the

difficulty of access to some rooftops led to collection of data over several days that included the 22nd, 23rd, 24th, 28th of January and 7th February of 2016. Surface albedo values were recorded using an LP PYRA 06 according to ASTM Standard E1918-06 (2006). Measurements were taken at a distance of 50 cm, levelly mounted above the surfaces (Figure 6.1). Mean albedo values were calculated from a number of readings which were taken at one minute intervals in different locations. This process was done for each of the categories. In addition, land surface temperatures (LST) were measured by an infrared camera. Then, the thermal images were analysed by FLIR Tools software to extract surface temperature values. The analysis was performed by calculating the mean surface temperature from several thermal images of each category based on a mean of all pixels in an image.

Figure 6.1 Measuring surface albedo by pyranometer with stand at 0.5 m from surface.

Table 6.1 Measurements of surface albedo and surface temperature in Perth city.

Materials	Albedo			LST			No. of Observations		Date	Actual time	Adjusted time
	Min	Max	Mean	Min	Max	Mean	Albedo	TIR			
New concrete	0.41	0.414	0.411 ± 0.0014	37.4	37.9	37.7 ± 0.289	8	3	7-Feb	9:42-9:54	10
Old concrete	0.203	0.216	0.209 ± 0.0049	45.8	48.9	47.5 ± 1.088	19	6	22-Jan	11:17-11:30	11:30
New black asphalt	0.062	0.072	0.065 ± 0.0026	54.5	57	55.7 ± 1.057	11	5	24-Jan	10:06-10:18	10
Old black asphalt	0.139	0.163	0.152 ± 0.0088	48.1	53.4	50.2 ± 1.904	24	9	24-Jan	9:40-9:55	10
New red asphalt	0.127	0.134	0.13 ± 0.0026	69.5	71.2	70.3 ± 0.622	10	5	7-Feb	2:07-2:18	2
Old red asphalt	0.136	0.165	0.148 ± 0.0122	65.2	68.7	67.2 ± 1.401	23	6	24-Jan	12:05-12:30	12:30
Rubber	0.134	0.142	0.137 ± 0.0025	51.7	58	54 ± 2.088	20	7	22-Jan	9:53-10:08	10
Red brick	0.143	0.2	0.171 ± 0.0268	51.9	57.9	55.3 ± 2.335	18	6	22-Jan	11:00-11:15	11
Yellow brick	0.246	0.249	0.247 ± 0.0009	59.5	60	59.7 ± 0.216	8	4	7-Feb	2:24-2:33	2:30
Red Tile	0.224	0.338	0.285 ± 0.0476	50.5	52.6	51.7 ± 0.853	29	5	22-Jan	10:40-10:52	11
Brown Tile	0.154	0.171	0.159 ± 0.0047	64	65.6	64.8 ± 0.541	14	7	7-Feb	12:00-12:15	12
Green Tile	0.235	0.245	0.242 ± 0.0042	56.9	60.2	58.8 ± 1.422	11	4	24-Jan	2:52-3:04	3
White Metal	0.493	0.522	0.511 ± 0.0095	47.7	49.9	49.5 ± 0.601	28	12	22-Jan	9:10-9:35	9:30
Red Metal	0.281	0.291	0.287 ± 0.0031	69.4	71.1	70.1 ± 0.680	18	5	22-Jan	11:50-12:05	12
Grey Metal	0.329	0.348	0.34 ± 0.0066	69.3	71.1	69.8 ± 0.780	22	5	22-Jan	12:30-12:45	12:30
Green Metal	0.247	0.267	0.256 ± 0.0084	55.3	59.1	57.2 ± 1.768	5	5	24-Jan	2:40-2:49	3
Brown Metal	0.204	0.209	0.206 ± 0.0017	66	66.9	66.5 ± 0.451	12	3	7-Feb	2:45-2:56	3
Grass	0.27	0.299	0.281 ± 0.0089	33.8	36.9	35.4 ± 1.154	31	7	23-Jan	9:50-10:15	10
Shrubs	0.217	0.238	0.224 ± 0.0063	33.6	36.7	35 ± 1.267	12	7	7-Feb	2:37-2:40	3
Trees	0.149	0.155	0.152 ± 0.0022	34.7	39.6	36.2 ± 1.583	10	9	22-Jan	11:36-11:45	11:30
Bare land	0.258	0.322	0.293 ± 0.0262	54.9	58	56.6 ± 1.128	20	5	24-Jan	2:23-2:30	2:30
Soil	0.277	0.279	0.278 ± 0.0008	57.5	58.4	58 ± 0.451	6	3	24-Jan	2:35-2:46	11:30
Mulch	0.183	0.211	0.202 ± 0.0089	50.2	53.1	51.9 ± 1.107	15	5	7-Feb	9:56-10:08	10
Water	0.025	0.045	0.031 ± 0.005	29.2	31.1	30.4 ± 0.520	21	14	23-Jan	10:44-11:10	11

As the aim of this chapter is to analyse thermal behaviour of dominant LULC categories within the urban environment, and to examine the relationship between field measurements and remotely sensed data, it was necessary to adjust all observed values to the time of the satellite overpass, which was 10 am local time. A new approach therefore involved taking other observations (training samples for some surfaces) of surface albedo and surface temperatures at 30 minutes intervals from 9 am to 3 pm local time. The purpose of this approach was to obtain semidiurnal variations of thermal values for the selected surfaces. All field measurements were initially adjusted to the nearest half hour to match them with the semidiurnal variations as shown in Table 6.1.

An important adjustment was applied to the values of surface albedo and surface temperature separately, based on some other factors as illustrated in the following sections.

6.3.1.1. Adjustment of the albedo mean values

In general, diurnal values of albedo vary with the solar zenith angle during the day. This means they are higher in the early morning and lower at noon (Zhang et al., 2012b; Rutan et al., 2014).

Field-based mean (n=6) semidiurnal values of albedo for old concrete, old black asphalt and red bricks are illustrated in Table 6.2. The albedo mean values measured between 9 am and 3 pm, for example, ranged from 0.302 to 0.297, 0.171 to 0.17 and 0.293 to 0.284 for old concrete, old black asphalt and red bricks, respectively. Despite these differences, the variation in albedo due to solar zenith angle for these surfaces for each 30 minutes interval was similar.

In general, it can be concluded that the maximum mean value of albedo occurred at 9 am, following which time albedo decreased to reach a minimum mean value at 12:30 pm, and then again increased in the same manner (Figure 6.2).

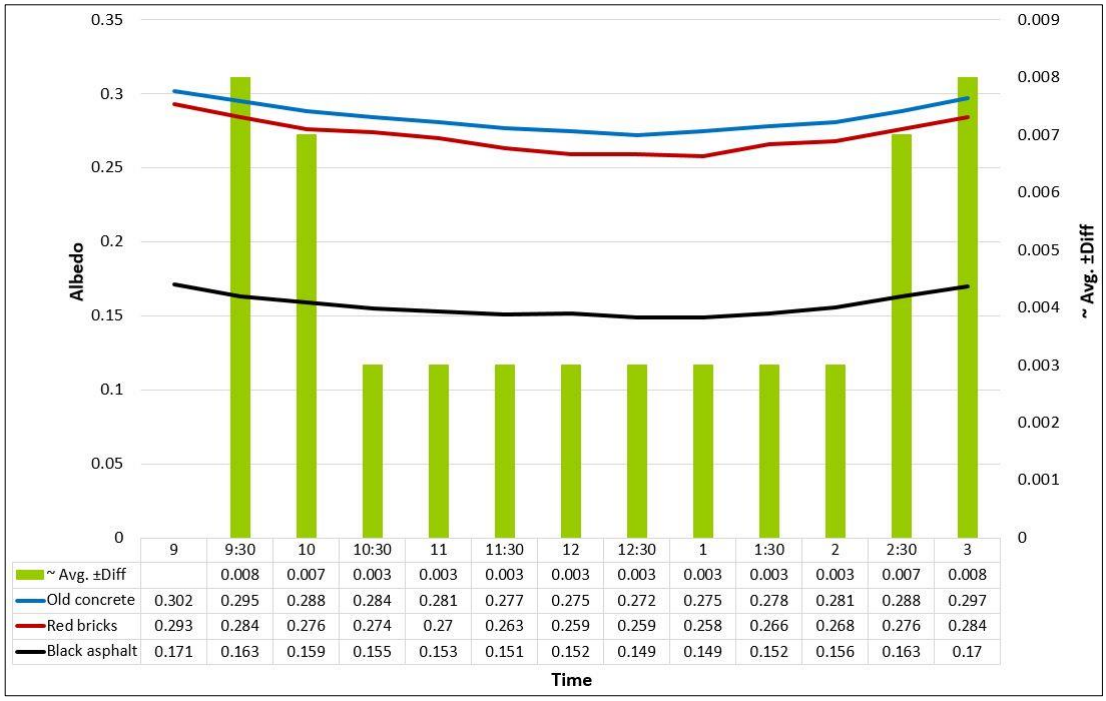

	9	9:30	10	10:30	11	11:30	12	12:30	1	1:30	2	2:30	3
~ Avg. ±Diff		0.008	0.007	0.003	0.003	0.003	0.003	0.003	0.003	0.003	0.003	0.007	0.008
Old concrete	0.302	0.295	0.288	0.284	0.281	0.277	0.275	0.272	0.275	0.278	0.281	0.288	0.297
Red bricks	0.293	0.284	0.276	0.274	0.27	0.263	0.259	0.259	0.258	0.266	0.268	0.276	0.284
Black asphalt	0.171	0.163	0.159	0.155	0.153	0.151	0.152	0.149	0.149	0.152	0.156	0.163	0.17

Figure 6.2 Temporal variation of surface albedo observed over old concrete, black asphalt and red ground bricks.

In order to adjust mean albedo values that were taken at different times to be comparable with data for 10 am, a correction was used that depended on the semidiurnal differences measured three surfaces in Figure 6.2, and extrapolated to all surfaces. For example, the value of old red asphalt (see Table 6.4) was converted from 0.148 at 12:30 pm to 0.163 at 10 am by adding differences over the five half hour intervals between measurement times (0.003 + 0.003 + 0.003 + 0.003 + 0.003).

6.3.1.2. Adjustment of the surface temperature mean values

In order to demonstrate thermal behaviour of LULC in terms of surface temperature, LULC surfaces were first thermally classified into seven categories based on their heat capacity. Secondly, one material was selected from each group to determine thermal variation from 9 am to 3 pm at 30 minutes intervals.

The first step was to classify urban LULC categories into discrete groups. These categories were classified according to their heat capacity, which were based on the standard heat capacity of each material stated in the literature (Jayalakshmy & Philip, 2010; Integrated Environmental Solutions, 2011; Dupont et al., 2014; Hens, 2016).

Heat capacity is defined as the amount of heat required to increase the temperature of a unit mass of a substance by one degree Celsius. The heat capacity values of selected LULC surfaces are shown in Table 6.2.

Table 6.2 Groups and heat capacity of urban LULC materials.

	Group	Materials	Heat Capacity J/(Kg*k)		Group	Materials	Heat Capacity J/(Kg*k)
1	Concrete	New concrete Old concrete	960	4	Metal	White Metal Red Metal Grey Metal Green Metal Brown Metal	480-530
2	Asphalt & Rubber	New black asphalt Old black asphalt New red asphalt Old red asphalt Rubber	1000	5	Vegetation	Grass Shrubs Trees	1300-2000
3	Bricks & Tiles	Red brick Yellow brick Red Tile Brown Tile Green Tile	800-835	6	Bare-soil	Bare land Soil Mulch	837-910
				7	Water	Water	4187

The second step was to determine the percentage change (increasing/decreasing) in the surface temperature at each half hour for one particular material from each group. This method was used to measure thermal behaviour of the LULC categories depending on their thermal accumulation.

Table 6.3 shows surface temperature observations for old concrete and old black asphalt on the 17th of February 2016, grass and red bricks on the 20th of March 2016, and for brown metal and soil on the 29th of March 2016. Measurements were taken during clear sky at half hour intervals for all these surfaces except soil for which the observation was conducted on an hourly basis.

Table 6.3 Percent change in surface temperature for old concrete, old black asphalt, brown metal, red ground bricks, grass and soil.

Time	Old concrete		Old B asphalt		Brown metal		Red brick		Grass		Soil	
	LST	%chg.	LST	%chg.	LST	%chg.	LST	%chg.	LST	%chg.	LST	%chg.
9	↑39.7	0.061	↑45.4	0.062	↑39.9	0.055	↑32.1	0.055	↑30.6	0.063	↑30.2	0.058
9:30	↑41.9	0.064	↑46.4	0.063	↑47.6	0.065	↑34.4	0.059	↑30.9	0.064		0.063
10	↑44.4	0.068	↑48.2	0.066	↑52	0.071	↑37.2	0.064	↑33.8	0.070	↑35.3	0.067
10:30	↑48.3	0.074	↑52.4	0.072	↑56.3	0.077	↑40.4	0.070	↑36.3	0.075		0.073
11	↑49.5	0.076	↑54.7	0.075	↑59.7	0.082	↑43.9	0.076	↑38.3	0.079	↑41.1	0.078
11:30	↑51.4	0.079	↑57.3	0.078	↑62.5	0.086	↑46.4	0.080	↑39.8	0.083		0.083
12	↑53.3	0.081	↑59.5	0.081	↑63.6	0.087	↑47.4	0.082	↕41.2	0.085	↑45.7	0.087
12:30	↑52.8	0.082	↑60	0.082	↑64.1	0.088	↑49.2	0.085	↓40.9	0.083		0.088
1	↑53.9	0.083	↑60.9	0.083	↕64.9	0.089	↑49.9	0.086	↓40.1	0.082	↕46.3	0.088
1:30	↑54.6	0.083	↑61.7	0.084	↓62.3	0.085	↕50.3	0.087	↓38.8	0.080		0.084
2	↑55.1	0.084	↑62	0.085	↓54.2	0.074	↓50.1	0.086	↓38.6	0.080	↓41.3	0.079
2:30	↕55.2	0.084	↕62.3	0.085	↓53.8	0.074	↓49.6	0.086	↓37.7	0.078		0.077
3	↓54.1	0.082	↓60.5	0.083	↓49.7	0.068	↓48.5	0.084	↓37	0.077	↓39.5	0.075

With regard to the surface temperature variations in Table 6.3, there appears to be differences in thermal performance between each of these materials. It is also important to note that the surface temperature peak times varied depending on the material. It can be concluded that the mean surface temperature of concrete and asphalt increases until 2:30 pm, and for red bricks until 1:30 pm, metal and soil until 1 pm and for vegetation cover until 12 pm, before beginning to decrease.

The mean value of LST for all categories was adjusted to the 10 am Landsat overpass time using the percent changes for the appropriate times of day. For example, the actual value of old red asphalt at 12:30 pm was 67.2 °C (see Table 6.4).The percent change in LST for this group of materials was applied in order to obtain an estimated value of 54 °C at 10 am.

6.3.2. Remotely sensed data

This section describes how surface albedo and surface temperature were derived from Landsat 8 images for the study areas.

6.3.2.1. Surface albedo

Surface reflectance level-2 products from Landsat 8 OLI, available from the U.S. Geological Survey website (USGS, 2018b), were used to retrieve the surface albedo. The formula of (Liang, 2000), which was normalised by Smith (2010) and is presented as Equation 6.1, was used to compute broadband albedos from the narrowband based on the surface reflectance values of the visible bands 2, 4, near-infrared band of 5, SWIR1 band of 6 and SWIR2 band of 7 of Landsat 8. These data were provided in 16-bit signed integers in Geotiff format with values of surface albedo ranging from 0 to 1. This procedure has been shown to produce accurate results in deriving shortwave broadband albedo from surface reflectance satellite data (i.e., Landsat) in previous studies (e.g., Naegeli et al., 2017; He et al., 2018).

$$\alpha = ((0.356\rho_2) + (0.130\rho_4) + (0.373\rho_5) + (0.085\rho_6) + (0.072\rho_7) - 0.018)/1.016 \quad (6.1)$$

Where:

α = Surface albedo

ρ_i = At-surface reflectance values of Landsat 8 bands of 1,2,4,5,6, and 7

6.3.2.2. Surface temperature

The surface temperatures were retrieved from thermal infrared band 10 of the Landsat 8 image. The procedure to estimate surface temperature from Landsat data was described in Section 4.3.2.

6.3.3. Validating surface albedo and land surface temperature

It was considered imperative to validate adjusted field data for surface albedo and surface temperature. Since thermal remote sensing has been successfully used in a range of applications, maps of surface albedo and surface temperature derived from the Landsat 8 image, which had already been validated with other thermal maps and metrological data (see Sections 4.4.2), were selected to verify the adjusted field data. For this purpose, a sampling method was applied to extract the mean value from each

map sample covering an area of 30 × 30 m for surface albedo and surface temperature, and targeted on field sampling coordinates (Figure 6.3).

In this work, albedo was derived from multispectral bands of Landsat 8 OLI data using surface reflectance level-2 products provided by the USGS. In order to interpret the results, a pan-sharpening technique was subsequently used. The ESRI pan-sharpening transformation algorithm was adopted, which uses both multispectral bands and a panchromatic band (Thomas et al., 2008; ESRI, 2015).

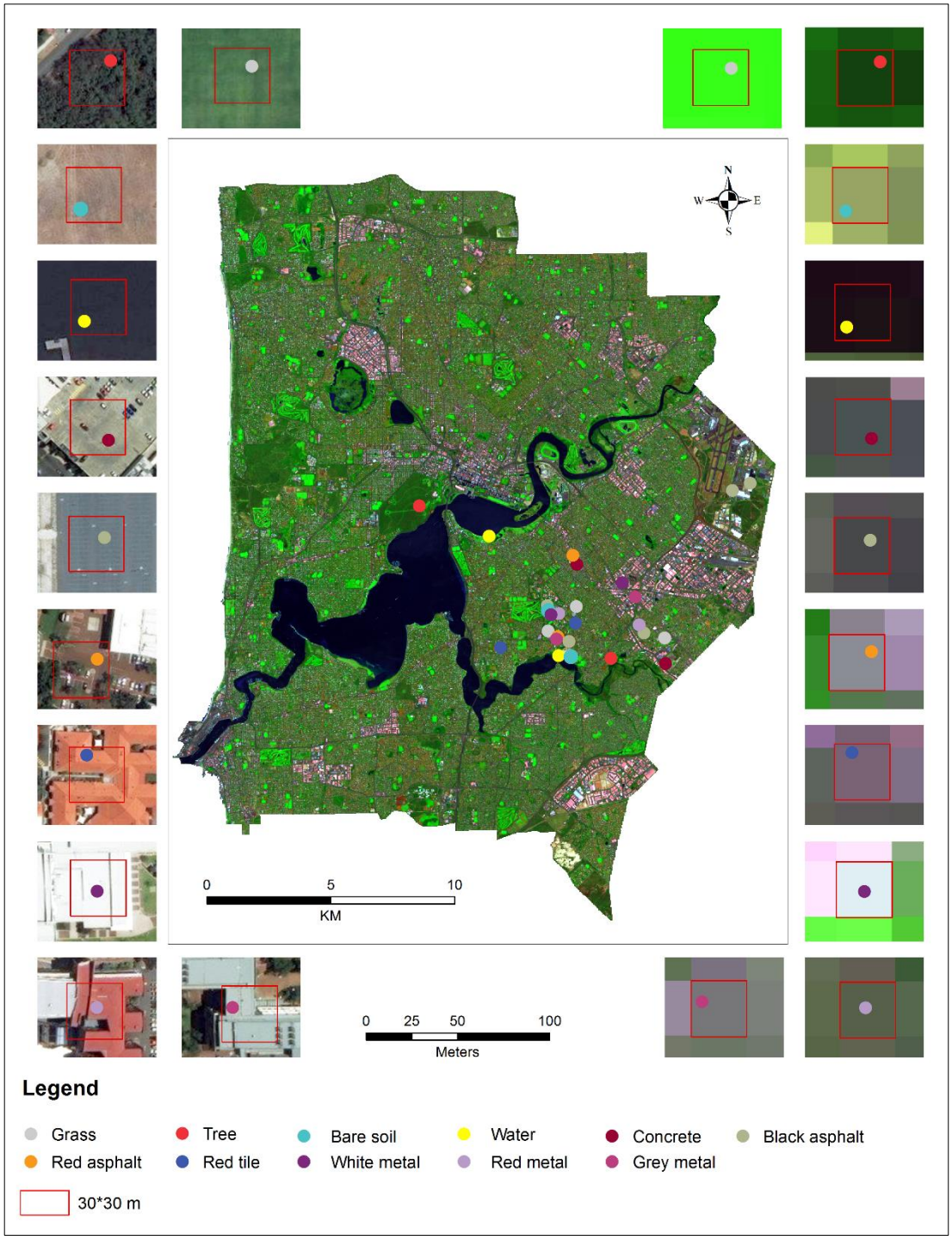

Figure 6.3 Location of field observations within the study area, sampling locations in-situ (left) and on Landsat (right).

The average value of each category was computed from several image areas that matched the field sample sites within the study area. As a result of the differing spatial resolutions, different numbers of categories (eleven and five) were selected to compare surface albedo and surface temperature, respectively. Regression analysis between

adjusted field work data and Landsat derived values of surface albedo and temperature for various categories was carried out.

6. 4. Results and discussion

This section first examines the relationship between Landsat derived surface albedo and surface temperatures and selected adjusted field measurements, as shown in Table 6.4. Then, the influence of thermal properties on the adjusted surface albedo and surface temperature mean values is assessed for the 24 LULC categories of Perth (Table 6.4 and Figure 6.4).

Table 6.4 Actual and adjusted surface albedo and temperature measurements for urban LULC surfaces.

Group	No	Materials	Actual measurements			Adjusted measurements		
			Albedo	LST °C	Time	Albedo	LST °C	Time
1	1	New concrete	0.411	37.7	10	0.411	37.7	10
	2	Old concrete	0.209	47.5	11:30	0.218	41	10
2	3	New black asphalt	0.065	55.7	10	0.065	55.7	10
	4	Old black asphalt	0.152	50.2	10	0.152	50.2	10
	5	New red asphalt	0.13	70.3	2	0.136	54.7	10
	6	Old red asphalt	0.148	67.2	12:30	0.163	54	10
	7	Rubber	0.137	54	10	0.137	54	10
3	8	Red brick	0.171	55.3	11	0.177	46.9	10
	9	Yellow brick	0.247	59.7	2:30	0.246	44.8	10
	10	Red Tile	0.285	51.7	11	0.291	43.8	10
	11	Brown Tile	0.159	64.8	12	0.171	50.9	10
	12	Green Tile	0.242	58.8	3	0.233	45.1	10
4	13	White Metal	0.511	49.5	9:30	0.504	54.1	10
	14	Red Metal	0.287	70.1	12	0.299	57.3	10
	15	Grey Metal	0.34	69.8	12:30	0.355	56.6	10
	16	Green Metal	0.256	57.2	3	0.247	59.8	10
	17	Brown Metal	0.206	66.5	3	0.197	69.6	10
5	18	Grass	0.281	35.4	10	0.281	35.4	10
	19	Shrubs	0.224	35	3	0.215	32	10
	20	Trees	0.152	36.2	11:30	0.161	30.7	10
6	21	Bare land	0.293	56.6	2:30	0.292	49.5	10
	22	Soil	0.278	58	11:30	0.287	47.2	10
	23	Mulch	0.204	51.9	10	0.204	51.9	10
7	24	Water	0.031	30.4	11	0.031	30.4	11

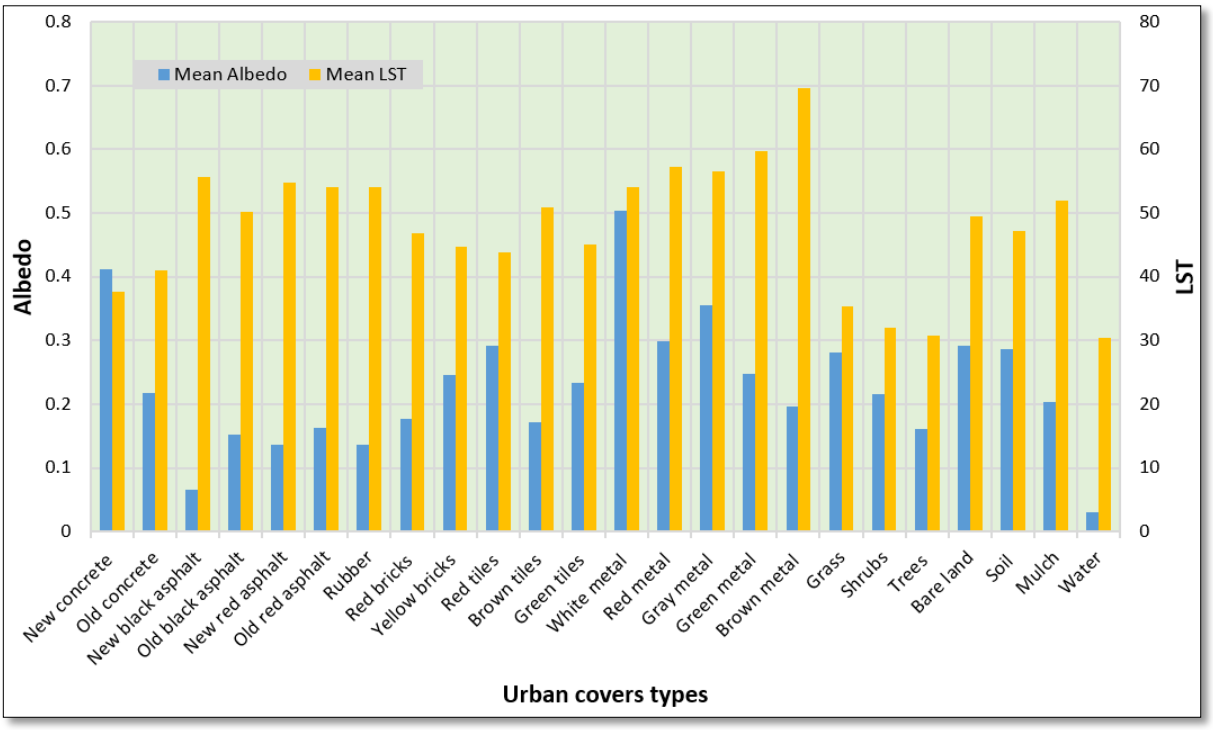

Figure 6.4 Adjusted surface albedo and temperature values.

6.4.1. Verifying adjusted field measurements with Landsat 8 derived values for surface albedo and temperature

Surface albedo and surface temperature play an effective role in a variety of studies, including urban studies, climate studies and environmental studies. Therefore the comparison of adjusted field values of these factors with the validated maps derived from Landsat 8 data was considered necessary for the following analysis.

For surface albedo, the mean values of eleven land use surfaces in Perth were selected for determining the correlation between field measurements and Landsat derived values (Table 6.5). Examination of the correlation coefficient of surface albedo from field data and Landsat showed a strong positive correlation ($r^2 = 0.936$) (Figure 6.5).

Table 6.5 Comparison between adjusted field based albedo and Landsat derived albedo.

	Surface albedo values			
	Materials	Field work	Landsat 8	Difference
1	Old concrete	0.218	0.228	-0.01
2	Old black asphalt	0.152	0.143	0.009
3	Old red asphalt	0.163	0.151	0.012
4	Red Tile	0.291	0.197	0.094
5	White Metal	0.504	0.463	0.041
6	Red Metal	0.299	0.241	0.058
7	Grey Metal	0.355	0.280	0.075
8	Grass	0.281	0.257	0.024
9	Trees	0.161	0.121	0.04
10	Bare-soil	0.287	0.272	0.015
11	Water	0.031	0.039	-0.008

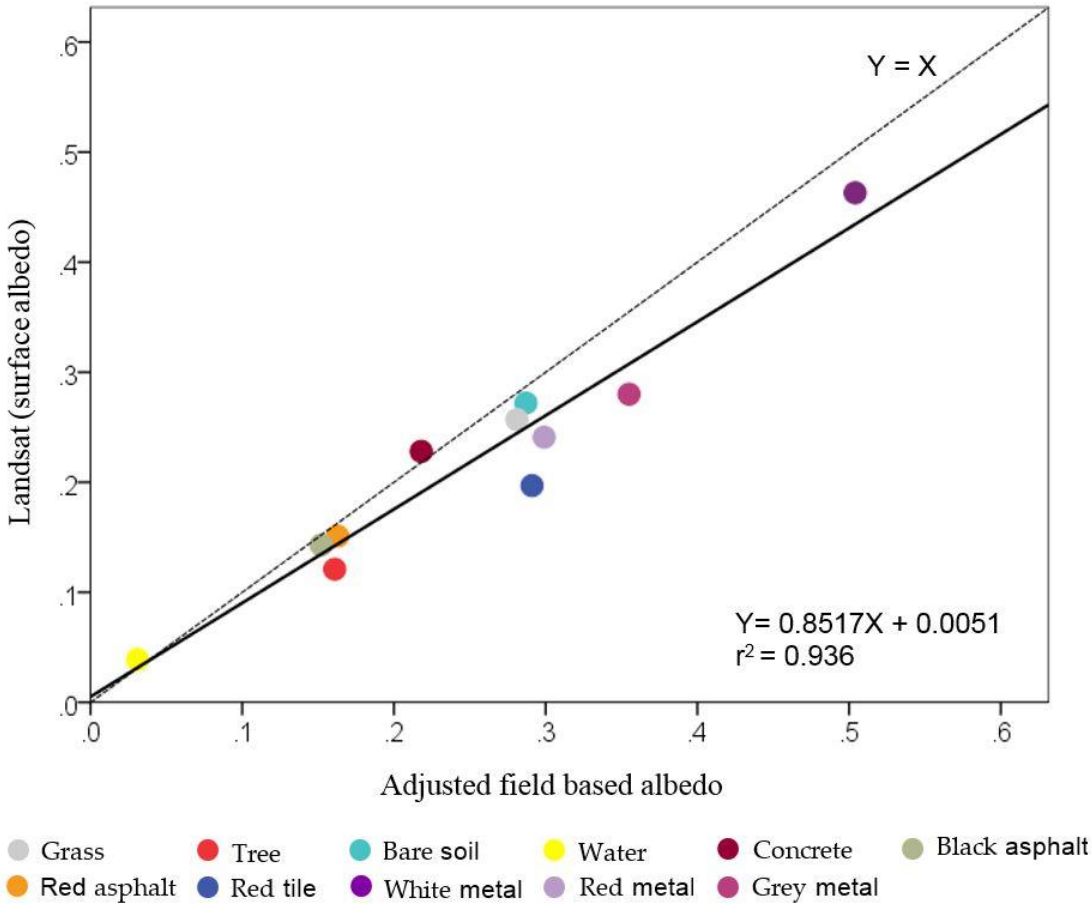

Figure 6.5 Relationship between adjusted field-based albedo and Landsat derived albedo.

The map in Figure 6.6 shows the spatial distribution of surface albedo, which reveals clear edge effects for most categories, especially those having a large area. This edge effect assisted in distinguishing the different urban cover surfaces and was used to identify the features.

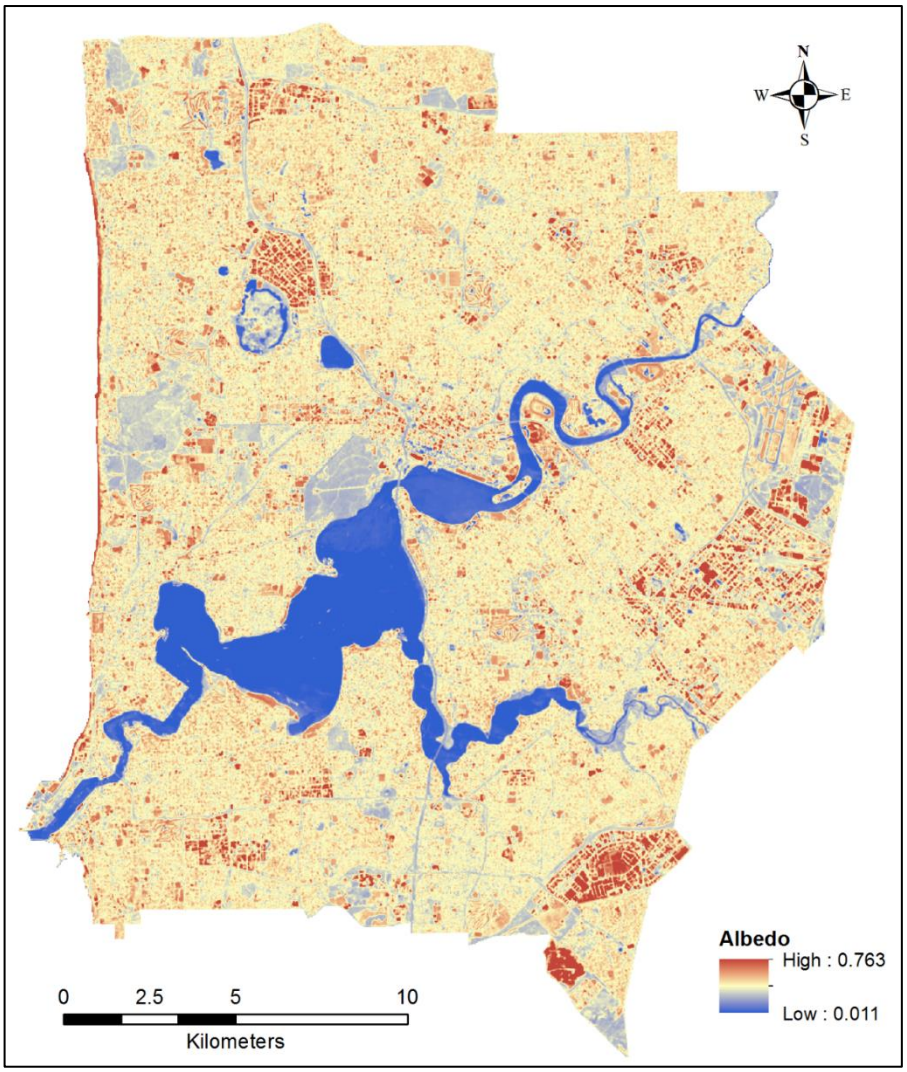

Figure 6.6 Surface albedo map of Perth as derived from the Landsat 8 image.

For surface temperature, the adjusted field work data was also verified using Landsat 8 data derived from band 10 (Figure 6.7), but using fewer categories, since it was difficult to extract individual values for LULC surfaces within the central metropolitan area of Perth. Therefore, the mean values of the categories were computed based on the weight of each category within the sampling grid square (see Section 6.3.3).

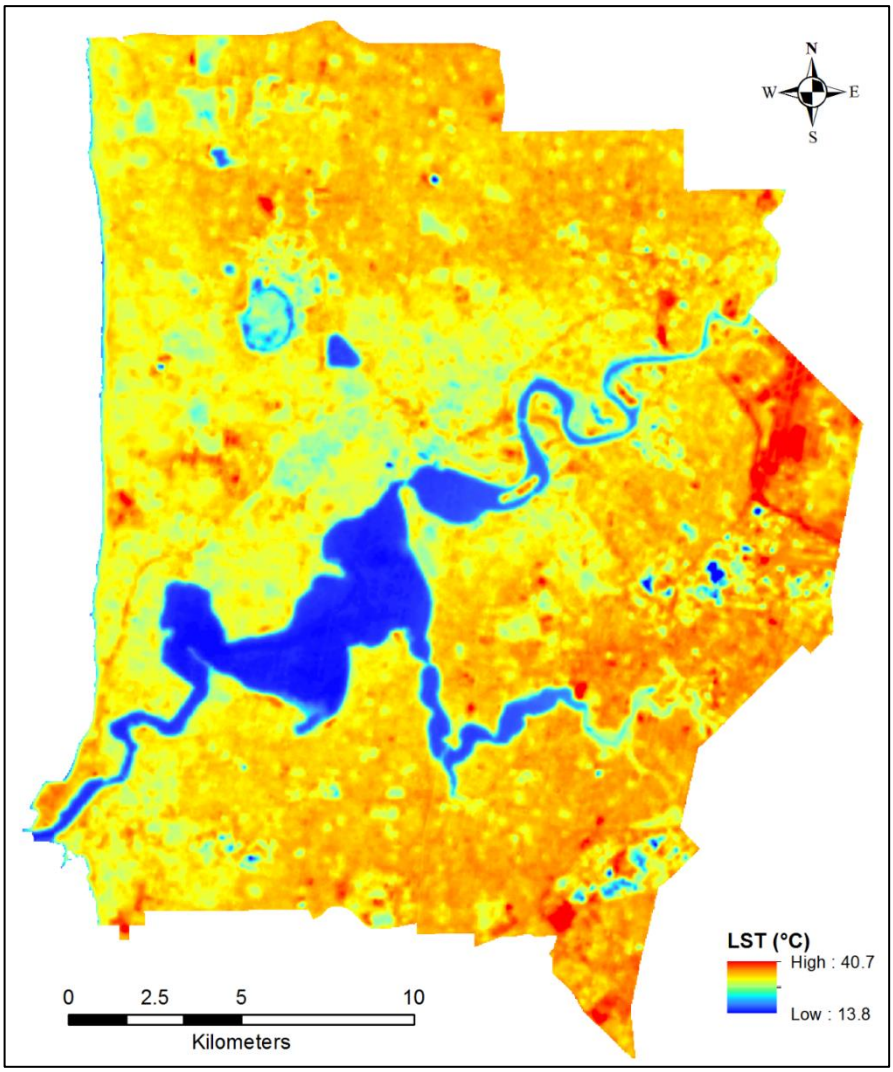

Figure 6.7 Land surface temperature map (in °C) of Perth.

As shown in Table 6.6 and Figure 6.8, a reasonably good agreement was found for these categories with a strong positive correlation (r^2= 0.868) between Landsat values and field data. However there were significant differences for certain categories.

Table 6.6 Comparison between field measurements and Landsat 8 data for surface temperature (°C).

Surface temperature mean values °C						
	Materials	Field work		Landsat 8	Difference	
		Raw	adjusted		Raw	adjusted
1	Grass	35.4	35.4	34.1	1.3	1.3
2	Trees	36.2	30.7	32.0	4.2	-1.3
3	Bare-soil	56.6	48.3	40.5	16.1	7.8
4	Water	30.4	30.4	27.1	3.3	3.3
5	Built-up	61.3	44.4	37.3	25.7	7.1

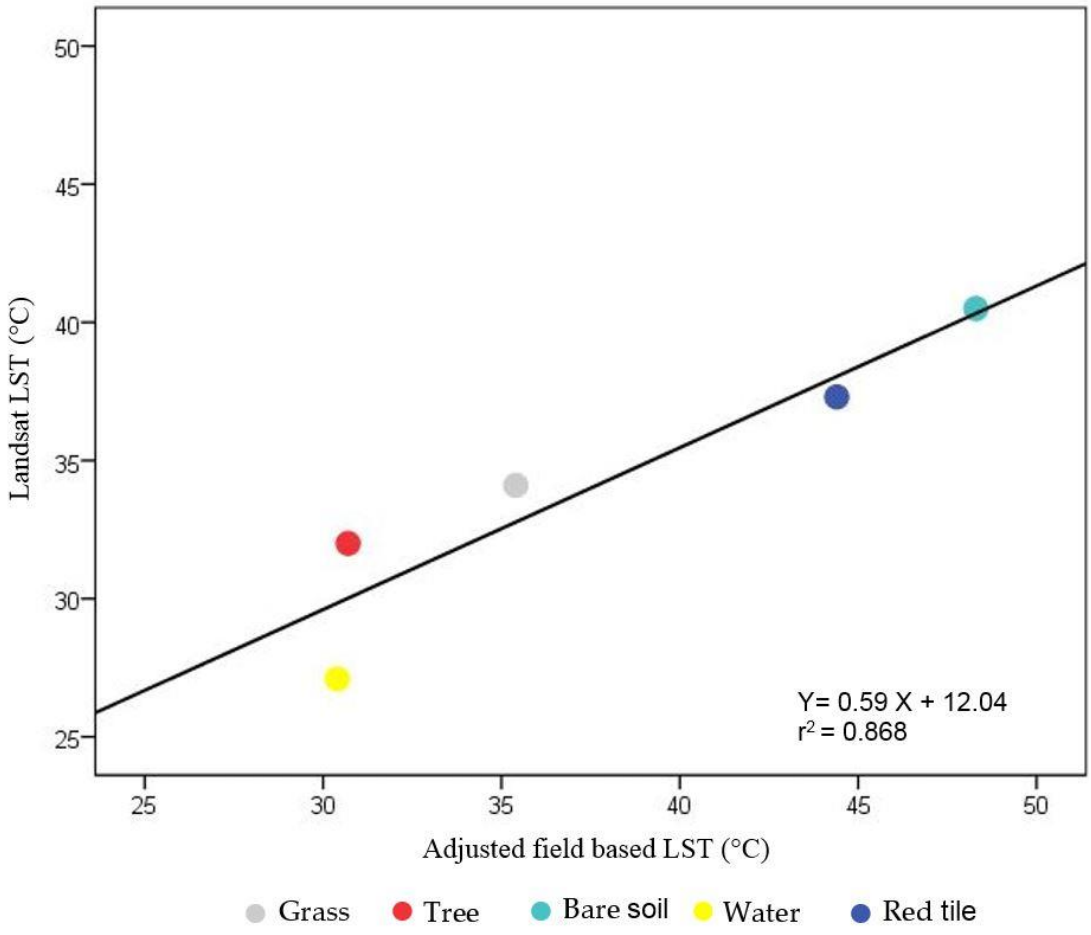

Figure 6.8 Relationship between adjusted field work data and Landsat 8 for LST.

A number of possible reasons, mostly associated with the circumstances of field measurements, are expected to have an effect on the LST values. The field measurements of water bodies in this study were taken from several different locations, which were twenty meters away from the edge of the rivers. These locations may not accurately represent the values for the middle of the river due to the depth of water, as well as the conditions of water in terms of purity. Hence some disparity between datasets may be expected. The analysis revealed that the extracted value from Landsat 8 was 27.1 °C whereas the field value was 30.4 °C for water bodies. This result was expected also because the thermal pixels of Landsat 8 cover a large area of water surface with differing depths. In contrast, field values of water were measured from shallow locations at 11 am (and were not adjusted for diurnal variation), and this delay may have allowed absorption of extra heat by those water bodies. According to Webb and Zhang (1997), the surface albedo and temperature of river water varies from one place to another depending on flow rates and the level of suspended materials.

The average values of bare-soil were significantly different in surface temperature between datasets (48.3 °C from field work, compared to 40.5 °C estimated from Landsat). The surface temperature values of bare-soil categories were observed from vacant land within the study area, which included homogeneous area of mulch, sandy soil, and bare-land. While, the categories represented by several heterogeneous areas included sandy soil, cultivated land, land covered by mulch and woody weeds for Landsat derived surface temperatures. As a result, in-situ value was higher than the estimated Landsat based surface temperature.

For built-up areas, LST obtained from field work represented the mean value of concrete, roof tiles and asphalt whose values varied, being 39.3 °C, 43.8 °C and 50.2 °C respectively. The difference in LST between field work and Landsat data was found to be 7.1 °C. This difference is related to the large pixel size of Landsat TIR bands which may have failed to truly represent each material within the complex built-up surfaces. Also, it can be concluded that the samples may have been influenced by the character of neighbouring surfaces.

In contrast, grass and tree categories did not demonstrate a substantial difference in surface temperature between datasets, which may be mainly due to the fact that these

categories included large areas completely covered by these surfaces. However, there is a slight observed variation which is related to conditions mentioned in section 6.4.2.

For the grass category, the value of surface temperature obtained from the field was 35.4 °C while the estimated value from Landsat was 34.1 °C. This difference may have occurred as a result of heterogeneous grass types in the study area. Estimated surface temperature from Landsat provided a mean value for one pixel (10,000 m^2 resampled to 900 m^2), but field data represented a small area (0.5 m^2) on the ground, which was a sufficiently small scale to be affected by heterogeneity.

Similarly, the trees category had a surface temperature of 30.7 °C from the field and 32.0 °C from Landsat 8. The field measurements were taken from two types of trees, which may have been unrepresentative of the entire category. Whereas, the satellite image is likely to encompass all types of trees. The observed temperature difference between methods may, therefore, be related to the density of different tree types as well as their different moisture content, which may have a variable effect in reducing surface temperatures.

An analysis and comparison of adjusted measurements is therefore found to be reasonable and satisfactory.

6.4.2. Thermophysical behaviour of urban LULC surfaces

The results of field measurements of surface albedo and surface temperature were reported for all selected LULC categories in Table 6.4 and Figure 6.4. It is apparent that there are variations in surface albedo and temperature values among categories resulting from the interaction of solar radiation and urban cover surfaces, as their optical properties such as reflectance, absorption, and transmittance vary considerably.

Generally, it may be seen that the metal group had the highest surface temperature (54.1-69.6 °C), followed by the asphalt (50.2-55.7 °C), bare land (47.2-51.9 °C), bricks (43.8-50.9 °C), concrete (37.7-41 °C), vegetation (30.7-35.4 °C) and water (30.4 °C) categories. In this study, surface albedo and surface temperature of impervious surfaces are characterised by a greater effect on the urban environment relative to non impervious surfaces. In particular, built-up areas with dark colours absorb solar radiation during the day and release it at night. On the other hand, it is apparent that

the thermal behaviour of vegetation has lower contribution to Perth's urban heat environment than other LULC surfaces, as dose the water category. Light coloured surfaces have higher values of albedo and lower surface temperatures compared with dark coloured surfaces, which have a lower albedo and higher surface temperatures.

Moreover, an inverse variation in trend over time between observed surface temperature and surface albedo was identified. It was found that surface temperature increases in the morning and reaches peak in the afternoon based on the type of material, and then started to decrease. Conversely, surface albedo decreases continuously, reaches its minimum at noon and then increases again. This outcome agrees with previous studies (Igusky, 2008; Zhang et al., 2012b) which described the relationship between the surface temperature and surface albedo. This difference produces different effects on the urban environment, depending on the types of land cover, time, geographic location, climate etc.

The following sections describe the results of different surfaces based on field analysis.

(1) Concrete group

This group included two types of concretes based on their age. The first type is new concrete with lighter colours and the second is old concrete with darker colours. New concrete had a higher albedo (0.411) and lower surface temperature (37.7 °C) compared with old concrete, which had an albedo of 0.218 and a surface temperature of 41 °C. The results showed that dropping albedo by approximately one half over time increased surface temperature by approximately 3.3 °C. This indicates that the albedo and temperature of concrete surfaces have an inverse behaviour with time, as described above.

(2) Asphalt and rubber group

This group had the highest heat absorption due to its dark and rough surfaces. In addition, they have high heat capacity and low thermal conductivity. Due to their thermal properties, these categories absorb heat and retain it for a long time, reaching their peak temperatures at 2:30 pm, hours later than most others categories. This group is also affected by aging, which leads to a change in the values of surface albedo and temperature with time. The measured temperature values for new black and red asphalt were higher than old black and red asphalt, which may be directly related to their

relative reflectance and absorption of radiation. Red asphalt, therefore, tends to have a more positive impact on urban environment than black asphalt. Rubber is used to cover concrete roofs, and has the same trends as asphalt in terms of thermal behaviour.

(3) Bricks and tiles group

These types of materials are highly variable and also occur in different colours. Red and yellow bricks that are used for paving ground and red, green and brown tiles which cover most roofs in the study area are made from clay. Yellow bricks had higher albedos and lower surface temperatures than red bricks. The highest albedo (0.291) and lowest surface temperature (43.8 °C) were observed for red tiles, followed by green tiles with 0.233 and 45.1°C respectively, and lowest albedo (0.171) and highest surface temperature (50.9 °C) was observed for brown tiles. It was observed that, despite the fact that this group has relatively low heat capacity, their thermal behaviour depends on surface characteristics. In this group, lighter coloured surfaces may be characterised by lesser thermal impacts, because these kinds of materials have higher reflectance of solar radiation.

(4) Metals group

The metallic material that covers some rooftops in the study area is mostly Colorbond® steel, which is composed of high quality pre-painted steel. According to BlueScope Steel (2012), the white colour may be characterised as a cool material compared with others coloured metals (in shades such as green, blue and brown), which have lower albedos and higher surface temperatures. The results confirmed that the white paint had the highest albedo and lowest surface temperature, and that albedo values reduced and surface temperature values increased gradually from colour to colour such as grey, red, green and brown (Table 6.4). It can also be seen that there was a significant difference between light colour (white) and dark colour (brown) in both values of albedo and surface temperature. Metals, in general, have high absorption and emittance of heat due to their heat capacity and thermal conductivity (Martinez, 2016).

(5) Vegetation group

In this group, vegetation areas included grass, shrubs, and trees, which have surface albedos ranging from 0.161 to 0.281 and surface temperatures ranging from 30.7 to 35.4 °C. This variation is due to the varying characteristics of plants, including density,

shape, water content, etc. In addition, vegetation cover has a wide variation in the values of its heat capacity, which in turn strongly depends on moisture content. The surface albedo mean values of grass, shrubs, and trees were found to be 0.281, 0.215 and 0.161, respectively. Surface temperature mean values were 35.4°C, 32 °C and 30.7 °C respectively. This group is unusual in its thermal behaviour compared with the other groups. These results indicate an inverse thermal behaviour of vegetation compared with non-vegetation categories, in that higher albedo correlates to higher surface temperatures. These results correspond with a previous study (Rajabi & Abu-Hijleh, 2011).

(6) Bare-soil group

This group consists of soil, bare land, and mulch. Its surface albedo mean value ranged from 0.204 to 0.292 and surface temperature mean values ranged from 47.2 to 51.9 °C. This wide range in values is related to the surface characteristics of materials. Surface albedo of bare land (0.292) was found to be higher than soil (0.287) and mulch (0.204). Whereas, its surface temperature value (49.5 °C) was higher than soil (47.2 °C) but less than mulch 51.9 °C. The categories of soil and mulch follow the general reverse correlation between surface albedo and temperature, but bare land does not appear to fit this relationship. This may occur due to the fact that bare land is partly covered with patches of dead grass, thus potentially increasing both values of albedo and surface temperature. However, mulch has low reflectance and high absorption of solar radiation, resulting in a higher thermal capacity. This may have led to a lower albedo value of 0.204 and higher surface temperature of 51.9 °C.

(7) Water group

This group involved only rivers, which represented a large, apparently homogeneous area. Its surface albedo and temperature were 0.031 and 30.4 °C, respectively. It can be inferred that water has a high absorption and low reflectance of radiation, and consequently stores more heat than other categories, due to its high heat capacity (Table 6.2).

In summary, the above results indicate that, despite the fact that each group has similar thermal properties, certain categories have different thermal behaviours depending on the surface characteristics of each category.

In general, lighter coloured surfaces have higher albedos and lower surface temperatures compared to darker coloured surfaces, which have lower albedos and higher surface temperature. Surface albedo and temperature of built-up categories are characterised by a greater impact on the environment compared with non-built up categories. Built-up areas with a dark colours are able to store more heat from solar radiation during the day and radiate in night. Also, as shown in Table 6.3, the thermal accumulation of the LULC categories depends on the time of day of radiation absorption. In this study, LULC categories that had higher thermal accumulation were asphalt and concrete: their surface temperature was higher than other categories, and their influence may be more evident after sunset.

In contrast with other types of materials that have the capability to store heat more throughout the day, metals can affect the urban environment during daytime because of their low heat capacity and accumulation.

On one hand, analysis of the surfaces in built-up areas showed that some categories such as white bare metal, new concrete, and red tiles reflect a significant part of incoming solar radiation, suggesting a mitigating effect on the development of any UHI. In contrast, other surfaces had low reflectance and high absorption, such as black asphalt, rubber, old concrete, red bricks, and dark coloured metal. These covers may produce significant amounts of heat, particularly after sunset, thus leading to an increased UHI effect.

6. 5. Chapter summary

In the urban environment, in-situ measurements of albedo and LST are necessary for assessing the thermal behaviour of LULC. This chapter presented a detailed analysis about the effect of the thermophysical performance of most urban LULC surfaces in Perth using field observations during hot summer days. Data from field work was adjusted using a method that corrected for the time of day of measurement. The adjusted data was correlated with a Landsat 8 image. Thereafter, these findings were discussed in more details to quantify effects of urban LULC surfaces on the UHI of Perth. The results confirmed that the use of the adjustment on field measurements is practical for identifying the thermophysical behaviour of urban LULC surfaces.

7. Conclusions and recommendations

7. 1. Introduction

This thesis evaluated the impact of the surface urban heat island (SUHI) in two cities, Baghdad and Perth, with the use of Landsat data and field measurements. It presented a comprehensive analysis, and addressed three main objectives. The first was to quantify the spatiotemporal expansion of impervious surfaces during the past five decades and assess its effects on the SUHI (chapter 4). The second was to examine the effect of spatial patterns of urban LULC categories on the LST pattern (chapter 5). The third was to investigate the influence of urban LULC characteristics on urban thermal environments (chapter 6).

The energy budget of the urban surface was defined by its surface temperature and albedo. Therefore, the adopted method regarding adjusting field observations with the Landsat data for LST and albedo can accurately contribute in evaluating the urban environments at local scale. Using urban landscape indices as a factor in determining surface temperature patterns can also add more information to the SUHI.

The most important finding of this work was that the spatial patterns of urban landscape and the characteristics of urban surfaces had significant impacts on the LST patterns that occurred in both cities, irrespective of the amount of urban expansion. The outcome of this study are expected to be valuable for researchers, urban planners, environmental engineers who work in urban thermal environment. It could further help to achieve sustainable development goals in the urban environment.

In this chapter, the results and discussions of these objectives are summarised, concluded, and further recommendations are given in the following three sections.

In this chapter, the results and discussions of these objectives are summarised, concluded, and further recommendations are given in the following three sections.

7. 2. Spatiotemporal dynamics of impervious surfaces and LST

Chapter 4 presented a quantitative evaluation of the spatiotemporal dynamics of impervious surfaces during the summers of 1976, 1984, 1992, 2000 and 2015 for

Baghdad, and 1974, 1988, 1997, 2008 and 2015 for Perth using multi-date Landsat data. The spatiotemporal variations of the LST pattern for the same datasets above (excepting the 1970s) as well as the temporal and seasonal variation of the SUHI for both cities were also investigated. The results revealed that:

a) The adopted approach for extracting impervious surfaces used in this work was effective with regard to the accuracy level of ISA maps.

b) Combining ISA maps with a zones division was another powerful approach described in chapter 4 for determining precise amounts and directions of built-up area changes over time.

c) The area of impervious surfaces for Baghdad increased by 18.6% during the period from 1976 to 2015, whereas Perth had increases of 14.1% during the period from 1974 to 2015. However, LST of built-up areas and then the SUHI intensity were significantly elevated in Baghdad in comparison to Perth.

d) Impervious surface area was proved to be an important indicator that can be effectively used to study the effects of urban heat islands in addition to other environmental issues.

e) Evaluation of the spatiotemporal variations of impervious surfaces and LSTs of two contrasting cities from developed and developing countries, each having hot summers, is expected to benefit researchers working within the area of urban thermal environment.

7.2.1. Recommendations

a) It may be important to investigate the relationship between impervious surface area and SUHI using higher spatial resolution datasets (e.g., Sentinel imagery). Spectral mixture analysis (SMA) can typically be used for the analysis (Tromp & Epema, 1998).

b) It is recommended that the spatiotemporal changes in major LULC categories (i.e., vegetation cover, water bodies, and bare land along with impervious

surfaces) be quantified, and their relationships with the LST pattern be compared.

c) The problem of spectrally-mixed pixels over urban areas using Landsat data, particularly between bright impervious surfaces and dry soil, still exists (Weng & Hu, 2008; Weng, 2012). Fusion of a nighttime thermal image with daytime multispectral bands, which were examined by the author (Naem et al., 2016), could be a feasible approach to overcome this problem using ISA techniques.

7. 3. Urban landscape pattern and LST

Chapter 5 first quantified the spatial distribution of land use and land cover (LULC) categories, as well as the intensity of impervious surfaces. It then examined the relationship between LST and each of the percent ISA and landscape metrics using, Shannon's diversity index (SHDI), modified Simpson's evenness index (MSIEI), Shannon's evenness index (SHEI), and patch density (PD). The analysis of the relationships was employed to understand the extent to which the urban thermal environment is influenced by the spatial patterns of land use and land cover (LULC) categories. The analysis revealed that:

a) Percent impervious surface area (PISA) and impervious surface analysis tool (ISAT) are useful parameters that can be used to provide detailed information about the distribution and amount of impervious surfaces in a specific area.

b) The differences between the two cities in the spatial distributions of impervious surfaces intensities and their effect on the LST pattern was pronounced.

c) Statistical analysis of the correlation coefficients indicated opposite relationships between Baghdad and Perth for the correlations for each of the landscape metrics with LST.

d) Creating a grid of 100 × 100 m, matching the spatial resolution of thermal Landsat data, was an appropriate scale to extract and analyse values of PISA, landscape metrics, and LST within the urban environment.

e) Support and regulation by local authorities for green infrastructure within a city, in addition to strong planning regulations, have a significant impact on the urban thermal environment.

f) Socioeconomic and political circumstances also had a significant effect on the behaviour of the urban thermal environments in the two cities.

g) Studying urban landscape patterns in two contrasting cities may be useful for formulating sustainable urban environmental management by determining the causative factors and devising pertinent strategies for mitigating the effect of SUHI in cities.

7.3.1. Recommendations

a) Since there are a considerable number of landscape metrics that have been previously used in assessing the pattern and structure of the landscape, it is recommended that other spatial metrics also be compared with the LST pattern, at different scales over an urban area to determine further appropriate metrics to be used in analysing LST.

b) In order to mitigate the effect of the UHI in Baghdad, it is recommended that a comprehensive environmental policy be implemented in terms of:

- Increases in vegetation cover and water bodies, including their optimal spatial distribution within residential, industrial and commercial areas.

- Implementing and monitoring environmental regulations and planning by the related authorities.

7. 4. Urban LULC characteristics and LST

Chapter 6 implemented an integrated approach, utilising field measurements and remotely sensed data, to investigate the thermophysical behaviour of urban LULC categories in Perth. In this study, a new hypothetical method was suggested for temporally adjusting the surface albedo and LST for all collected field data, to the time of the satellite overpass. The application and calibration of this method confirmed that

the adjusted field data was accurate and appropriate for analysing and characterising the impact various LULC categories on the urban thermal environment. This section of the thesis showed that:

a) Surface albedo and LST, retrieved from Landsat data, may be effectively used as parameters to locate hot and cold spots, and to quantify the thermal pattern.

b) Using albedo (at a scale of 30 × 30 m) along with LST (at 100 × 100 m), retrieved from Landsat data, it was possible to make thermal pattern interpretations of the urban areas to a good level of detail. However, field measurements of albedo and LST at a very fine scale over heterogeneous urban areas can provide further detailed information and more accurate outcomes for characterising the thermophysical behaviour of various urban LULC categories.

c) Adjustment values of surface albedo and LST collected from field measurements at the time of satellite overpass may be an appropriate approach in analysing urban thermal environments. The problem of time differences among field measurements, and satellite data, could be overcome by this approach.

d) The relationship between albedo and LST was found to be unusual for the vegetation group (i.e., grass, shrubs, and trees) compared with other LULC groups. This may be due to the physical characteristics of plants such as density, shape, water content, etc.

e) The colour of various materials (e.g., due to painting) in urban surfaces is an important factor in determining the thermal behaviour of surfaces.

7.4.1. Recommendations

a) In order to investigate thermophysical behaviour of a greater number of LULC categories, further comparison experiments between field measurements and remotely sensed data should be attempted. It is recommended to use high spatial resolution remote sensing data to accompany the field work.

b) The urban thermal environment may be greatly influenced by the characteristics of urban land use surfaces. Therefore, using suitable building and paving materials, which have high albedo reflectance and less absorbance and heat storage, may contribute to mitigating the UHI effect.

c) New technologies using Unmanned Aerial Vehicles (UAVs), which have been recently developed and devoted to use in remote sensing applications, can be employed to further characterise thermal behaviour of urban surfaces. This technique can provide significant advantages (Themistocleous, 2014):

- Various sensors can be installed onto the platform, which is important for a more complete picture of urban areas.
- A number of remote sensing techniques can be used with UAVs.
- Reduction in time, effort and cost compared with a hand-held instrument.
- Scale effects can be better considered when integrating UAVs data with the satellite data.

d) It is recommended that the approach applied in this thesis be a used to examine other different climatic sites and the thermophysical behaviour of their urban surfaces.

e) Further research to investigate the thermal behaviour of urban LULC surfaces in the evening or night, along with daytime, using both thermal remote sensing data and field measurements, should be conducted to improve our knowledge about their diurnal thermal variations.

References

ABS. (2012). Australian Bureau of Statistics, Geography and climate, Australian's climate. Retrieved from http://www.abs.gov.au/ausstats/abs@.nsf/Lookup/by%20Subject/1301.0~2012~Main%20Features~Australia's%20climate~143.

ABS. (2015). Australian Bureau of Statistics, Sunshine: Average Daily Sunshine Hours. Retrieved from http://www.bom.gov.au/watl/sunshine/.

Adebayo, Y. R. (1987). The effect of urbanization on some characteristics of relative humidity in Ibadan. *Journal of climatology, 7*(6), 599-607.

Ahmed, A. Q., Ossen, D. R., Jamei, E., Manaf, N. A., Said, I., & Ahmad, M. H. (2014). Urban surface temperature behaviour and heat island effect in a tropical planned city. *Theoretical and Applied Climatology, 119*(3-4), 493-514.

Akbari, H., Berdahl, P., Levinson, R., Wiel, S., Miller, B., & Desjarlais, A. (2006). *Cool color roofing materials*: Berkeley, California Energy Commission, PIER Building End-Use Energy Efficiency Program. CEC-500-2006-067.

Akbari, H., Davis, S., Huang, J., Dorsano, S., & Winnett, S. (1992). *Cooling our communities: a guidebook on tree planting and light-colored surfacing*. United States: Lawrence Berkeley Laboratory Report LBL-31587.

Akbari, H., Pomerantz, M., & Taha, H. (2001). Cool surfaces and shade trees to reduce energy use and improve air quality in urban areas. *Solar energy, 70*(3), 295-310.

Akbari, H., Rosenfeld, A., & Taha, H. (1990). *Summer heat islands, urban trees, and white surfaces*. Berkeley, California. Energy Analysis Program, Center for Building Science, Applied Science Division, Lawrence Berkeley Laboratory, University of California.

Al-Dabbas, M. A., Al-Zubaidi, A. A., & Al-Khafaji, R. (2015). Impact of climate changes on the hydrochemistry of Razaza Lake and Rahaliya–Shithatha Springs–Central Iraq. *Journal of Environment and Earth Science, 5*(6), 106-115.

Al-Waeely, A., Salman, S., Abdol-Reza, W., Chaichan, M., Kazem, H., & Al-Jibori, H. (2014). Evaluation of the spatial distribution of shared electrical generators and their environmental effects at Al-Sader City-Baghdad-Iraq. *International Journal of Engineering & Technology IJET-IJENS, 14*(2), 16-23.

Alasady, A. M. A. (2011). *Solar energy the suitable energy alternative for Iraq beyond oil*. Paper presented at the Proceedings of the international conference on petroleum and sustainable development (IPCBEE), Singapore.

Alcoforado, M. J., & Andrade, H. (2008). Global warming and the urban heat island *Urban ecology* (pp. 249-262): Springer.

Ali, S. H., Daood, N. A., & Ibrahim, L. K. (2015). Derivation of seasonal variation maps of the average precipitation in Iraq by using remote sensing data and geographical information system. *Arabian Journal of Geosciences, 8*(7), 4741-4753.

Angel, S., Parent, J., Civco, D. L., Blei, A., & Potere, D. (2011). The dimensions of global urban expansion: Estimates and projections for all countries, 2000–2050. *Progress in Planning, 75*(2), 53-107.

Arnold Jr, C. L., & Gibbons, C. J. (1996). Impervious surface coverage: the emergence of a key environmental indicator. *Journal of the American planning Association, 62*(2), 243-258.

Artis, D. A., & Carnahan, W. H. (1982). Survey of emissivity variability in thermography of urban areas. *Remote Sensing of Environment, 12*(4), 313-329.

Asaeda, T., Ca, V. T., & Wake, A. (1996). Heat storage of pavement and its effect on the lower atmosphere. *Atmospheric Environment, 30*(3), 413-427.

Asgarian, A., Amiri, B. J., & Sakieh, Y. (2015). Assessing the effect of green cover spatial patterns on urban land surface temperature using landscape metrics approach. *Urban Ecosystems, 18*(1), 209-222.

ASTM Standard E1918-06. (2006). *Standard test method for measuring solar reflectance of horizontal and low-sloped surfaces in the field*. ASTM International, West Conshohocken, PA.

Atkinson, B. (2003). Numerical modelling of urban heat-island intensity. *Boundary-Layer Meteorology, 109*(3), 285-310.

Ayanlade, A., & Jegede, O. O. (2015). Evaluation of the intensity of the daytime surface urban heat island: how can remote sensing help? *International Journal of Image and Data Fusion, 6*(4), 348-365.

Bagan, H., & Yamagata, Y. (2012). Landsat analysis of urban growth: How Tokyo became the world's largest megacity during the last 40 years. *Remote Sensing of Environment, 127*, 210-222.

Banzhaf, E., Grescho, V., & Kindler, A. (2009). Monitoring urban to peri-urban development with integrated remote sensing and GIS information: A Leipzig, Germany case study. *International Journal of Remote Sensing, 30*(7), 1675-1696.

Bao, T., Li, X., Zhang, J., Zhang, Y., & Tian, S. (2016). Assessing the distribution of urban green spaces and its anisotropic cooling distance on urban heat island pattern in Baotou, China. *ISPRS International Journal of Geo-Information, 5*(2), 1-13.

Bechtel, B., Zaksek, K., & Hoshyaripour, G. (2012). Downscaling land surface temperature in an urban area: A case study for Hamburg, Germany. *Remote Sensing, 4*(10), 3184-3200.

Becker, F., & Li, Z.-L. (1990). Towards a local split window method over land surfaces. *Remote Sensing, 11*(3), 369-393.

Bektas Balcik, F. (2014). Determining the impact of urban components on land surface temperature of Istanbul by using remote sensing indices. *Environmental Monitoring and Assessment, 186*(2), 859-872.

Blakely, E. J., & Carbonell, A. (2012). *Resilient coastal city regions: Planning for climate change in the United States and Australia*: Lincoln Institute of Land Policy.

BlueScope Steel. (2012). *Colobond steel general information-Datasheet*. B. Steel. Retrieved from http://www.bluescopesteel.com.au/files/dmfile/COLORBONDGeneral-Information-Datasheet_June2012.pdf.

Boardman, J. W., & Kruse, F. A. (1994). *Automated spectral analysis: A geological example using AVIRIS data, north Grapevine Mountains, Nevada.* Paper presented at the Proceeding of the ERIM tenth thematic conference on geologic remote sensing, Ann Arbor, MI (pp. 407-418).

Bokaie, M., Zarkesh, M. K., Arasteh, P. D., & Hosseini, A. (2016). Assessment of Urban Heat Island based on the relationship between land surface temperature and Land Use/ Land Cover in Tehran. *Sustainable Cities and Society, 23*, 94-104.

BOM. (2015). *Australian Bureau of Meteorology, Weather and climate data of Perth*. Retrieved from http://www.bom.gov.au/climate/data/index.shtml?bookmark=136.

Bonafoni, S., Baldinelli, G., Rotili, A., & Verducci, P. (2017). Albedo and surface temperature relation in urban areas: Analysis with different sensors. *Urban Remote Sensing Event (JURSE), held in Dubai, United Arab Emirates (6-8 March 2017)*. (pp. 1-4). IEEE.

Botequila Leitao, A., Miller, J., Ahern, J., & McGarigal, K. (2006). *Measuring landscapes, a professional planner's manual*: Island Press, Washington, DC.

Bounoua, L., DeFries, R., Collatz, G. J., Sellers, P., & Khan, H. (2002). Effects of land cover conversion on surface climate. *Climatic Change, 52*(1-2), 29-64.

Brabec, E., Schulte, S., & Richards, P. L. (2002). Impervious surfaces and water quality: A review of current literature and its implications for watershed planning. *Journal of Planning Literature, 16*(4), 499-514.

Cabral, P., Gilg, J.-P., & Painho, M. (2005). *Monitoring urban growth using remote sensing, GIS, and spatial metrics.* Paper presented at the Proc. SPIE 5884, remote sensing and modeling of ecosystems for sustainability II, San Diego, California, USA.

Chadchan, J., & Shankar, R. (2012). An analysis of urban growth trends in the post-economic reforms period in India. *International Journal of Sustainable Built Environment, 1*(1), 36-49.

Chapman, S., Watson, J., Salazar, A., Thatcher, M., & McAlpine, C. (2017). *The impact of urbanization and climate change on urban temperatures: a systematic review.*

Charabi, Y., & Bakhit, A. (2011). Assessment of the canopy urban heat island of a coastal arid tropical city: The case of Muscat, Oman. *Atmospheric Research, 101*(1), 215-227.

Chavez, P. S. (1988). An improved dark-object subtraction technique for atmospheric scattering correction of multispectral data. *Remote sensing of environment, 24*(3), 459-479.

Chen, X.-L., Zhao, H.-M., Li, P.-X., & Yin, Z.-Y. (2006). Remote sensing image-based analysis of the relationship between urban heat island and land use/cover changes. *Remote sensing of environment, 104*(2), 133-146.

Chen, Y.-C., Yao, C.-K., Honjo, T., & Lin, T.-P. (2018). The application of a high-density street-level air temperature observation network (HiSAN): Dynamic variation characteristics of urban heat island in Tainan, Taiwan. *Science of The Total Environment, 626*, 555-566.

Christen, A., & Vogt, R. (2004). Energy and radiation balance of a central European city. *International Journal of Climatology, 24*(11), 1395-1421.

City of Perth. (2016a). *Environment strategy*. Retrieved from https://www.perth.wa.gov.au/planning-development/environment-and-sustainability/sustainability-city.

City of Perth. (2016b). *Urban forest plan, 2016-2036*. Retrieved from https://www.perth.wa.gov.au/planning-development/city-initiatives/urban-forest-plan.

Colebatch, T. (2016). *Australia's urban boom: The latest evidence*. Retrieved from http://insidestory.org.au/australias-urban-boom-the-latest-evidence.

Confalonieri, U., Menne, B., Akhtar, R., Ebi, K. L., Hauengue, M., Kovats, R. S., . . . Woodward, A. (2007). Human health. In M. L. Parry, O. F. Canziani, J. P. Palutikof, P. J. v. d. Linden & C. E. Hanson (Eds.), *Climate change 2007: impacts, adaptation and vulnerability. Contribution of Working Group II to the Fourth Assessment Report of the Intergovernmental Panel on Climate Change* (pp. 391-431). Cambridge, UK: Cambridge University Press.

Congalton, R. G. (1991). A review of assessing the accuracy of classifications of remotely sensed data. *Remote sensing of environment, 37*(1), 35-46.

Connoley, T. (2013). *Mapping Perth's population growth*. Urban Development Institute of Australia.Retrieved from http://blog.udiawa.com.au/article/mapping-perths-population-growth-13.

CSO. (2012). The Central Organization for Statistics, Ministry of Planning, Iraq-Statistical data of population for Baghdad province. Retrieved from http://www.cosit.gov.iq.

Dai, Z., Guldmann, J.-M., & Hu, Y. (2018). Spatial regression models of park and land-use impacts on the urban heat island in central Beijing. *Science of The Total Environment, 626*, 1136-1147.

Davies, F., Middleton, D. R., & Bozier, K. E. (2007). Urban air pollution modelling and measurements of boundary layer height. *Atmospheric Environment, 41*(19), 4040-4049.

Davis, D. E. (2016). Reflections on the relations between development and urbanization: past trajectories and future challenges. *International Journal of Urban Sciences, 20*(1), 1-14.

Day, C., & Roaf, S. (2007). *Ecohouse: a design guide*: Routledge.

Deng, Y., Fan, F., & Chen, R. (2012). Extraction and analysis of impervious surfaces based on a spectral un-mixing method using Pearl River Delta of China Landsat TM/ETM+ imagery from 1998 to 2008. *Sensors, 12*(2), 1846-1862.

Dimoudi, A., & Nikolopoulou, M. (2003). Vegetation in the urban environment: microclimatic analysis and benefits. *Energy and buildings, 35*(1), 69-76.

Ding, F., & Xu, H. Q. (2008). Comparison of three algorithms for retrieving land surface temperature from Landsat TM thermal infrared band. *Journal of Fujian Normal University (Natural Science Edition), 24*(1), 91-96.

Duarte, D. H., Shinzato, P., dos Santos Gusson, C., & Alves, C. A. (2015). The impact of vegetation on urban microclimate to counterbalance built density in a subtropical changing climate. *Urban Climate, 14*, 224-239.

Dupont, C., Chiriac, R., Gauthier, G., & Toche, F. (2014). Heat capacity measurements of various biomass types and pyrolysis residues. *Fuel, 115*, 644-651.

Dwivedi, A., & Mohan, Buddhiraju K. (2018). Impact of green roof on micro climate to reduce Urban Heat Island. *Remote Sensing Applications: Society and Environment, 10*, 56-69.

Earl-Slater, A. (2002). *The handbook of clinical trials and other research*: Radcliffe Publishing.

Elsayed, I. S. (2012). A study on the urban heat island of the city of Kuala Lumpur, Malaysia. *Journal of King Abdulaziz University, 23*(2), 121-134.

Emmanuel, R., & Krüger, E. (2012). Urban heat island and its impact on climate change resilience in a shrinking city: The case of Glasgow, UK. *Building and Environment, 53*, 137-149.

EPA. (2014). *Reducing Urban Heat Islands: Compendium of Strategies, U.S. Environmental Protection Agency*. Retrieved from https://www.epa.gov/sites /production/files/2014-06/documents/basicscompendium.pdf.

ESRI. (2013). Environmental Systems Research Institute, ArcGIS Desktop software (Version 10.2). United States: Esri Inc, Redlands.

ESRI. (2015). Fundamentals of panchromatic sharpening, ArcGIS Help 10.4. Retrieved from http://desktop.arcgis.com/en/arcmap/10.3/manage-data/raster-and-images/fundamentals-of-panchromatic-sharpening.htm#ESRI_SECTION 1_E7746E90388943A4A24BFF776C6E87DF.

Estoque, R. C., & Murayama, Y. (2017). Monitoring surface urban heat island formation in a tropical mountain city using Landsat data (1987–2015). *ISPRS Journal of Photogrammetry and Remote Sensing, 133*, 18-29.

EXELIS. (2013). Environment for Visualizing Images (ENVI), image processing and analysis software (Version 5.1). United States.

Fall, S., Niyogi, D., Gluhovsky, A., Pielke, R. A., Kalnay, E., & Rochon, G. (2010). Impacts of land use land cover on temperature trends over the continental United States: assessment using the North American Regional Reanalysis. *International Journal of Climatology, 30*(13), 1980-1993.

Fathizad, H., Tazeh, M., Kalantari, S., & Shojaei, S. (2017). The investigation of spatiotemporal variations of land surface temperature based on land use changes using NDVI in southwest of Iran. *Journal of African Earth Sciences, 134*, 249-256.

FLIR E5. (2014). *FLIR E5 Datasheet*. Retrieved from http://www.infraredcamera warehouse.com/content/FLIR%20Datasheets/FLIR%20E5%20Datasheet.pdf.

Foody, G. M. (2002). Status of land cover classification accuracy assessment. *Remote sensing of environment, 80*(1), 185-201.

Ford, K. (1979). *Remote sensing for planners*: Center for Urban Policy Research.

Fouillet, A., Rey, G., Laurent, F., Pavillon, G., Bellec, S., Guihenneuc-Jouyaux, C., . . . Hémon, D. (2006). Excess mortality related to the August 2003 heat wave in France. *International archives of occupational and environmental health, 80*(1), 16-24.

Freestone, R. (2009). *Cities, citizens and environmental reform: Histories of Australian town planning associations*: Sydney University Press.

Gabriel, K. M., & Endlicher, W. R. (2011). Urban and rural mortality rates during heat waves in Berlin and Brandenburg, Germany. *Environmental pollution, 159*(8), 2044-2050.

Gallo, K. P., Tarpley, J. D., McNab, A. L., & Karl, T. R. (1995). Assessment of urban heat islands: A satellite perspective. *Atmospheric Research, 37*(1-3), 37-43.

Geoscience Australia. (2016). Digital Elevation Data. Retrieved from http://www.ga.gov.au/scientific-topics/national-location-information/digital-elevation-data.

Gillespie, A. (2014). Land Surface Emissivity. In E. G. Njoku (Ed.), *Encyclopedia of Remote Sensing* (pp. 303-311). New York, NY: Springer New York.

Giridharan, R., Lau, S. S. Y., Ganesan, S., & Givoni, B. (2007). Urban design factors influencing heat island intensity in high-rise high-density environments of Hong Kong. *Building and Environment, 42*(10), 3669-3684.

Goward, S. N. (1981). Thermal behavior of urban landscapes and the urban heat island. *Physical Geography, 2*(1), 19-33.

Green, A. A., Berman, M., Switzer, P., & Craig, M. D. (1988). A transformation for ordering multispectral data in terms of image quality with implications for noise removal. *IEEE Transactions on Geoscience and Remote Sensing, 26*(1), 65-74.

Griffith, J. A., Trettin, C. C., & O'Neill, R. V. (2002). A landscape ecology approach to assessing development impacts in the tropics: A geothermal energy example in Hawaii. *Singapore Journal of Tropical Geography, 23*(1), 1-22.

Gunter, F. R. (2013). *The political economy of Iraq: Restoring balance in a post-conflict society*: Edward Elgar Publishing Limited.

GWRC. (2010). *Estimating impervious surface area: A comparative assessment of CITY green and NOAA's impervious surface analysis tool (ISAT) methodologies*. Retrieved from www.deq.state.va.us/portals/0/deq/coastal zonemanagement/task12-03-09a.pdf.

Hajj, M. E., Bégué, A., Lafrance, B., Hagolle, O., Dedieu, G., & Rumeau, M. (2008). Relative Radiometric Normalization and Atmospheric Correction of a SPOT 5 Time Series. *Sensors (Basel, Switzerland), 8*(4), 2774-2791.

Hamdi, R. (2010). Estimating urban heat island effects on the temperature series of Uccle (Brussels, Belgium) using remote sensing data and a land surface scheme. *Remote Sensing, 2*(12), 2773-2784.

Hao, P., Niu, Z., Zhan, Y., Wu, Y., Wang, L., & Liu, Y. (2016). Spatiotemporal changes of urban impervious surface area and land surface temperature in Beijing from 1990 to 2014. *GIScience & Remote Sensing, 53*(1), 63-84.

Hathout, S. (2002). The use of GIS for monitoring and predicting urban growth in East and West St Paul, Winnipeg, Manitoba, Canada. *Journal of Environmental management, 66*(3), 229-238.

He, T., Liang, S., Wang, D., Cao, Y., Gao, F., Yu, Y., & Feng, M. (2018). Evaluating land surface albedo estimation from Landsat MSS, TM, ETM+, and OLI data based on the unified direct estimation approach. *Remote Sensing of Environment, 204*, 181-196.

Hens, H. S. (2016). *Applied building physics: Ambient conditions, building performance and material properties*. Berlin, Germany: Ernts & Sohn.

Heo, J., & FitzHugh, T. W. (2000). A standardized radiometric normalization method for change detection using remotely sensed imagery. *Photogrammetric Engineering and Remote Sensing, 66*(2), 173-181.

Herold, M., Couclelis, H., & Clarke, K. C. (2005). The role of spatial metrics in the analysis and modeling of urban land use change. *Computers, Environment and Urban Systems, 29*(4), 369-399.

Herold, M., & Menz, G. (2000). *Landscape metric signatures (LMS) to improve urban land use information derived from remotely sensed data.* Paper presented at the Proceedings of the 20th EARSeL Symposium, June 2000, pp. 251–256, Dresden, Germany.

Howard, L. (1833). *Climate of London deduced from meteorological observations* (Vol. 1-3). London: Harvey and Darton.

Hu, F., Liu, X. M., Li, L., & Wang, Y. (2006). Summer urban climate trends and environmental effect in the Beijing area. *Chinese Journal of Geophysics, 49*(3), 617-626.

Huang, G., Zhou, W., & Cadenasso, M. (2011). Is everyone hot in the city? Spatial pattern of land surface temperatures, land cover and neighborhood socioeconomic characteristics in Baltimore, MD. *Journal of environmental management, 92*(7), 1753-1759.

Hurd, J. D., & Civco, D. L. (2004). *Temporal characterization of impervious surfaces for the State of Connecticut.* Paper presented at the ASPRS Annual Conference Proceedings, Denver, Colorado, May 2004, (pp. CD-ROM).

Igusky, K. (2008). *Quantifying albedo and surface temperature over different land covers: Implications for carbon offsets.* (Master's Thesis). Duke University, Durham, NC, USA.

Imhoff, M. L., Zhang, P., Wolfe, R. E., & Bounoua, L. (2010). Remote sensing of the urban heat island effect across biomes in the continental USA. *Remote Sensing of Environment, 114*(3), 504-513.

IMO. (2015). *Iraqi Meteorological Organization, climate department, Baghdad weather*. Retrieved from http://www.meteoseism.gov.iq/index.php?name=Pages&op=page&pid=86.

Integrated Environmental Solutions. (2011). *Apache Tables User Guide - IES Virtual Environment 6.4. Integrated Environmental Solutions Limited*. Retrieved from www.iesve.com/downloads/help/ve64/Thermal/ApacheTables.pdf.

Jacobson, C. R. (2011). Identification and quantification of the hydrological impacts of imperviousness in urban catchments: A review. *Journal of environmental management, 92*(6), 1438-1448.

Jai, Y., & Zeng-Xiang, Z. (2003). *Dynamic study on landscape spatial pattern of land use in China based on RS and GIS.* Paper presented at the Proceedings of the Geoscience and Remote Sensing Symposium, 2003, IEEE International.

Janjai, S., Wanvong, W., & Laksanaboonsong, J. (2006). *The determination of surface albedo of Thailand using satellite data.* Paper presented at the Proceeding of the 2nd joint international conference on Sustainable Energy and Environment (SEE2006), Bangkok, Thailand.

Jassim, S. Z., & Goff, J. C. (2006). *Geology of Iraq*: DOLIN, sro, distributed by Geological Society of London.

Jauregui, E. (1991). Influence of a large urban park on temperature and convective precipitation in a tropical city. *Energy and buildings, 15*(3), 457-463.

Jayalakshmy, M., & Philip, J. (2010). Thermophysical properties of plant leaves and their influence on the environment temperature. *International Journal of Thermophysics, 31*(11-12), 2295-2304.

Jenks, M., & Burgess, R. (2000). *Compact cities: sustainable urban forms for developing countries*: London; New York: Spon Press.

Jensen, J. R. (2005). *Introductory Digital Image Processing: A Remote Sensing Perspective* (3rd ed.). Upper Saddle River.

Jiménez-Muñoz, J. C., & Sobrino, J. A. (2003). A generalized single-channel method for retrieving land surface temperature from remote sensing data. *Journal of Geophysical Research: Atmospheres, 108*(D22).

Jones, P. D., Groisman, P. Y., Coughlan, M., Plummer, N., Wang, W., & Karl, T. (1990). Assessment of urbanization effects in time series of surface air temperature over land. *Nature, 347*(6289), 169-172.

Kantzioura, A., Kosmopoulos, P., & Zoras, S. (2012). Urban surface temperature and microclimate measurements in Thessaloniki. *Energy and buildings, 44*, 63-72.

Kärdi, T. (2007). Remote sensing of urban areas: linear spectral unmixing of Landsat Thematic Mapper images acquired over Tartu (Estonia). *Estonian Journal of Ecology, 56*(1), 19-32.

Karl, T. R., Diaz, H. F., & Kukla, G. (1988). Urbanization: Its detection and effect in the United States climate record. *Journal of climate, 1*(11), 1099-1123.

Kennewell, C., & Shaw, B. J. (2008). Perth, Western Australia. *Cities, 25*(4), 243-255.

Khandelwal, S., & Goyal, R. (2010). *Effect of vegetation and urbanization over land surface temperature: Case study of Jaipur City.* Paper presented at the Proceedings of the EARSeL Symposium, pp. 177-183.

Kim, M., Lee, K., & Cho, G.-H. (2017). Temporal and spatial variability of urban heat island by geographical location: A case study of Ulsan, Korea. *Building and Environment, 126*, 471-482.

Kim, Y.-H., & Baik, J.-J. (2002). Maximum urban heat island intensity in Seoul. *Journal of Applied Meteorology, 41*(6), 651-659.

Kinga, I. (2015). The spatio-temporal analysis of impervious surfaces in Cluj-Napoca, Romania. *Geographia Technica, 10*(2), 50-58.

Kolokotroni, M., & Giridharan, R. (2008). Urban heat island intensity in London: An investigation of the impact of physical characteristics on changes in outdoor air temperature during summer. *Solar Energy, 82*(11), 986-998.

Konrad, C. P., & Booth, D. B. (2002). *Hydrologic trends associated with urban development for selected streams in the Puget Sound Basin, western Washington*: US Department of the Interior, US Geological Survey.

Kottmeier, C., Biegert, C., & Corsmeier, U. (2007). Effects of urban land use on surface temperature in Berlin: Case study. *Journal of urban planning and development, 133*(2), 128-137.

Kuang, W., Chi, W., Lu, D., & Dou, Y. (2014). A comparative analysis of megacity expansions in China and the U.S.: Patterns, rates and driving forces. *Landscape and Urban Planning, 132*, 121-135.

Kumar, K. S., Bhaskar, P. U., & Padmakumari, K. (2012). Estimation of land surface temperature to study urban heat island effect using landsat ETM+ image. *International journal of Engineering Science and technology, 4*(2), 771-778.

Kushari, B., & Kanitpong, K. (2011). *Surface albedo of Bangkok roads.* Paper presented at the Proceedings of the Eastern Asia Society for Transportation Studies.

Landsberg, H. E. (1981). *The urban climate* (Vol. 28): Academic press.

Le-Xiang, Q., Hai-Shan, C., & Chang, J. (2006). Impacts of land use and cover change on land surface temperature in the Zhujiang Delta. *Pedosphere, 16*(6), 681-689.

Li, G., Lu, D., Moran, E., & Hetrick, S. (2013a). Mapping impervious surface area in the Brazilian Amazon using Landsat Imagery. *GIScience & remote sensing, 50*(2), 172-183.

Li, H., Harvey, J., & Kendall, A. (2013b). Field measurement of albedo for different land cover materials and effects on thermal performance. *Building and environment, 59*, 536-546.

Li, X., Zhou, Y., Asrar, G. R., Imhoff, M., & Li, X. (2017). The surface urban heat island response to urban expansion: A panel analysis for the conterminous United States. *Science of The Total Environment, 605-606*, 426-435.

Li, Z.-L., Tang, B.-H., Wu, H., Ren, H., Yan, G., Wan, Z., . . . Sobrino, J. A. (2013c). Satellite-derived land surface temperature: Current status and perspectives. *Remote Sensing of Environment, 131*, 14-37. http://dx.doi.org/https://doi.org/10.1016/j.rse.2012.12.008.

Liang, S. (2000). Narrowband to broadband conversions of land surface albedo I: Algorithms. *Remote Sensing of Environment, 76*(2), 213-238.

Lin, Z., & Xu, H. (2016, 4-6 July 2016). *A study of Urban heat island intensity based on “local climate zones”: A case study in Fuzhou, China.* Paper presented at the 2016 4th International Workshop on Earth Observation and Remote Sensing Applications (EORSA).

Lindén, J., Grimmond, C. S. B., & Esper, J. (2015). Urban warming in villages. *Adv. Sci. Res., 12*(1), 157-162.

Liu, C., Frazier, P., & Kumar, L. (2007). Comparative assessment of the measures of thematic classification accuracy. *Remote Sensing of Environment, 107*(4), 606-616.

Liu, H., & Weng, Q. (2008). Seasonal variations in the relationship between landscape pattern and land surface temperature in Indianapolis, USA. *Environmental Monitoring and Assessment, 144*(1-3), 199-219.

Lo, C. (1981). Land use mapping of Hong Kong from Landsat images an evaluation. *International Journal of Remote Sensing, 2*(3), 231-252.

Lo, C., & Quattrochi, D. A. (2003). Land use and land cover change, urban heat island phenomenon, and health implications. *Photogrammetric Engineering & Remote Sensing, 69*(9), 1053-1063.

LP PYRA 06. (2007). *Instruction Manual of Albedometer*.

Lu, D., Li, G., Kuang, W., & Moran, E. (2014). Methods to extract impervious surface areas from satellite images. *International Journal of Digital Earth, 7*(2), 93-112.

Lu, D., Song, K., Zang, S., Jia, M., Du, J., & Ren, C. (2015). The Effect of Urban Expansion on Urban Surface Temperature in Shenyang, China: an Analysis with Landsat Imagery. *Environmental Modeling & Assessment, 20*(3), 197-210.

Lu, D., & Weng, Q. (2004). Spectral mixture analysis of the urban landscape in Indianapolis with Landsat ETM+ imagery. *Photogrammetric Engineering & Remote Sensing, 70*(9), 1053-1062.

Lu, D., & Weng, Q. (2006). Use of impervious surface in urban land-use classification. *Remote Sensing of Environment, 102*(1), 146-160.

Luck, M., & Wu, J. (2002). A gradient analysis of urban landscape pattern: A case study from the Phoenix metropolitan region, Arizona, USA. *Landscape Ecology, 17*(4), 327-339.

Madanian, M., Soffianian, A. R., Soltani Koupai, S., Pourmanafi, S., & Momeni, M. (2018). The study of thermal pattern changes using Landsat-derived land surface temperature in the central part of Isfahan province. *Sustainable Cities and Society, 39*, 650-661.

Madlener, R., & Sunak, Y. (2011). Impacts of urbanization on urban structures and energy demand: What can we learn for urban energy planning and urbanization management? *Sustainable Cities and Society, 1*(1), 45-53.

Maingi, J., Kepner, S., & Edmonds, W. (2002). Accuracy assessment of 1992 Landsat-MSS derived land cover for the upper San Pedro Watershed (US/Mexico). *Sponsored by Environmental Protection Agency, Las Vegas, NV. National Exposure Research Lab, 2002.*

Manteghi, G., bin Limit, H., & Remaz, D. (2015). Water Bodies an Urban Microclimate: A Review. *Modern Applied Science, 9*(6), 1.

Marshall, J. D. (2007). Urban land area and population growth: A new scaling relationship for metropolitan expansion. *Urban Studies, 44*(10), 1889-1904.

Martin, P., Baudouin, Y., & Gachon, P. (2015). An alternative method to characterize the surface urban heat island. *International Journal of Biometeorology, 59*(7), 849-861.

Martinez, I. (2016). Thermal effects on materials. Retrieved from http://webserver. dmt.upm.es/~isidoro/.

Mathew, A., Khandelwal, S., & Kaul, N. (2016). Spatial and temporal variations of urban heat island effect and the effect of percentage impervious surface area and elevation on land surface temperature: Study of Chandigarh city, India. *Sustainable Cities and Society, 26*, 264-277.

McFeeters, S. (1996). The use of the Normalized Difference Water Index (NDWI) in the delineation of open water features. *International journal of remote sensing, 17*(7), 1425-1432.

McGarigal, K., & Marks, B. J. (1995). *FRAGSTATS: spatial pattern analysis program for quantifying landscape structure*. Portland (OR): USDA Forest Service, Pacific Northwest Research Station; General Technical Report PNW-GTR-351: Retrieved from http://www.umass.edu/landeco/pubs/mcgarigal.marks.1995.pdf.

McGarigal, K. S., Cushman, S., Neel, M., & Ene, E. (2002). *FRAGSTATS: Spatial pattern analysis program for categorical maps*.

Meng, Q., Zhang, L., Sun, Z., Meng, F., Wang, L., & Sun, Y. (2018). Characterizing spatial and temporal trends of surface urban heat island effect in an urban main built-up area: A 12-year case study in Beijing, China. *Remote Sensing of Environment, 204*, 826-837.

Menon, S., Akbari, H., Mahanama, S., Sednev, I., & Levinson, R. (2010). Radiative forcing and temperature response to changes in urban albedos and associated CO2 offsets. *Environmental Research Letters, 5*(1), 014005.

Miran, A. (2017). *The Ministry of Planning and the United Nations Human Settlements Programme (UN-Habitat) Launched the Results of the Identification of Informal Settlements in Iraq*. UN Human Settlements Program. Retrieved from https://reliefweb.int/report/iraq/ministry-planning-and-united-nations-human-settlements-programme-un-habitat-launched.

Moghadam, H. S., & Helbich, M. (2013). Spatiotemporal urbanization processes in the megacity of Mumbai, India: A Markov chains-cellular automata urban growth model. *Applied Geography, 40*, 140-149.

Mohan, M., Kikegawa, Y., Gurjar, B., Bhati, S., Kandya, A., & Ogawa, K. (2009). Assessment of urban heat island intensities over Delhi. *The Seventh International Conference on Urban Climate, held in Yokohama, Japan (29 June - 3 July 2009).*

Murray, J., & Heggie, D. (2016). *From Urban to National Heat Island: the effect of anthropogenic heat output on climate change in high population industrial countries: National Heat Islands* (Vol. 4).

Naegeli, K., Damm, A., Huss, M., Wulf, H., Schaepman, M., & Hoelzle, M. (2017). Cross-Comparison of Albedo Products for Glacier Surfaces Derived from Airborne and Satellite (Sentinel-2 and Landsat 8) Optical Data. *Remote Sensing, 9*(2), 110.

Naem, M., Corner, R., & Dewan, A. (2016). *Diurnal and seasonal surface temperature variations: A case study in Baghdad.* Paper presented at the Proceedings of the 3rd Annual Conference of Research@Locate, 12-14 Apr 2016, Melbourne, Australia: CEUR.

NASA/GISS. (2018). NASA's Goddard Institute for Space Studies (GISS) Retrieved from https://climate.nasa.gov/vital-signs/global-temperature/.

Nieuwolt, S. (1966). The urban microclimate of Singapore. *J. Trop. Geog, 22*(1), 30-37.

NOAA Coastal Services Center. (2013). *Impervious Surface Analysis Tool (ISAT) for ArcGIS 10.x*. Retrieved from www.csc.noaa.gov.

Nordhaus, W. D. (2002). *The economic consequences of a war in Iraq*.

Núñez Peiró, M., Sánchez-Guevara Sánchez, C., & Neila González, F. J. (2017). Update of the Urban Heat Island of Madrid and Its Influence on the Building's Energy Simulation. In P. Mercader-Moyano (Ed.), *Sustainable Development and Renovation in Architecture, Urbanism and Engineering* (pp. 339-350). Cham: Springer International Publishing.

O'Connor, K., Stimson, R. J., & Daly, M. (2001). *Australia's changing economic geography: A society dividing*: Oxford University Press.

O'Neill, R. V., Krummel, J. R., Gardner, R. H., Sugihara, G., Jackson, B., DeAngelis, D. L., . . . Graham, R. L. (1988). Indices of landscape pattern. *Landscape Ecology, 1*(3), 153-162.

Oke, T. (1995). The heat island of the urban boundary layer: characteristics, causes and effects. In J. E. Cermak, A. G. Davenport, E. J. Plate & D. X. Viegas (Eds.), *Wind climate in cities* (pp. 81-107). Dordrecht, the Netherlands: Kluwer Academic.

Oke, T., Johnson, G., Steyn, D., & Watson, I. (1991). Simulation of surface urban heat islands under 'ideal'conditions at night Part 2: Diagnosis of causation. *Boundary-Layer Meteorology, 56*(4), 339-358.

Oke, T. R. (1973). City size and the urban heat island. *Atmospheric Environment, 7*(8), 769-779.

Oke, T. R. (1976). The distinction between canopy and boundary-layer urban heat islands. *Atmosphere, 14*(4), 268-277.

Oke, T. R. (1982). The energetic basis of the urban heat island. *Quarterly Journal of the Royal Meteorological Society, 108*(455), 1-24.

Oke, T. R. (1987). *Boundary layer climates*: Routledge.

Oke, T. R. (2006). Towards better scientific communication in urban climate. *Theoretical and Applied Climatology, 84*(1-3), 179-190.

Oliveira, S., Andrade, H., & Vaz, T. (2011). The cooling effect of green spaces as a contribution to the mitigation of urban heat: A case study in Lisbon. *Building and Environment, 46*(11), 2186-2194.

Onishi, A., Cao, X., Ito, T., Shi, F., & Imura, H. (2010). Evaluating the potential for urban heat-island mitigation by greening parking lots. *Urban forestry & Urban greening, 9*(4), 323-332.

Pal, S., & Ziaul, S. (2017). Detection of land use and land cover change and land surface temperature in English Bazar urban centre. *The Egyptian Journal of Remote Sensing and Space Science, 20*(1), 125-145.

Peel, M. C., Finlayson, B. L., & McMahon, T. A. (2007). Updated world map of the Köppen-Geiger climate classification. *Hydrology and Earth System Sciences, 4*(2), 439-473.

Peng, S., Piao, S., Ciais, P., Friedlingstein, P., Ottle, C., Bréon, F. o.-M., . . . Myneni, R. B. (2011). Surface urban heat island across 419 global big cities. *Environmental science & technology, 46*(2), 696-703.

Pham, T. D., Bailey, G., Marshall, J., Spurr, R., & Dwyer, L. (2013). *The economic impact of the current mining boom on the Australian tourism industry*: Tourism Research Australia Canberra.

Phelan, P. E., Kaloush, K., Miner, M., Golden, J., Phelan, B., Silva III, H., & Taylor, R. A. (2015). Urban heat island: mechanisms, implications, and possible remedies. *Annual Review of Environment and Resources, 40*, 285-307.

Prado, R. T. A., & Ferreira, F. L. (2005). Measurement of albedo and analysis of its influence the surface temperature of building roof materials. *Energy and Buildings, 37*(4), 295-300.

Prakash, A. (2000). Thermal remote sensing: concepts, issues and applications. *International Archives of Photogrammetry and Remote Sensing, 33*(B1; PART 1), 239-243.

Qin, Z., Karnieli, A., & Berliner, P. (2001). A mono-window algorithm for retrieving land surface temperature from Landsat TM data and its application to the Israel-Egypt border region. *International Journal of Remote Sensing, 22*(18), 3719-3746.

Radhi, H., Fikry, F., & Sharples, S. (2013). Impacts of urbanisation on the thermal behaviour of new built up environments: A scoping study of the urban heat island in Bahrain. *Landscape and Urban Planning, 113*, 47-61.

Rajabi, T., & Abu-Hijleh, B. (2011). The Study of Vegetation Effects on Reduction of Urban Heat Island in Dubai.

Rajagopalan, P., Lim, K. C., & Jamei, E. (2014). Urban heat island and wind flow characteristics of a tropical city. *Solar Energy, 107*, 159-170.

Rajasekar, U., & Weng, Q. (2009). Urban heat island monitoring and analysis using a non-parametric model: A case study of Indianapolis. *ISPRS Journal of Photogrammetry and Remote Sensing, 64*(1), 86-96.

Rao, P. (1972). Remote sensing of urban heat islands from an environmental satellite. *Bulletin of the American Meteorological Society, 53*(7), 647-648.

Rashed, T., Weeks, J. R., Gadalla, M. S., & Hill, A. G. (2001). Revealing the anatomy of cities through spectral mixture analysis of multispectral satellite imagery: A case study of the Greater Cairo region, Egypt. *Geocarto International, 16*(4), 7-18.

Rasul, A., Balzter, H., & Smith, C. (2016). Diurnal and seasonal variation of surface urban cool and heat islands in the semi-arid city of Erbil, Iraq. *Climate, 4*(3), 42.

Reis, J. P., Silva, E. A., & Pinho, P. (2014). Measuring space: A review of spatial metrics for urban growth and shrinkage. *The Routledge handbook of planning research methods*, 279.

Rooney, C., McMichael, A. J., Kovats, R. S., & Coleman, M. P. (1998). Excess mortality in England and Wales, and in Greater London, during the 1995 heatwave. *Journal of epidemiology and community health, 52*(8), 482-486.

Rosenfeld, A. H., Akbari, H., Romm, J. J., & Pomerantz, M. (1998). Cool communities: Strategies for heat island mitigation and smog reduction. *Energy and Buildings, 28*(1), 51-62.

Rouse Jr, J. W., Haas, R., Schell, J., & Deering, D. (1974). Monitoring vegetation systems in the Great Plains with ERTS, NASA SP-351. *Third ERTS-1 Symposium, held in NASA, Washington, DC (1974).* (pp. 309-317).

Rutan, D. A., Smith, G. L., & Wong, T. (2014). Diurnal variations of albedo retrieved from earth radiation budget experiment measurements. *Journal of Applied Meteorology and Climatology, 53*(12), 2747-2760.

Sabins, F. F. (2007). *Remote sensing: principles and applications*: Waveland Press.

Santamouris, M., Synnefa, A., & Karlessi, T. (2011). Using advanced cool materials in the urban built environment to mitigate heat islands and improve thermal comfort conditions. *Solar Energy, 85*(12), 3085-3102.

Santra, A., Santra Mitra, S., Mitra, D., & Sarkar, A. (2017). Relative Radiometric Normalisation - performance testing of selected techniques and impact analysis on vegetation and water bodies. *Geocarto International*, 1-16.

Sarrat, C., Lemonsu, A., Masson, V., & Guedalia, D. (2006). Impact of urban heat island on regional atmospheric pollution. *Atmospheric Environment, 40*(10), 1743-1758.

Scherer, D., Fehrenbach, U., Lakes, T., Lauf, S., Meier, F., & Schuster, C. (2014). Quantification of heat-stress related mortality hazard, vulnerability and risk in Berlin, Germany. *Journal of the Geographical Society of Berlin, 144*(3-4), 238-259.

Schindler, S., Poirazidis, K., & Wrbka, T. (2008). Towards a core set of landscape metrics for biodiversity assessments: A case study from Dadia National Park, Greece. *Ecological Indicators, 8*(5), 502-514.

Schowengerdt, R. A. (2006). *Remote sensing: models and methods for image processing*: Academic press.

Schueler, T. R. (1994). The importance of imperviousness. *Watershed protection techniques, 1*(3), 100-111.

Schwarz, N., Schlink, U., Franck, U., & Großmann, K. (2012). Relationship of land surface and air temperatures and its implications for quantifying urban heat island indicators—An application for the city of Leipzig (Germany). *Ecological Indicators, 18*, 693-704.

Scott, A. A., Misiani, H., Okoth, J., Jordan, A., Gohlke, J., Ouma, G., . . . Waugh, D. W. (2017). Temperature and heat in informal settlements in Nairobi. *PLoS ONE, 12*(11), e0187300.

Semenza , J. C., Rubin , C. H., Falter , K. H., Selanikio , J. D., Flanders , W. D., Howe , H. L., & Wilhelm , J. L. (1996). Heat-related deaths during the July 1995 heat wave in Chicago. *New England Journal of Medicine, 335*(2), 84-90.

Seto, K. C., Fragkias, M., Güneralp, B., & Reilly, M. K. (2011). A meta-analysis of global urban land expansion. *PloS ONE, 6*(8), e23777.

Seto, K. C., Güneralp, B., & Hutyra, L. R. (2012). Global forecasts of urban expansion to 2030 and direct impacts on biodiversity and carbon pools. *Proceedings of the National Academy of Sciences, 109*(40), 16083-16088.

Shao, J. (1991). Calculation of sunshine duration and saving of land use in urban building design. *Energy and Buildings, 15*(3), 407-415.

Sheng, L., Lu, D., & Huang, J. (2015). Impacts of land-cover types on an urban heat island in Hangzhou, China. *International Journal of Remote Sensing, 36*(6), 1584-1603.

Shrestha, M. K., York, A. M., Boone, C. G., & Zhang, S. (2012). Land fragmentation due to rapid urbanization in the Phoenix Metropolitan Area: Analyzing the spatiotemporal patterns and drivers. *Applied Geography, 32*(2), 522-531.

Silva, J. S., Silva, R. M. d., & Santos, C. A. G. (2018). Spatiotemporal impact of land use/land cover changes on urban heat islands: A case study of Paço do Lumiar, Brazil. *Building and Environment, 136*, 279-292.

Siyuan, W., Jingshi, L., & Cunjian, Y. (2007). Temporal change in the landscape erosion pattern in the Yellow River Basin, China. *International Journal of Geographical Information Science, 21*(10), 1077-1092.

SLIP Enabler. (2015). Imagery Subscription Service (SLIP). Retrieved from https:// www2.landgate.wa.gov.au/web/guest/57.

Slonecker, E. T., Jennings, D. B., & Garofalo, D. (2001). Remote sensing of impervious surfaces: A review. *Remote Sensing Reviews, 20*(3), 227-255.

Smith, R. (2010). The heat budget of the earth's surface deduced from space. *Yale University Center for Earth Observation: New Haven, CT, USA*.

Sobrino, J. A., Jiménez-Muñoz, J. C., & Paolini, L. (2004). Land surface temperature retrieval from LANDSAT TM 5. *Remote Sensing of Environment, 90*(4), 434-440.

Sobrino, J. A., Li, Z. L., Stoll, M. P., & Becker, F. (1996). Multi-channel and multi-angle algorithms for estimating sea and land surface temperature with ATSR data. *International Journal of Remote Sensing, 17*(11), 2089-2114.

Sobrino, J. A., Oltra-Carrió, R., Sòria, G., Jiménez-Muñoz, J. C., Franch, B., Hidalgo, V., . . . Romaguera, M. (2013). Evaluation of the surface urban heat island effect in the city of Madrid by thermal remote sensing. *International journal of remote sensing, 34*(9-10), 3177-3192.

Sobrino, J. A., & Raissouni, N. (2000). Toward remote sensing methods for land cover dynamic monitoring: Application to Morocco. *International Journal of Remote Sensing, 21*(2), 353-366.

Song, C., Woodcock, C. E., Seto, K. C., Lenney, M. P., & Macomber, S. A. (2001). Classification and change detection using Landsat TM data: When and how to correct atmospheric effects? *Remote Sensing of Environment, 75*(2), 230-244.

Stathopoulou, M., Cartalis, C., & Petrakis, M. (2007). Integrating Corine Land Cover data and Landsat TM for surface emissivity definition: application to the urban area of Athens, Greece. *International Journal of Remote Sensing, 28*(15), 3291-3304.

Stathopoulou, M., Synnefa, A., Cartalis, C., Santamouris, M., Karlessi, T., & Akbari, H. (2009). A surface heat island study of Athens using high-resolution satellite imagery and measurements of the optical and thermal properties of commonly used building and paving materials. *International Journal of Sustainable Energy, 28*(1-3), 59-76.

Stewart, I. D., & Oke, T. R. (2012). Local climate zones for urban temperature studies. *Bulletin of the American Meteorological Society, 93*(12), 1879-1900.

Streutker, D. R. (2002). A remote sensing study of the urban heat island of Houston, Texas. *International Journal of Remote Sensing, 23*(13), 2595-2608.

Streutker, D. R. (2003a). Satellite-measured growth of the urban heat island of Houston, Texas. *Remote Sensing of Environment, 85*(3), 282-289. http://dx.doi.org/https://doi.org/10.1016/S0034-4257(03)00007-5.

Streutker, D. R. (2003b). *A study of the urban heat island of Houston, Texas.* (PhD's Thesis). Rice University, Houston, Texas, USA.

Su, S., Xiao, R., Jiang, Z., & Zhang, Y. (2012). Characterizing landscape pattern and ecosystem service value changes for urbanization impacts at an eco-regional scale. *Applied Geography, 34*, 295-305.

Sukopp, H. (1998). Urban ecology - scientific and practical aspects. In J. Breuste, H. Feldmann & O. Uhlmann (Eds.), *Urban Ecology* (pp. 3-16). Berlin, Heidelberg: Springer Berlin Heidelberg.

Suppiah, R., Hennessy, K., Whetton, P., McInnes, K., Macadam, I., Bathols, J., . . . Page, C. (2007). Australian climate change projections derived from simulations performed for the IPCC 4th Assessment Report. *Australian Meteorological Magazine, 56*(3), 131-152.

Svensson, M. K., & Eliasson, I. (2002). Diurnal air temperatures in built-up areas in relation to urban planning. *Landscape and urban planning, 61*(1), 37-54.

Svirejeva-Hopkins, A., Schellnhuber, H. J., & Pomaz, V. L. (2004). Urbanised territories as a specific component of the Global Carbon Cycle. *Ecological Modelling, 173*(2), 295-312.

Swain, P. H., & Davis, S. M. (1978). *Remote sensing:The quantitative approach*: New York, McGraw-Hill.

Synnefa, A., Karlessi, T., Gaitani, N., Santamouris, M., Papakatsikas, C., & Aktis, S. (2009). Measurement of optical properties and thermal performance of coloured thin layer asphalt samples and evaluation of their impact on the urban environment. *The Second International Conference on Countermeasures to Urban Heat Islands, held in Berkeley, California, USA (2009).*

Synnefa, A., Santamouris, M., & Apostolakis, K. (2007). On the development, optical properties and thermal performance of cool colored coatings for the urban environment. *Solar Energy, 81*(4), 488-497.

Taha, H. (1997). Urban climates and heat islands: Albedo, evapotranspiration, and anthropogenic heat. *Energy and buildings, 25*(2), 99-103.

Taha, H., Akbari, H., Rosenfeld, A., & Huang, J. (1988). Residential cooling loads and the urban heat island-the effects of albedo. *Building and Environment, 23*(4), 271-283.

Taha, H., Sailor, D., & Akbari, H. (1992). *High-albedo materials for reducing building cooling energy use*. Lawrence Berkeley Laboratory, University of California, p. 73.

Taleghani, M., Sailor, D. J., Tenpierik, M., & van den Dobbelsteen, A. (2014). Thermal assessment of heat mitigation strategies: The case of Portland State University, Oregon, USA. *Building and Environment, 73*, 138-150.

Tan, M., & Li, X. (2015). Quantifying the effects of settlement size on urban heat islands in fairly uniform geographic areas. *Habitat International, 49*, 100-106.

Tang, F., & Xu, H. (2016). A study on the quantitative relationship between impervious surface and land surface temperature based on remote sensing technology.*The Fourth International Workshop on Earth Observation and Remote Sensing Applications, held in Guangzhou, China (4-6 July 2016).* (pp. 368-372). IEEE.

Themistocleous, K. (2014). *The use of UAV platforms for remote sensing applications: Case studies in Cyprus.* Paper presented at the Proceedings of Second International Conference of Remote Sensing and Geoinformation of the Environment (RSCy2014), SPIE.

Thi Van, T., & Xuan Bao, H. D. (2010). Study of the impact of urban development on surface temperature using remote sensing in Ho Chi Minh City, Southern Vietnam. *Geographical Research, 48*(1), 86-96.

Thomas, C., Ranchin, T., Wald, L., & Chanussot, J. (2008). Synthesis of Multispectral Images to High Spatial Resolution: A Critical Review of Fusion Methods Based on Remote Sensing Physics. *IEEE Transactions on Geoscience and Remote Sensing, 46*(5), 1301-1312.

Tiangco, M., Lagmay, A., & Argete, J. (2008). ASTER-based study of the night-time urban heat island effect in Metro Manila. *International Journal of Remote Sensing, 29*(10), 2799-2818.

Tromp, M., & Epema, G. F. (1998). Spectral mixture analysis for mapping land degradation in semi-arid areas. *Geologie en Mijnbouw, 77*(2), 153-160.

Tucker, C. J. (1979). Red and photographic infrared linear combinations for monitoring vegetation. *Remote sensing of Environment, 8*(2), 127-150.

Tucker, C. J., Vanpraet, C. L., Sharman, M., & Van Ittersum, G. (1985). Satellite remote sensing of total herbaceous biomass production in the Senegalese Sahel: 1980–1984. *Remote sensing of environment, 17*(3), 233-249.

Turner, B. (1994). Local faces, global flows: The role of land use and land cover in global environmental change. *Land Degradation & Development, 5*(2), 71-78.

Turner, M. G. (1990). Spatial and temporal analysis of landscape patterns. *Landscape Ecology, 4*(1), 21-30.

Turner, M. G. (2005). Landscape Ecology: What Is the State of the Science? *Annual Review of Ecology, Evolution, and Systematics, 36*(1), 319-344.

Turner, M. G., Gardner, R. H., & O'neill, R. V. (2001). *Landscape ecology in theory and practice* (Vol. 401): Springer.

Turner, R. E., Rabalais, N. N., Justic', D., & Dortch, Q. (2003). Global patterns of dissolved N, P and Si in large rivers. *Biogeochemistry, 64*(3), 297-317.

Tzavali, A., Paravantis, J., Mihalakakou, G., Fotiadi, A., & Stigka, E. (2015). *Urban heat island intensity: A literature review* (Vol. 24).

Uemoto, K. L., Sato, N. M., & John, V. M. (2010). Estimating thermal performance of cool colored paints. *Energy and Buildings, 42*(1), 17-22.

Unger, J., Gál, T. M., Rakonczai, J., Mucsi, L., Szatmári, J., Tobak, Z., & Van Leeuwen, B. (2009). Air temperature versus surface temperature in urban environment. *The Seventh International Conference on Urban Climate, held in Yokohama, Japan (29 June - 3 July 2009).*

United Nations. (2001). *The Components of Urban Growth in Developing Countries*. New York.

United Nations. (2014). *World Urbanization Prospects: The 2014 Revision*. New York.

USGS. (2015b). Using the USGS Landsat 8 Product. Retrieved from http://landsat.usgs.gov/Landsat8_Using_Product.php.

USGS. (2016a). Digital Elevation Aster Global DEM. Retrieved from http://earthexplorer.usgs.gov/.

USGS. (2016b). Landsat Missions Timeline. Retrieved from https://landsat.usgs.gov/landsat-missions-timeline.

USGS. (2018a). Landsat missions. Retrieved from http://earthexplorer.usgs.gov/.

USGS. (2018b). Landsat Surface Reflectance Level-2 Science Products. Retrieved from https://landsat.usgs.gov/landsat-surface-reflectance-data-products.

Valor, E., & Caselles, V. (1996). Mapping land surface emissivity from NDVI: Application to European, African, and South American areas. *Remote Sensing of Environment, 57*(3), 167-184.

Vlassova, L., Perez-Cabello, F., Nieto, H., Martín, P., Riaño, D., & de la Riva, J. (2014). Assessment of Methods for Land Surface Temperature Retrieval from Landsat-5 TM Images Applicable to Multiscale Tree-Grass Ecosystem Modeling. *Remote Sensing*, *6*(5), 4345.

Voogt, J. (2007). *How researchers measure urban heat islands*. Environmental Protection Agency (EPA), United States: Retrieved from https://www.epa.gov/sites/production/files/2014-07/documents/epa_how_to_measure_a_uhi.pdf.

Voogt, J. A. (2004). *Urban heat islands: hotter cities*. Washington, DC: American Institute of Biological Sciences.

Voogt, J. A., & Oke, T. R. (2003). Thermal remote sensing of urban climates. *Remote sensing of environment, 86*(3), 370-384.

Wang, K., Wang, J., Wang, P., Sparrow, M., Yang, J., & Chen, H. (2007). Influences of urbanization on surface characteristics as derived from the Moderate-Resolution Imaging Spectroradiometer: A case study for the Beijing metropolitan area. *Journal of Geophysical Research: Atmospheres, 112*(D22).

Wang, S., Ding, C., & Liu, J. (2009). Landscape evolution in the Yellow River Basin using satellite remote sensing and GIS during the past decade. *International Journal of Remote Sensing*, *30*(21), 5573-5591.

Wang, S. Y., Wang, G. Q., Zhang, Z. X., & Zhou, Q. B. (2003). *Analysis of landscape patterns and driving factors of land use in China*. Paper presented at the IGARSS 2003. 2003 IEEE International Geoscience and Remote Sensing Symposium. Proceedings (IEEE Cat. No.03CH37477).

Ward, A. D., Trimble, S. W., Burckhard, S. R., & Lyon, J. G. (2015). *Environmental hydrology*. Boca Raton: Crc Press.

Washington State Department of Ecology. (2017). What is climate change? Retrieved from http://www.ecy.wa.gov/climatechange/whatis.htm.

Webb, B., & Zhang, Y. (1997). Spatial and seasonal variability in the components of the river heat budget. *Hydrological processes, 11*(1), 79-101.

Weng, Q. (2012). Remote sensing of impervious surfaces in the urban areas: Requirements, methods, and trends. *Remote Sensing of Environment, 117*, 34-49.

Weng, Q., & Hu, X. (2008). Medium spatial resolution satellite imagery for estimating and mapping urban impervious surfaces using LSMA and ANN. *IEEE Transactions on Geoscience and Remote Sensing, 46*(8), 2397-2406.

Weng, Q., Hu, X., & Liu, H. (2009). Estimating impervious surfaces using linear spectral mixture analysis with multitemporal ASTER images. *International Journal of Remote Sensing, 30*(18), 4807-4830.

Weng, Q., & Lu, D. (2008). A sub-pixel analysis of urbanization effect on land surface temperature and its interplay with impervious surface and vegetation coverage in Indianapolis, United States. *International Journal of Applied Earth Observation and Geoinformation, 10*(1), 68-83.

Weng, Q., & Yang, S. (2004). Managing the adverse thermal effects of urban development in a densely populated Chinese city. *Journal of Environmental Management, 70*(2), 145-156.

Weng, Y.-C. (2007). Spatiotemporal changes of landscape pattern in response to urbanization. *Landscape and urban planning, 81*(4), 341-353.

Wong, N. H., & Chen, Y. (2008). *Tropical urban heat islands: climate, buildings and greenery*: Routledge.

Wu, C., & Murray, A. T. (2003). Estimating impervious surface distribution by spectral mixture analysis. *Remote sensing of Environment, 84*(4), 493-505.

Wu, H., Ye, L.-P., Shi, W.-Z., & Clarke, K. C. (2014). Assessing the effects of land use spatial structure on urban heat islands using HJ-1B remote sensing imagery in Wuhan, China. *International Journal of Applied Earth Observation and Geoinformation, 32*, 67-78.

Wu, J. J. (2008). Making the case for landscape ecology an effective approach to urban sustainability. *Landscape Journal, 27*(1), 41-50.

Xiao, H., Kopecká, M., Guo, S., Guan, Y., Cai, D., Zhang, C., . . . Yao, W. (2018). Responses of Urban Land Surface Temperature on Land Cover: A Comparative Study of Vienna and Madrid. *Sustainability, 10*(2).

Xiao, H., & Weng, Q. (2007). The impact of land use and land cover changes on land surface temperature in a karst area of China. *Journal of Environmental Management, 85*(1), 245-257.

Xiao, R.-b., Ouyang, Z.-y., Zheng, H., Li, W.-f., Schienke, E. W., & Wang, X.-k. (2007). Spatial pattern of impervious surfaces and their impacts on land surface temperature in Beijing, China. *Journal of Environmental Sciences, 19*(2), 250-256. http://dx.doi.org/https://doi.org/10.1016/S1001-0742(07)60041-2.

Xu, H. (2006). Modification of normalised difference water index (NDWI) to enhance open water features in remotely sensed imagery. *International Journal of Remote Sensing, 27*(14), 3025-3033.

Yang, L., Huang, C., Homer, C. G., Wylie, B. K., & Coan, M. J. (2003). An approach for mapping large-area impervious surfaces: Synergistic use of Landsat-7 ETM+ and high spatial resolution imagery. *Canadian Journal of Remote Sensing, 29*(2), 230-240.

Yang, L., Qian, F., Song, D.-X., & Zheng, K.-J. (2016). Research on Urban Heat-Island Effect. *Procedia Engineering, 169*, 11-18.

Yang, Q., Huang, X., & Li, J. (2017). Assessing the relationship between surface urban heat islands and landscape patterns across climatic zones in China. *Scientific Reports, 7*(1), 9337.

Yang, X., & Lo, C. (2000). Relative radiometric normalization performance for change detection from multi-date satellite images. *Photogrammetric Engineering and Remote Sensing, 66*(8), 967-980.

Yavaşlı, D. (2017). *Spatio-Temporal Trends of Urban Heat Island and Surface Temperature in Izmir, Turkey* (Vol. 5).

Yiftachel, O., & Hedgcock, D. (1993). Urban social sustainability: The planning of an Australian city. *Cities, 10*(2), 139-157.

Yow, D. M. (2007). Urban heat islands: Observations, impacts, and adaptation. *Geography Compass, 1*(6), 1227-1251.

Yu, X., & Lu, C. (2014). *Urban percent impervious surface and its relationship with land surface temperature in Yantai City, China.* Paper presented at the 35th International Symposium on Remote Sensing of Environment (ISRSE35).

Yuan, F., & Bauer, M. E. (2007). Comparison of impervious surface area and normalized difference vegetation index as indicators of surface urban heat island effects in Landsat imagery. *Remote Sensing of environment, 106*(3), 375-386.

Yuan, F., Wu, C., & Bauer, M. E. (2008). Comparison of spectral analysis techniques for impervious surface estimation using Landsat imagery. *Photogrammetric Engineering & Remote Sensing, 74*(8), 1045-1055.

Zhang, H., Qi, Z.-f., Ye, X.-y., Cai, Y.-b., Ma, W.-c., & Chen, M.-n. (2013a). Analysis of land use/land cover change, population shift, and their effects on spatiotemporal patterns of urban heat islands in metropolitan Shanghai, China. *Applied Geography, 44*, 121-133.

Zhang, P., Imhoff, M. L., Bounoua, L., & Wolfe, R. E. (2012a). Exploring the influence of impervious surface density and shape on urban heat islands in the northeast United States using MODIS and Landsat. *Canadian Journal of Remote Sensing, 38*(4), 441-451.

Zhang, Y.-F., Wang, X.-P., Pan, Y.-X., & Hu, R. (2012b). Diurnal relationship between the surface albedo and surface temperature in revegetated desert ecosystems, northwestern China. *Arid Land Research and Management, 26*(1), 32-43.

Zhang, Y., Balzter, H., Zou, C., Xu, H., & Tang, F. (2015). Characterizing bi-temporal patterns of land surface temperature using landscape metrics based on sub-pixel classifications from Landsat TM/ETM+. *International Journal of Applied Earth Observation and Geoinformation, 42*, 87-96.

Zhang, Y., Odeh, I. O. A., & Ramadan, E. (2013b). Assessment of land surface temperature in relation to landscape metrics and fractional vegetation cover in an urban/peri-urban region using Landsat data. *International Journal of Remote Sensing, 34*(1), 168-189.

Zhang, Z., Ji, M., Shu, J., Deng, Z., & Wu, Y. (2008). Surface urban heat island in Shanghai, China: Examining the relationship between land surface temperature and impervious surface fractions derived from Landsat ETM+ imagery. *The International Archives of the Photogrammetry, Remote Sensing and Spatial Information Sciences, 37*, 601-606.

Zhou, B., Rybski, D., & Kropp, J. P. (2017). The role of city size and urban form in the surface urban heat island. *Scientific Reports, 7*(1), 4791.

Zhou, D., Zhao, S., Liu, S., Zhang, L., & Zhu, C. (2014a). Surface urban heat island in China's 32 major cities: Spatial patterns and drivers. *Remote Sensing of Environment, 152*, 51-61.

Zhou, L., Dickinson, R., Tian, Y., Zeng, X., Dai, Y., Yang, Z. L., . . . Strahler, A. (2003). Comparison of seasonal and spatial variations of albedos from Moderate-Resolution Imaging Spectroradiometer (MODIS) and Common Land Model. *Journal of Geophysical Research, 108*(D15), 1-20.

Zhou, W., Huang, G., & Cadenasso, M. L. (2011). Does spatial configuration matter? Understanding the effects of land cover pattern on land surface temperature in urban landscapes. *Landscape and Urban Planning, 102*(1), 54-63.

Zhou, W., Qian, Y., Li, X., Li, W., & Han, L. (2014b). Relationships between land cover and the surface urban heat island: seasonal variability and effects of spatial and thematic resolution of land cover data on predicting land surface temperatures. *Landscape ecology, 29*(1), 153-167.

Appendix A

Accuracy assessment tables of impervious surface area and LULC maps

1. The study area of Baghdad

a. Error matrix of the ISA map in 1976

		Reference			
Classified map		Impervious	Non- impervious	Total	User's Accuracy
	Impervious	338	0	338	100
	Non- impervious	112	450	562	80
	Total	450	450	900	
	Producer's Accuracy	75	100		
	Overall accuracy	88			
	Kappa coefficient	0.75			

b. Error matrix of the ISA map in 1984

		Reference			
Classified map		Impervious	Non- impervious	Total	User's Accuracy
	Impervious	373	0	373	100
	Non- impervious	77	450	527	85
	Total	450	450	900	
	Producer's Accuracy	83	100		
	Overall accuracy	91			
	Kappa coefficient	0.83			

c. Error matrix of the ISA map in 1992

		Reference			
Classified map		Impervious	Non- impervious	Total	User's Accuracy
	Impervious	345	9	354	97
	Non- impervious	105	441	546	81
	Total	450	450	900	
	Producer's Accuracy	77	98		
	Overall accuracy	87			
	Kappa coefficient	0.75			

d. Error matrix of the ISA map in 2000

		Reference			
		Impervious	Non- impervious	Total	User's Accuracy
Classified map	Impervious	367	9	376	98
	Non- impervious	83	441	524	84
	Total	450	450	900	
	Producer's Accuracy	82	98		
	Overall accuracy	90			
	Kappa coefficient	0.8			

e. Error matrix of the ISA map in 2015

		Reference			
		Impervious	Non- impervious	Total	User's Accuracy
Classified map	Impervious	364	17	381	96
	Non- impervious	86	433	519	83
	Total	450	450	900	
	Producer's Accuracy	81	96		
	Overall accuracy	89			
	Kappa coefficient	0.77			

f. Error matrix of the LULC classified map in 2015

		Reference data					
		ISA	Green area	Bare land	Water	Total	User's Accuracy
Classified map	ISA	365	0	15	0	380	96
	Green area	28	134	19	9	190	71
	Bare land	57	19	103	0	179	58
	Water	0	36	7	108	151	72
	Total	450	189	144	117	900	
	Producer's Accuracy	81	71	72	92		
	Overall accuracy	79					
	Kappa coefficient	0.69					

2. The study area of Perth

a. Error matrix of the ISA map in 1974

		Reference			
		Impervious	Non- impervious	Total	User's Accuracy
Classified map	Impervious	330	0	330	100
	Non- impervious	120	450	570	79
	Total	450	450	900	
	Producer's Accuracy	73	100		
	Overall accuracy	87			
	Kappa coefficient	0.73			

b. Error matrix of the ISA map in 1988

		Reference			
		Impervious	Non- impervious	Total	User's Accuracy
Classified map	Impervious	393	9	402	98
	Non- impervious	57	441	498	89
	Total	450	450	900	
	Producer's Accuracy	87	98		
	Overall accuracy	93			
	Kappa coefficient	0.85			

c. Error matrix of the ISA map in 1997

		Reference			
		Impervious	Non- impervious	Total	User's Accuracy
Classified map	Impervious	401	49	450	89
	Non- impervious	49	401	450	89
	Total	450	450	900	
	Producer's Accuracy	89	89		
	Overall accuracy	89			
	Kappa coefficient	0.78			

d. Error matrix of the ISA map in 2008

		Reference			
		Impervious	Non- impervious	Total	User's Accuracy
Classified map	Impervious	385	56	441	87
	Non- impervious	65	394	459	86
	Total	450	450	900	
	Producer's Accuracy	86	88		
	Overall accuracy	87			
	Kappa coefficient	0.73			

e. Error matrix of the ISA map in 2015

		Reference			
		Impervious	Non- impervious	Total	User's Accuracy
Classified map	Impervious	412	53	465	89
	Non- impervious	38	397	435	91
	Total	450	450	900	
	Producer's Accuracy	92	88		
	Overall accuracy	90			
	Kappa coefficient	0.80			

f. Error matrix of the LULC classified map in 2015

		Reference data					
		ISA	Green area	Bare land	Water	Total	User's Accuracy
Classified map	ISA	396	0	4	0	400	99
	Green area	32	189	44	2	267	71
	Bare land	22	0	69	1	92	75
	Water	0	0	0	141	141	100
	Total	450	189	117	144	900	
	Producer's Accuracy	88	100	59	98		
	Overall accuracy	88					
	Kappa coefficient	0.83					

Appendix B

Section 1: The values of surface albedo and temperature retrieved from field work and Landsat 8 for various LULC surfaces, Perth

1. The surface albedo values of field measurements

	New concrete	Old concrete	New black asphalt	Old Black asphalt	New red asphalt	Old red asphalt
	0.414	0.214	0.072	0.161	0.129	0.162
	0.413	0.215	0.065	0.162	0.128	0.162
	0.411	0.201	0.065	0.155	0.129	0.162
	0.411	0.214	0.065	0.15	0.129	0.162
	0.41	0.213	0.065	0.14	0.128	0.162
	0.411	0.216	0.066	0.141	0.127	0.165
	0.411	0.213	0.062	0.141	0.134	0.164
	0.41	0.214	0.063	0.139	0.133	0.164
		0.209	0.066	0.141	0.133	0.164
		0.203	0.064	0.141	0.133	0.139
		0.204	0.063	0.14		0.14
		0.204		0.14		0.14
		0.204		0.163		0.141
		0.204		0.163		0.142
		0.208		0.163		0.142
		0.21		0.158		0.142
		0.21		0.157		0.142
		0.203		0.157		0.137
		0.208		0.157		0.136
				0.155		0.136
				0.155		0.136
				0.153		0.136
				0.153		0.137
				0.153		
Mean	0.411	0.209	0.065	0.152	0.130	0.148
SD	0.0014	0.0049	0.0026	0.0088	0.0026	0.0122
SE	0.0005	0.0011	0.0008	0.0018	0.0008	0.0025
Count	8	19	11	24	10	23
		Max value			Min value	

	Rubber	Red bricks	Yellow bricks	Red tiles	Brown tiles	Green tiles
	0.142	0.15	0.249	0.304	0.158	0.245
	0.141	0.15	0.248	0.307	0.157	0.244
	0.141	0.14	0.247	0.304	0.158	0.245
	0.141	0.148	0.247	0.303	0.162	0.244
	0.137	0.144	0.246	0.319	0.167	0.245
	0.139	0.143	0.247	0.316	0.171	0.245
	0.14	0.144	0.248	0.315	0.159	0.235
	0.138	0.143	0.247	0.315	0.155	0.245
	0.136	0.143		0.336	0.154	0.237
	0.136	0.194		0.338	0.155	0.236
	0.136	0.199		0.336	0.159	0.238
	0.136	0.199		0.335	0.157	
	0.136	0.2		0.335	0.157	
	0.136	0.2		0.32	0.159	
	0.136	0.196		0.319		
	0.135	0.195		0.321		
	0.135	0.194		0.324		
	0.134	0.193		0.324		
	0.135			0.224		
	0.135			0.224		
				0.224		
				0.226		
				0.227		
				0.228		
				0.229		
				0.229		
				0.224		
				0.225		
				0.226		
Mean	0.137	0.171	0.247	0.285	0.159	0.242
SD	0.0025	0.0268	0.0009	0.0476	0.0047	0.0042
SE	0.0006	0.0063	0.0003	0.0088	0.0013	0.0013
Count	20	18	8	29	14	11
		Max value			Min value	

	White metal	Red metal	Grey metal	Green metal	Brown metal	Grass
	0.501	0.283	0.333	0.267	0.207	0.286
	0.5	0.288	0.329	0.256	0.209	0.284
	0.501	0.286	0.329	0.26	0.207	0.283
	0.499	0.288	0.335	0.248	0.207	0.283
	0.499	0.287	0.335	0.247	0.206	0.278
	0.498	0.291	0.333		0.208	0.278
	0.503	0.291	0.335		0.208	0.278
	0.502	0.291	0.334		0.204	0.277
	0.504	0.29	0.335		0.205	0.278
	0.493	0.291	0.335		0.205	0.272
	0.504	0.281	0.34		0.204	0.272
	0.518	0.286	0.336		0.205	0.271
	0.518	0.286	0.344			0.271
	0.52	0.285	0.344			0.27
	0.522	0.284	0.345			0.27
	0.518	0.285	0.345			0.274
	0.523	0.285	0.345			0.273
	0.524	0.284	0.348			0.274
	0.522		0.348			0.274
	0.511		0.348			0.275
	0.522		0.347			0.299
	0.518		0.347			0.299
	0.512					0.297
	0.517					0.297
	0.506					0.297
	0.514					0.284
	0.519					0.281
	0.516					0.28
						0.281
						0.281
						0.281
Mean	0.511	0.287	0.340	0.256	0.206	0.281
SD	0.0095	0.0031	0.0066	0.0084	0.0017	0.0089
SE	0.0018	0.0007	0.0014	0.0037	0.0005	0.0016
Count	28	18	22	5	12	31
		Max value			Min value	

	Shrubs	Trees	Bare land	Soil	Mulch	Water
	0.228	0.15	0.303	0.279	0.211	0.045
	0.238	0.154	0.302	0.278	0.21	0.034
	0.225	0.155	0.301	0.278	0.211	0.032
	0.225	0.154	0.301	0.278	0.211	0.031
	0.223	0.153	0.302	0.277	0.206	0.035
	0.223	0.15	0.322	0.277	0.207	0.035
	0.233	0.15	0.321		0.206	0.031
	0.22	0.15	0.321		0.205	0.035
	0.219	0.15	0.32		0.203	0.031
	0.218	0.149	0.319		0.205	0.038
	0.221		0.261		0.201	0.034
	0.217		0.261		0.201	0.029
			0.262		0.191	0.028
			0.258		0.183	0.029
			0.258		0.186	0.029
			0.258			0.025
			0.259			0.026
			0.322			0.026
			0.301			0.026
			0.302			0.025
						0.026
Mean	0.224	0.152	0.293	0.278	0.202	0.031
SD	0.0063	0.0022	0.0262	0.0008	0.0089	0.0050
SE	0.0018	0.0007	0.0059	0.0003	0.0023	0.0011
Count	12	10	20	6	15	21
		Max value			Min value	

2. The surface temperature values of field measurements

	New concrete	Old concrete	New black asphalt	Old Black asphalt	New red asphalt	Old red asphalt
	37.9	46.8	56.4	48.6	70.4	67.8
	37.4	45.8	55.9	48.2	70.3	66.2
	37.9	47.2	57	48.6	71.2	68.6
		48.9	54.5	48.1	70	68.7
		48	54.8	50.9	69.5	65.2
		48		50.7		66.7
				53.4		
				50.9		
				52.2		
Mean	37.7	47.5	55.7	50.2	70.3	67.2
SD	0.289	1.088	1.057	1.904	0.622	1.401
SE	0.167	0.444	0.473	0.635	0.278	0.572
Count	3	6	5	9	5	6
		Max value			Min value	

	Rubber	Red bricks	Yellow bricks	Red tiles	Brown tiles	Green tiles
	53.4	54.5	60	51.8	65	60.2
	53.3	53.8	59.5	51.3	64.9	58.7
	58	57.9	59.6	50.5	64.2	59.5
	55.2	57.5	59.7	52.4	65.6	56.9
	54.1	56.4		52.6	65	
	52.4	51.9			64	
	51.7				64.6	
Mean	54.0	55.3	59.7	51.7	64.8	58.8
SD	2.088	2.335	0.216	0.853	0.541	1.422
SE	0.789	0.953	0.108	0.381	0.205	0.711
Count	7	6	4	5	7	4
		Max value			Min value	

	White metal	Red metal	Grey metal	Green metal	Brown metal	Grass
	47.7	70.2	71.1	57.8	66	33.8
	49.2	69.5	69.3	55.4	66.5	36.1
	49.9	69.4	70.1	55.3	66.9	34.4
	49.3	71.1	69.3	59.1		36.9
	49.6	70.1	69.4	58.5		36.3
	49.5					35.9
	49.9					34.6
	49.9					
	49.7					
	49.8					
	49.5					
	49.4					
Mean	49.5	70.1	69.8	57.2	66.5	35.4
SD	0.601	0.680	0.780	1.768	0.451	1.154
SE	0.173	0.304	0.349	0.791	0.260	0.436
Count	12	5	5	5	3	7
		Max value			Min value	

	Shrubs	Trees	Bare land	Soil	Mulch	Water
	34.2	37.6	56	58.4	52.3	30.8
	36.1	36.2	55.4	58	51.5	31.1
	36.7	39.6	56.6	57.5	50.2	30.6
	34.8	35.3	54.9		52.4	30.9
	33.7	34.7	57.5		53.1	30
	36.1	36.7	57.8			30.9
	33.6	34.8	56.7			30.6
		35.2	58			29.2
		35.7				30.1
						30
						30.6
						30
						30.9
						30.4
Mean	35.0	36.2	56.6	58.0	51.9	30.4
SD	1.267	1.583	1.128	0.451	1.107	0.520
SE	0.479	0.528	0.399	0.260	0.495	0.139
Count	7	9	8	3	5	14
		Max value			Min value	

3. The surface albedo values derived from Landsat 8

	Old concrete	Old Black asphalt	Old red asphalt	Red tiles	White metal	Red metal
	0.203	0.104	0.137	0.173	0.367	0.258
	0.248	0.135	0.174	0.244	0.375	0.224
	0.149	0.141	0.142	0.163	0.389	0.237
	0.225	0.132	0.145	0.193	0.478	0.232
	0.188	0.116	0.154	0.211	0.403	0.262
	0.291	0.171	0.17	0.192	0.587	0.229
	0.269	0.184	0.15	0.211	0.47	0.242
	0.232	0.145	0.158	0.175	0.635	
	0.284	0.129	0.136	0.186	0.437	
	0.196	0.134	0.146	0.196	0.505	
	0.219	0.202	0.147	0.219	0.496	
	0.192	0.152	0.151	0.196	0.417	
	0.227	0.118				
	0.274	0.142				
Mean	0.228	0.143	0.151	0.197	0.463	0.241
SD	0.0413	0.0269	0.0118	0.0223	0.0836	0.0145
SE	0.0110	0.0072	0.0034	0.0064	0.0241	0.0055
Count	14	14	12	12	12	7
		Max value			Min value	

	Grey metal	Grass	Trees	Bare land	water
	0.279	0.241	0.105	0.234	0.018
	0.195	0.273	0.117	0.237	0.049
	0.204	0.272	0.145	0.256	0.08
	0.249	0.235	0.138	0.25	0.048
	0.326	0.268	0.141	0.384	0.022
	0.296	0.267	0.119	0.301	0.041
	0.323	0.247	0.094	0.265	0.052
	0.392	0.256	0.106	0.321	0.044
	0.335	0.277	0.122	0.247	0.039
	0.205	0.269	0.114	0.225	0.032
		0.248	0.129	0.272	0.029
		0.236			0.032
					0.025
Mean	0.280	0.257	0.121	0.272	0.039
SD	0.0661	0.0154	0.0162	0.0470	0.0163
SE	0.0209	0.0044	0.0049	0.0142	0.0045
Count	10	12	11	11	13
		Max value		Min value	

4. The surface temperature values derived from Landsat 8

	Grass	Trees	Soil	Water	Built-up
	36.7	31.8	40.9	27.9	34.5
	36.4	31.7	40.5	27.2	34.8
	36.1	31.5	38.5	25.7	38.3
	36.4	32.3	40.9	27.3	36.7
	32.1	32	41	27.1	36.4
	32.3	32.3	41	26.9	37.1
	32.8	32.2	40.3	26.8	37.4
	33	32.8	40.8	27	39.5
	32.9	29.8	40.8	28.1	36.6
	33.4	29.9	39.3	28.5	37.6
	33.9	34.2	41.2	26.2	38.3
	33.7	33.1	39.8	27.1	39.7
	33.6	32.2	41.2	27.3	38.7
	34.6	32.6		26.4	36.4
Mean	34.1	32.0	40.5	27.1	37.3
SD	1.619	1.141	0.814	0.738	1.551
SE	0.433	0.305	0.226	0.197	0.414
Count	14	14	13	14	14
		Max value		Min value	

Section 2: Visible and thermal images of various LULC surfaces were acquired by the FLIR E5 infrared camera in the field, Perth

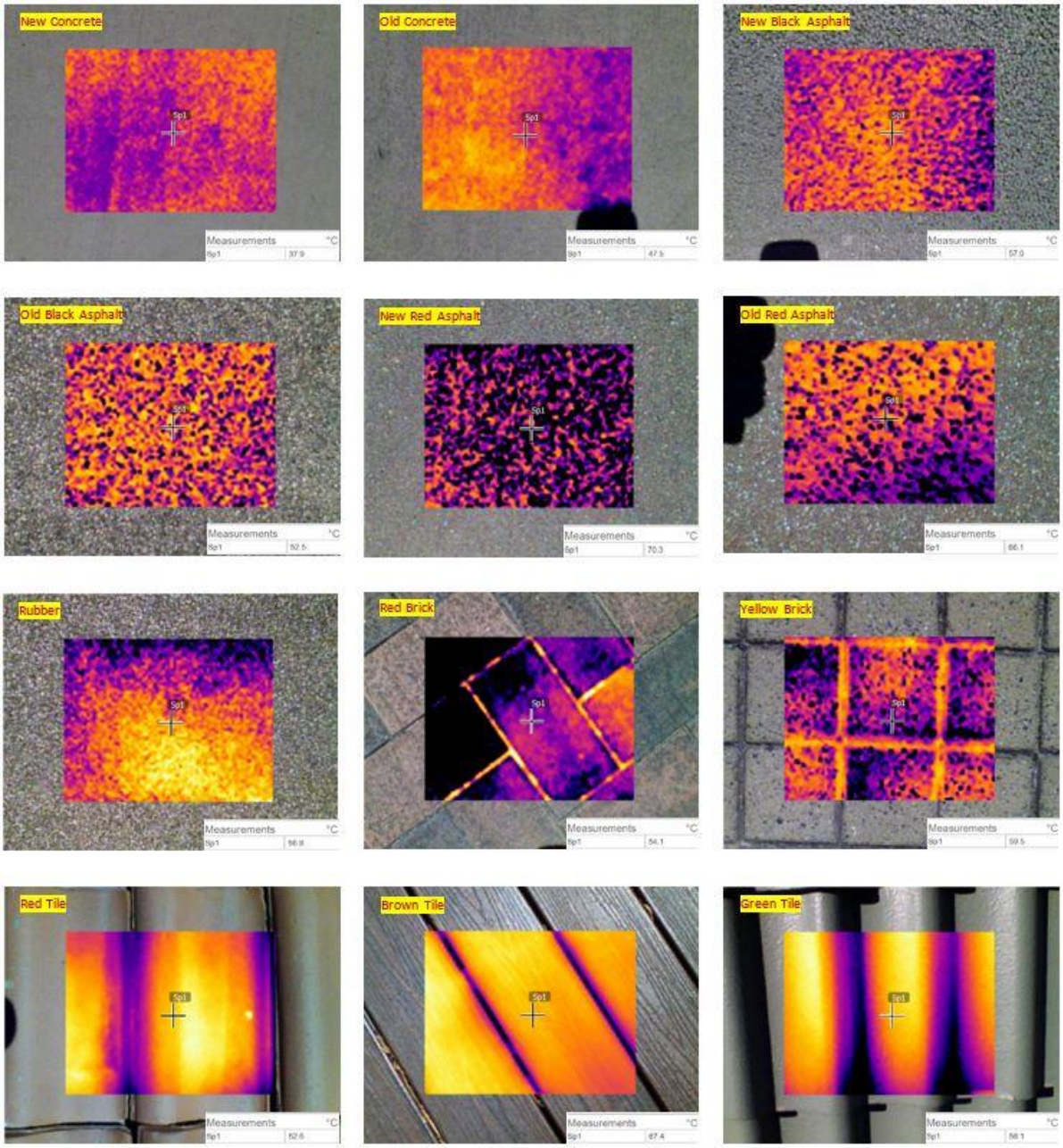

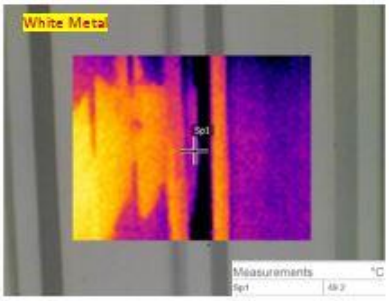
White Metal
Sp1
Measurements
°C
Sp1

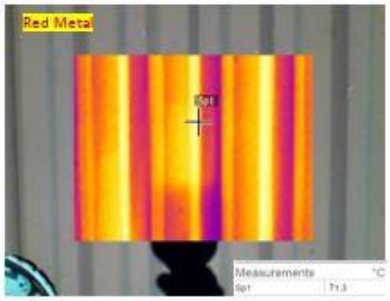
Red Metal
Sp1
Measurements
°C
Sp1

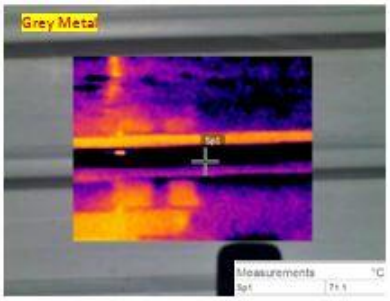
Grey Metal
Sp1
Measurements
°C
Sp1

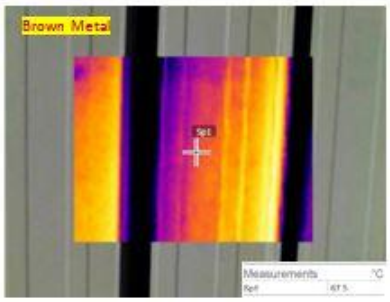
Brown Metal
Sp1
Measurements
°C
Sp1

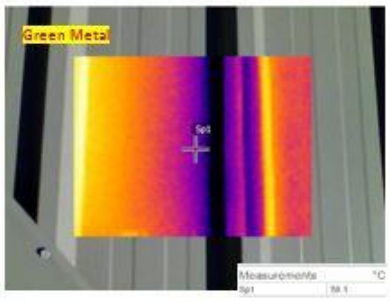
Green Metal
Sp1
Measurements
°C
Sp1

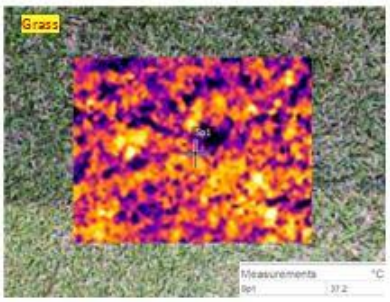
Grass
Sp1
Measurements
°C
Sp1

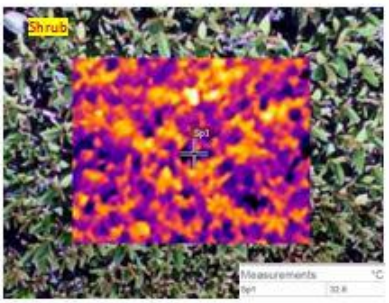
Shrub
Sp1
Measurements
°C
Sp1


Tree
Sp1
Measurements
°C
Sp1

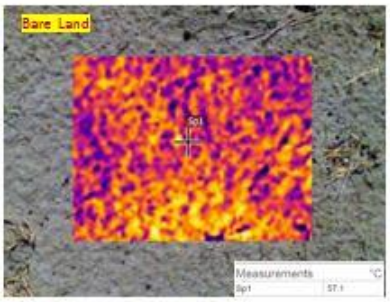
Bare Land
Sp1
Measurements
°C
Sp1

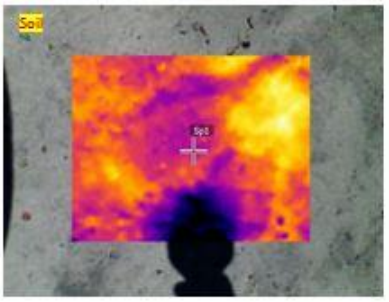
Soil
Sp1

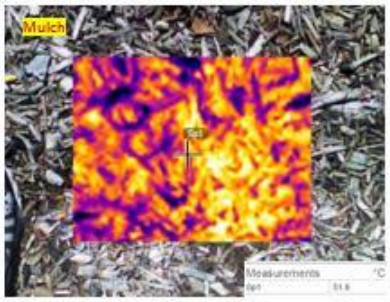
Mulch
Sp1
Measurements
°C
Sp1

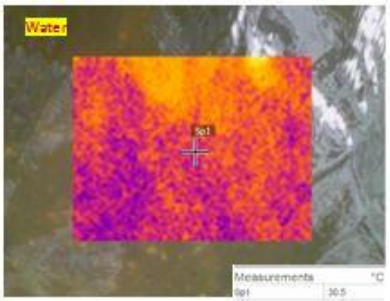
Water
Sp1
Measurements
°C
Sp1

Image showing the Pyranometer instrument used by the author for collecting albedo data in the field, Perth